Three studies on quantum phases of matter

Ming-Hao Li
Merton College
University of Oxford

A thesis submitted for the degree of
Doctor of Philosophy

Trinity 2024

To science.

Acknowledgements

To begin, I would like to thank my supervisor: Prof. Sid Parameswaran. In the years since I knew him, he has always been supportive of me both academically and personally. My research interests have broadened because of the insightful discussions with him, and the research presented in this thesis would not have been possible without his guidances.

Also, I would like to thank Prof. Nick Bultinck who has been like an extra supervisor to me. I am grateful that he introduced me to the fields of tensor network and Belgian Trappist beer.

I would like to thank Prof. Paul Fendley and Prof. Meng Cheng, the examiners for my viva. I greatly enjoyed the illuminating discussions.

I thank my parents and my brother for tolerating my long absence from home, and for their unwavering supports.

I would like to thank all the people I have had the chance to collaborate with: Prof. Jutho Haegeman, Prof. Titus Neupert, Prof. Apoorv Tiwari, Sounak Biswas and Quinten Mortier.

I sincerely thank all my other physicist friends that I made over the years: Michele Fava, Yves Kwan, Guanming Zhang, Jacob Robertson, Jovan Jovanovic, Jonathan Classen-Howes, Luisa Eck, Riccardo Senese, Konstantinos Vasiliou, Ziwei Wang, Abhishodh Prakash, Max McGinley, Yuchi He, Lukas Devos, Tatiana Vovk, Vladimir Zakharov, Aravindh Shankar, Alaric Sanders, Akshat Pandey, Zhou Yang, Xiangzhou Zhu, Han Zheng as well as many others.

I also thank my Merton friends, Cesare Vagge, Pavle Kravljanac, Hiroto Takahashi, Samuel Liebana Garcia and Uziel Gonzalez. I greatly enjoy conversations with you, which usually start with international politics and end with personal love stories.

A special thank goes to Bianca Sgorbati and Eleanor Wise. I will always fondly remember the films we watched, along with the enticing scents of home cooked pasta, British pie and beef stew.

Finally I thank my partner, Anita Breudel, who has always been there for me without fail. This journey is impossible without you.

Abstract

This is a thesis in three parts regarding the study of quantum phases of matter.

In the first part, we show that the gapless boundary signatures — namely, chiral/helical hinge modes or localized zero modes — of three-dimensional higher-order topological insulators and superconductors with inversion symmetry can be gapped without symmetry breaking upon the introduction of non-Abelian surface topological order. In each case, the fractionalization pattern that appears on the surface is 'anomalous' in the sense that it can be made consistent with symmetry only on the surface of a three dimensional higher-order insulator/superconductor. Our results show that the interacting manifestation of higher-order topology is the appearance of 'anomalous gapped boundaries' between distinct topological orders whose quasiparticles are related by inversion, possibly in conjunction with other protecting symmetries such as TRS and charge conservation. This part is based on the published work: **Ming-Hao Li**, Titus Neupert, S. A. Parameswaran and Apoorv Tiwari, *Anomalous gapped boundaries between surface topological orders in higher-order topological insulators and superconductors with inversion symmetry*, Phys. Rev. B 106, 125121.

In the second part, we extend the study of finite-entanglement scaling from one-dimensional gapless models to two-dimensional systems with a Fermi surface. In particular, we show that the entanglement entropy of a contractible spatial region with linear size L scales as $S \sim L \log[\xi f(L/\xi)]$ in the optimal tensor network, and hence area-law entangled, state approximation to a metallic state, where $f(x)$ is a scaling function which depends on the shape of the Fermi surface and ξ is a finite correlation length induced by the restricted entanglement. Crucially, the scaling regime can be realized with numerically tractable bond dimensions. We also discuss the implications of the Lieb-Schultz-Mattis theorem at fractional filling for tensor network state approximations of metallic states. This part is based on parts of the published work: Quinten Mortier*, **Ming-**

Hao Li*, Jutho Haegeman and Nick Bultinck, *Finite-entanglement scaling of 2D metals*, Phys. Rev. Lett. 131, 266202.

In the third part, we study fermionic quantum spin liquids (QSLs) on the three-dimensonal trillium lattice of corner-sharing triangles. We are motivated by recent experimental and theoretical investigations that have explored various classical and quantum spin liquid states on similar networks of triangular motifs with strong geometric frutstration. Using the framework of Projective Symmetry Groups (PSG), we obtain a classification of all symmetric Z_2 and $\mathsf{U}(1)$ QSLs on the trillium lattice. We find 2 Z_2 spin-liquids, and a single $\mathsf{U}(1)$ spin-liquid which is proximate to one of the Z_2 states. This small number of solutions reflecting the constraints imposed by the two non-symmorphic symmetries in the space group of trillium. This part is based on the unpublished work in collaboration with Dr. Sounak Biswas and Prof. S.A. Parameswaran.

* These authors have contributed equally to the work.

Contents

List of acronyms

AGSP Approximate Ground State Projector

BCS Bardeen–Cooper–Schrieffer

BFGS Broyden–Fletcher–Goldfarb–Shanno

BZ Brillouin Zone

CFT Conformal Field Theory

DMRG Density Matrix Renormalisation Group

EE Entanglement Entropy

FCC Face-Centered-Cubic

FS Fermi Surface

GFTNS Gaussian Fermionic Tensor Network States

GVW Gu-Verstraete-Wen

HHK Hyper-Hyper-Kagome

HK Hyper-Kagome

HOSPT Higher Order Symmetry Protected Topological (phase)

HOTI Higher Order Topological Insulator

HOTSC Higher Order Topological Superconductor

IGG Invariant Gauge Group

LHS Left Hand Side

MFT Mean Field Theory

MPS Matrix Product State

OPE Operator Product Expansion

PEPS Projected Entangled Pair State

PHS Particle Hole Symmetry

PSG Projective Symmetry Group

QSL Quantum Spin Liquid

RG Renormalisation Group

RHS Right Hand Side

RVB Resonating Valence Bond

SC Superconductor

SET Symmetry Enriched Topological (phase)

SG Symmetry Group

SPT Symmetry Protected Topological (phase)

SSH Su–Schrieffer–Heeger

STO Surface Topological Order

TI Topological Insulator

TNS Tensor Network State

TRIM time-reversal invariant momenta

TRS Time Reversal Symmetry

TSC Topological Superconductor

WZW Wess-Zumino-Witten (theory)

Chapter 1

Introduction

Since the beginning of history, our forebears have never ceased to ponder the transient nature of existence. In his late work *Timaeus* [1], Plato notes that, because of the constant transformation between things – "*...we apparently see what we've just been calling 'water' solidifying and turning into stones and earth ...*", it is difficult to give an identity to a thing when its identity can be transformed into another. As a solution to this difficulty, he proposes that things in their own rights are the *receptacles*, characterless objects that get characterised temporarily by the four elements, namely fire, water, air and earth. Plato then proceeds to construct a mathematical/geometrical theory for the four elements, which he assumes to be made of primary particles of certain shapes. More specifically, he assigns the tetrahedron for fire, the octahedron for air, the icosahedron for water, and the cube for earth. These Platonic solids are fundamentally made of triangles, and transformations of elements are achieved by the reassembling of the triangles.

Using modern terminologies, what Plato describes in his dialogue can be regarded as a theory of phase transitions. The term "phase" can be identified as Plato's element, and microscopic particles such as atoms and molecules replace Plato's triangle. As an example, today we know that the same constituent, namely the H_2O molecule, is the assembling unit simultaneously of ice, water and vapour. Different phases of matter are the consequences, more of different kinds of collective phenomena, rather than of the different fundamental units.

To a modern physicist, what mathematical principles are guiding the formation of different phases of matter? A remarkable theory was developed in the 1960s, largely due to Lev Landau [2, 3], in an attempt to explain the so-called *second order phase transitions*.

Chapter heading: owl motif, detail of the *fanggui*, Shang dynasty, Yinxu period (circa 14th – 12th/11th centuries B.C.), Meiyintang Collection # 65.

The Landau theory states that phases separated by second order phase transitions are characterised by different symmetries. A primary example is the 2D Ising model, a toy model for magnetism, which exhibits paramagnetic phase above a certain temperature T_c, and ferromagnetic phase below T_c. Across the transition, a Z_2 symmetry is broken. The second order phase transitions themselves, often called critical points/lines, exhibit universal features, such as scale invariance and critical exponents.

The Landau theory had been really successful, notably explaining BCS superconductors and gapless excitations such as phonons and spin waves associated with symmetry breaking. However, encounters with quantum Hall effects and high T_c superconductors from the 70s to the 80s demonstrated to us that phases cannot be distinguished merely by symmetries. In fact, in the past five decades, a kind of "*quantum new wave*" has emerged, in which a considerable amount of novel phases of matter beyond the Landau regime has been identified. It is an ongoing quest for the contemporary physicists to shift to a new paradigm which classifies and explains these novel phases of matter. Despite the absence of a new paradigm, a collection of research themes, which are not necessarily mutually exclusive, is discerned. The list includes:

- Fractionalisation: emergent quasi-particles that carry fractionalised charge and statistics, such as anyons;
- Band topology: systems with bulk topological invariant and protected anomalous edge theories, most famously gapless theories;
- Fermi surface states without quasi-particle excitations: non Fermi liquid states which exhibit anomalous transport properties, such as the strange metal phase in the cuprate systems;

The list can go on, but what is the common thread that connects the items? Today, it is widely believed that quantum many body entanglement plays a central role in the "*quantum new wave*", and it sometimes reminds me of the role that DNA plays in biological systems. Being a primary feature that distinguishes quantum world from the classical world, it is not surprising that it holds the key to the plethora of the exotic phases. Mathematically, we use entanglement entropy to quantify the amount of entanglement in a system. In many cases, we can distinguish the novel phases directly from the quantum entanglement entropy itself, e.g. topological entanglement entropy and Fermi surface entanglement entropy that depends on the Fermi surface geometry. Utilising our understanding of quantum entanglement, an efficient representation of typical many body quantum states, that can be stored on classical computers, is developed, namely the tensor network representation (I will explain later in

this chapter what "typical" means), greatly advancing the classical simulations of quantum matter.

Due to the richness of the phenomena, during my DPhil studies I have not committed myself to a singular research theme. Instead, three separate studies were conducted on the quantum phases of matter, namely the phases of matter at absolute zero temperature, when the quantum effects are the strongest and the most transparent. The first concerns the anyonic states on the surfaces of the inversion protected higher order topological phases, where we probe alternative anomalous surface states for these crystalline symmetry protected phases; the second turns to the study of finite entanglement scaling of 2D Gaussian fermionic tensor network states, demonstrating tensor network's capability to simulate the highly entangled Fermi surface states; finally we present a projective symmetry group study of the quantum spin liquid states on the 3D trillium lattice.

In the coming sections, we give a comprehensive pedagogical review of the prerequisites for the above three studies.

1.1 Symmetry protected topological phase and bulk boundary correspondence

1.1.1 Symmetry protected topological phase

The notion of bulk-boundary correspondence has been crucial in the studies of topological phases of matter. An example of the principle is the two dimensional topological insulator (2D TI), which has a bulk theory that is topological and gapped, as well as a one dimensional edge theory that is gapless [4, 5]. For certain topological phases, the stability of the gapless nature of the edge relies on the symmetries that are present in the system. In the system of 2D TI, the relevant symmetry group is $\mathsf{U}(1) \rtimes \mathcal{T}$, where $\mathcal{T}$ denotes the time reversal symmetry (TRS). To see why the symmetry protects the gapless nature of the edge modes, one notes that edge modes for 2D TI can be described by $\mathsf{U}(1)_1 \times \mathsf{U}(1)_{-1}$ Luttinger theory, and the symmetry explicitly prevents us from writing down a mass term in the Luttinger theory [6, 7]. Due to the demonstrated symmetry protection, these phases are usually termed *symmetry protected topological phases* (SPT phases) [8, 9, 10].

In understanding the principle of bulk-boundary correspondence, the notion of *anomaly* is very important [11, 12, 13, 14, 15]. In general, for a d-dimensional SPT phase protected by symmetry group G, the boundary theory of the SPT phase cannot exist on its own without breaking the symmetry. However, the boundary theory of a SPT phase does not necessarily take a unique form. Gapped and gapless theories can both be the boundary theory of a SPT as long as they have the correct anomaly corresponded to the SPT phase. Therefore one

can see that the bulk-boundary correspondence principle is not a correspondence between a SPT and a gapless boundary theory. Instead, it is a correspondence between a SPT and an anomalous boundary theory. Now we review this correspondence using a simple example.

1.1.1.1 't Hooft anomaly in 0D and projective representation of symmetry

Let us consider a generic quantum mechanical system, with the Hilbert space $\mathcal{H}$. The quantum states in the Hilbert space are defined up to a $\mathsf{U}(1)$ phase, i.e.

$$|\Psi\rangle \sim |\Psi'\rangle = e^{i\alpha}|\Psi\rangle, \tag{1.1}$$

where $\sim$ denotes equivalence. Indeed, under the insertion of phase, the transition amplitudes $|\langle\phi|\psi\rangle|^2$ are preserved, where $|\phi\rangle$ is another quantum state.

When the discussion of symmetry is involved in the context of quantum mechanics, one popular definition is that, under the symmetry action g, generic transition amplitudes $|\langle\phi|\psi\rangle|^2$ are preserved. Bearing this in mind, how do we establish a representation of a symmetry group G that corresponds to the Hilbert space? In 1931, Wigner proved the following theorem [16]:

Theorem 1 (Wigner's theorem)**.** *Given a symmetry element $g \in G$, where G is the relevant symmetry group, there exists a bijection ρ_g which acts on $\mathcal{H}$. The operator ρ_g is either linear and unitary, or anti-linear and anti-unitary.*

The operators ρ_g are not defined uniquely in the case when $\dim \mathcal{H} \geq 2$, since the following map $\rho_g \mapsto e^{i\alpha}\rho_g$ still preserves transition amplitudes. This phase ambiguity is most relevant in the case of projective representations of symmetry. In the following paragraphs, we construct an example.

Let us consider an Abelian symmetry group $G \equiv \mathsf{Z}_2 \times \mathsf{Z}_2 \equiv \{1, a, b, ab\}$. A projective representation is given as follows:

$$\rho_1 = \tau_0, \quad \rho_a = \tau_z, \quad \rho_b = \tau_y, \quad \rho_{ab} = i\tau_x, \tag{1.2}$$

where τ_0 is the identity matrix, and the rest of the τs are the Pauli matrices. The projective nature of the representation can be seen by examining the multiplication laws, which are denoted as $\rho_{g_1}\rho_{g_2} = \exp(i\alpha(g_1, g_2))\rho_{g_1 g_2}$. We have that $\alpha(a, b) = \alpha(ab, ab) = \pi$. One might hope that, upon the redefinition $\rho_g \mapsto e^{i\alpha}\rho_g$, these non-trivial phases can be eliminated. In fact this is not possible, since we cannot smoothly go from a projective representation to a non-projective one. The classification of projective representation of the group G is given by the second cohomology group $H^2(G, \mathsf{U}(1))$. In this specific case we have $H^2(\mathsf{Z}_2 \times \mathsf{Z}_2, \mathsf{U}(1)) =$

Z_2, therefore there is only 1 *non-trivial* projective representation up to the redefinition of phases.

The fact that $[\rho_a, \rho_b] \neq 0$ implies that there exists no G-invariant state. Let us assume the opposite, i.e. $\exists|\psi\rangle$ such that $\rho_a|\psi\rangle = \rho_b|\psi\rangle = |\psi\rangle$. The contradiction is clear when we realise that $\rho_a\rho_b|\psi\rangle \neq \rho_b\rho_a|\psi\rangle$, violating our earlier assumption. Consequently, this provides an obstruction for us to gauge the G symmetry, as gauging a symmetry in quantum mechanics means projecting to the G-invariant sector. The obstruction is the so-called *'t Hooft anomaly* [17].

As we will see in the coming section, the projective representation also constrains the spectrum of the compatible Hamiltonian. Through the example, we will see how SPT and 't Hooft anomaly can be connected.

1.1.1.2 A 1D SPT protected by $\mathsf{Z}_2 \times \mathsf{Z}_2$

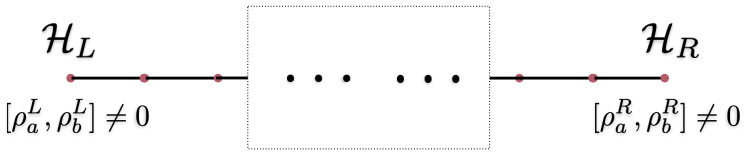

Figure 1.1: This figure portrays the cluster model on the 1D lattice with open boundary condition. The symmetry becomes fractionalised on the left and right edge, and admits projective representations locally.

In this section we present *the cluster model* which is described in some details in Ref. [18]. We consider a spin-$\frac{1}{2}$ model on a 1D lattice with open boundary condition, as demonstrated in Fig. 1.1. The Hamiltonian is given by:

$$H = -\sum_j \tau_x^{j-1}\tau_z^j\tau_x^{j+1}. \tag{1.3}$$

The cluster model has a $\mathsf{Z}_2 \times \mathsf{Z}_2$ symmetry. Suppose the number of sites is an even number N, we find the following representation of the symmetries:

$$\rho_a = \tau_z^1\tau_z^3\tau_z^5\ldots\tau_z^{N-1}, \quad \rho_b = \tau_z^2\tau_z^4\tau_z^6\ldots\tau_z^N. \tag{1.4}$$

Note that $[\rho_a, \rho_b] = 0$, but this will be violated in the ground state. Since the terms in the Hamiltonian commute, the ground state subspace has $\langle\tau_x^{j-1}\tau_z^j\tau_x^{j+1}\rangle = 1$ for all j. Consequently, $\langle\tau_x^1\tau_z^2\tau_z^4\tau_z^6\ldots\tau_z^{N-2}\tau_x^{N-1}\rangle = 1$. Somewhat surprisingly, the global symmetries a and b, when restricted to the ground state subspace, become operators that only act on the edge:

$$\rho_a|_{\text{GS}} = \tau_z^1\tau_x^2\tau_x^N, \quad \rho_b|_{\text{GS}} = \tau_x^1\tau_x^{N-1}\tau_z^N. \tag{1.5}$$

It is then natural for us to factorise the symmetry operators into left and right edge symmetry operator, namely: $\rho_a^L|_{\text{GS}} = \tau_z^1\tau_x^2$, $\rho_a^R|_{\text{GS}} = \tau_x^N$, $\rho_b^L|_{\text{GS}} = \tau_x^1$ and $\rho_b^R|_{\text{GS}} = \tau_x^{N-1}\tau_z^N$. The localised operators on the edge do not change the energy in the ground state subspace, and their existences are termed *symmetry fractionalisations*.

In contrast with the initial representation, the edge representation of symmetry is projective. More specifically,

$$(\rho_a^L\rho_b^L)|_{\text{GS}} = -(\rho_b^L\rho_a^L)|_{\text{GS}}, \quad (\rho_a^R\rho_b^R)|_{\text{GS}} = -(\rho_b^R\rho_a^R)|_{\text{GS}}. \tag{1.6}$$

Therefore, both the left and the right edge are individually two-fold degenerate, resulting the ground state to be four-fold degenerate. Indeed, the cluster model is a non-trivial SPT and its edge exhibits a typical 't Hooft anomaly.

As we notice, the boundary theory of the cluster model is gapless, as it is common in many of the SPT realisations. This does not necessarily need to be true at all times. Indeed, in the coming section we would like to present examples of anomalous gapped boundary theory for SPT.

1.1.2 Surface topological order

When interaction is absent, the surface of 3D TI hosts odd number of 2D gapless Dirac cone. In contrast with the free regime, when interaction is introduced, the surface of 3D TI can host a gapped theory without breaking the symmetries, at the cost of being topologically ordered i.e. there are anyons on the surface [19, 20]. This phenomenon is not exclusive to TI: 3D TSC and even bosonic SPT phases can also host anyons on their surfaces [21, 22, 23]. These surface topological orders (STOs) carry the same anomaly as the original gapless theories.

The STO for the 3D TI is the so-called $\mathcal{T}$-Pfaffian state, where the term was coined due to the fact that it is a time reversal symmetric variation of the Pfaffian/Moore-Read state [24]. The algebraic theory of $\mathcal{T}$-Pfaffian can be viewed as a product of two topological orders:

$$\mathcal{T}\text{-Pf} \equiv \overline{\text{Ising}} \times \mathsf{U}(1)_8/\mathbb{Z}_2. \tag{1.7}$$

The $\overline{\text{Ising}}$ topological order, the complex conjugated version of the traditional Ising topological order, has three anyons,

$$\overline{\text{Ising}} = \{1, \psi, \sigma\}, \tag{1.8}$$

with fusion rules:

$$\sigma \times \psi = \sigma, \sigma \times \sigma = 1 + \psi, \psi \times \psi = 1, \tag{1.9}$$

and topological spins:

$$\theta_1 = 1, \theta_\psi = -1, \theta_\sigma = e^{-i\frac{\pi}{8}}. \tag{1.10}$$

The topological spin of an anyon a encodes the phase that is picked up by the state when two as exchange position/half-braid.

The $\mathsf{U}(1)_8$ topological order has 8 anyons:

$$\mathsf{U}(1)_8 = \{0, 1, 2, 3, \ldots, 7\}, \tag{1.11}$$

with fusion rules:

$$p \times q = (p + q) \bmod 8, \tag{1.12}$$

and topological spins:

$$\theta_k = e^{i\frac{\pi}{8}k^2}. \tag{1.13}$$

The product is taken such that $1, \psi \in \overline{\text{Ising}}$ are combined with even $p \in \mathsf{U}(1)_8$, and $\sigma \in \overline{\text{Ising}}$ is combined with odd $p \in \mathsf{U}(1)_8$. Therefore we arrive at:

$$\mathcal{T}\text{-Pf} = \{1_0, 1_2, 1_4, 1_6, \psi_0, \psi_2, \psi_4, \psi_6, \sigma_1, \sigma_3, \sigma_5, \sigma_7\}. \tag{1.14}$$

The fusion rules and topological spins can be obtained as the product of the $\overline{\text{Ising}}$ topological order and the $\mathsf{U}(1)_8$ topological order. We list the topological spin here. Among the above

	1_0	1_2	1_4	1_6	ψ_0	ψ_2	ψ_4	ψ_6	σ_1	σ_3	σ_5	σ_7
θ	1	i	1	i	-1	$-i$	-1	$-i$	1	-1	-1	1

Table 1.1: Topological Spins for $\mathcal{T}$-Pfaffian topological order.

anyons, ψ_4 is special since it is a local object i.e. it braids trivially with everyone else. Also, it has topological spin -1 and $\mathsf{U}(1)$ charge e. Therefore we identify it to be the physical electron. The existence of such local object is a feature of fermionic topological order, indicating the non-modularity of the theory.

One can observe that algebraic theory of $\mathcal{T}$-Pfaffian is time reversal invariant, since most anyons have real topological spins with the exceptions $1_2, 1_6, \psi_2, \psi_6$. With these four anyons, we have:

$$\mathcal{T} : 1_2 \leftrightarrow \psi_2, 1_6 \leftrightarrow \psi_6. \tag{1.15}$$

By breaking TRS, one can obtain a purely 2D chiral topological order with the same anyon contents as the $\mathcal{T}$-Pfaffian. The edge of such 2D chiral topological order contains a Dirac mode and a counter propagating Majorana mode. It is described by the following Lagrangian density:

$$\mathcal{L} = \frac{2}{4\pi}\partial_x\phi(\partial_t - v_1\partial_x)\phi + i\gamma(\partial_t + v_2\partial_x)\gamma, \tag{1.16}$$

where ϕ denotes the bosonised Dirac mode, and γ is the Majorana mode. One notes that the chiral central charge of the edge is given by $c = \frac{1}{2}$.

The STO for the 3D $\nu = 3$ TSC is the $\mathsf{SO}(3)_3$ topological order. The $\mathsf{SO}(3)_3$ anyon model contains anyons $\{0, 1, 2, 3\}$ with fusion rules:

$$i \times j = \sum_{k=|i-j|}^{\min[i+j,6-(i+j)]} k, \tag{1.17}$$

and topological spins:

$$\{\theta_i\} = \{1, i, -i, -1\}. \tag{1.18}$$

The quantum dimension of the anyons is listed as the following:

$$\{d_i\} = \{1, 1+\sqrt{2}, 1+\sqrt{2}, 1\}. \tag{1.19}$$

From the above data, one can derive the S-matrix, which encodes the braiding information, via the Kitaev ribbon formula [25]. By breaking TRS, one can also obtain a purely 2D chiral topological order with the same anyon contents as the above. The edge of such 2D chiral topological order is described by the $\mathfrak{so}(3)_3$ Wess-Zumino-Witten (WZW) theory. Furthermore, the chiral central charge of the edge is given by $c = \frac{9}{4}$. The above two topological orders we described are very useful for our construction in Chapter 2.

1.1.3 Higher order topological phases

In the picture mentioned above, one notes that the relevant symmetries are on-site, and the bulk-boundary correspondence principle relates a d-dimensional bulk to a $(d-1)$-dimensional boundary. In recent years, researchers have come to realise that the introduction of crystalline symmetries to the system can generalise the standard notion of bulk-boundary correspondence. More specifically, the presence of certain crystalline symmetries can establish a d-dimensional bulk to $d-k$-dimensional boundary correspondence, and such systems are termed k-th order topological topological insulators/superconductors (TIs/TSCs) [26, 27]. Physically, the correspondence is manifested by the existence of hinge/corner gapless modes in the system. Examples of these *higher-order topological phases* include: 1.) 3D phases with hinge modes (second-order phases); 2.) 2D phases with corner modes (second-order phases); 3.) 3D phases with corner modes (third-order phases). In this generalised regime, the standard TIs and TSCs can be classified as first-order topological phases, whereas the k-th order topological phases are referred to as higher order topological insulators/topological superconductors (HOTIs/HOTSCs). Examples of higher order topological phases are constructed in Chapter 2.

1.2 Area law and tensor network states

1.2.1 Entanglement entropy and the area law

In this thesis we study quantum phases of matter, i.e. phases of matter at $T = 0$. At equilibrium, the quantum system rests in its ground state, which encodes the information of the phases. It turns out that we can draw quite general conditions on the entanglement entropy for the systems that appear in nature, namely the *scaling laws*. Before we give a precise statement on this, let us review what entanglement entropy is.

Let us consider first a density matrix ρ, and we define an entropy quantity $S \equiv -\mathrm{Tr}[\rho \log \rho]$. Interpreting the density matrix as a statistical ensemble, and it can be diagonalised with R non-zero eigenvalues $\{\lambda_1, \ldots, \lambda_R\}$, the entropy defined before is evaluated as:

$$S = -\sum_{i=1}^{R} \lambda_i \log \lambda_i, \tag{1.20}$$

bearing close resemblance with the Gibbs entropy. The direct consequence of the above definition is that, for a pure state $\rho \equiv |\psi\rangle\langle\psi|$, the entropy is 0, whilst for mixed states, the entropy is non-zero. Such behaviours lend itself abilities to measure quantum entanglement, whose presences indicate that the entangled subsystem encodes only partial information about the whole. In other words, when we partition the entire system into entangled parts A and B, the reduced density matrix $\rho_A \equiv \mathrm{Tr}_B[\rho]$ is a mixed density matrix, and thus the entropy:

$$S_E \equiv -\mathrm{Tr}[\rho_A \log \rho_A] \neq 0. \tag{1.21}$$

At this point, we can start calling the defined quantity *entanglement entropy*, which is also referred to as the *von Neumann entropy* in the literature.

How does the entanglement entropy of a random pure state look like? This question was considered by Page [28]. Suppose the system is partitioned into A and B, with Hilbert space dimension $m \equiv d^{N_A}$ and $n \equiv d^{N_B}$ respectively, where d is the local Hilbert space dimension, and N_A and N_B are the sizes of the subsystems ($N_A \leq N_B$). Taking the average defined against the unitary invariant Haar measure on the space of unit vector $|\psi\rangle$ in the $m \times n$ Hilbert space of the entire system, Page conjectured that:

$$S_E = \sum_{k=n+1}^{mn} \frac{1}{k} - \frac{m-1}{2n}. \tag{1.22}$$

At large n, the above formula has an asymptotic expansion:

$$S_E = \log m - \frac{m^2-1}{2mn} + \sum_{j=1}^{\infty} B_{2j} \frac{m^{2j}-1}{2jm^{2j}n^{2j}}$$

$$\sim \log m - \frac{m}{2n} = N_A \log d - \frac{d^{N_A}}{2d^{N_B}}, \tag{1.23}$$

where B_{2j} are the Bernoulli numbers and the last line holds when $m >> 1$. Despite Eq. 1.22 being only a conjecture by Page, it was later proved rigorously in [29, 30].

Identifying N_A as the "volume" of subsystem A, the aforementioned scaling behaviour of the entanglement entropy for a random pure state is the so called *volume law*. It is then somewhat surprising when we discover that the ground states of typical quantum many body systems defy the *volume law*, and instead obey a different kind of scaling law. Indeed, Hastings proved rigorously [31] an area law for gapped local 1D quantum systems. We now carefully state the theorem as follows.

Theorem 2 (Area law in 1D)**.** *Consider a Hamiltonian $H = \sum_{j\in\{1,\dots N\}} H_{j,j+1}$, where $H_{j,j+1}$ is supported on site j and $j+1$ only, and $||H_{j,j+1}|| \leq J$. Suppose the Hamiltonian has an unique ground state with energy gap ΔE. Consider subsystem $A = \{1, \dots, N_A\}$, we have:*

$$S_E(A) \leq S_{\max} = c_0 \xi \log(6\xi) \log(d) 2^{6\xi \log(d)}, \tag{1.24}$$

where d is the local Hilbert space dimension, c_0 is of order unity constant, $\xi \equiv \max(2v/\Delta E, \xi_C)$, v is the velocity of sound associated with the Lieb-Robinson bound and ξ_C is of order unity.

We note that $S_{\max}$ is a constant and does not scale with subsystem size N_A, i.e. it is proportional to the area of $|\partial A| = \text{const}$. Since this proof, there has been a series of works that attempt to improve and generalise the theorem. Notably in Ref. [32, 33, 34], using the Chebyshev-based Approximate Ground State Projector (AGSP) technique, Hastings' results on the 1D area laws are exponentially improved. The bound given in the proof by Hastings scales like $\exp(\mathcal{O}(\xi \log(d)))$, whereas the improved version gives $\mathcal{O}(\xi \log^3(d))$. An area law is also proved for 2D frustration free spin systems using the same technique.

Is the existence of an energy gap a necessary condition for the area law? In 1D this is generally true. However, in higher dimension, even critical systems can be shown to respect the area law, e.g. the critical bosons [35]. Today, it is generally believed that the ground states for quantum systems with gapped local Hamiltonians feature the area law in general dimensions, which are arguably the most "typical" settings in nature. Therefore, to probe the ground state properties, we need to deal with states that are much less entangled than a random quantum state. Indeed, the designers for the tensor network states took note of that, as we will see in the coming discussions.

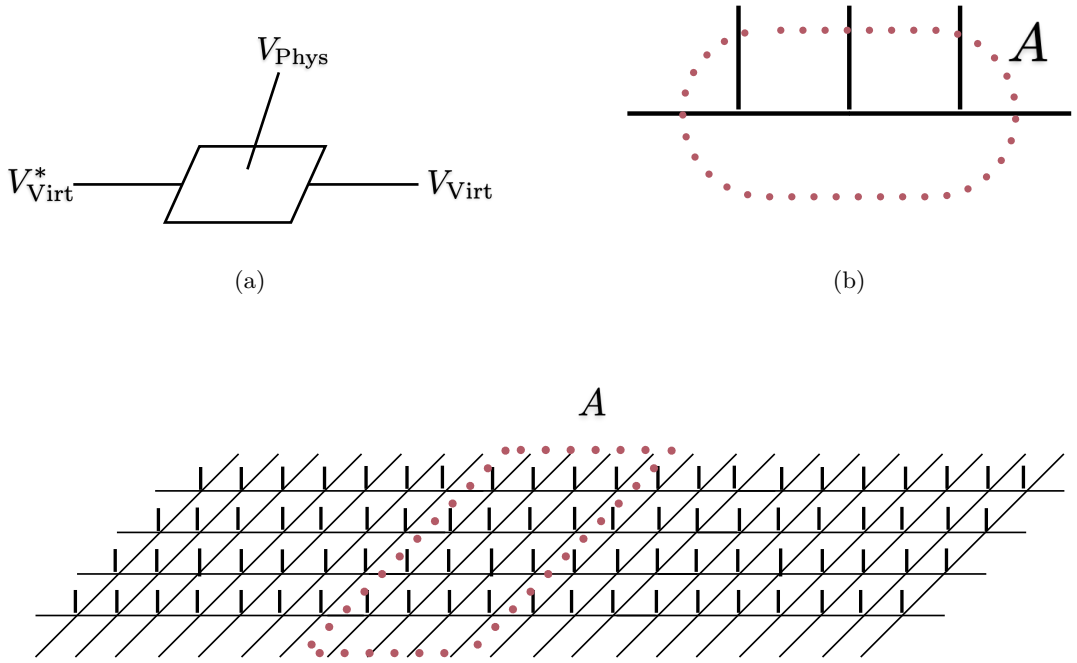

(a) (b)

(c)

Figure 1.2: (a) A local tensor with three open legs, the horizontal legs are to be contracted with the neighbouring tensors, and the vertical leg denotes physical degrees of freedom; (b) A 1D matrix product state, where A denotes a subsystem; (c) A 2D projected entangled pair state, where A denotes a subsystem.

1.2.2 Tensor network states

Tensor network states are built out of local tensors such as the one in Fig. 1.2a. Denoting the tensor as T, we have $T \in V^*_{\text{Virt}} \otimes V_{\text{Phys}} \otimes V_{\text{Virt}}$, where V_{Virt} and V^*_{Virt} are the virtual Hilbert space and its dual that contain virtual degrees of freedom to be contracted, with dimension D, and V_{Phys} is the local physical Hilbert space with dimension d. Suppose the basis for V^*_{Virt} is span$\{\langle i|\}$, for V_{Phys} is span$\{|j\rangle\}$, and for V_{Virt} is span$\{|k\rangle\}$, the local tensor is explicitly:

$$T = \sum_{i,j,k} C_{ijk} \langle i| \otimes |j\rangle \otimes |k\rangle. \tag{1.25}$$

To build tensor network states, we contract the virtual degrees of freedom so that only the physical degrees of freedom are left. In the language of the tensor diagrams, contractions are denoted by the connected legs. The reason why we introduce the virtual degrees of freedom is to sustain quantum entanglement through the networks, and the dimension of

the virtual Hilbert space, called the *bond dimension* D, serves as a control parameter for entanglement. We will make this statement precise in the coming discussion.

1.2.2.1 The matrix product states

The matrix product states (MPS) are the 1D examples of tensor network states, and Fig. 1.2b gives an example of MPS in the tensor diagram language. Suppose we have N physical sites, with periodic boundary condition, the MPS state is formally:

$$|\Psi\rangle_{\text{MPS}} = \sum_{j_1,\ldots,j_N} \text{Tr}[T^{j_1}T^{j_2}\ldots T^{j_N}]|j_1\rangle \otimes |j_2\rangle \otimes \cdots \otimes |j_N\rangle. \tag{1.26}$$

The contractions of the virtual legs take the forms of matrix products, hence the name.

A generic many body state on these N physical sites is:

$$|\Psi\rangle = \sum_{j_1,\ldots,j_N} C_{j_1,\ldots,j_N}|j_1\rangle \otimes |j_2\rangle \otimes \cdots \otimes |j_N\rangle. \tag{1.27}$$

Comparing the number of parameters in the above two states, we observe that:

$$\#(|\Psi\rangle_{\text{MPS}}) = o(NdD^2), \quad \#(|\Psi\rangle) = o(d^N). \tag{1.28}$$

When N is large, it is quite clear that $o(d^N) >> o(NdD^2)$. Why, then, do we believe that the MPS can encode enough information to represent $|\Psi\rangle$? The secret lies in the area law. Making a subsystem cut as we did in Fig. 1.2b, because of the matrix product structure, the Schmidt rank of the state is at most D^2. Thus we obtain an upper bound for the entanglement entropy for the subsystem:

$$S_E \leq 2\log D \sim |\partial A|, \tag{1.29}$$

which is an area law. It is then not surprising that the MPS can be used to simulate the ground states of 1D quantum gapped local Hamiltonians.

Historically, White discovered a powerful algorithm to simulate 1D quantum system, termed the density matrix renormalisation group (DMRG) [36, 37]. It was quite a mystery at that time regarding why DMRG was that successful. Later it was realised that, formulated in the MPS language, what DMRG does is variationally optimising the MPS [38, 39, 40]. Moreover, it was shown in Ref. [41] that all 1D area law states can be efficiently and faithfully represented as MPS. Together with the Hastings' proof on the area laws for the ground states of 1D quantum gapped local Hamiltonian, the mystery was finally solved.

In the coming paragraphs, we derive some important properties for the MPS. For simplicity, we consider the case when the MPS is uniform at the thermodynamical limit with

open boundary condition. The derivations follow closely Ref. [42], which is one of the canonical texts on the uniform MPS methods. We first write down the state $|\Psi(T)\rangle$:

$$|\Psi(T)\rangle = \ldots$$ 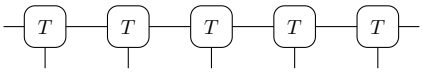 $$\ldots. \tag{1.30}$$

The first thing we would like to comment is that the MPS has gauge redundancies, i.e. the following transformation leaves $|\Psi(T)\rangle$ invariant:

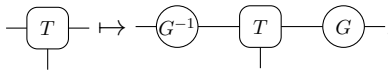 $$. \tag{1.31}$$

To fix a gauge, *canonical forms* can be found for the MPS tensor T. To proceed we need to first introduce the transfer matrix:

$$E =$$ 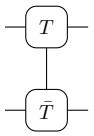 $$. \tag{1.32}$$

Using this $D^2 \times D^2$ operator, we can normalise the MPS. Note that the leading eigenvalue of E is a positive number λ_0. By rescaling $T \mapsto T/\sqrt{\lambda_0}$, we ensure that $\langle\Psi(\bar{T})|\Psi(T)\rangle = 1$. Next, by solving eigenvalue equations for the leading eigenvector, we can find the left and right fixed points l and r:

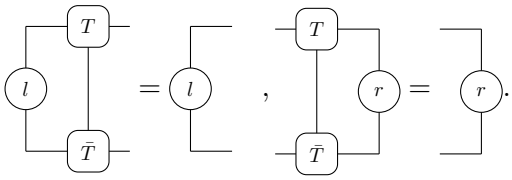 $$. \tag{1.33}$$

Decomposing $l = L^\dagger L$, we perform the following gauge transformation:

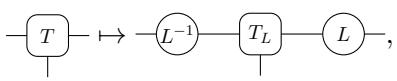 $$, \tag{1.34}$$

such that:

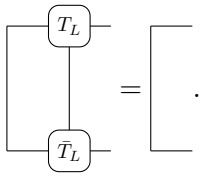 $$. \tag{1.35}$$

The post-transformation tensor T_L is called the *left-orthonormal form*. Similarly we can define the *right-orthonormal form* T_R. If we further define $C \equiv LR$, the following condition between T_L and T_R exists:

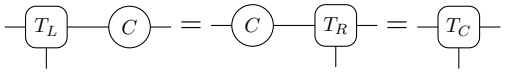 $$, \tag{1.36}$$

where

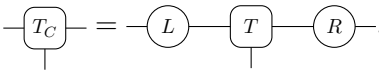

(1.37)

These forms serve as the key ingredients for us to set the gauge. Indeed, choosing a generic site (it is called the central site because our system is infinite), and we transform all the left tensors into the left-orthonormal forms, and the right tensors into the right-orthonormal form, we arrive at the so-called *mixed gauge*. In the diagrammatical language, we perform:

$$|\Psi(T)\rangle = \ldots$$

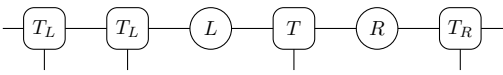

$$= \ldots$$

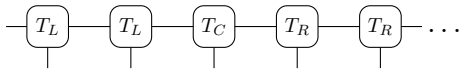

$$= \ldots$$

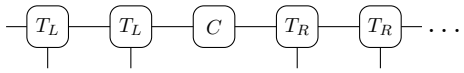

(1.38)

In the mixed gauge, it is clear to see that the singular value decomposition of $C = USV^\dagger$ gives us the Schmidt decomposition of the state at the bond, and the entanglement entropy is directly evaluated as:

$$S_E = -\sum_i C_i^2 \log(C_i^2), \tag{1.39}$$

where C_is are the singular values of C. Using the canonical forms, we can exactly calculate the scalar product for two MPS, and the complexity is $o(dD^3)$. In fact, calculating expectation values of local operators as well as correlation functions has similar complexity.

Another property we mention here is that the correlation functions on the MPS always decay exponentially. Consider a correlation function:

$$\langle\Psi(\bar{T})|O_0 O_{n+1}|\Psi(T)\rangle =$$

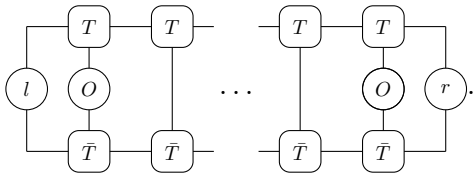

(1.40)

To evaluate the expression, we perform an eigen-decomposition for the transfer matrix products in between the two sites:

$$E^n =$$

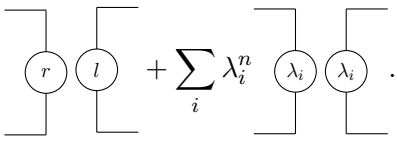

$$+ \sum_i \lambda_i^n \quad .$$

(1.41)

The first term on the right hand side will clearly give us the disconnected part of the correlation function. The connected correlation function is then:

$$\langle\Psi(\bar{T})|O_0 O_{n+1}|\Psi(T)\rangle - \langle\Psi(\bar{T})|O_0|\Psi(T)\rangle\langle\Psi(\bar{T})|O_{n+1}|\Psi(T)\rangle$$

$$= \sum_i (\lambda_i)^n$$ 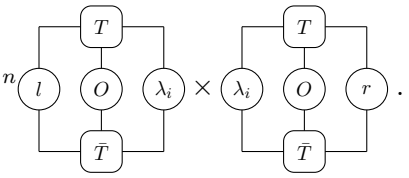 (1.42)

From the expression, we can observe that the connected correlation function has exponential decay, and the largest eigenvalue in the expression $\lambda_{\max}$ determines the correlation length $\xi = -1/\log(|\lambda_{\max}|)$. Note that $\lambda_{\max}$ is the second largest eigenvalue of the transfer matrix E, since the true largest eigenvalue is 1 after normalization.

The above derivations were done in the case of infinite uniform MPS in the open boundary condition. In the case of finite MPS without translation invariance in the open boundary condition, canonical forms can still be found iteratively. The complexity for calculating the scalar product for two MPS of N sites becomes $o(NdD^3)$. In the case of finite MPS without translation invariance in the periodic boundary condition, canonical forms can no longer be found due to the existence of loops, but the scalar product for two MPS of N sites can still be calculated, with the complexity $o(NdD^5)$.

To summarise, the MPS admit: 1.) the area law of entanglement entropy; 2.) finite correlation length; 3.) efficient exact contractions; 4.) canonical forms in the case of open boundary conditions. Much of the success of MPS based simulations relies on the last two properties. The question is, can we still afford such luxury with its higher dimensional counter parts?

1.2.2.2 Projected entangled pair states

The projected entangled pair states (PEPS) are the natural higher dimensional generalisations of MPS, and Fig. 1.2c gives an example of PEPS in the tensor diagram language. In this chapter we consider only the 2D case. Comparing with the MPS, the local tensor that is used to build the tensor network is five legged instead of three.

Making a subsystem cut as we did in Fig. 1.2c, which is a square region with size $L_s \times L_s$, the Schmidt rank of the state is at most D^{4L_s}. Thus we obtain an upper bound for the entanglement entropy for the subsystem:

$$S_E \leq 4L_s \log D \sim |\partial A|, \tag{1.43}$$

which is an area law similar to the case of MPS. In fact, the similarity does not extend much further.

A novice practitioner of PEPS will undoubtedly be surprised about the fact that PEPS can sustain correlation functions with polynomial decay, in sharp contrast with MPS. Indeed, in Ref. [43], a beautiful example is constructed. The key idea here is a correspondence

between PEPS and classical statistical physical systems. We consider the 2D classical Ising model as a pedagogical example, which has the classical Hamiltonian:

$$H = \sum_{\langle i,j \rangle} h(\sigma_i, \sigma_j) = -\sum_{\langle i,j \rangle} \sigma_i \sigma_j, \quad \sigma_i = \pm 1, \tag{1.44}$$

where $\langle i, j \rangle$ denotes the nearest neighbour bonds. We first prepare a product state $\bigotimes_i |+\rangle_i$, where $|+\rangle = |\uparrow\rangle + |\downarrow\rangle$, and the PEPS state is constructed by:

$$|\Psi_{H,\beta}\rangle = \exp[-\frac{\beta}{2} \sum h(\sigma_i, \sigma_j)] \bigotimes_i |+\rangle_i. \tag{1.45}$$

Each of the $\exp[-\frac{\beta}{2} h(\sigma_i, \sigma_j)]$s is a kind of local gate that acts on the product state $\bigotimes_i |+\rangle_i$, creating entanglement with bond dimension $D = 2$. The contraction of the PEPS leads to the classical partition function for the Ising model, namely:

$$\langle \Psi_{H,\beta} | \Psi_{H,\beta} \rangle = \mathcal{Z}(\beta) \equiv \sum_{\{\sigma\}} e^{-\beta \sum_{\langle i,j \rangle} h(\sigma_i, \sigma_j)}. \tag{1.46}$$

Moreover, the correlation functions evaluated on the PEPS can be identified as the classical correlation functions for the Ising model:

$$\frac{\langle \Psi_{H,\beta} | \sigma_i \sigma_j | \Psi_{H,\beta} \rangle}{\langle \Psi_{H,\beta} | \Psi_{H,\beta} \rangle} = \frac{1}{\mathcal{Z}(\beta)} \sum_{\{\sigma\}} \sigma_i \sigma_j e^{-\beta \sum_{\langle i,j \rangle} h(\sigma_i, \sigma_j)}. \tag{1.47}$$

The 2D classical Ising model on square lattices becomes critical at $\beta_c = \frac{1}{2} \log(1 + \sqrt{2})$, and the correlation function becomes:

$$\frac{\langle \Psi_{H,\beta_c} | \sigma_i \sigma_j | \Psi_{H,\beta_c} \rangle}{\langle \Psi_{H,\beta_c} | \Psi_{H,\beta_c} \rangle} \sim \frac{a}{|\vec{r}_i - \vec{r}_j|^{1/4}}. \tag{1.48}$$

Remarkably, we have shown that at a modest bond dimension $D = 2$, PEPS is capable of representing a state that has polynomially decaying correlation function. It should be noted though, that the critical state here is a classical critical state. Aside from this, we should also bear in mind that in 2D, criticality does not necessarily lead to the violations of the area law as we mentioned earlier. Again we see evidence that entanglement entropy should serve as a measure of simulation capability.

The demonstrated simulation power of PEPS has likely cheered up the mood of the aforementioned practitioner. However, much to our inconvenience, there is no canonical form for PEPS due to loops, whose presences prevent us from making sensible Schmidt decompositions. Despite efforts seeking a generalised version of canonical form for PEPS (see Ref. [44] for example), no widely accepted solution has been found. In fact, exactly calculating the scaler product of two generic PEPS of N sites has the complexity $o(\exp(N))$.

More precisely, it has been shown that the complexity class of contracting generic PEPS tensor is $\#P$-hard in the number of tensors [45, 46].

To overcome this difficulty, algorithms have been developed to approximately contract PEPS, such as the boundary MPS methods [47], and corner transfer matrix methods [48].

Alternatively, we can also study restricted tensor network states that *can* be contracted efficiently, examples include isometric tensor network [49], as well as Gaussian fermionic tensor networks that we utilise in Chapter 3.

1.2.2.3 Fermionic tensor network states

The most commonly used TNS represent spin wave functions, and hence are bosonic, i.e. the constituent tensors are simply arrays of complex numbers. To every index of the bosonic tensors we can associate a vector space with a particular choice of basis, and the arrays of complex numbers represent the components of the tensors in these basis.

Fermionic TNS are defined as a natural extension of conventional bosonic TNS. In particular, to every index of a fermionic tensor one associates a *super* vector space V [50]. A super vector space is a Z_2 graded vector space, which means that it comes with an operator Z^f which squares to the identity (the fermion parity operator), and partly induces a canonical choice of basis such that basis vectors are eigenstates of Z^f. States which are eigenstates of Z^f are called homogeneous states, and the parity of a homogeneous state $|i\rangle$ is denoted as

$$\mathsf{Z}^f|i\rangle = (-1)^{|i|}|i\rangle\,,\ |i| \in \{0,1\}\,. \tag{1.49}$$

The subspace of V spanned by the vectors which are even under Z^f is denoted as V^0, and is called the even subspace. The odd subspace is denoted as V^1. The properties of a super vector space V naturally carry over to its dual space V^*, which is also graded. The natural action of dual vectors on vectors gives rise to the evaluation map $\mathcal{C}$, and we can choose a canonical dual basis $\langle i|$ such that

$$\mathcal{C} : V^* \otimes V \to \mathbb{C} : \langle i| \otimes |j\rangle \to \delta_{ij}\,. \tag{1.50}$$

It then also follows that $\langle i|\mathsf{Z}^f = (-1)^{|i|}\langle i|$ so that $|i\rangle$ and $\langle i|$ have the same parity. The Z_2 grading induced by Z^f becomes important when vectors are 'reordered'. More precisely, when working with tensor products of super vector spaces, one always uses the following canonical isomorphism,

$$\mathcal{F} : V \otimes W \to W \otimes V : |i\rangle \otimes |j\rangle \to (1)^{|i||j|}|j\rangle \otimes |i\rangle\,, \tag{1.51}$$

which encodes the fermionic anticommutation relations. The same reordering rule is used when one or two of the vectors involved are dual vectors. *Tensor contraction* is then

defined as the following sequence of steps: (1) take the tensor product of the tensors to be contracted, (2) use $\mathcal{F}$ to bring the vectors and dual vectors corresponding to the legs which are to be contracted next to each other, and (3) use the evaluation $\mathcal{C}$ as defined in Eq. 1.50 to contract the legs. This procedure is unambiguous up to an innocuous overall minus sign as long as the tensors respect the superselection rule which comes with super vector spaces: all tensors need to have a well-defined fermion parity. For more details we refer to Ref. [50].

There exists an isomorphism between polynomials of M Grassmann numbers and a super vector space of dimension 2^M. To illustrate how this isomorphism works, consider the case of a single Grassmann number θ. To every monomial we associate a basis state of the super vector space as follows,

$$\theta^n \cong |n\rangle\,, \quad n \in \{0,1\}\,. \tag{1.52}$$

The dual space is isomorphic to polynomials of another Grassmann number $\bar{\theta}$,

$$\bar{\theta}^n \cong \langle n|\,, \quad n \in \{0,1\}\,. \tag{1.53}$$

The evaluation map is then given by the following Berezin integral,

$$\mathcal{C} : \langle n| \otimes |m\rangle \cong \bar{\theta}^n \theta^m \to \int \mathrm{d}\theta \int \mathrm{d}\bar{\theta}\, e^{\bar{\theta}\theta} \bar{\theta}^n \theta^m = \langle n|m\rangle = \delta_{nm}\,. \tag{1.54}$$

This explains the presence of the factors $e^{\bar{\theta}_{\mathbf{x}}\theta_{\mathbf{x}+\mathbf{e}_{x/y}}}$ in the definition of the Gaussian fermionic tensor network states later in Eq. 3.2: they ensure that the Berezin integral implements the tensor contraction according to the conventional evaluation map of the super vector spaces associated with the legs of the fermionic tensors. The canonical isomorphism $\mathcal{F}$ defined in Eq. 1.51 is implemented automatically via the anticommutation relations of Grassmann numbers. The mapping of monomials of Grassmann numbers to basis states of a super vector space generalizes straightforwardly to the case with more than one Grassmann number.

1.2.3 Area law breaking states and finite entanglement scaling

The discussions earlier made it clear to us that the representation capability of tensor network states relies on the area law. Despite the fact that the area law are "typical" ground states of local quantum systems, there are crucial scenarios in which the ground states of local quantum systems become more entangled than the area law. The study of how well suited TNS can be used to represent these states is called *finite entanglement scaling*. In the coming discussions, we discuss the area law breaking states in 1D and higher dimension and give a summary of our understanding of finite entanglement scaling.

1.2.3.1 Area law breaking in 1D: conformal field theories

In this section we prove that the entanglement entropy for conformal field theory in $1+1$D (2D CFTs), usually describing 1D quantum systems at criticality, violates the area law by a logarithmic correction. The proof was initially given in Ref. [51], but the arguments presented here follow closely with Ref. [52].

Consider a quantum many body system in one dimension. We would like to compute the density matrix at finite inverse temperature β:

$$\rho(\{\phi''\}|\{\phi'\}) \equiv Z(\beta)^{-1}\langle\{\phi''\}|e^{-\beta H}|\{\phi'\}\rangle, \tag{1.55}$$

where $Z(\beta)^{-1}$ is the partition function. The density matrix can be written as a path integral in the canonical sense:

$$\rho = Z^{-1}\int D[\phi]\prod_x \delta(\phi(x,0)-\phi')\prod_x \delta(\phi(x,\beta)-\phi'')e^{-S_E}, \tag{1.56}$$

where $S_E(x,\tau)$ is the corresponding Euclidean action.

It is simple to verify $\mathrm{Tr}\rho = 1$, which is done by setting $\phi' = \phi''$. In the relevant scenario, we consider a subsystem $A \equiv (u,v)$ at $\tau = 0$, and we want to compute $\rho_A \equiv \mathrm{Tr}_{\bar{A}}\rho$. Now, recalling computing $Z(\beta)$, which requires us to sew $\tau = 0$ and $\tau = \beta$ together. The path integral is then done on a spacetime manifold which is sewed in the τ direction. Computing $\rho_A \equiv \mathrm{Tr}_{\bar{A}}\rho$ requires us to do the same path integral, albeit leaving an open cut for interval A along $\tau = 0$.

The replica trick involves dealing with the object, $\mathrm{Tr}\rho_A^n$, which can be again written as a path integral, defined on the spacetime manifold $\mathcal{R}_n$, which is constructed by: 1.) take n copies of the original spacetime manifold responsible for computing ρ_A (sewed object with open cut A), labeled by $1 \le k \le n$; 2.) sew the cuts such that $\phi'_k = \phi''_{k+1}$ and $\phi'_n = \phi''_1$ for $x \in A$. The resulting spacetime manifold is then an n-sheeted object $\mathcal{R}_n$. And we have $\mathrm{Tr}\rho_A^n = Z_n(A)/Z^n$. Let us then note that:

$$S_A = -\lim_{n\to 1}\partial_n \mathrm{Tr}\rho_A^n = -\lim_{n\to 1}\partial_n \sum_i \lambda_i^n = \sum_i \lambda_i \log\lambda_i, \tag{1.57}$$

where λ_is are the eigenvalues of ρ. Thus, the task of computing the entanglement entropy S_A is converted to the computation of $\mathrm{Tr}\rho_A^n$. In the generic cases, the converted task is not much simpler. However, since our n-sheeted Riemann surface $\mathcal{R}_n$ is two dimensional, the uniformisation theorem states that $\mathcal{R}_n$ can be conformally mapped to the Riemann sphere/complex plane. Thus allowing the full power of 2D CFTs.

For clarity, we first consider the case when then subsystem is a single interval, the entire system is infinite at zero temperature. In other words, we denote $A \equiv (u,v)$ as a single

interval with length l, and the single sheet of the Riemann surface is then infinite in both the x and the τ directions. The Riemann surface $\mathcal{R}_n$ is flat everywhere except at the points where the sheets are connected, therefore the partition function can be equivalently expressed as an expectation value of certain fields evaluated in a model on $\mathbb{C}$. These fields are usually called *branch point twist fields*, denoted as $\mathcal{T}_n(u,0)$ and $\tilde{\mathcal{T}}_n(v,0)$. More specifically, let us first denote the partition function for the original theory on $\mathcal{R}_n$ as:

$$\mathcal{Z}_{\mathcal{R}_n} = \int D[\phi] \exp[-\int_{\mathcal{R}_n} dx d\tau \mathcal{L}[\phi](x,\tau)]. \tag{1.58}$$

We further define a model which is made of n copies of the original model on $\mathbb{C}$:

$$\int_{\mathcal{C}_{u,v}} D[\phi_1, \dots \phi_n] \exp[-\int_{\mathcal{R}_n} dx d\tau \mathcal{L}^{(n)}[\phi_1, \dots \phi_n](x,\tau)] = \langle \mathcal{T}_n(u,0), \tilde{\mathcal{T}}_n(v,0) \rangle_{\mathcal{L}^{(n)},\mathbb{C}}, \tag{1.59}$$

where $\mathcal{C}_{u,v}$ denotes restricted path integral with $\phi_i(x,0^+) = \phi_{i+1}(x,0^-)$ for $x \in [u,v]$, and $\mathcal{L}^{(n)}[\phi_1, \dots \phi_n] = \sum_i \mathcal{L}[\phi_i]$. Introducing the branch point twist fields takes care of the restriction on the path integral. Generally we have:

$$\langle O(x,\tau;i) \rangle_{\mathcal{L},\mathcal{R}_n} = \frac{\langle O_i(x,\tau) \mathcal{T}_n(u,0) \tilde{\mathcal{T}}_n(v,0) \rangle_{\mathcal{L}^{(n)},\mathbb{C}}}{\langle \mathcal{T}_n(u,0) \tilde{\mathcal{T}}_n(v,0) \rangle_{\mathcal{L}^{(n)},\mathbb{C}}}, \tag{1.60}$$

where $O(x,\tau;i)$ denotes the operator O from the original theory on the ith sheet, and $O_i(x,\tau)$ denotes the operator O from the ith replica theory on the complex plane $\mathbb{C}$.

The following map $w \mapsto z \equiv ((w-u)/(w-v))^{1/n}$ maps the entire $\mathcal{R}_n$ to the Riemann sphere $\mathcal{C} \cup \{\infty\}$. Specifically $u \mapsto 0$ and $v \mapsto \infty$. We will also refer to the Riemann sphere as $\mathcal{C}$ in the following text.

In 2D CFT, the holomorphic component of the stress tensor $T(w)$ behaves as follows in a conformal transformation:

$$T(w) = \left(\frac{dz}{dw}\right)^2 T(z) + \frac{c}{12}\{z,w\}, \tag{1.61}$$

where z is the coordinate of $\mathcal{C}$, c is the central charge of the CFT and $\{.,.\}$ denotes the Schwartzian derivative $(z'''z' - (3/2)z''^2)/z'^2$. If we take the expectation values of both sides, we note that $\langle T(z) \rangle_{\mathcal{C}} = 0$ because of translational and rotational invariance. Thus we have:

$$\langle T(w) \rangle_{\mathcal{L},\mathcal{R}_n} = \frac{c}{12}\{z,w\} = \frac{c}{24}(1 - \frac{1}{n^2}) \frac{(v-u)^2}{(w-u)^2(w-v)^2}. \tag{1.62}$$

Using Eq. 1.60, we obtain:

$$\frac{\langle T_i(x,\tau) \mathcal{T}_n(u,0) \tilde{\mathcal{T}}_n(v,0) \rangle_{\mathcal{L}^{(n)},\mathbb{C}}}{\langle \mathcal{T}_n(u,0) \tilde{\mathcal{T}}_n(v,0) \rangle_{\mathcal{L}^{(n)},\mathbb{C}}} = \frac{c}{24}(1 - \frac{1}{n^2}) \frac{(v-u)^2}{(w-u)^2(w-v)^2}, \tag{1.63}$$

where $T_i(x,\tau)$ is the stress tensor for the ith replica theory. Therefore the total stress tensor expectation value is obtained by timing the above by n, namely:

$$\frac{\langle T^{(n)}(x,\tau)\mathcal{T}_n(u,0)\tilde{\mathcal{T}}_n(v,0)\rangle_{\mathcal{L}^{(n)},\mathbb{C}}}{\langle \mathcal{T}_n(u,0)\tilde{\mathcal{T}}_n(v,0)\rangle_{\mathcal{L}^{(n)},\mathbb{C}}} = \frac{c}{24}(n-\frac{1}{n})\frac{(v-u)^2}{(w-u)^2(w-v)^2}. \tag{1.64}$$

From here we can read off the scaling dimensions of $\mathcal{T}_n$ and $\tilde{\mathcal{T}}_n$, $\Delta_n = \frac{c}{12}(n-\frac{1}{n})$, which leads to:

$$\mathrm{Tr}[\rho_A^n] \sim \mathcal{Z}_n(A) \sim \langle \mathcal{T}_n(u,0)\tilde{\mathcal{T}}_n(v,0)\rangle_{\mathcal{L}^{(n)},\mathbb{C}} = |u-v|^{-2\Delta_n}. \tag{1.65}$$

The entanglement entropy is then:

$$S_E = \frac{c}{3}\log(\frac{l}{a}) + \text{const}, \tag{1.66}$$

which defies the area law by a logarithmic correction.

The violation of the area law means that we can never use a MPS to exactly represent the 1D critical state governed by CFT. However, by increasing the bond dimension of the MPS we use, we can indeed systematically improve the simulation precision. The finite bond dimension D of the MPS induces a finite correlation length ξ, and in the vicinity of criticality, it was observed empirically that a power law, $\xi \sim D^\kappa$, exists [53]. It was later proved in Ref. [54] that:

$$\kappa = \frac{6}{c(\sqrt{\frac{12}{c}}+1)}. \tag{1.67}$$

1.2.3.2 Area law breaking in higher dimension: states with Fermi surfaces

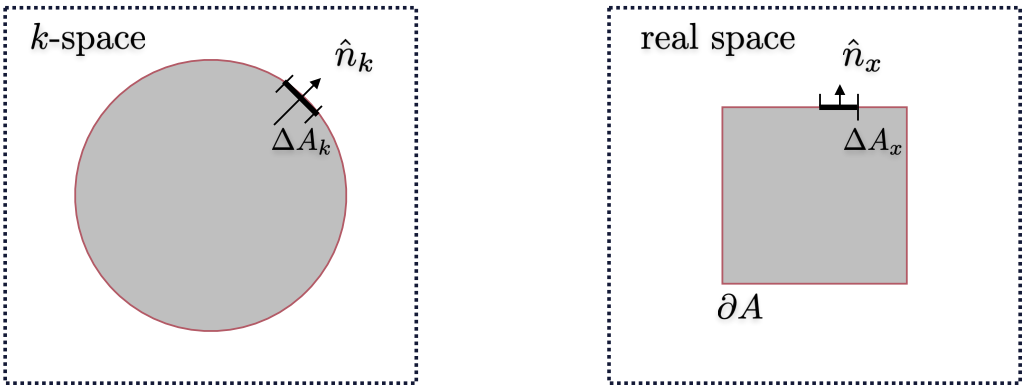

Figure 1.3: We present a diagram that demonstrates the double integration in Eq. 1.68 in 2D.

In higher dimension, the most well known example of quantum systems with ground states that break the area law is the class of states with Fermi surface. In fact, a geometrical formula that captures the leading contributions to the entanglement entropy was suggested in Ref. [55] for the free Fermi surface:

$$S_E = \frac{L^{d-1}}{(2\pi)^{d-1}} \frac{\log L}{12} \oint \oint |\hat{n}_x \cdot \hat{n}_k| dA_x dA_k, \tag{1.68}$$

where the double integral is performed along the Fermi surface as well as the boundary of the subsystem A, L is the size of the subsystem L, $\hat{n}_k$ and $\hat{n}_x$ are the normal vectors on the Fermi surface and real space boundary ∂A respectively, as demonstrated in Fig. 1.3. The conjectured formula, often referred to as the *Widom formula*, has been numerically tested such as in Ref. [56]. The relevant mathematical conjecture invoked in the paper was later proved in Ref. [57]. However, we found the intuitive arguments given in Ref. [58] very illuminating in understanding the origin of Eq. 1.68.

The fundamental reason behind the success of Eq. 1.68, is that the low energy excitations of the Fermi liquids can be viewed as a collection of large number of decoupled chiral modes, with each mode being relativistic, and thus captured by the conformal field theory (CFT) approach. This approach is often termed the *patch construction of the Fermi liquids*. The patch construction of Fermi surfaces can justified using the non-linear bosonization formalism [59]. Using the co-adjoint orbit methods, the leading terms in a free Fermi surface action can be written as:

$$I = -\frac{p_F^{d-1}}{2} \int \frac{dt d^d x d^{d-1} p}{(2\pi)^d} v_F (\hat{n}_\theta \cdot \nabla \phi)^2, \tag{1.69}$$

where θ parameterised the Fermi surface and ϕ is the bosonised field, and v_F is the Fermi velocity. In 1D the above results reduce to the well known action for Luttinger liquid, and the integration over Fermi surface becomes a sum over fields ϕ_L and ϕ_R. Indeed we see that the action can be viewed as a collection of massless chiral bosons.

The entanglement entropy of the Fermi surface can be viewed as the summing up the contributions from these chiral modes. Take the 2D case demonstrated in Fig. 1.3 as an example, given ΔA_x, the chiral mode density is given by $\Delta A_x / 2\pi$. We then include the $|\hat{n}_x \cdot \hat{n}_k|$ factor to count of number of modes perpendicular to ΔA_x. Thus the number of modes that contribute to entanglement for infinitesimal ΔA_x and ΔA_k is $\Delta A_x \Delta A_k |\hat{n}_x \cdot \hat{n}_k| / 2\pi$. Each chiral mode contributes $\Delta S_E = \log L / 6$ using Eq. 1.66 where $c = 1/2$. Summing up the contributions along the Fermi surface as well as ∂A, including a factor $1/2$ to avoid double counting, we arrive at:

$$S_E = \frac{\log L}{24\pi} \oint \oint |\hat{n}_x \cdot \hat{n}_k| dA_x dA_k, \tag{1.70}$$

which is indeed the Widom formula in 2D.

Does the Widom formula still hold for non-Fermi liquids? Attempts to resolve this have been carried out [60, 61], without reaching a consensus. It is possible that the non-linear bosonisation methods can help with this, since it allow us to write down non Fermi liquid models that are quadratic in terms of the bosonised field [59]. This has recently also been noted in Ref. [62].

We have seen in the finite entanglement scaling of MPS that, despite that the CFT states possess logarithmic violations to the area law, the simulation precision using MPS can be systematically improved. Will PEPS be capable in doing the same? In Chapter 3 we give an attempt to answer this question.

1.3 Parton construction of quantum spin liquids and projective symmetry group

1.3.1 Resonating valence bond states: a ballad by Anderson

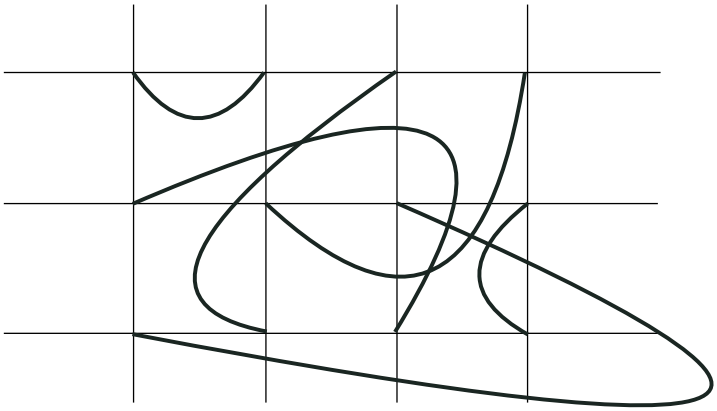

Figure 1.4: This figure portrays a spin singlet configuration that covers the 2D square lattice. The RVB states are made of superpositions of configurations like this.

The quantum spin liquid states (QSLs) are usually defined by what they are not. This is because of its conglomeration of research themes, such as fractionalisation, emergent gauge fields, projective symmetry and topological order. The list can go on, but it is quite difficult to pick out one theme from the list and assign it as the defining feature of the QSLs. In his seminal work [63] on the resonating valence bond state (RVB), written in 1973, Anderson in fact gives an enlightening statement on why RVB states should be called quantum spin liquids, " ... *We visualize the relation between the two as being that of a quantum liquid vs. a quantum solid. The Néel state is like a solid: it has condensed into a spin lattice, whereas*

the real ground state is a fluid of mobile valence bonds, i.e. pairs of spins correlated together into singlets. " Indeed, in contrast with the Néel state which has long range order for the spin correlation function, the RVB states that Anderson constructs are meant to have short range or power law decaying correlation.

How do the RVB states look like? Let us consider a configuration as illustrated in Fig. 1.4, where each thick curve connecting two lattice sites (i, j) denotes a spin singlet $(|\uparrow_i\downarrow_j\rangle - |\downarrow_i\uparrow_j\rangle)/\sqrt{2}$, and the RVB state is:

$$|\Psi_{\rm RVB}\rangle = \sum_P a(P)|(i_1, j_1)\dots(i_n, j_n)\rangle, \tag{1.71}$$

where P denotes a singlet configuration, so the RVB state is a generic superposition of these configurations. The superposition amplitudes $a(P)$ usually serve as variational parameters. To make progress, one of the choices to restrict $a(P)$ is by factorisation:

$$a(P) = \prod_k \varphi(|i_k - j_k|), \tag{1.72}$$

where φs are functions that select what types of valence bonds are favoured. In Ref. [64], a variational study using the above RVB ansatz was performed for quantum Heisenberg model on the 2D square lattice. It was shown that, if we set:

$$\varphi(x) \sim \frac{1}{x^k}, \tag{1.73}$$

then the Néel order is destroyed for $k \geq 5$.

However, we would like to remark here that, the valence bonds configuration states are generically not orthonormal or linearly independent, and thus form an overly complete basis. Also, Anderson initially proposed that the RVB state, instead of the Néel ordering state, is the true ground state for the spin-1/2 quantum Heisenberg model on the 2D triangular lattice. This claim, unfortunately, seems to be refuted by the state of the art numerics. It is surprising that the RVB idea was revitalised by Anderson in the late 1980s in a very different context, when physicists were confronted with the mysterious cuprate high T_c superconductivity. Anderson notes [65] that, upon Gutzwiller projection which enforces single occupancy constraint, the projected BCS wavefunction becomes a natural RVB state. More explicitly:

$$P_G|\Psi_{\rm BCS}\rangle = P_G \prod_{\vec{k}} (u_{\vec{k}} + v_{\vec{k}} c^\dagger_{k,\uparrow} c^\dagger_{-k,\downarrow})|0\rangle = P_G (\sum_{(i,j)} \varphi(i-j) c^\dagger_{i,\uparrow} c^\dagger_{j,\downarrow})^{N/2}|0\rangle, \tag{1.74}$$

where $P_G \equiv \prod_i (1 - n_{i,\uparrow} n_{i,\downarrow})$ being the Gutzwiller projector, and $\varphi(i-j)$ is the Fourier transform of $v_{\vec{k}}/u_{\vec{k}}$.

Anderson had hoped that, upon doping, the RVB state will become a superconductor and the singlet pairs will start carrying supercurrents. However, the program was not fully successful. Despite this, Anderson's proposal has opened door to the so-called *parton construction of quantum spin liquids*. For more than 10 years after Ref. [65], a sizeable number of QSLs were identified, with fascinating properties such as fractionalised particles and topological order. Eventually, these efforts were synthesised into an unifying framework by Xiao-Gang Wen [66] which allows systematic constructions of mean field QSLs given the symmetry. What was also manifested in this framework is that symmetry becomes *projective*, and its reincarnation – the projective symmetry group (PSG) – serves as an order parameter for the so-called "*quantum order*" à la Wen. In the coming section, we give a review of this framework following the discussions in Ref. [66].

1.3.2 Parton construction: formalism

The classification of projective symmetry groups corresponds to the classification of disordered mean-field phases of spin models with Heisenberg exchange interactions. To introduce this construction, we start with the Heisenberg model on a given spatial lattice,

$$H = \sum_{\{i,j\}} J_{ij} \vec{S}_i \cdot \vec{S}_j. \tag{1.75}$$

First, we decompose the spins into Abrikosov fermions as follows :

$$\vec{S}_i = \sum_{\alpha,\beta} \frac{1}{2} f^\dagger_{i\alpha} \vec{\sigma}_{\alpha\beta} f_{i\beta}. \tag{1.76}$$

This enlarges the dimension of the Hilbert space on each lattice site from two to four, and consequently, the Hilbert space must be projected back to the original spin Hilbert space by imposing the constraint of exactly one fermion per lattice site, $\sum_\alpha f^\dagger_{i\alpha} f_{i\alpha} = \mathrm{Id}$. One recovers the usual spin commutation relations $[S^m, S^n] = i\epsilon_{lmn} S^l$ in the projected Hilbert space. The one fermion per site constraint $\sum_\alpha f^\dagger_{i\alpha} f_{i\alpha} = \mathrm{Id}$ also implies $\sum_{\alpha,\beta} f_{i\alpha} f_{i\beta} \epsilon_{\alpha\beta} = 0$. The above equation maps the spin Hilbert space to the subspace of the Abrikosov fermion Hilbert space in which the fermion occupation number on each site is 1. This means that, on the operator level, we strictly have $\sum_\alpha f^\dagger_{i\alpha} f_{i\alpha} = \mathrm{Id}$. Indeed, by using the identity, we can verify that $[S^m, S^n] = i\epsilon_{lmn} S^l$. In fact, a second constraint, as a consequence of the first one, is also introduced: $\sum_{\alpha,\beta} f_{i\alpha} f_{i\beta} \epsilon_{\alpha\beta} = 0$. One can verify this constraint by considering $\sum_{\alpha,\beta} f_{i\alpha} f_{i\beta} \epsilon_{\alpha\beta} \sum_\gamma f^\dagger_{i\gamma} f_{i\gamma} |\psi\rangle$, where $\sum_\gamma f^\dagger_{i\gamma} f_{i\gamma} |\psi\rangle = |\psi\rangle$.

In terms of the Abrikosov fermions, the Heisenberg Hamiltonian reads (up to some constants)

$$H = \sum_{\{i,j\}} \sum_{\alpha\beta\mu\nu} J_{ij} \frac{1}{4} (f^\dagger_{i\alpha} \vec{\sigma}_{\alpha\beta} f_{i\beta}) \cdot (f^\dagger_{j\mu} \vec{\sigma}_{\mu\nu} f_{j\nu})$$

$$= \sum_{\{i,j\}} \sum_{\alpha\beta} -\frac{1}{2} J_{ij} (f^\dagger_{i\alpha} f_{j\alpha} f^\dagger_{j\beta} f_{i\beta} + \frac{1}{2} f^\dagger_{i\alpha} f_{i\alpha} f^\dagger_{j\beta} f_{j\beta}). \tag{1.77}$$

We study this Hamiltonian in a mean field approximation, by introducing parameters for expectation values of operators

$$\eta_{ij}\epsilon_{\alpha\beta} = -2\langle f_{i\alpha} f_{j\beta}\rangle, \quad \chi_{ij}\delta_{\alpha\beta} = 2\langle f^\dagger_{i\alpha} f_{j\beta}\rangle; \tag{1.78}$$

where $\eta_{ij} = \eta_{ji}$ and $\chi_{ij} = \chi^\dagger_{ji}$.

As is usual, we expand operators in Eq. 1.77 in terms of fluctuations about their expectation values and ignore terms which are quadratic in fluctuations, leading to

$$\begin{aligned} H_{\text{MFT}} = &- \sum_{\langle i,j\rangle} \frac{3}{8} J_{ij} (\chi_{ji} f^\dagger_{i\mu} f_{j\mu} + \eta_{ij} f^\dagger_{i\mu} f^\dagger_{j\mu} + h.c. \\ &- |\chi_{ij}|^2 - |\eta_{ij}|^2) + \sum_i (\mu^3_i (f^\dagger_{i\uparrow} f_{i\uparrow} - f_{i\downarrow} f^\dagger_{i\downarrow}) \\ &+ \frac{1}{2}(\mu^1_i + i\mu^2_i) f_{i\mu} f_{i\nu} \epsilon_{\mu\nu} + h.c.). \end{aligned} \tag{1.79}$$

We note that we have introduced the Lagrange multipliers μ^m_i to impose the one-fermion-per-site constraint at a mean-field level. The Lagrange multipliers μ^m_i as well as the parameters χ_{ij} and η_{ij} are determined self consistently.

To facilitate further discussion on the $\mathsf{SU}(2)$ gauge structure of the mean-field Hamiltonian, it is convenient to introduce a spinor representation

$$\psi \equiv \begin{bmatrix} \psi_1 \\ \psi_2 \end{bmatrix} \equiv \begin{bmatrix} f_\uparrow \\ f^\dagger_\downarrow \end{bmatrix}. \tag{1.80}$$

In terms of these spinors, the mean-field Hamiltonian can be be compactly rewritten as:

$$\begin{aligned} H_{\text{MFT}} = &\sum_{\langle i,j\rangle} \frac{3}{8} J_{ij} [\frac{1}{2} \text{Tr}(U^\dagger_{ij} U_{ij}) - (\psi^\dagger_i U_{ij} \psi_j + h.c.)] \\ &+ \sum_i \mu^l_i \psi^\dagger_i \tau^l \psi_i, \end{aligned} \tag{1.81}$$

where the mean field parameters χ_{ij} and η_{ij} have been recast into

$$U_{ij} \equiv \begin{bmatrix} \chi^\dagger_{ij} & \eta_{ij} \\ \eta^\dagger_{ij} & -\chi_{ij} \end{bmatrix}. \tag{1.82}$$

The constraint implementing projection into the spin Hilbert space at the mean-field level now has the form:

$$\langle \psi^\dagger_i \tau^l \psi_i \rangle = 0. \tag{1.83}$$

$\{U_{ij}\}$ and $\{\mu_i^m\}$ can be viewed as variational parameters which specify the mean-field "ansatz": the word referring to both the mean-field Hamiltonian and the wave function corresponding to its ground state. Variationally optimizing the parameters to obtain the lowest energy ground state is equivalent to determining the parameters self consistently.

The spinor representation makes the $\mathsf{SU}(2)$ gauge redundancy of the mean-field Hamiltonian manifest. The Hamiltonian is invariant, trivially, under the site-dependent gauge transformation $\psi_i \mapsto W_i\psi_i$ and $U_{ij} \mapsto W_iU_{ij}W_j^\dagger$, where $W_i \in \mathsf{SU}(2)$. The origin of the gauge redundancy lies in Eq. 1.76: it is easy to check that this $\mathsf{SU}(2)$ gauge transformation on the spinor leaves the physical spin operator invariant. Therefore, the mean-field anstaz parametrised by U_{ij} and the one parametrised by $W_iU_{ij}W_j^\dagger$ share the same physical spin wave functions, *i.e.*, the same wave function after projecting the fermionic Hilbert space into the physical spin Hilbert space. This has significant consequences for what we require of symmetric mean-field ansatzes. Consider the action of a symmetry $g : U_{ij} \mapsto U_{g(i)g(j)}$. For a symmetric ansatz we no longer require $U_{g(i)g(j)} = U_{ij}$ — but only that there exists transformations $G_g(n) \in \mathsf{SU}(2)$ for all sites n, such that $G_g(g(i))U_{g(i)g(j)}G_g^\dagger(g(j)) = U_{ij}$ — the gauge redundancy then implies that physical properties of the state represented by the ansatz have not changed. The physical transformations together with the gauge transformation, $(G_g(i), g)$, which leaves the ansatz invariant, constitute the *projective symmetry group* (PSG). The PSG characterises the symmetries of the ansatz, and serves to classify and characterise different mean field spin liquid states.

From the preceding discussion on the gauge structure it is clear that not all fluctuations of the mean-field parameters $\{U_{ij}\}$ are physical: the unphysical fluctuations between gauge inequivalent states must be described by gauge fields in the effective theory. The effective theories, then, are likely to be fermions coupled to gauge fields. The gauge structure of the low energy theory is in general, however, not given by the high energy gauge group $\mathsf{SU}(2)$, but typically broken down to a global Z_2, $\mathsf{U}(1)$ or $\mathsf{SU}(2)$. The low-energy gauge structure is determined by the "invariant gauge group" (IGG) [66], is a special subgroup of the PSG comprised of pure gauge transformations which leave the ansatz invariant, *i.e.*, $\mathcal{G} = \{W_i | W_iU_{ij}W_j^\dagger = U_{ij}, W \in \mathsf{SU}(2)\}$. Given the central importance of the IGG, one usually labels QSLs by the IGG, leading to the terminology of "Z_2, $\mathsf{U}(1)$, or $\mathsf{SU}(2)$" QSLs. Another way to see the low energy gauge structure is by examining the fluxes. Let us consider all flux operators $\mathcal{P}(\mathcal{C}_i)$ for closed loops $\mathcal{C}_i$ sharing the *same starting point*. By the Anderson-Higgs mechanism, when all $\mathcal{P}(\mathcal{C}_i) \sim \tau_0$, the $\mathsf{SU}(2)$ gauge structure is unbroken; when generically $[\mathcal{P}(\mathcal{C}_i), \mathcal{P}(\mathcal{C}_j)] = 0$, the $\mathsf{SU}(2)$ gauge structure is broken down to $\mathsf{U}(1)$; when there exist $[\mathcal{P}(\mathcal{C}_i), \mathcal{P}(\mathcal{C}_j)] \neq 0$, the $\mathsf{SU}(2)$ gauge structure is broken down to Z_2.

As seen from above, the PSGs, therefore, play the role of "universality" classes of mean-field QSL phases, resolving quantum disordered states with the same physical symmetries.

A typical programme of investigation of symmetric spin liquid ground states on a given spatial lattice involves the enumeration of all PSGs, given all physical symmetries (the ones in the space group, time reversal) and the IGG. This allows the construction of corresponding mean-field ansatzes and the consequent investigation of spin liquid phases. In the following section, we construct a 2D Z_2 quantum spin liquid state to illuminate the formalism [67].

1.3.3 A gapped Z_2 quantum spin liquid with topological order

Consider a Heisenberg model on the 2D square lattice, with the inclusion of the next nearest neighbour coupling. The model is sometimes referred to as the $J_1 - J_2$ model, where J_1 denotes the strength of the neighbour coupling and J_2 denotes the strength of the next neighbour coupling.

A mean field ansatz invoking the parton construction was presented in Ref. [67]. Using the notation we established earlier, this mean field ansatz can be represented as:

$$\begin{aligned} U_{i,i+\hat{x}} = U_{i,i+\hat{y}} &= -\chi\tau_z \equiv U_1, \\ U_{i,i+\hat{x}+\hat{y}} &= \Delta_1\tau_x + \Delta_2\tau_y \equiv U_2, \\ U_{i,i-\hat{x}+\hat{y}} &= \Delta_1\tau_x - \Delta_2\tau_y \equiv U_3, \\ \mu^x \neq 0, \quad \mu^y = \mu^z &= 0. \end{aligned} \tag{1.84}$$

We first consider two loops, namely $\mathcal{C}_1 = i \to i+\hat{x} \to\to i+\hat{x}+\hat{y} \to i$ and $\mathcal{C}_2 = i \to i+\hat{y} \to\to i-\hat{x}+\hat{y} \to i$. Evaluating the flux operators on these two loops, we obtain that:

$$\mathcal{P}(\mathcal{C}_1) = \chi^2 U_2, \quad \mathcal{P}(\mathcal{C}_2) = \chi^2 U_3, \tag{1.85}$$

which generically do not commute with each other. Since we mentioned earlier, when the flux operators on the lattices do not commute, the IGG is fully broken from $\mathsf{SU}(2)$ to Z_2. This is how we know that the above ansatz describes a Z_2 quantum spin liquid state.

Diagonalising the mean field spinon Hamiltonian, we observe that the spinon bands are given by $E_\pm = \pm\sqrt{\epsilon_1^2(\vec{k}) + \epsilon_2^2(\vec{k}) + \epsilon_3^2(\vec{k})}$, where:

$$\begin{aligned} \epsilon_1(\vec{k}) &= 2J_1\chi(\cos(k_x) + \cos(k_y)), \\ \epsilon_2(\vec{k}) &= 2J_2\Delta_1(\cos(k_x+k_y) + \cos(k_x-k_y)) + \mu^x, \\ \epsilon_3(\vec{k}) &= 2J_2\Delta_2(\cos(k_x+k_y) - \cos(k_x-k_y)). \end{aligned} \tag{1.86}$$

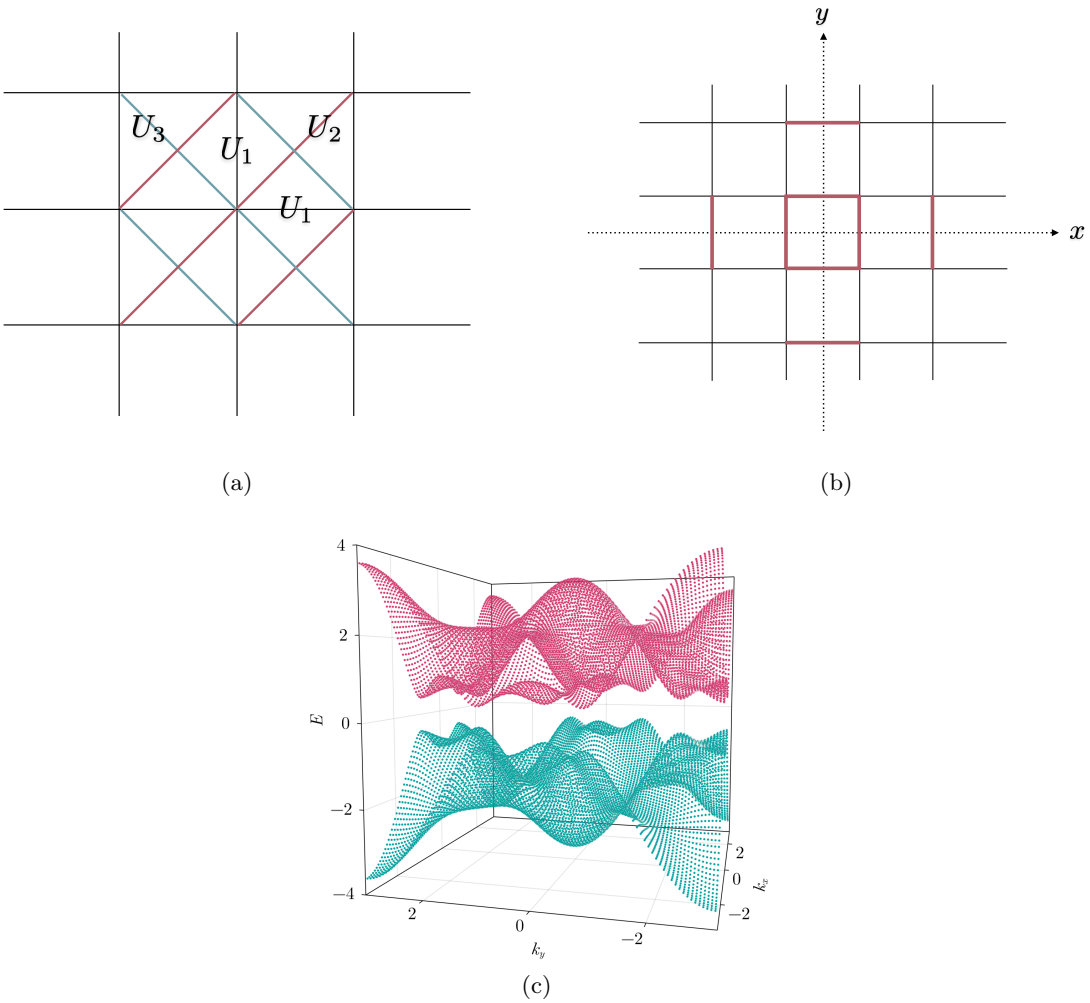

Figure 1.5: (a) A Z_2 spin liquid, the Z_2 sRVB state, on the 2D square lattice; (b) The gauge transformed ansatz with π flux through the two holes of the torus; (c) The spinon band structure where the green band is the filled band, featuring a gapped band structure for the Z_2 sRVB state.

Since the spinons are half filled by construction, the dispersion relation tells us that these spinons are gapped as shown in Fig. 1.5c.

We now turn to the analysis of symmetry on this ansatz. This ansatz is apparently translational symmetric, and also symmetric under parity symmetry $\hat{x} \leftrightarrow \hat{y}$. However, under the $\frac{\pi}{2}$ rotation, the original ansatz is mapped to:

$$\begin{aligned} \tilde{U}_{i,i+\hat{x}} &= \tilde{U}_{i,i+\hat{y}} = -\chi\tau_z, \\ \tilde{U}_{i,i+\hat{x}+\hat{y}} &= \Delta_1\tau_x - \Delta_2\tau_y, \\ \tilde{U}_{i,i-\hat{x}+\hat{y}} &= \Delta_1\tau_x + \Delta_2\tau_y, \\ \mu^x \neq 0, \quad \mu^y &= \mu^z = 0. \end{aligned} \tag{1.87}$$

It seems that the transformed ansatz is not the same as the original ansatz. We note that we can perform the following gauge transformation $W(i) \equiv (-1)^i \tau_x$, such that:

$$W(i)\tilde{U}_{ij}W^\dagger(j) = U_{ij}. \tag{1.88}$$

Therefore, despite the fact that the ansatz is not apparently symmetric under the $\frac{\pi}{2}$ rotation, it is symmetric up to a further gauge transformation. In other words, the PSG element $(G_g(i), g)$ leaves the ansatz invariant. After the Gutzwiller projection, the physical spin wave function will be explicitly symmetric under the $\frac{\pi}{2}$ rotation. A similar action by time reversal symmetry exists for this ansatz too. In fact, this Z_2 ansatz does preserve the full symmetry of the lattice, and it is usually referred to as the Z_2 short-ranged resonating valence bond (sRVB) state.

The Z_2 sRVB state carries non-trivial Z_2 topological order, as pointed out in Ref. [67]. The easiest way to see this is to consider the Z_2 sRVB state on a torus, i.e. imposing the periodic boundary condition. Let us introduce (p, q), which can take value 0 or 1, to label the class of gauge transformations that we are to perform, which are:

$$W_i^{(p,q)} = (-1)^{p\theta(x)}(-1)^{q\theta(y)} \tag{1.89}$$

, where $\theta(x) = 0$ if $x < 0$, and $\theta(x) = 1$ if $x < 0$ (similarly for y). The ansatz U_{ij} is transformed as $\tilde{U}_{ij}^{(p,q)} = W_i^{(p,q)} U_{ij} W_j^{(p,q)\dagger}$. When $p = 1$, the U_{ij}s passing the x-axis pick up -1 signs, and similarly the U_{ij}s passing the y-axis pick up -1 signs when $q = 1$. In Fig. 1.5b, we demonstrate the case when $p = q = 1$, and the coloured links are the links that change signs.

The gauge transformations do not change the energy of the state, but in this crucial case, the ground states corresponding to different pairs of (p, q) are in fact different states. Consider the global flux operators on a closed loop $\mathcal{C}_x$ around the torus along the x-axis, we immediately see that $\mathcal{P}^{(0,0)}(\mathcal{C}_x) = -\mathcal{P}^{(1,0)}(\mathcal{C}_x)$. Therefore the (p, q) pairs label the π flux through the two holes of the torus, leading to a ground state degeneracy of 4. In general, the Z_2 gapped spin liquid on the genus g Riemann surface has a ground state degeneracy of 2^{2g}. Moreover, these different ground states cannot be tunnelled into each other through local fluctuations [67]. Unsurprisingly, this is a common feature for the Z_2 gauge theory, and it demonstrated that the Z_2 gauge theory is the low energy effective theory of the Z_2 sRVB state. Indeed, the Z_2 sRVB, a gapped Z_2 quantum spin liquid, carries a topological order.

1.4 The structure of the thesis

As we finish the pedagogical review on the prerequisites, the introductory chapter is closed with a structure of the remaining parts for this thesis.

In Chapter 2, we construct the surface topological orders for the 3D inversion symmetric higher order topological insulators and superconductors. The chapter is based on the published paper [68].

In Chapter 3, we study the finite entanglement scaling of 2D gaussian fermionic tensor network states when they are used to simulate 2D Fermi surfaces. The chapter is based on parts of the published paper [69].

In Chapter 4, the quantum spin liquid states are constructed using the projective symmetry group analysis. The chapter is based on an unpublished manuscript in collaboration with Dr. Sounak Biswas and Prof. Sid Parameswaran.

Finally we will close with Chapter 5, where we present the conclusions and the outlooks from these studies.

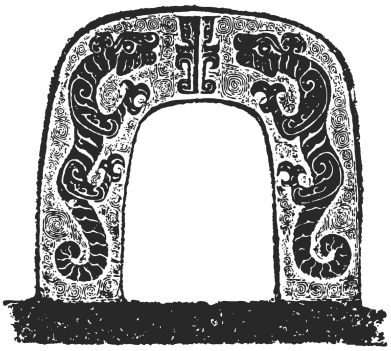

Chapter 2

Anomalous gapped boundaries between surface topological orders in higher-order topological insulators and superconductors with inversion symmetry

2.1 Introduction

In this work, we construct topologically ordered surface terminations for three dimensional electronic topological insulators and superconductors both with and without TRS (classes A, AII, AIII, D, DIII, CII and BDI within the Altland-Zirnbauer classification scheme) whose higher-order topology is enabled by the additional presence of three-dimensional spatial inversion symmetry, denoted $\mathcal{I}$. A band-theoretic classification indicates that the surfaces of such phases host one-dimensional chiral or helical Dirac hinge modes along an inversion-invariant line, or degenerate zero-dimensional corner modes at antipodal points, which cannot be gapped by any symmetric free-fermion perturbation [27]. We show that these hinge and corner modes may be gapped out upon introducing an inversion-symmetric configuration of fractionalized phases with non-Abelian anyons on the surface. The surface now realizes a fully gapped and symmetric topologically ordered state. Crucially, this surface fractionalization pattern is anomalous as it would be impossible to assemble a configuration of topological orders with the relevant symmetry properties for a system in purely two dimensions, i.e. without invoking the mode contributed by the three dimensional bulk.

Chapter heading: tiger motif, detail of the *you*, Shang dynasty (circa 16th – 12th/11th centuries B.C.), Cernuschi Museum in France and Sumitomo Collection in Japan.

Compared with Ref. [70], this work discusses the action of crystalline symmetry on the STO beyond merely arranging the STOs in a symmetry-respecting configuration.

The rest of the chapter is organized as follows. In Section 2.2 and 2.3, we present the construction of surface topological order for second and third order inversion symmetric topological phases respectively. The main results of the chapter are summarised in Table 2.1. Technical details are collected in several appendices.

	Second Order Topology		Third Order Topology	
AZ Class	Hinge Modes	STOs	Zero Modes	STOs
A	Chiral Dirac	2D $\mathcal{T}$-Pfaffian [†]		
AIII			Dirac	$(\mathsf{SO}(3)_3)^4$ [‡]
AI				
BDI			Majorana	$(\mathsf{SO}(3)_3)^2$
D	Chiral Majorana	$\mathsf{SO}(3)_3$	Majorana	$(\mathsf{SO}(3)_3)^2$
DIII	Helical Majorana	$\mathsf{SO}(3)_3 \times \overline{\mathsf{SO}(3)_3}$	Majorana Kramers Pair	$(\mathsf{SO}(3)_3 \times \overline{\mathsf{SO}(3)_3})^2$
AII	Helical Dirac	2D $\mathcal{T}$-Pfaffian$\times$2D $\mathcal{T}$-Pfaffian		
CII			Majorana Kramers Pair	$(\mathsf{SO}(3)_3 \times \overline{\mathsf{SO}(3)_3})^2$
C	Chiral Majorana	[§]		
CI				

[†] The 2D $\mathcal{T}$-Pfaffian has the same anyon content of $\mathcal{T}$-Pfaffian, albeit without TRS.

[‡] Also enriched by $\mathsf{U}(1)$ charge conservation symmetry. No microscopic construction provided.

[§] Note that there is no STO for 2nd order class C. The 2nd order class C can be obtained by breaking the TRS in the first order class CI, similar to the case of 2nd order class A which is obtained by breaking the TRS in the first order class AII. The STO for the 2nd order class C should have the same anyon content as the STO for the first order class CI, which was excluded in Ref. [71]. In the above paper, the authors argue that, due to disorder, interaction is always relevant in the first order class CI, and will cause spontaneous symmetry breaking of TRS, thus ruling out STOs that preserve TRS.

Table 2.1: Summary of surface topological order for all inversion symmetric higher order topological phases in the AZ classes. The shaded entries denote the absence of gapless modes or STO. The superscripts that appear in the column of third order STO denote the number of copies of the topological order e.g. $(\mathsf{SO}(3)_3)^2$ means two copies of $\mathsf{SO}(3)_3$. The STO we put on the surface is always inversion symmetric since we place a topological order and its inversion symmetric partner on the surface so that the original gapless line/point modes can be gapped.

2.2 Surface topological order for second order topological phases

2.2.1 Class A + inversion: HOTI with chiral Dirac hinge mode

A second-order topological insulator (HOTI) protected solely by inversion symmetry can be obtained by perturbing a 3D topological insulator with a surface mass term that breaks TRS ($\mathcal{T}$) but preserves inversion symmetry ($\mathcal{I}$) [27]. The bulk of the 3D topological insulator can be captured by the Bloch Hamiltonian

$$H(\vec{k}) = \sum_i \sin(k_i)\sigma_i \otimes \tau_x - (2 - \sum_i \cos(k_i))\sigma_0 \otimes \tau_z, \tag{2.1}$$

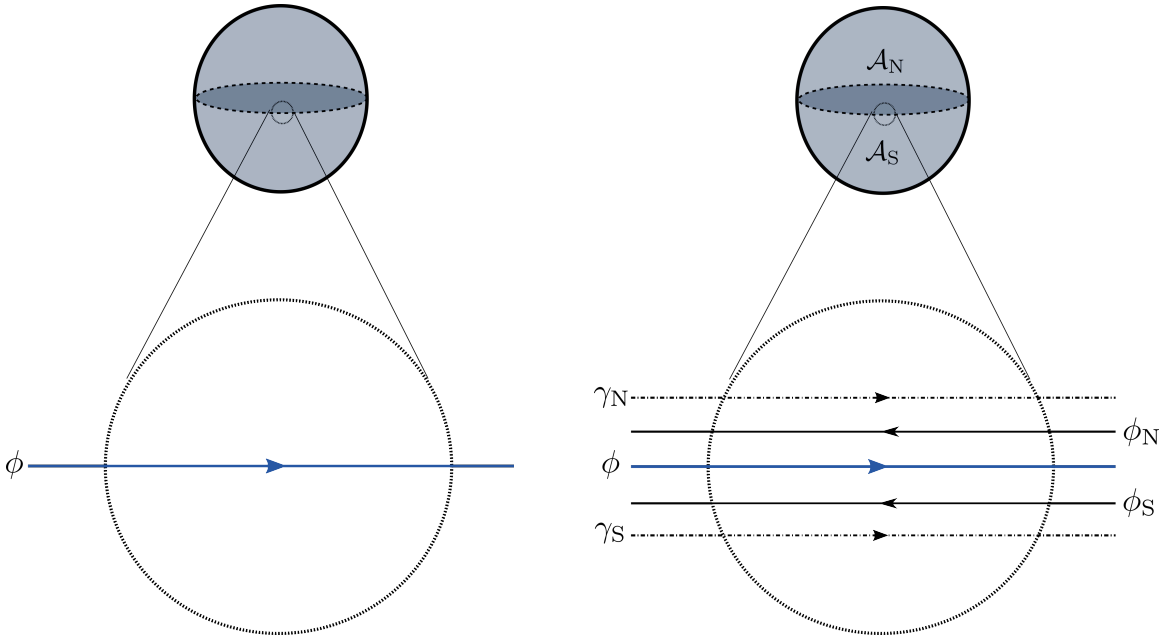

(a) Before pasting STO (b) After pasting STO

Figure 2.1: Surface topological order for second order topological phases protected by inversion symmetry in A class. ϕ denotes the chiral Dirac hinge mode. The edge modes of STOs are $\phi_{N/S}$, the Dirac edge modes, and $\gamma_{N/S}$, the Majorana edge modes.

where $\vec{\sigma}, \vec{\tau}$ are Pauli matrices that act on spin and orbital degrees of freedom respectively. Inversion symmetry and TRS are given by $\mathcal{I} = \sigma_0 \otimes \tau_z$ and $\mathcal{T} = i\sigma_y \otimes \tau_0 \mathcal{K}$ respectively, where $\mathcal{K}$ denotes complex conjugation. In order to construct the hinge state we first inspect the linearized surface Hamiltonian which takes the form [27]

$$h(\vec{k}, \vec{r}) = -(\vec{k} \times \hat{n}_{\vec{r}}) \cdot \vec{\tilde{\sigma}}, \tag{2.2}$$

where $\hat{n}_{\vec{r}}$ is the unit vector normal to the surface, which is assumed to be spherical. The projected surface Hamiltonian is expressed in a rotated $\tilde{\sigma}$ basis in which the symmetry operators act as $\mathcal{I} = -\tilde{\sigma}_0$ and $\mathcal{T} = i\tilde{\sigma}_y \mathcal{K}$. The surface hinge mode is obtained by perturbing the 3D TI with a TRS breaking mass term of the form $\delta h(\vec{r}) = m_{\vec{r}}(\hat{n}_{\vec{r}} \cdot \vec{\tilde{\sigma}})$. Inversion symmetry imposes the constraint $m_{\vec{r}} = -m_{-\vec{r}}$ on the mass profile, signalling the vanishing of the mass term along some inversion symmetric curve. For concreteness, we consider the setup illustrated in Fig. 2.1 wherein the mass changes sign across the equator. It is known that such a domain wall hosts a chiral fermionic mode [72]. In order to gap out the chiral hinge mode, we induce topological orders denoted as $\mathcal{A}_N$ and $\mathcal{A}_S$ on the top/bottom halves of the surface. It is worth noting that the calculations below will be similar to the calculations in Ref. [70], albeit with an explicit treatment of crystalline symmetry. 3D inversion symmetry imposes $\mathcal{A}_S = \bar{\mathcal{A}}_N$, where $\bar{\mathcal{A}}$ denotes the orientation-reversed version

of $\mathcal{A}$. The topological order $[\text{Ising} \times \mathsf{U}(1)_{-8}]/\mathsf{Z}_2$ is a suitable choice for $\mathcal{A}_\text{N}$. This is the same topological order as the $\mathcal{T}$-Pfaffian, if we ignore TRS, therefore we refer to it as 2D $\mathcal{T}$-Pfaffian. The edge theory of $\mathcal{A}_\text{N}$ contains a chiral Majorana mode and an anti-chiral compact boson mode. These are the edge fields corresponding to the bulk Ising and $\mathsf{U}(1)_{-8}$ topological orders respectively. Concretely, the edge of $\mathcal{A}_\text{N}$ and $\mathcal{A}_\text{S}$ are described by the Lagrangians [20, 19]

$$\begin{aligned}\mathcal{L}_{\partial\mathcal{A}_\text{N}} &= -\frac{2}{4\pi}\partial_x\phi_\text{N}(\partial_t-\partial_x)\phi_\text{N} + i\gamma_\text{N}(\partial_t+\partial_x)\gamma_\text{N},\\ \mathcal{L}_{\partial\mathcal{A}_\text{S}} &= -\frac{2}{4\pi}\partial_x\phi_\text{S}(\partial_t-\partial_x)\phi_\text{S} + i\gamma_\text{S}(\partial_t+\partial_x)\gamma_\text{S}.\end{aligned} \tag{2.3}$$

where γ_N and γ_S are Majornana-Weyl modes while ϕ_N and ϕ_S are compact bosonic modes. The chiral hinge additionally contains a single Dirac mode contributed by the HOTI bulk which can be described by the bosonized Lagrangian [73, 74, 75]

$$\mathcal{L}_0 = \frac{1}{4\pi}\partial_x\phi(\partial_t+\partial_x)\phi, \tag{2.4}$$

where ϕ is a compact boson. The combined Lagrangian describing the equatorial hinge is therefore given by

$$\mathcal{L}_\text{Hinge} = \mathcal{L}_{\partial\mathcal{A}_\text{N}} + \mathcal{L}_{\partial\mathcal{A}_\text{S}} + \mathcal{L}_0. \tag{2.5}$$

The two Majorana modes can be combined into a Dirac mode which can be subsequently bosonized and written in terms of the compact boson ϕ_M using

$$\psi_\text{M} \sim e^{i\phi_\text{M}(x)} \sim e^{-i\frac{\pi}{4}}\gamma_\text{N} + e^{i\frac{\pi}{4}}\gamma_\text{S}, \tag{2.6}$$

where we have suppressed the Klein factors for brevity [76]. The benefit of bosonizing the Majorana pair is that it allows for the description of the hinge in terms of the K-matrix Luttinger liquid formalism which is easier to work with. The hinge is then described by the Lagrangian

$$\mathcal{L}_\text{Hinge} = \frac{1}{4\pi}\partial_x\Phi^\mathsf{T}K\partial_t\Phi - \frac{1}{4\pi}\partial_x\Phi^\mathsf{T}\partial_x\Phi, \tag{2.7}$$

where $\Phi^\mathsf{T} = (\phi_\text{M}, \phi_\text{N}, \phi_\text{S}, \phi)$, the $K = \text{diag}(1,-2,-2,1)$ and the charge vector $t^\mathsf{T} = (0,1,1,1)$. Our intention is to add to Eq. (2.7) generic interactions represented by cosine terms that gap out all the hinge modes when driven to strong coupling

$$\delta\mathcal{L} = \sum_{I=1,2}\delta\mathcal{L}_I = \sum_{I=1,2}\lambda_I(x)\cos[\Lambda_I^\mathsf{T}K\Phi - \alpha_I] \tag{2.8}$$

Apart from being simultaneously gappable (see App. 2.A for details), the gapping vectors Λ_I need to satisfy a number of symmetry criteria related to inversion, charge conservation

and gauge symmetry derived from a Z_2 redundancy in our description of the hinge. First, the inversion symmetry acts as $\mathcal{I} : \Phi(x) \mapsto \mathrm{I}\Phi(-x)$ where $\mathrm{I} = (-1) \oplus \sigma^x \oplus (+1)$. Second, in order to respect $\mathsf{U}(1)$ symmetry, we impose charge neutrality condition, namely we require that $\Lambda^\mathsf{T} t = 0$. Finally, due to the fermionic nature of $\mathcal{A}_\mathrm{N}$ and $\mathcal{A}_\mathrm{S}$, an additional gauge symmetry $\mathsf{Z}_2^\mathrm{N} \times \mathsf{Z}_2^\mathrm{S}$ is imposed. The generators g_α of Z_2^α (where $\alpha = \mathrm{N}, \mathrm{S}$) implement the transformation

$$\mathsf{g}_{\mathrm{N,S}} : \phi_{\mathrm{N,S}} \mapsto \phi_{\mathrm{N,S}} \pm \frac{\pi}{2}, \quad \gamma_{\mathrm{N,S}} \mapsto -\gamma_{\mathrm{N,S}}. \tag{2.9}$$

Since the fermionic operator $\Psi_\alpha \simeq \gamma_\alpha e^{2i\phi_\alpha}$ is invariant under Z_2^α, the gauge symmetry imposes that any admissible cosine term tunnels only local operators, that is, fermions or combinations thereof. Additionally, as a consequence of the $\mathsf{Z}_2^\mathrm{N} \times \mathsf{Z}_2^\mathrm{S}$ symmetry we need to fix the compactification $\phi_{\mathrm{N,S}} \sim \phi_{\mathrm{N,S}} + \pi$. Two cosine terms are required to open a gap for the combined hinge theory. The first gapping vector can be chosen to be $\Lambda_1^\mathsf{T} = (0, -2, -2, 4)$. Such a term is inversion-symmetric if $\lambda_1(x) = \lambda_1(-x)$ [see Eq. (2.8)] therefore λ_1 can be chosen to be constant and $\alpha = 0$, i.e.,

$$\delta\mathcal{L}_1 = \lambda_1 \cos\left(4\phi_\mathrm{N} + 4\phi_\mathrm{S} + 4\phi\right). \tag{2.10}$$

This gapping term also respects $\mathsf{U}(1)$ and $\mathsf{Z}_2^\mathrm{N} \times \mathsf{Z}_2^\mathrm{S}$ symmetry as can be checked explicitly. Upon adding Eq. (2.10) to the original gapless hinge described by Eq. (2.7), the combination of fields $\langle \phi_\mathrm{N} + \phi_\mathrm{S} + \phi \rangle$ acquire a vacuum/groundstate expectation value, thereby breaking the $\mathsf{Z}_2^\mathrm{N} \times \mathsf{Z}_2^\mathrm{S}$ symmetry into a diagonal Z_2 subgroup denoted as $\mathsf{Z}_2^\mathrm{diag}$, generated by $\mathsf{g}_\mathrm{diag} := \mathsf{g}_\mathrm{N}\mathsf{g}_\mathrm{S}$ with the action

$$\mathsf{g}_\mathrm{diag} : \phi_\mathrm{N} \mapsto \phi_\mathrm{N} + \frac{\pi}{2}, \phi_\mathrm{S} \mapsto \phi_\mathrm{S} - \frac{\pi}{2}, \phi_\mathrm{M} \mapsto \phi_\mathrm{M} + \pi. \tag{2.11}$$

The second gapping vector can be chosen as $\Lambda_2^\mathsf{T} = (2, 1, -1, 0)$. Since the two gapping vectors $\Lambda_{1,2}$ satisfy the Haldane criterion $\Lambda_i^\mathsf{T} K \Lambda_j = 0$, the bosonic fields $\Lambda^\mathsf{T} K \Phi$ can simultaneously acquire a vacuum expectation value. The second gapping term $\delta\mathcal{L}_2$ is also charge neutral since $\Lambda_2^\mathsf{T} t = 0$ as well as invariant under the residual $\mathsf{Z}_2^\mathrm{diag}$ symmetry. Finally, the term is $\delta\mathcal{L}_2$ is inversion symmetric if $\alpha_2 = n\pi$ and $\lambda_2(-x) = (-1)^n \lambda_2(x)$. By choosing $n \in \mathbb{Z}_\mathrm{even}$, we can fix λ_2 to be constant everywhere.

To summarize, we have shown that the two cosine terms corresponding to $\Lambda_{1,2}$ satisfy the symmetry requirements as well as the Haldane criteria. Therefore, they can be simultaneously driven to strong coupling thereby completely gapping out the hinge without breaking any symmetry. We note that an inversion symmetric configuration of $\mathcal{A}_\mathrm{N}$ and $\mathcal{A}_\mathrm{S}$ illustrated in Fig. 2.1 without the mode contributed from the bulk is clearly ingappable on the hinge as the modes on the hinge carry a non-vanishing chiral central charge. Therefore as a pattern of 2D inversion symmetric topological order, $\mathcal{A}_\mathrm{N} \oplus \mathcal{A}_\mathrm{S}$ is anomalous and cancels the higher-order anomaly coming from the bulk.

2.2.2 Class AII + inversion: HOTI with helical Dirac hinge mode

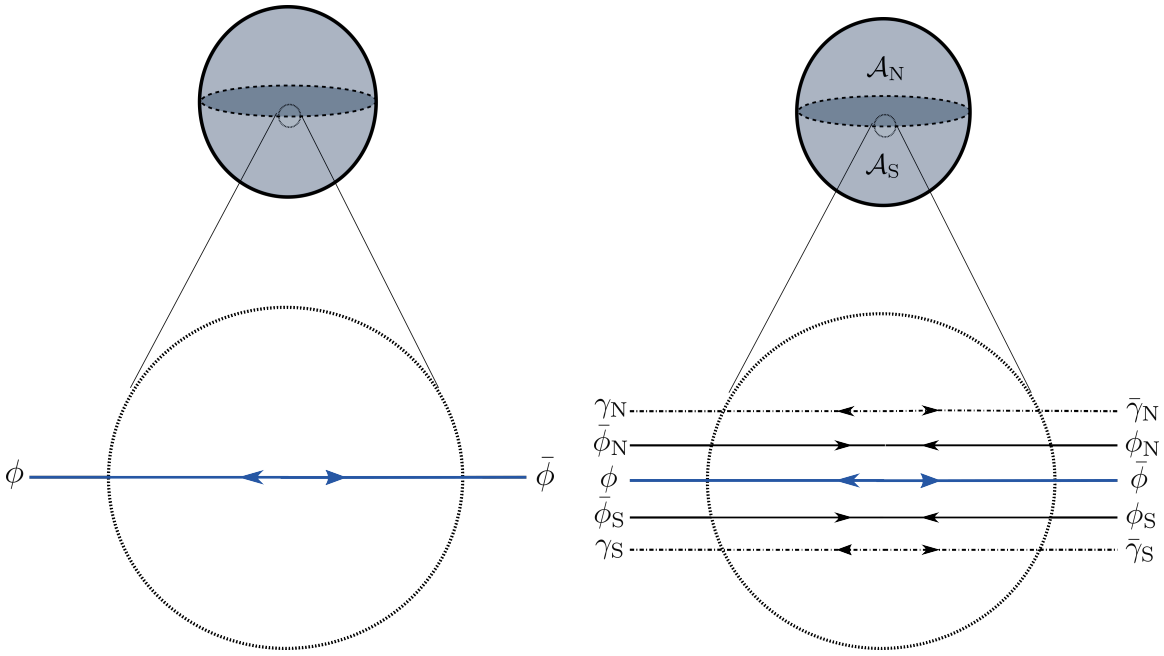

(a) Before pasting STO

(b) After pasting STO

Figure 2.2: Surface topological order configuration for inversion and TRS protected higher-order topological insulator. The $\phi/\bar{\phi}$ denote the helical Dirac hinge modes. The edge modes of STOs are $\phi_{N/S}$ and $\bar{\phi}_{N/S}$, the Dirac edge modes; and $\gamma_{N/S}$ and $\bar{\gamma}_{N/S}$, the Majorana edge modes.

It was shown in Refs. [27, 77] that TRS-invariant insulators (with $\mathcal{T}^2 = -1$) enriched by additional inversion symmetry can support non-trivial second-order topology. On inversion symmetric open geometries, models within the non-trivial second-order phase host robust helical Dirac modes along an inversion symmetric hinge on the surface. The helical hinge modes are similar to those obtained on the edge of a quantum spin Hall insulator and form a Kramer's pair which is stable against interactions [4]. Here we show that these modes can be gapped out by inducing topological order on the surface. Before getting into the details of the surface topological order, we briefly review the free fermion model for the helical HOTI. The strategy is to start with a doubled model and subsequently add a perturbation that gaps out the surface leaving behind a robust hinge. In this case, the parent theory consists of two 3D topological insulators. We consider the same geometrical settings as in Fig. 2.2. The surface Hamiltonian is given by

$$h_1(\vec{k}, \vec{r}) = \tau_0 \otimes (\vec{k} \times \hat{n}_{\vec{r}}) \cdot \vec{\sigma}. \tag{2.12}$$

The inversion and TRS are represented by $\mathcal{I} = \tau_0 \otimes (-\sigma_0)$ and $\mathcal{T} = \tau_0 \otimes (i\sigma_y \mathcal{K})$. A surface

mass term that respects TRS can be added to the Hamiltonian

$$\delta h_1(\vec{r}) = \tau_y \otimes m_{\vec{r}}(\hat{n}_{\vec{r}} \cdot \vec{\sigma}). \tag{2.13}$$

Inversion symmetry demands that $\mathcal{I}\delta h_1(\vec{r})\mathcal{I}^{-1} = \delta h_1(-\vec{r})$ which further imposes the condition $m_{\vec{r}} = -m_{-\vec{r}}$, signalling the vanishing of the mass term along some inversion symmetric curve. For reasons identical to the chiral HOTI case, this indicates the existence of gapless helical modes along the equator. TRS in the above construction acts within each flavor of the above model, i.e diagonally in the $\vec{\tau}$ space. We find it convenient to work with an equivalent description of the helical HOTI in which TRS acts by switching fermion flavors, such that the model can be thought of as a stacking of a chiral HOTI with its time-reversed copy. We consider the following Hamiltonian which is related to $h_1 + \delta h_1$ by a unitary transformation

$$\begin{aligned} h_2(\vec{k}, \vec{r}) = \tilde{\tau}_0 \otimes (\lambda_y \tilde{\sigma}_y + m_{\vec{r}} n_x \tilde{\sigma}_x + m_{\vec{r}} n_z \tilde{\sigma}_z) \\ + \tilde{\tau}_z \otimes (\lambda_x \tilde{\sigma}_x + \lambda_z \tilde{\sigma}_z + m_{\vec{r}} n_y \tilde{\sigma}_y), \end{aligned} \tag{2.14}$$

where $\vec{\lambda} \equiv \vec{k} \times \hat{n}_{\vec{r}}$. TRS is represented by

$$\mathcal{T} = i\tilde{\tau}_y \otimes \tilde{\sigma}_0 \mathcal{K}, \quad \mathcal{T}^2 = -1. \tag{2.15}$$

Upon performing an analysis similar to the one described above one is left with a surface which is gapped everywhere except an inversion symmetric hinge which hosts a pair of gapless helical modes $\left\{\psi, \bar{\psi}\right\}$ that form a Kramers doublet.

A natural candidate for an STO that can gap out the helical hinge mode is given by stacking the STO from the previous section and its time-reversed copy. It remains to be shown that this construction furnishes modes on the hinge that are robust by themselves, but when considered along with the helical modes contributed by the bulk lead to a completely gapped hinge. As illustrated in Fig. 2.2, we set up the STO configuration by placing $(\mathcal{A}_{\mathrm{N}}, \mathcal{A}_{\mathrm{S}})$ on the northern/southern hemispheres of a spherical surface geometry. Here $\mathcal{A}_{\mathrm{N,S}}$ stand for the product topological orders consisting of 2D $\mathcal{T}$-Pfaffian topological orders and their time-reversed copies. The edge theory contains 8 modes. We divide these into bosonic modes $\Phi = (\phi_{\mathrm{N}}, \phi_{\mathrm{S}}, \bar{\phi}_{\mathrm{N}}, \bar{\phi}_{\mathrm{S}})^{\mathsf{T}}$ and fermionic modes $\Gamma = (\gamma_{\mathrm{N}}, \gamma_{\mathrm{S}}, \bar{\gamma}_{\mathrm{N}}, \bar{\gamma}_{\mathrm{S}})^{\mathsf{T}}$. The action of TRS is encoded in the matrices $T_\Phi := \sigma^x \otimes \mathrm{Id}_2$ and $T_\Gamma = i\sigma^y \otimes \mathrm{Id}_2$ such that under TRS

$$\mathcal{T} : \begin{bmatrix} \Phi \\ \Gamma \end{bmatrix} \longmapsto \begin{bmatrix} T_\Phi \Phi \\ T_\Gamma \Gamma \end{bmatrix}, \quad i \longmapsto -i. \tag{2.16}$$

As before we need to impose a gauge symmetry that ensures that the cosine terms only tunnel combinations of fields that are built from local fermionic operators. The full fermionic

gauge symmetry group is $\mathsf{Z}_2^4 = \prod_\alpha \mathsf{Z}^\alpha$ where $\alpha = \mathrm{N}, \mathrm{S}, \bar{\mathrm{N}}, \bar{\mathrm{S}}$. The generators of this group denoted as g_α act as

$$\mathsf{g}_\alpha : \begin{bmatrix} \gamma_\alpha \\ \phi_\alpha \end{bmatrix} \longmapsto \begin{bmatrix} -\gamma_\alpha \\ \phi_\alpha \end{bmatrix} + s_\alpha \begin{bmatrix} 0 \\ \frac{\pi}{2} \end{bmatrix}, \tag{2.17}$$

where $s_\alpha = -1$ for $\alpha = \mathrm{S}, \mathrm{S}_T$ and $+1$ otherwise. Inversion squares to $+1$ and simply maps the fields on the northern hemisphere to their counterparts on the southern hemisphere and vice versa. We now proceed to gap out the edge modes. Firstly we combine the Majorana fermions into Dirac fermions

$$\begin{aligned} \psi_\mathrm{M} &\sim e^{i\phi_\mathrm{M}} \sim e^{-i\frac{\pi}{4}}\gamma_\mathrm{N} + e^{i\frac{\pi}{4}}\gamma_\mathrm{S}, \\ \bar{\psi}_\mathrm{M} &\sim e^{-i\bar{\phi}_\mathrm{M}} \sim e^{i\frac{\pi}{4}}\bar{\gamma}_\mathrm{N} + e^{-i\frac{\pi}{4}}\bar{\gamma}_\mathrm{S}. \end{aligned} \tag{2.18}$$

Since the Majorana fermions are themselves Kramers pairs, the action of TRS can be deduced as

$$\mathcal{T} : \begin{bmatrix} \phi_\mathrm{M} \\ \bar{\phi}_\mathrm{M} \end{bmatrix} \longmapsto \begin{bmatrix} \bar{\phi}_\mathrm{M} \\ \phi_\mathrm{M} + \pi \end{bmatrix}. \tag{2.19}$$

The edge is now effectively described by the following K-matrix and charge vector t

$$\begin{aligned} K &= \mathrm{diag}(-1, 2, 2, -1, 1, -2, -2, 1), \\ t &= (0, 1, 1, 1, 0, 1, 1, 1)^\mathsf{T}, \end{aligned} \tag{2.20}$$

in the basis $(\phi_\mathrm{M}, \phi_\mathrm{N}, \phi_\mathrm{S}, \phi, \bar{\phi}_\mathrm{M}, \bar{\phi}_\mathrm{N}, \bar{\phi}_\mathrm{S}, \bar{\phi})^\mathsf{T}$. Consider the gapping terms

$$\begin{aligned} \delta\mathcal{L} = &\cos[4\phi_\mathrm{N} + 4\phi_\mathrm{S} + 4\phi] + \cos[2\phi_\mathrm{N} - 2\phi_\mathrm{S} - 2\phi_\mathrm{M}] \\ &+ \cos[4\bar{\phi}_\mathrm{N} + 4\bar{\phi}_\mathrm{S} + 4\bar{\phi}] + \cos[2\bar{\phi}_\mathrm{N} - 2\bar{\phi}_\mathrm{S} - 2\bar{\phi}_\mathrm{M}]. \end{aligned} \tag{2.21}$$

Note that this expression is basically the gapping term for an inversion symmetric HOTI plus its time-reversed copy. Thus, we only need to check whether the above expression breaks TRS. Clearly, it does not break TRS explicitly; however, since both $\langle\bar{\phi}_\mathrm{N} + \bar{\phi}_\mathrm{S} + \bar{\phi}\rangle$ and $\langle\bar{\phi}_\mathrm{N} - \bar{\phi}_\mathrm{S} - \bar{\phi}_\mathrm{M}\rangle$ transform to their TRS copies with extra π phase, naively it seems like TRS is broken spontaneously. We note that the gauge group is now broken to $\mathsf{Z}_2^{\mathrm{diag}} \times \bar{\mathsf{Z}}_2^{\mathrm{diag}}$, where

$$\begin{aligned} &\mathsf{g}_{\mathrm{diag}} : \phi_\mathrm{N} \mapsto \phi_\mathrm{N} + \frac{\pi}{2}, \phi_\mathrm{S} \mapsto \phi_\mathrm{S} + \frac{\pi}{2}, \phi_\mathrm{M} \mapsto \phi_\mathrm{M} + \pi, \\ &\bar{\mathsf{g}}_{\mathrm{diag}} : \bar{\phi}_\mathrm{N} \mapsto \bar{\phi}_\mathrm{N} + \frac{\pi}{2}, \bar{\phi}_\mathrm{S} \mapsto \bar{\phi}_\mathrm{S} + \frac{\pi}{2}, \bar{\phi}_\mathrm{M} \mapsto \bar{\phi}_\mathrm{M} + \pi. \end{aligned} \tag{2.22}$$

We can see that $\langle\phi_\mathrm{N} + \phi_\mathrm{S} + \phi\rangle \sim \langle\phi_\mathrm{N} + \phi_\mathrm{S} + \phi\rangle + \pi$, $\langle\phi_\mathrm{N} - \phi_\mathrm{S} - \phi_\mathrm{M}\rangle \sim \langle\phi_\mathrm{N} - \phi_\mathrm{S} - \phi_\mathrm{M}\rangle + \pi$ as they are related to each other by a gauge transformation. Therefore TRS is not broken spontaneously either. Finally, we emphasize that without inversion symmetry, the above STO is non-anomalous as we can paste a copy of a quantum spin Hall liquid on, e.g., the southern hemisphere, with its edge modes residing on the equator and gap out the helical modes contributed by the STO without invoking the bulk.

2.2.3 Class D + inversion: HOTSC with chiral Majorana hinge mode

We briefly review the free fermion model for the chiral HOTSC in class D. The strategy to construct a second-order phase is to start with a class DIII topological superconductor and add a TRS-breaking perturbation that gaps out the surface leaving behind a robust hinge protected by inversion symmetry. The surface Hamiltonian is given by [27]

$$h(\vec{k},\vec{r}) = -(\vec{k}\times\hat{n}_{\vec{r}})\cdot\vec{\sigma}, \tag{2.23}$$

The inversion, time reversal and particle-hole symmetries are generated by $\mathcal{I} = -\sigma_0$, $\mathcal{T} = i\sigma_y\mathcal{K}$ and $\mathcal{P} = -(\hat{n}_{\vec{r}}\cdot\vec{\sigma})\sigma_y\mathcal{K}$. The surface can be deformed by the mass term

$$\delta h(\vec{r}) = m_{\vec{r}}(\hat{n}_{\vec{r}}\cdot\vec{\sigma}), \tag{2.24}$$

that breaks TRS. Inversion symmetry demands that $\mathcal{I}\delta h(\vec{r})\mathcal{I}^{-1} = \delta h(-\vec{r})$ which further imposes the condition $m_{\vec{r}} = -m_{-\vec{r}}$, signalling the vanishing of the mass term along some inversion symmetric curve which hosts gapless chiral modes. Due to the additional particle-hole symmetry as compared with the class A chiral HOTI, these are Majorana as opposed to Dirac modes. Before turning to the surface topological order, we first inspect the stability of the chiral hinge modes to inversion symmetric surface pasting of $p\pm ip$ superconductors. Let us consider the situation where there are $N_\pm$ chiral co-propagating Majorana hinge modes denoted as $\chi_i^\pm$ with $i = 1,\ldots,N_\pm$ that transform under inversion as

$$\mathcal{I}: \begin{bmatrix}\chi_i^\pm(\theta)\\ \chi_i^\pm(\theta+\pi)\end{bmatrix} \mapsto \begin{bmatrix}\pm i\chi_i^\pm(\theta+\pi)\\ \mp i\chi_i^\pm(\theta)\end{bmatrix}, \tag{2.25}$$

where θ is introduced to parameterize the equator on which the Majoranas are propagating. The above symmetry action can be derived from the bulk symmetry using a recursive Jackiw-Rebbi procedure (see App. 2.C) [78] and satisfies the basis-invariant relations $\{\mathcal{I},\mathcal{P}\} = 0$, $[\mathcal{I},\mathcal{T}] = 0$ and $\mathcal{I}^2 = 1$. we can always paste a $p+ip$ and $p-ip$ topological superconductor on the northern and southern hemispheres respectively, which contribute a pair of chiral hinge modes denoted as $\gamma^{\mathrm{N,S}}$. The inversion action on these modes is represented as

$$\mathcal{I}: \begin{bmatrix}\gamma^{\mathrm{N}}(\theta)\\ \gamma^{\mathrm{N}}(\theta+\pi)\\ \gamma^{\mathrm{S}}(\theta)\\ \gamma^{\mathrm{S}}(\theta+\pi)\end{bmatrix} \mapsto \begin{bmatrix}i\gamma^{\mathrm{S}}(\theta+\pi)\\ -i\gamma^{\mathrm{S}}(\theta)\\ i\gamma^{\mathrm{N}}(\theta+\pi)\\ -i\gamma^{\mathrm{N}}(\theta)\end{bmatrix}. \tag{2.26}$$

Consider the linear combinations $\gamma^\pm = (\gamma^{\mathrm{N}}\pm\gamma^{\mathrm{S}})/\sqrt{2}$ that transform under inversion as

$$\mathcal{I}: \begin{bmatrix}\gamma^\pm(\theta)\\ \gamma^\pm(\theta+\pi)\end{bmatrix} \mapsto \begin{bmatrix}\pm i\gamma^\pm(\theta+\pi)\\ \mp i\gamma^\pm(\theta)\end{bmatrix}. \tag{2.27}$$

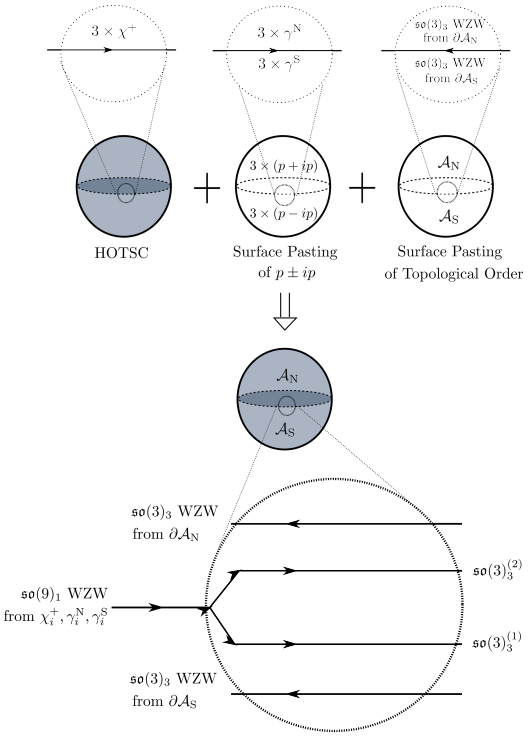

Figure 2.3: An illustration of the procedure used to gap out the $(3,0)$ configuration of chiral Majorana modes χ_i with $i = 1, 2, 3$. We introduce $\gamma_i^{N/S}$ Majoranas by pasting $p \pm ip$ superconductors on the surface and end up with a total of nine Majorana modes on the hinge. These are subsequently gapped out by introducing the STO $\mathcal{A}_{N,S}$ on the northern and southern hemispheres respectively. The nine Majorana modes are described by the $\mathsf{SO}(9)_1$ WZW which splits into two copies of $\mathsf{SO}(3)_3$ theories that gap out upon coupling to the edge modes provided by the STOs.

Henceforth we denote left/right-moving modes with/without an overbar. The configuration (N_+, N_-) with net $N_+ + N_-$ right movers can always be transformed to $(N_+ - 1, N_- - 1)$ by surface pasting. Therefore we have the equivalence relation

$$(N_+, N_-) \sim (N_+ - n, N_- - n), \tag{2.28}$$

where $n \in \mathbb{Z}$. Consequently, we can always transform a configuration (N_+, N_-) into a configuration with all positive parity modes $(N_+ - N_-, 0)$. For this reason we will only need to consider the stability of such modes under surface pasting of topologically ordered phases. The classification of inversion symmetry-protected higher-order phases in class D is given by the group Z_4 which can be indexed by $(N_+, 0)$ (See Sec. 2.3 for details). For the present discussion it will suffice to construct the STO for the generator of Z_4 which may be treated as $(3, 0)$. Since an odd number of Majorana fermions cannot be tamed by Abelian bosonization, the K-matrix approach we previously employed must be abandoned. Instead, we use non-Abelian bosonization to approach the problem. We remark here that

the method in this section is similar in spirit to Ref. [79, 80], however, adapted to inversion symmetry.

We consider the HOTSC to have a spherical geometry as illustrated in Fig. 2.3 with three chiral majorana modes χ_i^+ on the inversion-symmetric equator. In order to show that the chiral hinge can be gapped, we find it convenient to proceed in two steps. First we add additional degrees of freedom on the hinge by a purely surface pasting of $p \pm ip$ superconductors that preserves the inversion symmetry. In the second step, we induce inversion-symmetric topological order on the surface to gap out the combined hinge modes contributed by the $p \pm ip$ superconductors and the bulk higher-order superconductor. We begin by adding three copies of a $p + ip$ superconductor on the northern hemisphere and three copies of a $p - ip$ superconductor on the southern hemisphere. As a result, we end up with 6 additional Majorana modes on the equator which we label as $\{\gamma_i^{\mathrm{N}}, \gamma_i^{\mathrm{S}}\}$, with $i = 1, \ldots, 3$. The hinge is described by the $\mathfrak{so}(9)_1$ WZW theory [81]

$$S = \int \mathrm{d}t\mathrm{d}\theta i \Psi^{\mathsf{T}} (\partial_t - \partial_\theta) \Psi, \tag{2.29}$$

where we have introduced a 9 component Majorana spinor field Ψ. The operator product expansion (OPE) of the Majorana operators satisfies the standard relations

$$\begin{aligned} \chi_i^+(z)\chi_j^{\mathrm{N}}(w) &\sim \frac{\delta_{ij}}{z-w} + \ldots, \\ \gamma_i^{\mathrm{N}}(z)\gamma_j^{\mathrm{N}}(w) &\sim \frac{\delta_{ij}}{z-w} + \ldots, \\ \gamma_i^{\mathrm{S}}(z)\gamma_j^{\mathrm{S}}(w) &\sim \frac{\delta_{ij}}{z-w} + \ldots. \end{aligned} \tag{2.30}$$

We introduce $\mathfrak{so}(9)_1$ currents which can be expressed as fermion biliears,

$$\mathcal{J}^{\mathsf{A}}(z) = \frac{i}{2} \Psi^\dagger(z) \Sigma^{\mathsf{A}} \Psi(z), \tag{2.31}$$

where A is a Lie-algebra index, Σ^{A} are the generators of the $\mathfrak{so}(9)$ lie algebra and z are holomorphic coordinates defined as $z = \theta + it$ on the hinge. The currents $\left\{\mathcal{J}^{\mathsf{A}}\right\}_{\mathsf{A}=1,\ldots\dim(\mathfrak{so}(9))}$ satisfy the OPE

$$\mathcal{J}^{\mathsf{A}}(z)\mathcal{J}^{\mathsf{B}}(w) \sim \frac{\delta^{\mathsf{AB}}}{(z-w)^2} + \frac{i f_C^{AB} \mathcal{J}^C(w)}{z-w} + \ldots, \tag{2.32}$$

where $f_{\mathsf{C}}^{\mathsf{AB}}$ are the structure constants for $\mathfrak{so}(9)$. The action of inversion on the different Majorana operators is as follows

$$\begin{aligned} &\mathcal{I} : \chi_i^+(\theta) \longrightarrow i\chi_i^+(\theta + \pi), \\ &\mathcal{I} : \gamma_i^{\mathrm{N}}(\theta) \longrightarrow i\gamma_i^{\mathrm{S}}(\theta + \pi), \\ &\mathcal{I} : \gamma_i^{\mathrm{S}}(\theta) \longrightarrow i\gamma_i^{\mathrm{N}}(\theta + \pi). \end{aligned} \tag{2.33}$$

In order to construct the surface topological order that can absorb the Majorana hinge modes, it is useful to work with an embedding of $\mathfrak{so}(3)_3^{(1)} \times \mathfrak{so}(3)_3^{(2)} \subset \mathfrak{so}(9)_1$. Since inversion symmetry is an essential part of our setup, we need to be careful about its action on the various embedded components. We work with a choice of embedding such that the two copies of $\mathfrak{so}(3)_3$ are swapped under the action of inversion. Let us index the components of the spinor Ψ by a tuple (i,j) where $i,j = 1,2,3$. We define the different components such that they have the following simple transformation rule under inversion

$$\mathcal{I} : \Psi_{(i,j)}(\theta) \longmapsto i\Psi_{(j,i)}(\theta+\pi) \tag{2.34}$$

with

$$\begin{aligned}
&\Psi_{(i,i)} = \chi_i^+, \\
&\Psi_{(2,3)} = \gamma_1^{\mathrm{N}}, \quad \Psi_{(3,2)} = \gamma_1^{\mathrm{S}}, \\
&\Psi_{(3,1)} = \gamma_2^{\mathrm{N}}, \quad \Psi_{(1,3)} = \gamma_2^{\mathrm{S}}, \\
&\Psi_{(1,2)} = \gamma_3^{\mathrm{N}}, \quad \Psi_{(2,1)} = \gamma_3^{\mathrm{S}}.
\end{aligned} \tag{2.35}$$

In order to construct the $\mathfrak{so}(3)_3$ current operators, consider the matrices defined as $\sigma^{\mathsf{a},1} := \mathrm{L}^{\mathsf{a}} \otimes \mathrm{Id}_3$ and $\sigma^{\mathsf{a},2} := \mathrm{Id}_3 \otimes \mathrm{L}^{\mathsf{a}}$, $\mathsf{a} = 1,2,3$, where L^{a} are the generators of $\mathfrak{so}(3)$ in the fundamental representation. These matrices generate two decoupled $\mathfrak{so}(3)$ algebras

$$\left[\sigma^{\mathsf{a},\kappa}, \sigma^{\mathsf{b},\kappa'}\right] = \delta^{\kappa\kappa'} f_{\mathsf{c}}^{\mathsf{ab}} \sigma^{\mathsf{c},\kappa}. \tag{2.36}$$

Using this decomposition we define the following $\mathfrak{so}(3)_3 \times \mathfrak{so}(3)_3$ currents

$$\mathcal{J}^{\mathsf{a},\kappa} = \frac{i}{2} \Psi^\dagger \sigma^{\mathsf{a},\kappa} \Psi, \tag{2.37}$$

which explicitly take the form

$$\begin{aligned}
\mathcal{J}^{1,1} &= \frac{i}{2}\left[\left(\gamma_3^{\mathrm{S}}\right)^{(\dagger)} \gamma_2^{\mathrm{N}} + \left(\chi_2^+\right)^{(\dagger)} \gamma_1^{\mathrm{S}} + \left(\gamma_1^{\mathrm{N}}\right)^{(\dagger)} \chi_3^+\right] + \mathrm{h.c.}, \\
\mathcal{J}^{1,2} &= \frac{i}{2}\left[\left(\gamma_3^{\mathrm{N}}\right)^{(\dagger)} \gamma_2^{\mathrm{S}} + \left(\chi_2^+\right)^{(\dagger)} \gamma_1^{\mathrm{N}} + \left(\gamma_1^{\mathrm{S}}\right)^{(\dagger)} \chi_3^+\right] + \mathrm{h.c.}, \\
\mathcal{J}^{2,1} &= \frac{i}{2}\left[\left(\chi_1^+\right)^{(\dagger)} \gamma_2^{\mathrm{N}} + \left(\gamma_3^{\mathrm{N}}\right)^{(\dagger)} \gamma_1^{\mathrm{S}} + \left(\gamma_2^{\mathrm{S}}\right)^{(\dagger)} \gamma_3^+\right] + \mathrm{h.c.}, \\
\mathcal{J}^{2,2} &= \frac{i}{2}\left[\left(\chi_1^+\right)^{(\dagger)} \gamma_2^{\mathrm{S}} + \left(\gamma_3^{\mathrm{S}}\right)^{(\dagger)} \gamma_1^{\mathrm{N}} + \left(\gamma_2^{\mathrm{N}}\right)^{(\dagger)} \chi_3^+\right] + \mathrm{h.c.}, \\
\mathcal{J}^{3,1} &= \frac{i}{2}\left[\left(\chi_1^+\right)^{(\dagger)} \gamma_3^{\mathrm{S}} + \left(\gamma_3^{\mathrm{N}}\right)^{(\dagger)} \chi_2^+ + \left(\gamma_2^{\mathrm{S}}\right)^{(\dagger)} \gamma_1^{\mathrm{N}}\right] + \mathrm{h.c.}, \\
\mathcal{J}^{3,2} &= \frac{i}{2}\left[\left(\chi_1^+\right)^{(\dagger)} \gamma_3^{\mathrm{N}} + \left(\gamma_3^{\mathrm{S}}\right)^{(\dagger)} \chi_2^+ + \left(\gamma_2^{\mathrm{N}}\right)^{(\dagger)} \gamma_1^{\mathrm{S}}\right] + \mathrm{h.c.}.
\end{aligned} \tag{2.38}$$

The reason why we write $(\dagger)$ on the Majorana operator is to remind ourselves of the subtlety related to the imaginary action of inversion, e.g., if $\mathcal{I} : \chi_i^+(\theta) \mapsto i\chi_i^+(\theta+\pi)$, then $\mathcal{I}$:

$(\chi_i^+(\theta))^{(\dagger)} \mapsto (\chi_i^+(\theta+\pi))^{(\dagger)}(-i)$. We can verify that inversion acts as $\mathcal{I} : \mathcal{J}^{\mathsf{a},1} \leftrightarrow \mathcal{J}^{\mathsf{a},2}$ on the $\mathfrak{so}(3)$ currents. From the standard OPE for Majorana operators, we can extract the OPE for the $\mathfrak{so}(3)_3$ currents, and verify that the level is indeed 3 (see App. 2.B). The stress tensor decomposes as

$$T_{\mathfrak{so}(9)_1} = T_{\mathfrak{so}(3)_3^{(1)}} + T_{\mathfrak{so}(3)_3^{(2)}}, \tag{2.39}$$

which means that the chiral central charges of the embedded sectors add up to give the chiral central charge of the $\mathfrak{so}(9)_1$ WZW theory. Having formulated the hinge modes as two copies of $\mathfrak{so}(3)_3$, it is a straightforward task to gap them out by adding surface topological order. We introduce $\mathcal{A}_{\mathrm{N}} = \overline{\mathcal{A}_{\mathrm{S}}} = \overline{\mathsf{SO}(3)_3}$ whose edge conformal field theories and corresponding current operators we denote as $\overline{\mathfrak{so}(3)}_{3,\mathrm{N/S}}$ and $\bar{\mathcal{J}}^{\mathsf{a}}_{\mathrm{N/S}}$, respectively [79]. Under inversion the currents transform as

$$\mathcal{I} : \bar{\mathcal{J}}^{\mathsf{a}}_{\mathrm{N}}(\theta) \longmapsto \bar{\mathcal{J}}^{\mathsf{a}}_{\mathrm{S}}(\theta+\pi). \tag{2.40}$$

The hinge modes $\mathcal{J}^{\mathsf{a},\kappa}$ and the edge modes of the surface topological order $\bar{\mathcal{J}}^{\mathsf{a}}_{\mathrm{N/S}}$ can together be gapped out upon adding the gapping term

$$\delta\mathcal{L} = \lambda(\theta) \sum_{\mathsf{a}=1}^{3} \Big[\bar{\mathcal{J}}^{\mathsf{a}}_{\mathrm{N}}(\theta)\mathcal{J}^{\mathsf{a},1}(\theta) + \bar{\mathcal{J}}^{\mathsf{a}}_{\mathrm{S}}(\theta)\mathcal{J}^{\mathsf{a},2}(\theta) \Big], \tag{2.41}$$

which is inversion symmetric if $\lambda(\theta) = \lambda(\theta+\pi)$. Therefore, we can choose λ to be constant. To summarize, we have shown that the hinge modes $(3,0)$ can first be mapped to $(3,6)$ by purely surface pasting of $p \pm ip$ superconductors. Thereafter, two copies of $\mathfrak{so}(3)_3$ can be embedded in the $(3,6)$ configuration which can be gapped out by a surface pasting of $\mathsf{SO}(3)_3$ topological order. We remark that, if we try to directly gap out a single chiral majorana, i.e., the configuration $(1,0)$, without the procedure of pasting $p \pm ip$, the situation requires us to use a fermionic surface topological order with chiral central charge equal to $1/4$, provided that the gapping channel can be found. We do not know of such a fermionic topological order that is not the one we used, up to a condensation with a bosonic anti-chiral phase. Eventually we decided to use our current strategy laid out in this section.

2.2.4 Class DIII + inversion: HOTSC with helical Majorana hinge modes

Class DIII superconductors enriched by inversion symmetry support non-trivial second and third-order topological phases which host robust helical modes and Majorana Kramers zero modes on inversion symmetric loci on the surface [27]. The helical hinge modes are similar to those obtained on the edge of a 2D TRS invariant topological superconductor, i.e they contain a Majorana Kramers' pair of counter-propagating modes. Here we show that these modes can be gapped out if we allow for the possibility of surface topological order.

First we briefly review the free-fermion model for the helical HOTSC. We can start with two class DIII topological superconductors with opposite topological index and add symmetry-respecting perturbations that gap out the surface, leaving behind a robust hinge. The surface Hamiltonian prior to adding such a mass term is given by

$$h(\vec{k},\vec{r}) = -\rho_z \otimes (\vec{k} \times \hat{n}_{\vec{r}}) \cdot \vec{\sigma}, \tag{2.42}$$

where ρ_μ and σ_μ are the Pauli matrices in the orbital and spin space respectively. The inversion, time reversal and particle-hole symmetries are generated by $\mathcal{I} = -\rho_z \otimes \sigma_0$, $\mathcal{T} = \rho_0 \otimes i\sigma_y\mathcal{K}$ and $\mathcal{P} = -\rho_z \otimes (\hat{n}_{\vec{r}} \cdot \vec{\sigma})\sigma_y\mathcal{K}$. To perturb the Hamiltonian, we add the following mass term that respects the symmetries

$$\delta h(\vec{r}) = m_{\vec{r}}\rho_x \otimes \sigma_0. \tag{2.43}$$

Inversion symmetry demands that $\mathcal{I}\delta h(\vec{r})\mathcal{I}^{-1} = \delta h(-\vec{r})$ which further imposes the condition $m_{\vec{r}} = -m_{-\vec{r}}$, signalling the vanishing of the mass term along some inversion symmetric curve which we choose to be at the equator. After Jackiw-Rebbi projection, we may verify that a pair of helical Majorana modes resides at the hinge.

The classification of inversion symmetry enriched higher-order phases in class DIII is given by the group Z_4 which can be indexed by the number of Majorana helical hinge modes modulo 4 (See Sec. 2.3 for details). For the present discussion it will suffice to construct the STO for the generator of Z_4 which may be treated as $(3, 0)$. We first show that an odd number of helical modes is stable to weak interaction, and they are only unstable to adding topological order on the surface.

2.2.4.1 Stability of odd number of helical hinge modes

For concreteness, let us begin with the setup with three pairs of helical Majorana modes on the hinge. The Lagrangian density for the Majorana modes can be written as

$$\mathcal{L} = \sum_{j=1}^{2n+1} \Big[i\chi_j(\partial_t - \partial_x)\chi_j + i\bar{\chi}_j(\partial_t + \partial_x)\bar{\chi}_j \Big], \tag{2.44}$$

with $n = 1$ which is the non-chiral $\mathfrak{so}(3)_1$ WZW theory. For simplicity, we drop the explicit hermitian conjugation from the equations in this subsection as they do not play a role unless we are dealing with a imaginary symmetry representation such as inversion in Eq. (2.76). Here we are only interested in the stability of pairs of helical-modes under TRS which has a real representation. The holomorphic and anti-holomorphic currents that generate the $\mathfrak{so}(3)$ current algebra are

$$\mathcal{J}^{\mathsf{a}} = \frac{i}{2}\chi_j \mathrm{L}^{\mathsf{a}}_{jk}\chi_k = \frac{i}{2}\epsilon^{\mathsf{a}jk}\chi_j\chi_k$$

$$\bar{\mathcal{J}}^{\mathsf{a}} = \frac{i}{2}\bar{\chi}_j \mathrm{L}^{\mathsf{a}}_{jk}\bar{\chi}_k = \frac{i}{2}\epsilon^{\mathsf{a}jk}\bar{\chi}_j\bar{\chi}_k, \tag{2.45}$$

where $\mathsf{a} = 1, \ldots, \dim(\mathfrak{so}(3))$, and as before L^{a} are the generators for the $\mathfrak{so}(3)$ Lie algebra. The model is TRS invariant with the TRS action given by Eq. (2.75) for each pair $(\chi_j, \bar{\chi}_j)$. We are interested in the stability of this model to TRS invariant perturbations. More precisely, whether the theory can be completely gapped out without breaking TRS. At the quadratic level we can add the following terms to the Hamiltonian

$$\begin{aligned}\delta H &= \sum_{j,k,l} i m_j \epsilon^{jkl}(\chi_k\bar{\chi}_l + \bar{\chi}_k\chi_l) + \sum_j i\widetilde{m}_j\chi_j\bar{\chi}_j \\ &= \sum_j \left[m_j\mathcal{O}^j + i\widetilde{m}_j\chi_j\bar{\chi}_j\right],\end{aligned} \tag{2.46}$$

where, in the second second line we have defined the fermion bilinear $\mathcal{O}^j = i\epsilon^{jkl}(\chi_k\bar{\chi}_l + \bar{\chi}_k\chi_l)$. TRS imposes that $\widetilde{m}_j = -\widetilde{m}_j = 0$, while there are no such constraints on m_j. The operators $\mathcal{O}^j$ satisfy the algebra

$$\left[\mathcal{O}^j, \mathcal{O}^k\right] = 4(\chi_j\chi_k + \bar{\chi}_j\bar{\chi}_k), \tag{2.47}$$

which suggests that these operators cannot condense/acquire a ground state expectation value simultaneously. This may pose an obstruction to symmetrically gapping out the theory. Since the model is quadratic, we simply diagonalize the Hamiltonian and check whether this is the case. The full Hamiltonian reads

$$\begin{aligned}H &= \sum_j \int \mathrm{d}x \Big\{ iv\left(\chi_j\partial_x\chi_j - \bar{\chi}_j\partial_x\bar{\chi}_j\right) + \sum_j i m_j\mathcal{O}^j \Big\} \\ &= \int_k dk \Psi_k^{\mathsf{T}} H(k) \Psi_k,\end{aligned} \tag{2.48}$$

where in the second line, we have introduced the spinor $\Psi^{\mathsf{T}} = (\chi_1, \bar{\chi}_1, \chi_2, \bar{\chi}_2, \chi_3, \bar{\chi}_3)$ and transformed to momentum space. The explicit form of $H(k)$ is

$$H(k) = vk\mathrm{Id}_3 \otimes \sigma^z + \sum_j i m_j \mathrm{L}^j \otimes \sigma^y. \tag{2.49}$$

The spectrum of $H(k)$ is gapless with the eigenvectors $|\psi_1\rangle = (m_1, m_2, m_3)^{\mathsf{T}} \otimes (1, 0)^{\mathsf{T}}$ and $|\psi_2\rangle = (m_1, m_2, m_3)^{\mathsf{T}} \otimes (0, 1)^{\mathsf{T}}$ having eigenvalues $\pm vk$. We are able to find the above two vectors due to the simple condition that

$$\mathrm{Ker}\Big[\sum_j m_j \mathrm{L}^j\Big] \neq \varnothing, \tag{2.50}$$

which follows from the fact that $\mathrm{L} \equiv \sum_j m_j \mathrm{L}^j$ is a generic 3×3 anti-symmetric matrix, and is therefore singular, since

$$\det(\mathrm{L}^{\mathsf{T}}) = \det(-\mathrm{L}) = (-1)^3 \det(\mathrm{L}). \tag{2.51}$$

The above argument can be directly generalized to any odd number of helical modes, since the corresponding L will always be singular, and result in the existence of gapless eigenvectors. More generally, we may use a mathematical theorem [82] that states any antisymmetric matrix L can be block diagonalized by conjugating with an orthogonal matrix. We can then verify that for an even number of helical modes, we can block diagonalize the Hamiltonian into 2×2 blocks with a gapped spectrum.

Having established the stability of an odd number of helical modes at the non-interacting level, we proceed to examine the effect of four fermion or current-current interaction terms for the $\mathfrak{so}(3)_1 \times \overline{\mathfrak{so}(3)}_1$ theory. The action of TRS on the currents is

$$\mathcal{T} : \mathcal{J}^{\mathsf{a}} \longleftrightarrow -\bar{\mathcal{J}}^{\mathsf{a}}. \tag{2.52}$$

Therefore the general form of TRS invariant current-current interaction terms is

$$\delta H_{\mathsf{int}} = \sum_{\mathsf{a}} \lambda_{\mathsf{a}} \mathcal{J}^{\mathsf{a}} \bar{\mathcal{J}}^{\mathsf{a}} + \sum_{\mathsf{a},\mathsf{b}} \lambda_{\mathsf{ab}} \left(\mathcal{J}^{\mathsf{a}} \bar{\mathcal{J}}^{\mathsf{b}} + \bar{\mathcal{J}}^{\mathsf{a}} \mathcal{J}^{\mathsf{b}} \right). \tag{2.53}$$

We examine the λ_{a} terms first. The term $\mathcal{J}^{\mathsf{a}} \bar{\mathcal{J}}^{\mathsf{a}}$ can be decomposed into two kinds of bilinears: those of the form $\chi^j \bar{\chi}^j$, $j \neq \mathsf{a}$, and those of the form $\mathcal{O}^{\mathsf{a}}$. In other words if λ_{a} were to flow to strong coupling, at least one of these bilinears would be expected to acquire a groundstate expectation value. Since the former kind breaks TRS, this would lead to a groundstate that spontaneously breaks TRS. Alternatively, we could consider the scenario where $\mathcal{O}^{\mathsf{a}}$ acquires an expectation value. An important observation is that

$$\left(\mathcal{O}^j\right)^2 \propto \mathcal{J}^j \bar{\mathcal{J}}^j, \tag{2.54}$$

up to a constant term. Therefore, by ramping up λ^1 for example, we can gap out the modes $\chi_{2,3}$ and $\bar{\chi}_{2,3}$ by condensing $\mathcal{O}^{\mathsf{1}} \propto (\chi_2 \bar{\chi}_3 + \bar{\chi}_2 \chi_3)$. Crucially though, we cannot gap out the entire theory by simultaneously condensing $\mathcal{O}^{1,2,3}$, as these operators satisfy the non-trivial algebra in Eq. (2.47). This can be understood as a generalization of the Haldane criterion to non-Abelian current algebras.

Next, we turn to the terms of the form $\lambda_{\mathsf{ab}}(\mathcal{J}^{\mathsf{a}} \bar{\mathcal{J}}^{\mathsf{b}} + \bar{\mathcal{J}}^{\mathsf{a}} \mathcal{J}^{\mathsf{b}})$. We are interested in how the groundstate at $\lambda_{\mathsf{ab}} \to \infty$ transforms under TRS. To this end, we decouple the interaction term into possible products of fermion bilinears and ask whether we can find a decoupling where each bilinear is invariant under TRS. Let us illustrate this procedure with an explicit example. Consider the term

$$\begin{aligned} \mathcal{J}^1 \bar{\mathcal{J}}^2 + \bar{\mathcal{J}}^1 \mathcal{J}^2 &= (i\chi_2\chi_3)(i\bar{\chi}_1\bar{\chi}_3) + (i\bar{\chi}_2\bar{\chi}_3)(i\chi_1\chi_3) \\ &= (i\chi_3\bar{\chi}_3)(i\bar{\chi}_1\chi_2 - i\chi_1\bar{\chi}_2). \end{aligned} \tag{2.55}$$

This is the only possible decoupling for the term proportional to λ_{12}; the terms proportional to the other λ_{ab}'s all have similarly unique decouplings. Crucially, both the bilinears in the decoupling transform non-trivially under TRS and such an interaction cannot have a TRS invariant groundstate.

The above considerations generalize to any odd number of helical modes. For an even number of helical modes, say $2n$, we can construct an interaction term that gaps out all the modes while preserving the TRS. Consider the matrices $\widetilde{\mathrm{L}}^{\mathsf{a}}_{2n}$ with $\mathsf{a} = 1, \ldots, n$ which generate a $\mathfrak{so}(2)^n$ subgroup $\mathfrak{so}(2n)$. The matrix $\mathrm{L}^{\mathsf{a}}_{2n}$ basically generates rotations in $x_{2\mathsf{a}-1}$-$x_{2\mathsf{a}}$ plane in $\mathbb{R}^{2n}$. Then we can construct the currents

$$\mathcal{J}^{\mathsf{a}} := \frac{i}{2}\chi_j \widetilde{\mathrm{L}}^{\mathsf{a}}_{2n,jk}\chi_k = i\chi_{2\mathsf{a}-1}\chi_{2\mathsf{a}}, \tag{2.56}$$

and analogously we define the antiholomorphic currents $\bar{\mathcal{J}}^{\mathsf{a}}$. Then we may write down the interaction term

$$\begin{aligned}\delta H &= \lambda \sum_{\mathsf{a}=1}^{n} \mathcal{J}^{\mathsf{a}}\bar{\mathcal{J}}^{\mathsf{a}} \\ &= \lambda \sum_{\mathsf{a}=1}^{n} (i\chi_{2\mathsf{a}-1}\bar{\chi}_{2\mathsf{a}} + i\bar{\chi}_{2\mathsf{a}-1}\chi_{2\mathsf{a}})^2 + \text{const.}.\end{aligned} \tag{2.57}$$

Since the terms $(i\chi_{2\mathsf{a}-1}\bar{\chi}_{2\mathsf{a}} + i\bar{\chi}_{2\mathsf{a}-1}\chi_{2\mathsf{a}})$ are TRS invariant and commute mutually for all a, adding such a term gaps out all $2n$ helical modes simultaneously.

2.2.4.2 Gapping out the surface with topological order

In this subsection, we describe the STO for second-order 3D class DIII HOTSC protected by inversion symmetry. Here we start with the system that originally carries three pairs of helical Majorana modes along the hinge. Since the class DIII hinge modes can be regarded as a stack of class D hinge modes with their time-reversed partners, a natural candidate of the STO for class DIII is given by stacking the STO for class D with its time-reversed partner which is $\mathsf{SO}(3)_3 \times \overline{\mathsf{SO}(3)_3}$.

We consider the HOTSC to have a spherical geometry with three pairs of helical Majorana modes $\chi_i, \bar{\chi}_i$ propagating along the equator on the surface. First we add three copies of class DIII superconductors on the northern and southern hemisphere, ending up with 6 additional pairs of helical Majorana modes on the equator which we label as $\gamma_i^{\mathrm{N/S}}, \bar{\gamma}_i^{\mathrm{N/S}}$. The hinge is described by the $\mathfrak{so}(9)_1 \times \overline{\mathfrak{so}(9)_1}$ WZW theory. The action of inversion on the

different Majorana operators is as follows

$$\mathcal{I}: \begin{bmatrix} \chi_i \\ \gamma_i^{\mathrm{N}} \\ \gamma_i^{\mathrm{S}} \\ \bar{\chi}_i \\ \bar{\gamma}_i^{\mathrm{N}} \\ \bar{\gamma}_i^{\mathrm{S}} \end{bmatrix} (\theta) \longrightarrow \begin{bmatrix} i\chi_i \\ i\gamma_i^{\mathrm{S}} \\ i\gamma_i^{\mathrm{N}} \\ -i\bar{\chi}_i \\ -i\bar{\gamma}_i^{\mathrm{S}} \\ -i\bar{\gamma}_i^{\mathrm{N}} \end{bmatrix} (\theta + \pi). \tag{2.58}$$

Next, we carry out the conformal embedding procedure i.e. we embed $\mathfrak{so}(3)_3 \times \mathfrak{so}(3)_3 \subset \mathfrak{so}(9)_1$ and $\overline{\mathfrak{so}}(3)_3 \times \overline{\mathfrak{so}}(3)_3 \subset \overline{\mathfrak{so}}(9)_1$. Since the recipe is identical to that described for the holomorphic CFT in Sec. 2.2.3, we do not repeat the procedure here. Eventually, we end up with chiral and anti-chiral current operators that transform under the inversion-symmetry action as

$$\mathcal{I}: \begin{bmatrix} \mathcal{J}^{\mathsf{a},1} \\ \bar{\mathcal{J}}^{\mathsf{a},1} \end{bmatrix} (\theta) \longmapsto \begin{bmatrix} \mathcal{J}^{\mathsf{a},2} \\ \bar{\mathcal{J}}^{\mathsf{a},2} \end{bmatrix} (\theta + \pi), \tag{2.59}$$

where 'a' labels the generators of $\mathfrak{so}(3)$. Similarly, under TRS, the currents transform as

$$\mathcal{T}: \mathcal{J}^{\mathsf{a},\kappa} \longleftrightarrow -\bar{\mathcal{J}}^{\mathsf{a},\kappa}, \tag{2.60}$$

where $\kappa \in \{1, 2\}$. In order to gap out these current operators, we introduce topological order $\mathcal{A}_{\mathrm{N}}$ and $\mathcal{A}_{\mathrm{S}}$ on the northern and southern hemispheres, respectively, with $\mathcal{A}_{\mathrm{N}} = \mathsf{SO}(3)_3 \times \overline{\mathsf{SO}(3)}_3$. Conveniently, the symmetry transformation properties of the edge modes induced on the hinge from the topological order are identical to those of the aforementioned modes obtained from the conformal embedding procedure. We denote the modes provided by the topological orders on the northern and southern hemispheres with subscripts N and S. Under inversion and TRS,

$$\begin{aligned} \mathcal{I}: \mathcal{J}^{\mathsf{a}}_{\mathrm{N,S}}(\theta) &\longmapsto \mathcal{J}^{\mathsf{a}}_{\mathrm{S,N}}(\theta + \pi), \\ \mathcal{I}: \bar{\mathcal{J}}^{\mathsf{a}}_{\mathrm{N,S}}(\theta) &\longmapsto \bar{\mathcal{J}}^{\mathsf{a}}_{\mathrm{S,N}}(\theta + \pi), \\ \mathcal{T}: \mathcal{J}^{\mathsf{a}}_{\mathrm{N,S}}(\theta) &\longleftrightarrow -\bar{\mathcal{J}}^{\mathsf{a}}_{\mathrm{N,S}}(\theta). \end{aligned} \tag{2.61}$$

The hinge modes $\mathcal{J}^{\mathsf{a},\kappa}, \bar{\mathcal{J}}^{a,\kappa}$ and the edge modes of the surface topological order $\mathcal{J}^{\mathsf{a}}_{\mathrm{N/S}}, \bar{\mathcal{J}}^{\mathsf{a}}_{\mathrm{N/S}}$ can together be gapped out upon adding the gapping term

$$\begin{aligned} \delta\mathcal{L} = \lambda(\theta) \sum_{\mathsf{a}=1}^{3} \Big[&\bar{\mathcal{J}}^{\mathsf{a}}_{\mathrm{N}}(\theta)\mathcal{J}^{\mathsf{a},1}(\theta) + \bar{\mathcal{J}}^{\mathsf{a}}_{\mathrm{S}}(\theta)\mathcal{J}^{\mathsf{a},2}(\theta) \\ &+ \mathcal{J}^{\mathsf{a}}_{\mathrm{N}}(\theta)\bar{\mathcal{J}}^{\mathsf{a},1}(\theta) + \mathcal{J}^{\mathsf{a}}_{\mathrm{S}}(\theta)\bar{\mathcal{J}}^{\mathsf{a},2}(\theta) \Big], \end{aligned} \tag{2.62}$$

which is TRS invariant, and inversion symmetric if $\lambda(\theta) = \lambda(\theta + \pi)$. Therefore, we can choose λ to be constant.

2.3 Surface topological order for third order topological phases

In this subsection, we discuss the surface topological order for third order topological phases protected by inversion symmetry in addition to possible Altland-Zirnbauer symmetries. In total there are five Altland-Zirnbauer classes that support non-trivial third-order topology upon imposing inversion symmetry. These are D, BDI, AIII, DIII and CII. In what follows we present the STO for classes D, BDI and AIII together, as these classes and consequently their STOs are closely related.

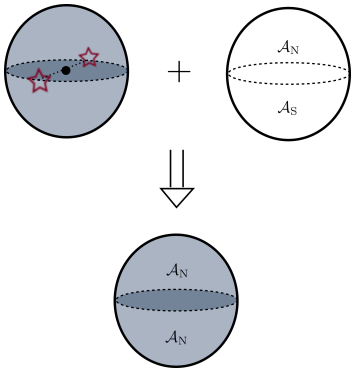

Figure 2.4: Surface topological order for third order topological phases protected by inversion symmetry. In the picture, the red stars denote the zero modes located at antipodal points of the surface.

2.3.1 Class D, BDI and AIII

We begin with the discussion of class D. Note that the third-order inversion-symmetric class D superconductor can be obtained by stacking two copies of second-order inversion-symmetric class D superconductors whose surface contains the configuration $(1,0)\oplus(1,0) = (2,0) \sim (1,-1)$ in the notation used in Sec. 2.2.3. The configuration $(1,-1)$ contains a pair of counter-propagating chiral modes χ^+ and $\bar{\chi}^-$ which are unstable to a mass term $im(\theta)(\chi^+(\theta))^{(\dagger)}\bar{\chi}^-(\theta)$. The inversion symmetry imposes that $m(\theta+\pi) = -m(\theta)$ and consequently, the mass vanishes at two anti-podal points which contain Majorana zero-modes. Furthermore since we can always gap out Majorana modes in pairs, $(2,0)\oplus(2,0) = (4,0) \sim (0,0)$. This agrees with the result [83, 27] that 3D class D higher-order topological superconductors enriched by inversion symmetry are classified by Z_4 which is an extension of Z_2 (second-order phases) by Z_2 (third-order phases).

Here we describe the procedure to gap out two surface Majorana zero modes (or equivalently the (2,0) configuration) by pasting inversion symmetric surface topological order. First we start with the configuration $(-6,-6)$ which is obtained by pasting 6 inversion symmetric copies of $p \pm ip$ on the surface. Next we paste $\mathfrak{so}(3)_3 \times \mathfrak{so}(3)_3$ on the northern and

southern hemispheres which effectively provides additional modes corresponding to $(12, 6)$. Upon such a surface pasting, we end up with $(-6, -6) \oplus (12, 6) = (6, 0) \sim (2, 0)$. Since we can create two Majorana zero modes on antipodal points on the surface without manipulating the bulk, we can always absorb the surface modes contributed by a third order class D superconductor.

Having obtained the STO for class D, we now proceed to discuss the surface topological order for 3D inversion TSC in BDI class. According to Ref. [27], 3D inversion-symmetric TSC in class BDI has a third order phase but no non-trivial first or second order phases. Conveniently, we make use of the notion of *block state* introduced in Ref. [84, 85]. Generically, a block state $|\Psi\rangle$ has the form $|\Psi\rangle = \bigotimes_{b\in B} |\psi_b\rangle$, where B is a collection of blocks, and block b is a d_b-dimensional system embedded in a d-dimensional space. In our case, the wavefunction of a non-trivial third order phase is physically equivalent (up to a inversion-symmetric finite depth unitary circuit) to a block state $|\Psi\rangle = |\Psi_1\rangle \otimes |\Psi_a\rangle$ where $|\Psi_1\rangle$ denotes a state in the non-trivial phase of the 1D BDI Majorana chain embedded in the 3D space with inversion symmetry, and $|\Psi_a\rangle$ denotes a state, describing the rest of the 3D space, in the trivial phase. The 1D BDI Majorana chain can be described by the following Hamiltonian

$$\hat{H} = \frac{1}{2}\int dx \hat{\psi}^\dagger(x) H(x) \hat{\psi}(x), \tag{2.63}$$

where

$$H(x) = -i\tau_y \partial_x + m(x)\tau_z, \quad \hat{\psi}^\dagger = (a_x^\dagger, a_x), \tag{2.64}$$

with $a_x^\dagger$ being a complex fermion creation operator. The Altland-Zirnbauer symmetries are represented as

$$\mathcal{T} = \mathcal{K}, \quad \mathcal{P} = \tau_x \mathcal{K}, \quad \mathcal{I} = \tau_z. \tag{2.65}$$

The mass profile $m(x)$ is positive (negative) inside (outside) the chain. If we denote the two edges of this chain as x^+ and x^- separately, then Jackiw-Rebbi procedure shows that these two edges host Majorana zero modes γ_{x^+} and γ_{x^-}, which have the form [18]

$$\begin{aligned} \gamma_{x^+} &= \int dx \frac{1}{\sqrt{2}}(a_x + a_x^\dagger) e^{\int_{x_a}^x dx' m(x')}, \\ \gamma_{x^-} &= \int dx \frac{i}{\sqrt{2}}(-a_x + a_x^\dagger) e^{-\int_{x_b}^x dx' m(x')}, \end{aligned} \tag{2.66}$$

where $x_{a/b}$ are parameters that ensure the normalization condition $\int dx e^{2\int_{x_a}^x dx' m(x')} = \int dx e^{-2\int_{x_b}^x dx' m(x')} = 1$. The actions of TRS and inversion are as follows

$$\mathcal{T}\gamma_{x^+}\mathcal{T}^{-1} = \gamma_{x^+}, \quad \mathcal{T}\gamma_{x^-}\mathcal{T}^{-1} = -\gamma_{x^-}. \tag{2.67}$$

$$\mathcal{I}\gamma_{x^+}\mathcal{I}^{-1} = i\gamma_{x^-}, \quad \mathcal{I}\gamma_{x^-}\mathcal{I}^{-1} = -i\gamma_{x^+}. \tag{2.68}$$

The above symmetry actions satisfy the basis invariant relations $\{\mathcal{I},\mathcal{P}\}=0$, $[\mathcal{I},\mathcal{T}]=0$, $\mathcal{T}^2=1$ and $\mathcal{I}^2=1$, independently agreeing with Ref. [27]. We thus propose that the STO for 3D third order inversion TSC in BDI class to be $\mathsf{SO}(3)_3\times\overline{\mathsf{SO}(3)_3}$, which is the same as we found for the 3D third order inversion TSC in D class. Recall that in Section 2.2.3, we showed that an inversion symmetric surface realization of $\mathsf{SO}(3)_3$ contains a gapless modes (denoted as $\mathcal{J}^{\mathsf{a}}_{\mathrm{N/S}}$ currents) appearing on an inversion-symmetric line (chosen as the equator for our convenience). We then used such a current mode to gap out the 9 chiral Majorana modes on the equator contributed by the bulk as well as the surface pasting of $p\pm ip$ superconductors. Similarly, $\mathsf{SO}(3)_3\times\overline{\mathsf{SO}(3)_3}$, which is the proposed STO for class BDI, has 9 pairs of counter-propagating Majorana modes, without the contribution from the bulk. Let us denote these modes as $\alpha_i,\bar{\alpha}_i$ with $i=1,\ldots,9$. The TRS action on the Majorana modes is

$$\mathcal{T}: i\mapsto -i,\ \begin{bmatrix}\alpha_i\\ \bar{\alpha}_i\end{bmatrix}\mapsto\begin{bmatrix}\bar{\alpha}_i\\ \alpha_i\end{bmatrix}. \tag{2.69}$$

While the inversion acts naturally on the current operators contributed by the STO on the equatorial hinge as

$$\mathcal{I}:\begin{bmatrix}\mathcal{J}^{\mathsf{a}}_{\mathrm{N}}\\ \bar{\mathcal{J}}^{\mathsf{a}}_{\mathrm{N}}\end{bmatrix}(\theta)\longleftrightarrow\begin{bmatrix}\mathcal{J}^{\mathsf{a}}_{\mathrm{S}}\\ \bar{\mathcal{J}}^{\mathsf{a}}_{\mathrm{S}}\end{bmatrix}(\theta+\pi). \tag{2.70}$$

After the conformal embedding, we regroup the Majoranas as $\chi_i,\gamma_i^{(1)},\gamma_i^{(2)},\bar{\chi}_i,\bar{\gamma}_i^{(1)},\bar{\gamma}_i^{(2)}$, where the definition is taken as

$$\begin{aligned}\chi_{1,2,3}\equiv&\alpha_{1,2,3},\\ \gamma^{(1)}_{1,2,3}\equiv&\ \alpha_{4,5,6},\\ \gamma^{(2)}_{1,2,3}\equiv&\ \alpha_{7,8,9},\end{aligned} \tag{2.71}$$

and similarly for the $\bar{\chi}_i,\bar{\gamma}_i^{(1)},\bar{\gamma}_i^{(2)}$. Inversion action on the Majoranas is

$$\mathcal{I}:\begin{bmatrix}\chi_i\\ \gamma_i^{(1)}\\ \gamma_i^{(2)}\\ \bar{\chi}_i\\ \bar{\gamma}_i^{(1)}\\ \bar{\gamma}_i^{(2)}\end{bmatrix}(\theta)\longrightarrow\begin{bmatrix}i\chi_i\\ i\gamma_i^{(2)}\\ i\gamma_i^{(1)}\\ -i\bar{\chi}_i\\ -i\bar{\gamma}_i^{(2)}\\ -i\bar{\gamma}_i^{(1)}\end{bmatrix}(\theta+\pi). \tag{2.72}$$

We now proceed to gap these modes in groups. For the γ's and $\bar{\gamma}$'s, we can write the following gapping term

$$\delta\hat{H}_1=\sum_i m_1(\theta)(i(\gamma_i^{(1)})^{(\dagger)}\bar{\gamma}_i^{(1)}-i(\gamma_i^{(2)})^{(\dagger)}\bar{\gamma}_i^{(2)}), \tag{2.73}$$

which gaps all the γ and $\bar{\gamma}$. For the χ's, $\bar{\chi}$'s, we can write the following gapping term:

$$\delta\hat{H}_2 = \sum_i m_{2,i}(\theta)(i\chi_i^{(\dagger)}\bar{\chi}_i). \tag{2.74}$$

Note that inversion forces $m_{2,i}(\theta) = -m_{2,i}(\theta + \pi)$, and each counter propagating $\chi, \bar{\chi}$ contributes a pair of Majorana zero modes. Since we have three pairs of counter-propagating $\chi, \bar{\chi}$, two pairs of Majorana zero modes will be gapped out, and we are therefore left with one protected pair of Majorana zero modes on the equator located at inversion-symmetric positions. Furthermore, the Jackiw-Rebbi procedure shows that these Majorana zero modes transform in the exact same way as in Eq. (2.67) and Eq. (2.68). Thus the zero modes from the STO can gap out the zero modes from the BDI bulk.

What about the third order inversion symmetric topological phase in AIII? According to Ref. [27], a 3D inversion symmetric TI in class AIII has only a third-order implementation. Physically, this phase can be thought of as a 1D AIII Su-Schrieffer-Heeger (SSH) chain which is in non-trivial phase inserted into a 3D manifold. There is a close connection between the 1D SSH chain and the 1D BDI chain, as pointed out in Ref. [18]. We can establish an exact mapping from two copies of the BDI Kitaev chain to one copy of SSH chain. The two dangling Majorana zero modes form a Dirac zero mode, which is the dangling zero mode of the SSH chain. Since two copies of Kitaev chain have an emergent $\mathsf{O}(2)$ symmetry, its subgroup $\mathsf{SO}(2)$ corresponds to the $\mathsf{U}(1)$ symmetry for the AIII chain. Crucially, the TRS in the BDI chain corresponds to the sub-lattice/chiral symmetry of the AIII chain (We comment that the TRS is still anti-unitary in the Fock space after the mapping, but it is unitary on the single-particle Hamiltonian [18]). Therefore, we naturally conclude that the STO for the 3D third order AIII phase is equivalent to the STO for two copies of 3D third order BDI phase, with chiral symmetry implemented in the same way as the TRS in the STO for BDI phase.

2.3.2 Class DIII

In this subsection, we discuss the STO for third order class DIII HOTSC. To that end, we first demonstrate the fact that, for 3D class DIII HOTSC protected by inversion, the classification is Z_4, which is an extension of Z_2 (second-order phases) by Z_2 (third-order phases). Consider the second-order case, where there is a pair of helical hinge modes. We denote the Majorana hinge modes as $(\chi, \bar{\chi})$. The TRS action on these modes is

$$\mathcal{T} : \begin{bmatrix} \chi(\theta) \\ \bar{\chi}(\theta) \end{bmatrix} \mapsto \begin{bmatrix} \bar{\chi}(\theta) \\ -\chi(\theta) \end{bmatrix}, \tag{2.75}$$

while the inversion action on these modes is

$$\mathcal{I}: \begin{bmatrix} \chi(\theta) \\ \bar{\chi}(\theta) \\ \chi(\theta+\pi) \\ \bar{\chi}(\theta+\pi) \end{bmatrix} \mapsto \begin{bmatrix} i\chi(\theta+\pi) \\ -i\bar{\chi}(\theta+\pi) \\ -i\chi(\theta) \\ i\bar{\chi}(\theta) \end{bmatrix}. \tag{2.76}$$

As in the case of Class D, the above action can be derived using recursive Jackiw-Rebbi procedures. Now suppose we have two copies of such helical modes $(\chi_1, \bar{\chi}_1, \chi_2, \bar{\chi}_2)$, with symmetry action exactly the same as the above. A gapping term can be written down in the 1D model

$$\delta\hat{h} = \int \mathrm{d}\theta \left[im(\theta) \left(\chi_1^{(\dagger)}(\theta)\bar{\chi}_2(\theta) + \bar{\chi}_1^{(\dagger)}(\theta)\chi_2(\theta) \right) \right]. \tag{2.77}$$

The above term is TRS invariant, and inversion symmetry imposes $m(\theta) = -m(\theta+\pi)$. Thus the 1D system is gapped out except at two inversion symmetric points. Furthermore, these two point modes can be gapped out if we take a double stacking of this model. We therefore conclude that the class DIII HOTSC protected by inversion has classification Z_4, which is an extension of Z_2 (second-order phases) by Z_2 (third-order phases).

To gap out the third order topology, we make use of the fact that the third order phase is obtained by two copies of second order phase. Now since the STO for the second order phase is $\mathsf{SO}(3)_3 \times \overline{\mathsf{SO}(3)_3}$, we conclude that the STO for third order topological phase is two copies of $\mathsf{SO}(3)_3 \times \overline{\mathsf{SO}(3)_3}$ topological order.

2.3.3 Class CII

We now briefly discuss the STO for the third order 3D HOTSC in class CII. Similarly to the case AIII, we can view the 3D inversion-symmetric third order CII phase as a 1D inversion-symmetric CII chain embedded in a 3D manifold. The 1D CII chain always has even number of Majorana zero modes at its edge, instead of single Majorana zero mode at the edge of Kitaev chain. we can view the edge zero modes for CII chain as a Kramers' pair of Majorana zero modes, similar to the edge mode in the case of 1D DIII chain. However 1D CII chain has a $2\mathsf{Z}$ classification whereas the 1D DIII chain has a Z_2 classification [86]. Here we briefly look at the following linearised 1D model for CII chain taken from Ref. [87]

$$H(k) = -k\tau_z\sigma_y + m\tau_x, \quad \mathcal{T} = \sigma_y\mathcal{K}, \quad \mathcal{P} = \tau_y\mathcal{K}. \tag{2.78}$$

The chain is in the topological phase when $m > 0$, and the zero modes are trapped at the $m = 0$ domain wall. We perform the Jackiw-Rebbi projection to track the symmetry action on the zero modes, and found that $\mathcal{T}_{\text{edge}} \sim \mathcal{P}_{\text{edge}} \sim i\sigma_y\mathcal{K}$. Because of this, stacking any number of copies of CII chains cannot enable us to gap these zero modes out, as TRS must commute with the mass term, whereas the PHS must anti-commute with the mass term.

The fact that CII can be viewed as a stacking of a Kitaev chain and its TRS copy with $\mathcal{P}^2 = -1$ implementation of PHS leads us to conjecture that the STO for the third order 3D inversion CII phase to be the same as the STO for the third order 3D DIII phase, with the $\mathcal{P}^2 = -1$ implementation of PHS on the STO level.

2.A K-matrix Luttinger liquids

In this appendix, we briefly review the K-matrix theory of Luttinger liquids [73, 74, 88]. 2D Abelian topological orders can be described by n emergent $\mathsf{U}(1)$ gauge fields coupled via a Chern-Simons action [89]. If the 2D system has a boundary, the boundary can be described by $\mathsf{U}(1)$ compact boson theory [74]. Specifically, the bulk Lagrangian and the boundary Lagrangian can be written as:

$$\begin{aligned}\mathcal{L}_{\text{bulk}} &= \frac{K_{IJ}}{4\pi}\epsilon_{\mu\nu\sigma}a^{I,\mu}\partial^{\nu}a^{J,\sigma},\\ \mathcal{L}_{\text{boundary}} &= K_{IJ}\partial_t\phi^I\partial_x\phi^J - V_{IJ}\partial_x\phi^I\partial_x\phi^J\\ &\quad + \sum_j g_j\cos[l_{j,I}^{\mathsf{T}}\phi^I + \alpha].\end{aligned} \tag{2.79}$$

In the bulk Lagrangian, the K_{IJ} is a symmetric integer matrix which describes the Chern-Simons coupling of emergent gauge fields a_μ^I. By requiring the gauge invariance of the theory on a $2+1d$ manifold with boundary, the boundary must carry degrees of freedom ϕ^I described by the corresponding boundary action. The sine-Gordon terms are derived by local Hermitian gapping terms i.e. $\cos[l_{j,I}^{\mathsf{T}}\phi^I + \alpha] \sim e^{il_{j,I}^{\mathsf{T}}\phi^I} + e^{-il_{j,I}^{\mathsf{T}}\phi^I}$, where l^{T}s are integer vectors (usually referred to as the gapping vectors). For the convenience of discussion, we also introduce the concept boundary gapping lattice $\Gamma^{\partial} = \{l_j\}$, namely the lattice spanned by gapping vectors.

The advantage of focusing on the K-matrix is that we can represent quasiparticles in a convenient algebraic way. Let us denote the order of the K-matrix as n, i.e., there are n gauge fields in the bulk, and a quasiparticle can be represented by a n-components vector l. The braiding phase between two quasiparticles is given by $\theta_{ll'} = 2\pi lK^{-1}l'$, and the topological spin (exchange phase) of the quasiparticle l is given by $\theta_l = \theta_{ll}/2 = \pi lK^{-1}l$. To identify local particles i.e. bosons/fermions in the theory, we require the local particle to braid trivially with all particles, thus resulting in the constraint $l = K\Lambda$, where Λ is an integer vector.

To have a fully gapped boundary, there are certain criteria that the sine-Gordon terms have to satisfy. More concretely, we look at:

$$\delta\mathcal{L}_{\text{boundary}} = \sum_j g_j\cos[l_{j,I}^{\mathsf{T}}\phi^I + \alpha]. \tag{2.80}$$

Physically, by writing such terms, quasiparticles l_js are condensed on the boundary. For all quasiparticles to condense, we require the following conditions [90]

1. The condensed quasiparticles have bosonic self-statistics: $\forall l_j \in \Gamma^\partial, l_{j,I}^\mathsf{T} K_{IJ}^{-1} l_{j,J} \in 2\mathsf{Z}$.
2. The condensed quasiparticles mutually braid trivially.
3. The bosonic fields corresponding to the condensed quasiparticles can acquire classical values at the same time: $\forall l_j, l_i \in \Gamma^\partial, l_{i,I}^\mathsf{T} K_{IJ}^{-1} l_{j,J} = 0$. This condition is also known as the *Haldane criterion*.
4. The condensed quasiparticles must be local/non-fractional particles: $\forall l_{j,I}, l_{j,I} = K_{IJ}\Lambda_{j,J}$, where $\Lambda_{j,J}$ is an integer vector.
5. Completeness: $\forall l_{j,I} = K_{IJ}\Lambda_{j,J}$, if $l_{j,I}^\mathsf{T} K_{IJ}^{-1} l_{j,J} = 0$, and $l_{j,I}^\mathsf{T} K_{IJ}^{-1} l_{i,J} = 0$ for $\forall l_{i,J} \in \Gamma^\partial$, then $l_{j,I} \in \Gamma^\partial$.
6. Non-chirality: the boundary theory must have p left movers and p right movers to begin with.

So far we have ignored the existence of global symmetries. It is beyond the scope of this appendix to introduce a complete inclusion of symmetry in the K-matrix formalism. We wish only to describe the more relevant symmetry to this chapter here. Crucially, we usually have a global $\mathsf{U}(1)$ symmetry if the system under discussion is a fermionic insulating system, e.g., quantum Hall systems and topological insulators. The presence of the global $\mathsf{U}(1)$ symmetry is usually signalled by the coupling of the original degrees of freedom to a background gauge field A^I:

$$\begin{aligned} \delta\mathcal{L}_{\text{bulk},\mathsf{U}(1)} &= -\frac{1}{2\pi} t_I \epsilon_{\mu\nu\sigma} A^\mu \partial^\nu a^{I,\sigma} \\ \delta\mathcal{L}_{\text{boundary},\mathsf{U}(1)} &= \frac{1}{2\pi} t_I \epsilon_{\mu\nu} \partial^\mu \phi^I A^\nu, \end{aligned} \tag{2.81}$$

where t_I is an integer vector usually referred to as the electric charge vector. Quasiparticle l's electric charge is given by $q_l = \frac{1}{2\pi} l^\mathsf{T} K^{-1} t$. Upon the introduction of the global $\mathsf{U}(1)$ symmetry, the quasiparticle condensation on the boundary is further restricted: only the charge neutral particles can be condensed ,i.e., $\forall l_j, l_j K^{-1} t = 0$.

2.B $\mathsf{SO}(N)_1$ Wess-Zumino-Witten theory

In this appendix, we briefly review the chiral $\mathsf{SO}(N)_1$ WZW conformal field theory which describes N chiral Majorana fermions on a $1{+}1d$ manifold [81]. The $\mathsf{SO}(N)$ global symmetry

arises due to the flavor symmetry of the N chiral Majorana fermions $\chi_i \mapsto O_{ij}\chi_j, O_{ij} \in \mathsf{SO}(N)$. Since this is a continuous symmetry, there exists corresponding Noether currents:

$$J^{\mathsf{a}} = \frac{i}{2}\chi_l L^{\mathsf{a}}_{lm}\chi_m, \mathsf{a} = 1, \ldots, \frac{N(N-1)}{2}, \tag{2.82}$$

where L^{a}s are anti-symmetric $N \times N$ matrices that generate the $\mathfrak{so}(N)$ Lie algebra. Majorana fermions operators have the following OPE:

$$\chi_{\mathsf{a}}(z)\chi_{\mathsf{b}}(w) = \frac{\delta^{\mathsf{ab}}}{z-w} + \ldots, \tag{2.83}$$

from which the OPE for currents is derived:

$$J^{\mathsf{a}}(z)J^{\mathsf{b}}(w) = \frac{\delta^{\mathsf{ab}}}{(z-w)^2} + \frac{if_{\mathsf{abc}}J^{\mathsf{c}}(w)}{z-w} + \ldots, \tag{2.84}$$

where f_{abc} is the structure constant for $\mathfrak{so}(N)$. The energy momentum tensor is obtained via the Sugawara construction, and is equivalent to the free fermion energy momentum tensor

$$T(z) = \frac{1}{2(N-1)}\vec{J}(z)\cdot\vec{J}(z) = -\frac{1}{2}\sum_i \chi_i\partial\chi_i(z). \tag{2.85}$$

The OPE of the energy momentum tensor is given by:

$$T(z)T(w) = \frac{N/4}{(z-w)^4} + \frac{2T(w)}{(z-w)^2} + \frac{\partial_w T(w)}{z-w} + \ldots, \tag{2.86}$$

from which we can read off the chiral central charge $c_- = N/2$. A procedure termed the conformal embedding allows us to decompose the original WZW theory into two smaller theories i.e. $\mathfrak{so}(N^2)_1 \supseteq \mathfrak{so}(N)^{(1)}_N \times \mathfrak{so}(N)^{(2)}_N$. For illustration purpose, we will review the conformal embedding for $\mathfrak{so}(9)_1 \supseteq \mathfrak{so}(3)^{(1)}_3 \times \mathfrak{so}(3)^{(2)}_3$. The original $\mathfrak{so}(9)_1$ theory has 9 Majorana fermions, denoted by a pair of indices $(i,j), i,j = 1,2,3$. We introduce a spinor Ψ to simplify the notation, thus all Majoranas are denoted by $\Psi_{(i,j)}$. The current of the $\mathfrak{so}(9)_1$ theory is given by:

$$J^j = \frac{i}{2}\Psi_{(a_1,a_2)}\Sigma^j_{(a_1,a_2),(b_1,b_2)}\Psi_{(b_1,b_2)}, j = 1,2,\ldots,36, \tag{2.87}$$

where Σ^j is the generator of the Lie algebra $\mathfrak{so}(9)$. To perform conformal embedding, we consider the following currents:

$$J^{j,(\kappa)} = \frac{i}{2}\Psi_{(a_1,a_2)}\sigma^{j,(\kappa)}_{(a_1,a_2),(b_1,b_2)}\Psi_{(b_1,b_2)}, \tag{2.88}$$

where $j = 1,2,3; \kappa = 1,2$

$$\begin{aligned}\sigma^{j,(1)}_{(a_1,a_2),(b_1,b_2)} &= \Lambda^j_{a_1,b_1}\delta_{a_2,b_2},\\ \sigma^{j,(2)}_{(a_1,a_2),(b_1,b_2)} &= \delta_{a_1,b_1}\Lambda^j_{a_2,b_2}.\end{aligned} \tag{2.89}$$

Note that Λ^j are the generators for $\mathfrak{so}(3)$. In the fundamental representation, these take the following form

$$\Lambda^1 = \begin{bmatrix} 0 & 0 & 0 \\ 0 & 0 & 1 \\ 0 & -1 & 0 \end{bmatrix}, \Lambda^2 = \begin{bmatrix} 0 & 0 & 1 \\ 0 & 0 & 0 \\ -1 & 0 & 0 \end{bmatrix}, \Lambda^3 = \begin{bmatrix} 0 & 1 & 0 \\ -1 & 0 & 0 \\ 0 & 0 & 0 \end{bmatrix}. \tag{2.90}$$

Explicitly, the currents of the sub-theories in terms of Majorana fermions are

$$\begin{aligned} J^{1,(1)} &= i(\chi_2\chi_3 + \chi_5\chi_6 + \chi_8\chi_9) \\ J^{2,(1)} &= i(\chi_1\chi_3 + \chi_4\chi_6 + \chi_7\chi_9) \\ J^{3,(1)} &= i(\chi_1\chi_2 + \chi_4\chi_5 + \chi_7\chi_8) \\ J^{1,(2)} &= i(\chi_4\chi_7 + \chi_5\chi_8 + \chi_6\chi_9) \\ J^{2,(2)} &= i(\chi_1\chi_7 + \chi_2\chi_8 + \chi_3\chi_9) \\ J^{3,(2)} &= i(\chi_1\chi_4 + \chi_2\chi_5 + \chi_3\chi_6), \end{aligned} \tag{2.91}$$

where we have used the notation

$$\begin{aligned} &\Psi_{(1,1)} = \chi_1, \Psi_{(2,2)} = \chi_5, \Psi_{(3,3)} = \chi_9; \\ &\Psi_{(1,2)} = \chi_4, \Psi_{(2,3)} = \chi_8, \Psi_{(3,1)} = \chi_3; \\ &\Psi_{(2,1)} = \chi_2, \Psi_{(3,2)} = \chi_6, \Psi_{(1,3)} = \chi_7. \end{aligned} \tag{2.92}$$

The OPEs computed for these currents takes the form

$$J^{\mathsf{a},(u)}(z)J^{\mathsf{b},(u)}(w) = \frac{3\delta^{\mathsf{ab}}}{(z-w)^2} + \frac{i\epsilon_{\mathsf{ab}j}J^j(w)}{z-w} + \ldots, \tag{2.93}$$

where the level 3 is determined by double contraction. Note that $J^{\mathsf{a},(1)}(z)J^{\mathsf{b},(2)}(w)$ is non-singular, so that the two sub-theories are decoupled. Thus we conclude that $J^{i,(u)}$ forms $\mathfrak{so}(3)_3^{(u)}$ current algebra. Furthermore, it was shown in Ref. [80] that

$$T_{\mathfrak{so}(9)_1} = T_{\mathfrak{so}(3)_3^{(1)}} + T_{\mathfrak{so}(3)_3^{(2)}}. \tag{2.94}$$

Thus the conformal embedding is complete.

2.C Jackiw-Rebbi projection procedures

In a seminal work, Jackiw and Rebbi [78] identified a generic mechanism where fermionic zero modes appear localized on the mass domain walls of a 1D Dirac fermionic system. Their approach has been generalized in the condensed matter literature to study zero modes localized at the boundaries of bulk topological phases, e.g., Dirac mode at the end of the SSH chain. In this chapter, we have used this procedure to track the symmetry action on

the gapless modes of the higher order topological phase. We demonstrate the procedure in this appendix for the second order inversion HOTSC in class D.

First, we start with one copy of 3D bulk Hamiltonian of class DIII TSC with inversion symmetry. After a series of Jackiw-Rebbi procedures, we end up with a chiral Majorana hinge modes on which the symmetry actions have explicit forms. Note that we will break TRS in the process, so eventually the system is a class D TSC with inversion symmetry. The bulk Hamiltonian is:

$$\hat{H} = \frac{1}{2}\sum_{\vec{k}} \hat{\psi}^\dagger_{\vec{k}} H(\vec{k}) \hat{\psi}_{\vec{k}}, \tag{2.95}$$

where

$$\begin{aligned} H(\vec{k}) &= (-k_x\tau_x\sigma_z - k_y\tau_y + k_z\tau_x\sigma_x) + \lambda\tau_z, \\ \hat{\psi}^\dagger_{\vec{k}} &= (c^\dagger_{\vec{k},\uparrow}, c^\dagger_{\vec{k},\downarrow}, c_{-\vec{k},\uparrow}, c_{-\vec{k},\downarrow}). \end{aligned} \tag{2.96}$$

The symmetries are represented as follows:

$$\mathcal{T} = i\sigma_y\mathcal{K}, \quad \mathcal{P} = \tau_x\mathcal{K}, \quad \mathcal{I} = \tau_z. \tag{2.97}$$

Note that here $\vec{\sigma}, \vec{\tau}$ are Pauli matrices in different spaces. σ is the spin space, and τ is the Nambu space. The 3D system lives inside a 3D ball, of which the boundary is S^2. Specifically we will pay attention to the gapless modes near $x^\pm = (\pm 1, 0, 0)$, as these two points are related to each other by inversion. The strategy is as follows: first we perform Jackiw-Rebbi from 3D to 2D so that we end up with a system which is a 2D stacked system $H_{x^-} \oplus H_{x^+}$ with a 3D inversion symmetry which relates system x^- and x^+ to each other; second we write a mass term $m(z)\Gamma$ in the stacked 2D system, and observe the behavior of the term under inversion symmetry. If $m(z) = -m(-z)$, then the stacked system hosts gapless mode along the hinge.

The mass coefficient $\lambda \equiv \lambda(x)$ has the behaviour such that $\lambda = 1$ inside the superconductor, and $\lambda = -1$ outside the superconductor. Let us investigate the surface modes near x^+. If we denote the surface eigenstate of the first quantized Hamiltonian as $|\varphi\rangle$, then

$$(i\tau_x\sigma_z\partial_x + \lambda(x)\tau_z)|\varphi\rangle = 0, \tag{2.98}$$

as we require the state to have no dispersion along the x-direction. The above equation is equivalent to

$$\partial_x|\varphi\rangle = i\lambda(x)\tau_x\tau_z\sigma_z|\varphi\rangle = \lambda(x)\tau_y\sigma_z|\varphi\rangle. \tag{2.99}$$

The above equation implies that $|\varphi\rangle$ is an eigenstate of $\tau_y\sigma_z$. There are four eigenstates of $\tau_y\sigma_z$:

$$|+,1\rangle = (e^{-i\frac{\pi}{4}}, 0, e^{+i\frac{\pi}{4}}, 0)^\mathsf{T};$$

$$
\begin{aligned}
|+,2\rangle &= (0, e^{+i\frac{\pi}{4}}, 0, e^{-i\frac{\pi}{4}})^{\mathsf{T}};\\
|-,1\rangle &= (e^{+i\frac{\pi}{4}}, 0, e^{-i\frac{\pi}{4}}, 0)^{\mathsf{T}};\\
|-,2\rangle &= (0, e^{-i\frac{\pi}{4}}, 0, e^{+i\frac{\pi}{4}})^{\mathsf{T}},
\end{aligned} \tag{2.100}
$$

where the phases are added so that boundary excitations are explicitly Majorana fermions. Using these eigenstates, the Eq. (2.99) can be reduced to:

$$
\partial_x|\varphi,\pm\rangle = \pm\lambda(x)|\varphi,\pm\rangle, \tag{2.101}
$$

for which the solutions are:

$$
|\varphi,\pm\rangle = \exp[\pm\int_{x_0}^{x} dx'\lambda(x')]|\pm\rangle, \tag{2.102}
$$

where x_0 is a constant to fix the normalisation condition. We therefore see that the states with positive eigenvalues are the normalisable states near x^+.
We further define the following matrix:

$$
U = \frac{1}{\sqrt{2}}[|+,1\rangle, |+,2\rangle, |-,1\rangle, |-,2\rangle]. \tag{2.103}
$$

The first quantized Hamiltonian of the combined system is:

$$
H_{\text{comb}}(\vec{k}) = U^\dagger H(\vec{k}) U = -k_y s_z \tilde{\sigma}_z + k_z \tilde{\sigma}_x, \tag{2.104}
$$

where "comb" stands for "x^+ and x^- combined". Note that we have omitted the exponential factor in the definition of U for convenience. The exponential factor is only useful in telling us that the effective Hamiltonian is describing the physics near x^+, and writing it down explicitly helps us remove the $-k_x\tau_x\sigma_z + \lambda(x)\tau_z$ term after the projection. The s-space is now the space of x^+ and x^-.

We can now examine the representation of symmetries in this basis:

$$
\begin{aligned}
\mathcal{T}_{\text{comb}} &= U^\dagger \mathcal{T} U = i\tilde{\sigma}_y \mathcal{K},\\
\mathcal{P}_{\text{comb}} &= U^\dagger \mathcal{P} U = \mathcal{K},\\
\mathcal{I}_{\text{comb}} &= U^\dagger \mathcal{I} U = -s_y \tilde{\sigma}_z.
\end{aligned} \tag{2.105}
$$

We conclude here, that we have obtained a stacked 2D system, of which the Hamiltonian is:

$$
\hat{H}_{\text{comb}} = \frac{1}{2}\sum_{\vec{k}} [\hat{\psi}_{\vec{k}}^{x^+\dagger}, \hat{\psi}_{\vec{k}}^{x^-\dagger}] H_{\text{comb}}(\vec{k}) \begin{bmatrix} \hat{\psi}_{\vec{k}}^{x^+} \\ \hat{\psi}_{\vec{k}}^{x^-} \end{bmatrix}, \tag{2.106}
$$

with symmetries having representations as in Eq. (2.105). We can have more explicit form of the spinor:

$$\begin{bmatrix} \hat{\psi}^{x^+}_{\vec{k}} \\ \hat{\psi}^{x^-}_{\vec{k}} \end{bmatrix} = \begin{bmatrix} \gamma^{x^+}_{-\vec{k},\uparrow} \\ \gamma^{x^+}_{\vec{k},\downarrow} \\ \gamma^{x^-}_{\vec{k},\uparrow} \\ \gamma^{x^-}_{-\vec{k},\downarrow} \end{bmatrix} = U^\dagger \hat{\psi}_{\vec{k}}. \tag{2.107}$$

In terms of $c, c^\dagger$, the Majoranas are:

$$\begin{aligned} \gamma^{x^+}_{-\vec{k},\uparrow} &= \frac{1}{\sqrt{2}}(e^{i\frac{\pi}{4}} c_{\vec{k},\uparrow} + e^{-i\frac{\pi}{4}} c^\dagger_{-\vec{k},\uparrow}) \\ \gamma^{x^+}_{\vec{k},\downarrow} &= \frac{1}{\sqrt{2}}(e^{-i\frac{\pi}{4}} c_{\vec{k},\downarrow} + e^{i\frac{\pi}{4}} c^\dagger_{-\vec{k},\downarrow}) \\ \gamma^{x^-}_{\vec{k},\uparrow} &= \frac{1}{\sqrt{2}}(e^{-i\frac{\pi}{4}} c_{\vec{k},\uparrow} + e^{i\frac{\pi}{4}} c^\dagger_{-\vec{k},\uparrow}) \\ \gamma^{x^-}_{-\vec{k},\downarrow} &= \frac{1}{\sqrt{2}}(e^{i\frac{\pi}{4}} c_{\vec{k},\downarrow} + e^{-i\frac{\pi}{4}} c^\dagger_{-\vec{k},\downarrow}). \end{aligned} \tag{2.108}$$

Let us add a surface perturbation which breaks TRS, i.e., a mass term on the whole surface of the 3D system that depends only on z. On our combined system, this perturbation is represented as $m(z)\Gamma$, where Γ is some matrix. Such a term is $m(z)\tilde{\sigma}_y$. Also this term breaks TRS explicitly. By imposing $\mathcal{I}_{\text{comb}} m(z)\tilde{\sigma}_y \mathcal{I}^{-1}_{\text{comb}} = m(-z)\tilde{\sigma}_y$, we end up with $m(z) = -m(-z)$. Thus we can conclude that the class D TSC with inversion symmetry hosts hinge modes, i.e., it hosts second order topology, which is consistent with the previous work.

We now proceed to perform Jackiw-Rebbi procedures on the combined 2D system, so that symmetries on the 1D hinge modes will manifest.

The first quantized Hamiltonian with perturbation is:

$$H_{\text{comb}} + \delta H_{\text{comb}} = -k_y s_z \tilde{\sigma}_z + k_z \tilde{\sigma}_x + m(z)\tilde{\sigma}_y, \tag{2.109}$$

in which we assign the behavior of $m(z)$ to be

$$m(z) = \begin{cases} -1, \text{ if } z < 0 \\ 0, \text{ if } z = 0 \\ +1, \text{ if } z > 0 \end{cases}. \tag{2.110}$$

If we denote the hinge eigenstate of the first quantized Hamiltonian as $|\varphi\rangle$, then

$$(-i\sigma_x \partial_z + m(z)\tilde{\sigma}_y)|\varphi\rangle = 0, \tag{2.111}$$

as we require the state to have no dispersion along the z-direction. The above equation is equivalent to

$$\partial_z |\varphi\rangle = -im(z)\tilde{\sigma}_x \tilde{\sigma}_y |\varphi\rangle = m(z)\tilde{\sigma}_z |\varphi\rangle. \tag{2.112}$$

The above equation implies that $|\varphi\rangle$ is an eigenstate of $s_0\tilde{\sigma}_z$. There are four eigenstates of $s_0\tilde{\sigma}_z$:

$$\begin{aligned}
|+,1\rangle &= (1,0,0,0)^{\mathsf{T}};\\
|+,2\rangle &= (0,0,1,0)^{\mathsf{T}};\\
|-,1\rangle &= (0,1,0,0)^{\mathsf{T}};\\
|-,2\rangle &= (0,0,0,1)^{\mathsf{T}}.
\end{aligned} \tag{2.113}$$

Using these eigenstates, the Eq. (2.112) can be reduced to:

$$\partial_z|\varphi,\pm\rangle = \pm m(z)|\varphi,\pm\rangle, \tag{2.114}$$

for which the solutions are:

$$|\varphi,\pm\rangle = \exp[\pm\int_{z_0}^{z} dz' m(z')]|\pm\rangle, \tag{2.115}$$

where z_0 is a constant to fix the normalisation condition. We therefore see that the states with positive eigenvalues are the normalisable states.

We further define the following matrix:

$$U' = [|+,1\rangle, |+,2\rangle, |-,1\rangle, |-,2\rangle]. \tag{2.116}$$

Note that U' will take us to the space $\zeta \otimes \tilde{s}$ which can be read off by studying the basis. ζ is the space of normalisable states and non-normalisable states. We intend to keep the normalisable states as hinge states, therefore keep the $--$ block of the ζ space.

The first quantized Hamiltonian of hinge state is:

$$U'^{\dagger}(H_{\text{comb}} + \delta H_{\text{comb}})U'|_{--} = U'^{\dagger}(-k_y s_z \tilde{\sigma}_z)U'|_{--} = k_y \tilde{s}_z. \tag{2.117}$$

The symmetries are:

$$\begin{aligned}
\mathcal{P}_{\text{hinge}} &= U'^{\dagger}\mathcal{P}_{\text{comb}}U'|_{--} = \mathcal{K},\\
\mathcal{I}_{\text{hinge}} &= U'^{\dagger}\mathcal{I}_{\text{comb}}U'|_{--} = \tilde{s}_y.
\end{aligned} \tag{2.118}$$

And the spinor is:

$$\hat{\mathrm{X}}_{\vec{k}} = (\chi_{\vec{k}}^{x^+}, \chi_{-\vec{k}}^{x^-})^{\mathsf{T}}. \tag{2.119}$$

The explicit form can be obtained in the following way:

$$\hat{\mathrm{X}}_{\vec{k}} = U'^{\dagger}\begin{bmatrix}\hat{\psi}_{\vec{k}}^{x^+}\\ \hat{\psi}_{\vec{k}}^{x^-}\end{bmatrix}|_{\text{lower}}, \tag{2.120}$$

since the normalisable states correspond to the $--$ block of the Hamiltonian. We can have more explicit forms from this expression:

$$\begin{aligned}\chi_{\vec{k}}^{x^-} &= \gamma_{-\vec{k},\downarrow}^{x^-} \\ \chi_{-\vec{k}}^{x^+} &= \gamma_{\vec{k},\downarrow}^{x^+}.\end{aligned} \tag{2.121}$$

Therefore we can conclude that the 1D hinge Hamiltonian is:

$$\hat{H}_{\text{hinge}} = \frac{1}{2}\sum_{\vec{k}} \hat{\mathrm{X}}_{\vec{k}}^{\dagger}(k_y\tilde{s}_z)\hat{\mathrm{X}}_{\vec{k}} = \frac{1}{2}\sum_{k} \hat{\mathrm{X}}_{\vec{k}}^{\dagger}H_{\text{hinge}}(\vec{k})\hat{\mathrm{X}}_{\vec{k}}, \tag{2.122}$$

with symmetries defined as in Eq. (2.118).

We use θ to parametrise the full hinge which has periodicity π, and $x^- = 0, x^+ = \pi$. The action of inversion is therefore:

$$I_{\text{hinge}} : \begin{bmatrix}\chi(\theta)\\ \chi(\theta+\pi)\end{bmatrix} \mapsto \tilde{s}_y \begin{bmatrix}\chi(\theta)\\ \chi(\theta+\pi)\end{bmatrix} = \begin{bmatrix}-i\chi(\theta+\pi)\\ i\chi(\theta)\end{bmatrix}. \tag{2.123}$$

We conclude that, the 3D class D TSC with inversion symmetry hosts a single chiral Majorana hinge mode χ on the surface with symmetries defined as above.

2.D Third-order class DIII inversion-symmetric superconductor

In this appendix, we show that the surface zero modes of 3D class DIII topological superconductor with inversion are stable to weakly-interacting surface perturbations.

We proceed to describe the weakly-interacting surface perturbation. Specifically, if we specify that the great circle connecting the antipodal corner modes as the equator, then we paste one copy of 2D TRS invariant topological superconductor on the northern hemisphere surface and another copy of 2D TRS invariant topological superconductor on the southern hemisphere surface, and these two copies are related to each other by inversion symmetry. To show that the original point modes are stable under this perturbation, it is sufficient to show that the pasted 2D model will not host any new corner modes on the equator, as these new corner modes will be able to be used to 'annihilate' the original point modes.

Our effectively 2D model, which can be called N-S model, has the following Hamiltonian:

$$H = (-k_x\sigma_z\tau_x - k_y\tau_y + \lambda\tau_z)\zeta_0, \tag{2.124}$$

where ζ denotes the N-S orbital space. The symmetries in this model are as follows:

$$\mathcal{T} = \sigma_y\mathcal{K}, \quad \mathcal{P} = \tau_x\mathcal{K}, \quad \mathcal{I} = \zeta_x\tau_z, \tag{2.125}$$

note that inversion switches the N-S orbitals.

The 1D edge of the N-S model, i.e. the equator, can be completely gapped out without leaving point modes behind. This can be shown by introducing the following gapping term in the bulk:

$$\delta H = m_{\vec{r}}\sigma_x\tau_x\zeta_y, \tag{2.126}$$

which is TRS invariant and PHS respecting. At the same time, by requiring $\mathcal{I}\delta H(\vec{r})\mathcal{I}^{-1} = \delta H(-\vec{r})$, we necessarily arrive at $m_{\vec{r}} = m_{-\vec{r}}$. To see what this means on the equator, we invoke the projection procedures as before. Upon projection, the 1D Hamiltonian and the gapping term become:

$$h = -k_S\sigma_z\zeta_0, \delta h = -m_{\vec{r}}(\hat{n}_{\vec{r}} \times \vec{\sigma})_z\zeta_y, \tag{2.127}$$

with symmetries:

$$\mathcal{T}_S = \sigma_y\mathcal{K}, \quad \mathcal{P}_S = -(\hat{n}_{\vec{r}} \cdot \vec{\sigma})\sigma_y\mathcal{K}, \quad \mathcal{I}_S = -\zeta_x. \tag{2.128}$$

Note that here k_S denotes momentum perpendicular to $\hat{n}_{\vec{r}}$. Here we can see again, by requiring $\mathcal{I}_S\delta h(\vec{r})\mathcal{I}_S^{-1} = \delta h(-\vec{r})$, we necessarily arrive at $m_{\vec{r}} = m_{-\vec{r}}$.

Thus we have proved that the edge of N-S model can be completely gapped without breaking symmetries or leaving corner modes, and consequently, the corner modes that arise from the third order topology of the 3D class DIII topological superconductor with inversion symmetry are stable under such surface perturbation.

Chapter 3

Finite-Entanglement Scaling of 2D Metals

3.1 Introduction

In this study we extend the finite-entanglement scaling analysis to two dimensions and show that a similar scaling collapse is possible for the entanglement entropy of metals, i.e., states with a Fermi surface, despite the fact that there is no underlying CFT describing the long-wavelength physics. Our results show that by exploiting the scaling collapse, moderate (and numerically tractable) bond dimensions already give rise to a sufficiently high numerical accuracy to reliably access all information about the Fermi surface that is contained in the Widom formula, and hence apply the general approach of "entanglement spectroscopy" to metallic systems. Some interesting previous works have studied finite-correlation-length scaling for 2D TNS [91, 92, 93, 94], but these works did not consider area-law-violating ground states.

Chapter heading: fish motif, detail of the *pan*, Shang dynasty, Erligang period (circa 17th/16th – circa 14th centuries B.C.), source unknown.

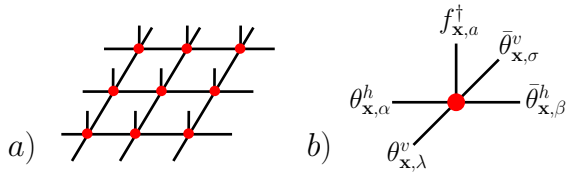

Figure 3.1: (a) A 2D tensor network on a 3×3 square lattice. (b) The assignment of physical creation operators $f^\dagger_{\mathbf{x}}$ to the physical index, and virtual Grassmann variables $\theta_{\mathbf{x}}, \bar{\theta}_{\mathbf{x}}$ to the virtual indices, of a Gaussian fermionic tensor.

3.2 Gaussian fermionic TNS

For concreteness we will perform our analysis on a square lattice. Since we are interested in 2D states with a Fermi surface we use fermionic projected entangled-pair states (PEPS) [95, 96, 48, 97, 98, 99]. In particular, we will be working with *Gaussian* fermionic tensors, which produce either a Slater determinant or a Bardeen-Cooper-Schrieffer (BCS) pairing (or pfaffian) state after contraction of the virtual indices. To define the Gaussian tensors, we assign fermion creation operators $f^\dagger_{\mathbf{x},a}$ ($a \in \{1,\dots,N\}$) to the physical index of the tensor at site $\mathbf{x}$, and Grassmann variables $\theta^h_{\mathbf{x},\alpha}, \bar\theta^h_{\mathbf{x},\beta}, \theta^v_{\mathbf{x},\lambda}, \bar\theta^v_{\mathbf{x},\sigma}$ ($\alpha,\beta,\lambda,\sigma \in \{1,\dots,M\}$) to the virtual indices, as in Fig. 3.1. The Grassmann variables square to zero, are mutually anticommuting, and also anticommute with the creation operators $f^\dagger_{\mathbf{x},a}$. The Gaussian tensor at site $\mathbf{x}$ is defined as

$$\hat T_{\mathbf{x}} = \exp\left(\frac{1}{2}\chi_{\mathbf{x}}^T A \chi_{\mathbf{x}}\right), \tag{3.1}$$

where the column vector $\chi_{\mathbf{x}} \equiv (f^\dagger_{\mathbf{x}}, \theta^h_{\mathbf{x}}, \bar\theta^h_{\mathbf{x}}, \theta^v_{\mathbf{x}}, \bar\theta^v_{\mathbf{x}})$ collects the N creation operators and $4M$ Grassmann variables assigned to site $\mathbf{x}$ and the antisymmetric matrix $A \in \mathbb{C}^{(N+4M)\times(N+4M)}$ contains the variational parameters. Note that A is independent of $\mathbf{x}$, which means that we are restricting ourselves to translation-invariant states. With the definition of the tensors in place, we can now define the (unnormalized) contracted Gaussian fermionic TNS (GfTNS) via the Berezin integral [100]

$$|\psi\rangle = \int [D\theta] \int [D\bar\theta] \prod_{\mathbf{x}} e^{\bar\theta^{h\,T}_{\mathbf{x}} \theta^h_{\mathbf{x}+\mathbf{e}_x}} e^{\bar\theta^{v\,T}_{\mathbf{x}} \theta^v_{\mathbf{x}+\mathbf{e}_y}} \hat T_{\mathbf{x}} |0\rangle\,, \tag{3.2}$$

where $|0\rangle$ is the physical Fock vacuum and $\mathbf{e}_{x/y}$ are unit vectors along the x/y-direction. Every Grassmann variable spans a two-dimensional super vector space, so the bond dimension of the GfTNS is $D = 2^M$.

Because we are considering translationally invariant states, the Gaussian Grassmann integral in Eq. 3.2 can be further simplified by going to momentum space. Working with a large but finite system of $N_s = N_x N_y$ sites and (anti-)periodic boundary conditions while defining $\chi_{\mathbf{k}} = \frac{1}{\sqrt{N_s}} \sum_{\mathbf{x}} e^{i\mathbf{k}\cdot\mathbf{x}} \chi_{\mathbf{x}}$, we can write

$$|\psi\rangle = \int [D\theta] \int [D\bar\theta] \exp\left(\frac{1}{2}\sum_{\mathbf{k}} \chi^T_{-\mathbf{k}} [A + M(\mathbf{k})] \chi_{\mathbf{k}}\right) |0\rangle\,.$$

Here, $M(\mathbf{k})$ is defined as $M(\mathbf{k}) = \mathbf{0}_N \oplus \tilde M(\mathbf{k})$, with $\mathbf{0}_N$ a $N \times N$ zero matrix, and

$$\tilde M(\mathbf{k}) = \begin{pmatrix} \mathbf{0}_M & -e^{ik_x}\mathbb{1}_M \\ e^{-ik_x}\mathbb{1}_M & \mathbf{0}_M \end{pmatrix} \oplus \begin{pmatrix} \mathbf{0}_M & -e^{ik_y}\mathbb{1}_M \\ e^{-ik_y}\mathbb{1}_M & \mathbf{0}_M \end{pmatrix}. \tag{3.3}$$

Writing $A = \begin{pmatrix} B & -C^T \\ C & D \end{pmatrix}$, with $N \times N$ submatrix B, $4M \times N$ submatrix C, and $4M \times 4M$ submatrix D, we finally obtain

$$|\psi\rangle \propto \mathrm{e}^{\frac{1}{2}\sum_{\mathbf{k}} f^\dagger_{-\mathbf{k}}(B+C^T[D+\tilde{M}(\mathbf{k})]^{-1}C)f^\dagger_{\mathbf{k}}}|0\rangle\,. \tag{3.4}$$

Here, we have assumed that $D + \tilde{M}(\mathbf{k})$ is non-degenerate at every $\mathbf{k}$ and refer to Ref. [69] for the degenerate case.

The construction of GfTNS as presented here was introduced in Ref. [97], and has been used in previous studies [101, 98, 102, 103]. There also exists an alternative formulation in terms of density matrices [95].

The state in Eq. 3.4 takes the form of a general BCS pairing state. Given that we set out to study states with a Fermi surface, the reader might worry that we are using TNS which contract to pairing states. The reason for this is simply that a finite-D Gaussian fTNS with explicit charge conservation symmetry always has an integer particle number at every momentum which is constant throughout the Brillouin zone, and therefore cannot represent or even closely approximate a state with a Fermi surface. This is not an embarrassing shortcoming of GfTNS, but a direct consequence of the Lieb-Schultz-Mattis theorem, which states that one cannot have a trivial insulator at noninteger fillings [104, 105, 106, 107]. In particular, in Ref. [108], it was shown that if a general, explicitly translationally invariant and U(1)-symmetric fTNS is forced to have a filling $\nu = p/q$, with p and $q > 1$ coprime integers, then the tensors necessarily have a purely virtual $\mathbb{Z}_{2q}$ symmetry. The entanglement entropy (EE) in a generic tensor network state with such virtual symmetry scales as $S = \alpha L - \ln 2q + \mathcal{O}(L^{-1})$, which implies that the fTNS has nontrivial topological order [109, 110, 111, 112]. So the incompatibility of Gaussianity and explicit U(1) symmetry at fractional filling $\nu = p/q$ for fTNS is a manifestation of the simple fact that Slater determinants cannot represent states with nontrivial topological order. The only way for a translationally invariant GfTNS to introduce finite entanglement in a metallic state is therefore to open a small superconducting gap at the Fermi surface.

3.3 Spinless Fermi surface

We first consider the case with $N = 1$, i.e., spinless fermions with a single orbital per site. To obtain the GfTNS, we minimize the energy of the following simple hopping Hamiltonian:

$$H = -t\sum_{\langle ij\rangle} f_i^\dagger f_j - t'\sum_{\langle\langle ij\rangle\rangle} f_i^\dagger f_j + h.c. - \mu\sum_i f_i^\dagger f_i\,, \tag{3.5}$$

where the first (second) sum is over nearest (next-nearest) neighbours. We choose the chemical potential μ such that there is a single electron pocket centered at the Γ point.

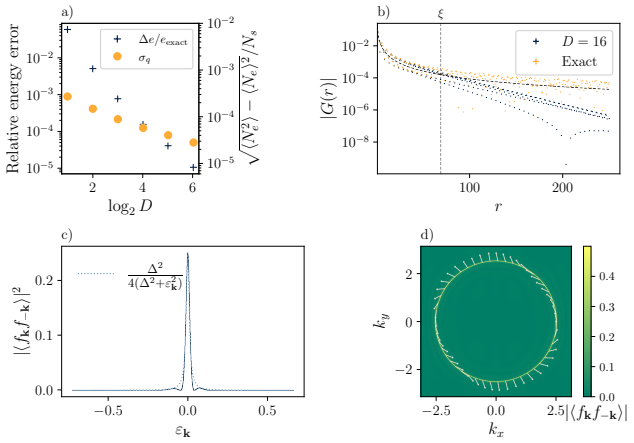

Figure 3.2: Results for spinless fermions with $t'/t = 0.353$ at half filling of $N_s = 999^2$ sites. (a) Relative difference in energy per site (denoted as $\Delta e/e_{\text{exact}}$) between the exact ground state and the optimized GfTNS as a function of bond dimension D; and the standard deviation σ_q of the particle number per site of the optimized GfTNS. (b) $|\langle f_r f_0\rangle|$ for $D = 16$ GfTNS vs the exact ground state. Near ξ, which is extracted from the EE, $|G(r)|$ for GfTNS starts to decay much faster than the power law behaviour for that of the exact ground state. (c) $|\langle f_{\mathbf{k}} f_{-\mathbf{k}}\rangle|^2$ at $D = 32$ along a radial direction in the Brillouin zone as a function of the single-particle energy $\varepsilon_{\mathbf{k}}$ of H (Eq. 3.5). (d) $\langle f_{\mathbf{k}} f_{-\mathbf{k}}\rangle$ at $D = 32$ throughout the Brillouin zone. The color map denotes the magnitude, the arrows the complex phase.

With periodic boundary conditions, the total number of electrons in the spinless Fermi sea is odd for every system size. If a state at momentum $\mathbf{k}$ is occupied, then so is the state at $-\mathbf{k}$. So the electrons appear in pairs, except at the time-reversal invariant momenta (TRIM). Here, the only TRIM which is occupied is the center of Brillouin zone $\mathbf{k} = 0$; hence the overall fermion parity is odd. The tensors defined in Eq. 3.1 have even fermion parity, and therefore the GfTNS also necessarily has even parity (for every system size). This is reflected in the fact that the wave function in Eq. 3.4 with $N = 1$ always leaves the states at the TRIM empty. It is possible to fix this discrepancy by inserting an additional Grassmann variable "on the virtual level" in Eq. 3.2, which makes the fTNS have odd parity (this Grassmann variable is identical to the string operators that have appeared in fTNS constructions [113] of the $p_x + ip_y$ superconductor [114]). Here, however, we will use a simpler way to sidestep this issue and work with antiperiodic boundary conditions such that the spinless Fermi surface state always has even fermion parity.

We choose μ to fix the total particle number N_e at half filling, i.e., $\nu = N_e/N_s = 1/2$, and use $t'/t = 0.353$ to realise an almost circular Fermi surface. We have optimized the GfTNS to minimize its energy $\langle H\rangle$, at different bond dimensions D (see Sec. 3.5 for details of the numerical simulations). Fig. 3.2(a) depicts the difference in energy of the optimal GfTNS compared the exact result, as well as the standard deviation of the total particle number

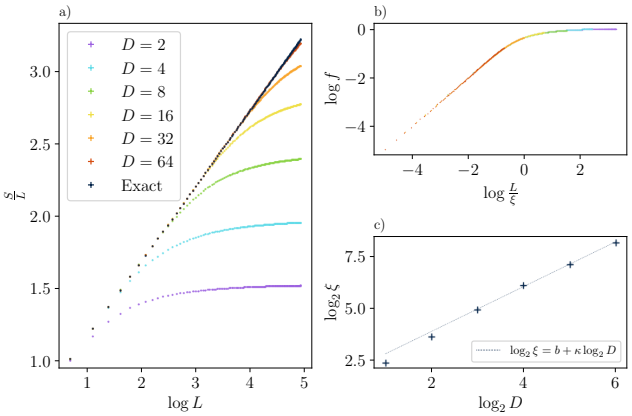

Figure 3.3: (a) Scaling collapse of the entanglement entropy S of a $L \times L$ square region in the optimized GfTNS for spinless fermions at half filling with $t'/t = 0.353$ and $N_s = 999^2$, obtained at different bond dimensions D. (b) Collapse of the GfTNS entanglement entropies using the scaling law of Eq. 3.7. (c) Linear fit of the correlation length ξ as a function of D obtained from the scaling collapse of S, with $\kappa = 1.074$.

per site, i.e., $\sigma_q \equiv \sqrt{\langle N_e^2 \rangle - \langle N_e \rangle^2}/N_s$. The latter is a quantifier for the charge conservation symmetry breaking in the GfTNS. We see that both the energy error and σ_q decrease as a function of D, indicating—similarly as Ref. [115]—that the optimised GfTNS provides an approximation to the exact metallic ground state which improves systematically with bond dimension. Fig. 3.2(b) shows the correlation function $G(\mathbf{r}) = \langle f^\dagger_{\mathbf{r}+\mathbf{r}'} f_{\mathbf{r}'} \rangle$ of the $D = 16$ GfTNS, which agrees with the exact result for $|\mathbf{r}| \lesssim \xi \approx 70$. Note that $\xi \ll N_x = N_y$, such that we can take our results to be representative of the thermodynamic limit. In Fig. 3.2(c) and 3.2(d) we plot the pairing function $\langle f_{\mathbf{k}} f_{-\mathbf{k}} \rangle$ for $D = 32$, both along a radial cut, and throughout the entire Brillouin zone. $|\langle f_{\mathbf{k}} f_{-\mathbf{k}} \rangle|^2$ is peaked at the Fermi surface, and can be approximated by the BCS expression $\Delta^2/4(\Delta^2 + \varepsilon^2_{\mathbf{k}})$, where $\varepsilon_{\mathbf{k}}$ is the single-particle dispersion of H. Fig. 3.2(d) illustrates that the phase of $\langle f_{\mathbf{k}} f_{-\mathbf{k}} \rangle$ winds by 2π along the Fermi surface, i.e., it is a $p_x + ip_y$ gap. We explain how the GfTNS deals with the chiral topology of the weak-pairing $p_x + ip_y$ superconductor [114, 116, 102] in the Ref. [69].

The leading term in the EE of a square $L \times L$ spatial region R in a 2D state with a single spinless Fermi surface is given by

$$S = \frac{\log(\Lambda L)}{24\pi} \oint_{\partial R} \oint_{\mathrm{FS}} |\mathrm{d}S_{\mathbf{x}} \cdot \mathrm{d}S_{\mathbf{k}}| \,, \tag{3.6}$$

where Λ is a nonuniversal inverse length scale, and the integrals are over the boundary of R and over the Fermi surface, and $\mathrm{d}S_{\mathbf{x}}$ ($\mathrm{d}S_{\mathbf{k}}$) is a surface element of ∂R (the Fermi surface) [55]. For the special case of a circular Fermi surface with radius k_F, this general expression evaluates to $S_{\mathrm{circ}} = \frac{2k_F L}{3\pi} \log \Lambda L$.

In Fig. 3.3(a), we plot the EE S as a function of L, directly calculated from the correlation matrix of the optimized GfTNS at different D. This plot shows our main result, which is that the leading contribution to the EE at finite D can be written as

$$S_{\mathrm{fTNS}} = \log\left(\Lambda\xi f(L/\xi)\right) \times \frac{1}{24\pi} \oint_{\partial R} \oint_{FS} \left|\mathrm{d}S_{\mathbf{x}} \cdot \mathrm{d}S_{\mathbf{k}}\right|, \tag{3.7}$$

where ξ is the finite-bond-dimension-induced correlation length, and $f(x)$ is a scaling function which satisfies $f(x \ll 1) \sim x$ and $f(x \gg 1) = \text{constant}$. Fig. 3.3(a) shows how the optimized GfTNS at different D approximate the $L \log L$ scaling of the EE, while Fig. 3.3(b) directly plots the scaling function $f(x)$ onto which the numerical data obtained at different D can be collapsed. Note that to obtain the scaling collapse we have only one tuning parameter ξ if we require that the GfTNS results agree with the exact result at small L. The length scale ξ obtained from the EE of the $D = 16$ GfTNS (see 3.A) is indicated as the vertical dashed line in the plot of $G(\mathbf{r})$ in Fig. 3.2(b). This shows that ξ agrees with the physical correlation length, i.e., the length scale at which the exponential decay of correlations in the GfTNS sets in. Finally, Fig. 3.3(c) confirms that ξ increases monotonically as a function of D. For the moderate bond dimensions used in this work, ξ seems to follow a power law as a function of D. However, based on both analytical [117] and numerical (see 3.B) results in 1D, which show that Gaussian fermionic matrix product states (GfMPS) cannot reproduce the power-law scaling $\xi \propto D^{\kappa}$ of generic MPS, we anticipate that for GfTNS, deviations from the power-law relation between ξ and D could occur at higher D. For general (i.e., non-Gaussian) fTNS, we nevertheless conjecture that $\xi \propto D^{\kappa}$.

3.4 Properties of the scaling function

Similarly to the scaling functions of gapless systems with conformal symmetry in the IR, $f(x)$ is expected to be insensitive to lattice-scale details. We also expect that $f(x)$ will depend on the shape of the Fermi surface, in analogy to the finite-temperature entropy scaling functions for Fermi liquids [118]. To verify the first expectation we have performed numerical data collapses of the EE obtained at different fillings, while keeping the FS approximately circular. These results (see 3.A), confirm that the EE at different fillings can indeed be collapsed on the same curve. By tuning away from $t'/t = 0.353$ in either direction, which changes the FS to being either more diamondlike or more squarelike, we observe that the results collapse on different scaling functions, thus confirming the dependence of $f(x)$ on the FS geometry (see 3.A).

3.5 Gu-Verstraete-Wen formalism for spinless fermions: optimisation method and additional results

In this section, we describe our numerical method to optimise GfTNS for 2D states with a Fermi surface composed of a single spinless fermion in detail. We apply the Gu-Verstraete-Wen (GVW) formalism for Gaussian tensor networks, as introduced in [97]. As $N = 1$, the B submatrix of A now reduces to zero so that

$$|\psi\rangle = \int D[\theta]D[\bar{\theta}] \prod_{\mathbf{x}} \exp\left(\bar{\theta}^{h^T}_{\mathbf{x}} \theta^{h}_{\mathbf{x}+\mathbf{e}_x}\right) \exp\left(\bar{\theta}^{v^T}_{\mathbf{x}} \theta^{v}_{\mathbf{x}+\mathbf{e}_y}\right) \exp\left(\frac{1}{2}\theta^T_{\mathbf{x}} D \theta_{\mathbf{x}}\right) \exp\left(\theta^T_{\mathbf{x}} C f^\dagger_{\mathbf{x}}\right) |0\rangle \ , \tag{3.8}$$

where $\theta_{\mathbf{x}} \equiv (\theta^{h^T}_{\mathbf{x}}, \bar{\theta}^{h^T}_{\mathbf{x}}, \theta^{v^T}_{\mathbf{x}}, \bar{\theta}^{v^T}_{\mathbf{x}})^T$ collects the virtual Grassmann numbers associated to site $\mathbf{x}$ and $f^\dagger_{\mathbf{x}}$ creates the spinless fermion on site $\mathbf{x}$. Furthermore, D is a complex antisymmetric $4M \times 4M$ matrix, whereas C is a complex vector of length $4M$. The number of (complex) variational parameters in this state thus seems to be $8M^2 + 2M$. However, the state has gauge redundancies which can be eliminated. The origin of the gauge redundancies can be discerned by examining a single term $\exp\left(\bar{\theta}^{h^T}_{\mathbf{x}} \theta^{h}_{\mathbf{x}+\mathbf{e}_x}\right)$, which is invariant under

$$\bar{\theta}^{h^T}_{\mathbf{x}} \mapsto \bar{\theta}^{h^T}_{\mathbf{x}} W^{-1}, \quad \theta^{h}_{\mathbf{x}+\mathbf{e}_x} \mapsto W \theta^{h}_{\mathbf{x}+\mathbf{e}_x} \qquad \forall\, W \in GL(M, \mathbb{C})\,. \tag{3.9}$$

Similarly we can also transform θ^v and $\bar{\theta}^v$. To keep the translation invariance explicit, we can apply the same transformation to every bond. Since we are integrating the Grassmann variables out, we can check that the resulting Gaussian state is invariant under these transformations.

To make the discussions more transparent, let us write D and C in terms of blocks,

$$D \equiv \begin{bmatrix} D_{hh} & D_{h\bar{h}} & D_{hv} & D_{h\bar{v}} \\ D_{\bar{h}h} & D_{h\bar{h}} & D_{\bar{h}v} & D_{\bar{h}\bar{v}} \\ D_{vh} & D_{v\bar{h}} & D_{vv} & D_{v\bar{v}} \\ D_{\bar{v}h} & D_{\bar{v}\bar{h}} & D_{\bar{v}v} & D_{\bar{v}\bar{v}} \end{bmatrix}, \quad C \equiv \begin{bmatrix} C_h \\ C_{\bar{h}} \\ C_v \\ C_{\bar{v}} \end{bmatrix}. \tag{3.10}$$

There are two independent gauge transformations, $W_{\mathbf{x}}$ and $W_{\mathbf{y}}$, transforming, for instance, the blocks D_{hh} and D_{vv} in the following way,

$$D_{hh} \mapsto W^T_{\mathbf{x}} D_{hh} W_{\mathbf{x}}, \quad D_{vv} \mapsto W^T_{\mathbf{y}} D_{vv} W_{\mathbf{y}}\,. \tag{3.11}$$

Because D_{hh} and D_{vv} are antisymmetric, they admit real normal forms [119],

$$D_{hh} = U_h^T \left(\bigoplus_{i=1}^{\lfloor \frac{M}{2} \rfloor} \begin{bmatrix} 0 & \alpha_i \\ -\alpha_i & 0 \end{bmatrix} (\oplus[0]) \right) U_h\,, \quad D_{vv} = U_v^T \left(\bigoplus_{i=1}^{\lfloor \frac{M}{2} \rfloor} \begin{bmatrix} 0 & \beta_i \\ -\beta_i & 0 \end{bmatrix} (\oplus[0]) \right) U_v, \tag{3.12}$$

where U_h and U_v are unitary matrices, $\{\alpha_i, \beta_i\}$ are non-negative real numbers and the direct sums $\oplus[0]$ only appear when M is odd. Therefore, by choosing

$$W_{\mathbf{x}} \equiv U_h^\dagger \left(\bigoplus_{i=1}^{\lfloor \frac{M}{2} \rfloor} \begin{bmatrix} \frac{1}{\sqrt{\alpha_i}} & 0 \\ 0 & \frac{1}{\sqrt{\alpha_i}} \end{bmatrix} (\oplus[1]) \right) , \quad W_{\mathbf{y}} \equiv U_v^\dagger \left(\bigoplus_{i=1}^{\lfloor \frac{M}{2} \rfloor} \begin{bmatrix} \frac{1}{\sqrt{\beta_i}} & 0 \\ 0 & \frac{1}{\sqrt{\beta_i}} \end{bmatrix} (\oplus[1]) \right) , \tag{3.13}$$

we bring D_{hh} and D_{vv} into very simple form $J^{\oplus \lfloor \frac{M}{2} \rfloor} (\oplus[0])$ with $J = i\sigma_y$. Thus, the gauge degrees of freedom are eliminated by fixing D_{hh} and D_{vv} in our GfTNS, thereby reducing the number of complex variational parameters to $7M^2 + 3M$. We optimised GfTNS with and without fixed gauge and found matching energies, thus not only confirming the validity of the gauge fixing procedure but also providing confidence that the optimisation procedure (as described in the next paragraph) is not struggling with local minima. However, the optimisation with gauge degrees of freedom removed convergence significantly faster, which was crucial to obtain converged results for the larger bond dimensions D used in this study.

To evaluate the energy of the GfTNS, we go to momentum space,

$$\begin{aligned} |\psi\rangle &= \int [D\theta] \int [D\bar{\theta}] \exp\left(\frac{1}{2} \sum_{\mathbf{k}} \theta_{-\mathbf{k}}^T [D + \tilde{M}(\mathbf{k})] \theta_{\mathbf{k}} + \theta_{-\mathbf{k}}^T C f_{\mathbf{k}}^\dagger \right) |0\rangle \\ &= \prod_{\mathbf{k}} \frac{1}{\sqrt{1 + |g_{\mathbf{k}}|^2}} \exp\left(\frac{1}{2} g_{\mathbf{k}} f_{-\mathbf{k}}^\dagger f_{\mathbf{k}}^\dagger \right) |0\rangle , \end{aligned} \tag{3.14}$$

where $g_{\mathbf{k}} \equiv C^T [D + \tilde{M}(\mathbf{k})]^{-1} C = C^T S(\mathbf{k})^{-1} C$ and where $\tilde{M}(\mathbf{k})$ is defined as in Eq. 3.3 in the main text. Consequently, the modal occupation and pairing term expectation values are given by Eq. 3.21. Using this and the fact that we can rewrite the free-fermion Hamiltonian from Eq. 3.5 as $H = \sum_{\mathbf{k}} H(\mathbf{k}) f_{\mathbf{k}}^\dagger f_{\mathbf{k}}$ with $H(\mathbf{k}) = -2t (\cos k_x + \cos k_y) - 2t' (\cos(k_x + k_y) + \cos(k_x - k_y)) - \mu$, we obtain the energy density,

$$e = \frac{1}{N_s} \langle \psi | H | \psi \rangle = \frac{1}{N_s} \sum_{\mathbf{k}} H(\mathbf{k}) \frac{|g_{\mathbf{k}}|^2}{(1 + |g_{\mathbf{k}}|^2)} . \tag{3.15}$$

The above expression serves as our cost function $e \equiv e(z)$ with the variational parameters in z encoding D and C. More concretely, the first $7M^2 - M$ elements of this complex vector, denoted as z_D, encode the gauge independent entries of D. The last $4M$ entries, denoted as z_C, correspond directly to C. The gradient of the cost function w.r.t. (the complex conjugate of) z can hence be expressed as

$$2 \frac{\partial e}{\partial \bar{z}} = \frac{2}{N_s} \sum_{\mathbf{k}} H(\mathbf{k}) \frac{g_{\mathbf{k}}(z)}{(1 + |g_{\mathbf{k}}(z)|^2)^2} \frac{\partial \bar{g}_{\mathbf{k}}(\bar{z})}{\partial \bar{z}} , \tag{3.16}$$

where

$$\frac{\partial g_{\mathbf{k}}}{\partial z_D} = -C^T S^{-1}(\mathbf{k}) \frac{\partial S(\mathbf{k})}{\partial z_D} S^{-1}(\mathbf{k}) C , \quad \frac{\partial g_{\mathbf{k}}}{\partial z_C} = \frac{\partial C^T}{\partial z_C} S^{-1}(\mathbf{k}) C + C^T S^{-1}(\mathbf{k}) \frac{\partial C}{\partial z_C} . \tag{3.17}$$

It should be noted that $\partial S(\mathbf{k})/\partial z_D$ and $\partial C/\partial z_C$ are sparse matrices/vectors. Considering z_D as example, each entry in z_D is associated with an ordered pair (i, j), such that $(\partial S(\mathbf{k})/\partial z_D)_{ij} = -(\partial S(\mathbf{k})/\partial z_D)_{ji} = 1$, and the rest of the matrix is 0. Having the analytical form of the cost function and the gradient, we use the quasi-Newton BFGS method, implemented in the `Optim.jl` package [120], to optimise the cost function. We observed that, for this problem, the BFGS method greatly outperforms alternative methods. We also remark that it is not difficult to work out the analytical expression of the Hessian of our cost function. While this enables the use of the second-order Newton's method, we found that it is too expensive in practice.

In addition to the result in the main text, we further optimised GfTNS and performed scaling collapses for Fermi surfaces with different fillings and shapes, the results for which are collected in Fig. 3.4 and Table 3.1. The four columns in the figure correspond to: 1) $t'/t = 0.353$, with $\mu = 0.754$ that enforces the filling to be 0.5; 2) $t'/t = 0.353$, with $\mu = 0.449$ that enforces the filling to be 0.45; 3) $t'/t = 0.353$, with $\mu = 1.00$ that enforces the filling to be 0.55; 4) $t'/t = 0.2$, with $\mu = 0.476$ that enforces the filling to be 0.5; 5) $t'/t = 0.5$, with $\mu = 0.963$ that enforces the filling to be 0.5. For all of these cases, we observe a similar scaling of energy error/correlation length with the bond dimension. Furthermore, we find that the scaling function is independent of the filling fraction (comparing cases 1, 2 and 3), but does show an (albeit weak) dependence on the shape of the Fermi surface (comparing case 1 with 4 and 5), as demonstrated in Fig. 3.6 . The former is quite remarkable. Indeed, deriving a general scaling law for the EE (as in Ref. [121]), one could start from the exact ground state EE, given by $S = \alpha\, k_F L \log \Lambda L$ for a circular Fermi surface. Simultaneously scaling L by a factor $\frac{1}{s}$ and k_F by s (thus scaling the periodicity of the Friedel oscillations in real-space by a factor $\frac{1}{s}$) while maintaining the same Λ should then decrease $\exp\left(\frac{S}{\alpha\, k_F L}\right)$ by a factor s. For an optimal GfTNS, the same reasoning applies but now also the correlation length should be scaled down, yielding the scaling hypothesis,

$$\exp\left(\frac{S(k_F, L, \xi)}{\alpha\, k_F L}\right) = s \exp\left(\frac{S(s k_F, \frac{L}{s}, \frac{\xi}{s})}{\alpha\, k_F L}\right) . \tag{3.18}$$

Setting $s = \xi$, one obtains

$$S(k_F, L, \xi) = \alpha\, k_F L \log \xi + S\left(k_F\, \xi, \frac{L}{\xi}, 1\right) = \alpha\, k_F L \log\left(\xi \Lambda f\left(k_F \xi, \frac{L}{\xi}\right)\right), \tag{3.19}$$

where everything was written down with a single logarithm by defining the scaling function via $S\left(k_F\, \xi, \frac{L}{\xi}, 1\right) = \alpha\, k_F L \log\left(\Lambda f\left(k_F \xi, \frac{L}{\xi}\right)\right)$. Here the Λ prefactor was added to make f dimensionless. We thus retrieve the same scaling law as in Eq. 3.7 but now also depending on $k_F \xi$. Based on Fig. 3.6, this additional dependence drops out. For different Fermi surface

t'/t	μ/t	n_{filling}	$D=4$	$D=8$	$D=16$	$D=32$	$D=64$
0.353	0.754	0.50	12.4	30.2	68.9	141.8	287.5
0.353	0.449	0.45	11.8	28.1	63.4	132.1	265.0
0.353	1.000	0.55	13.3	33.4	77.6	163.6	321.1
0.200	0.476	0.50	13.5	34.4	80.9	170.1	322.8
0.500	0.963	0.50	11.6	27.3	60.1	127.6	244.8

Table 3.1: The collection of correlation lengths, for the spinless case, obtained via the scaling collapse procedure.

shapes on the other hand, the scaling function does change. Drawing intuition from the finite temperature behavior of Fermi surface EE [118], this does not come as a surprise. We leave a detailed analysis to a future study.

3.A Performing the scaling collapse

Once optimised, real-space correlation functions like

$$\langle f_{\mathbf{x}}^\dagger f_{\mathbf{y}}\rangle = \frac{1}{N_s}\sum_{\mathbf{k}} e^{i\mathbf{k}\cdot(\mathbf{x}-\mathbf{y})}\, n(\mathbf{k}) \qquad \text{and} \qquad \langle f_{\mathbf{x}} f_{\mathbf{y}}\rangle = \frac{1}{N_s}\sum_{\mathbf{k}} e^{-i\mathbf{k}\cdot(\mathbf{x}-\mathbf{y})}\, x(\mathbf{k})\,. \tag{3.20}$$

(here for $N=1$) can easily be calculated for GfTNS by (inverse) Fourier transforming

$$n(\mathbf{k}) = \langle f_{\mathbf{k}}^\dagger f_{\mathbf{k}}\rangle = \frac{|g_{\mathbf{k}}|^2}{1+|g_{\mathbf{k}}|^2} \qquad \text{and} \qquad x(\mathbf{k}) = \langle f_{\mathbf{k}} f_{-\mathbf{k}}\rangle = \frac{g_{\mathbf{k}}}{1+|g_{\mathbf{k}}|^2}\,. \tag{3.21}$$

One then constructs a real-space correlation matrix C, consisting of

$$C_{\mathbf{x},\mathbf{y}} = C_{\mathbf{x}-\mathbf{y}} = \begin{pmatrix} \langle f_{\mathbf{x}}^\dagger f_{\mathbf{y}}\rangle & \langle f_{\mathbf{x}}^\dagger f_{\mathbf{y}}^\dagger\rangle \\ \langle f_{\mathbf{x}} f_{\mathbf{y}}\rangle & \langle f_{\mathbf{x}} f_{\mathbf{y}}^\dagger\rangle \end{pmatrix} \tag{3.22}$$

blocks for all combinations of $\mathbf{x}$ and $\mathbf{y}$. Restricting to vectors comprised in an $L\times L$ subregion, the resulting correlation matrix $C_{L\times L}$ can be used to calculate the entanglement entropy. Indeed, for a Gaussian state, $S=-\sum \zeta\log\zeta$ with ζ the eigenvalues of $C_{L\times L}$. Now recall the scaling hypothesis for the EE from Eq. 3.7. For a circular Fermi surface it reduces to

$$S = \alpha\, k_F L \log\left(\xi\Lambda f\left(\frac{L}{\xi}\right)\right), \tag{3.23}$$

with L a length scale proportional to the circumference of the real space region, k_F the Fermi momentum, an inverse length scale proportional to the circumference of the Fermi surface and $\alpha=\frac{2}{3\pi}$ a dimensionless prefactor depending on the shape of both. Together with the UV cut-off Λ, the latter can be determined from the exact ground state so that the only tunable parameters in the scaling law are the correlation lengths. These infrared length scales, depending on the bond dimension D of the GfTNS approximation, should be

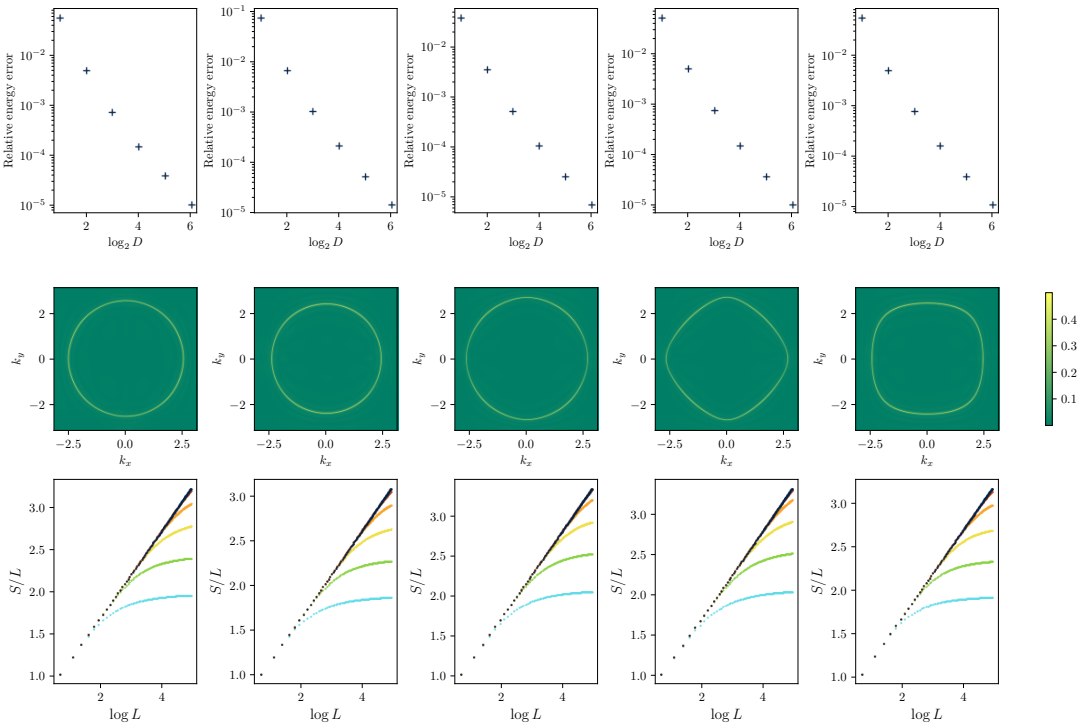

Figure 3.4: Collection of additional GfTNS results for the spinless model. The columns correspond to different parameter choices for $(t, t', n_{\text{filling}})$, respectively $(1, 0.353, 0.5)$, $(1, 0.353, 0.45)$, $(1, 0.353, 0.55)$, $(1, 0.2, 0.5)$ and $(1, 0.5, 0.5)$. The system size for the optimisation of these GfTNS is $N_s = 1000^2$. The first row collects the relative energy errors for the GfTNS. The second row collects $\langle f_{\mathbf{k}} f_{-\mathbf{k}} \rangle$ at $D = 32$ throughout the Brillouin zone. The color map denotes the magnitude. The third row collects the EE of a $L \times L$ region. The color of the data is chosen to match that of Fig. 3.3 for bond dimensions $D = 4, 8, 16, 32, 64$, while the $D = 2$ results have been omitted because they offer a poor description of the Fermi surface.

such that the results are described by a single scaling function f. To this end, we rewrite the scaling law as

$$\log\left(f\left(\frac{L}{\xi}\right)\right) = \frac{S}{\alpha\, k_F L} - \log(\xi\Lambda)\,. \tag{3.24}$$

For the correct ξ, plotting the right-hand side of the equation versus (the logarithm of) $\frac{L}{\xi}$ should thus yield a single curve. However, this leaves an overall scale undetermined as setting $\tilde{\xi} = s\xi$ simply leads to a redefined scaling function $\tilde{f}(x) = \frac{1}{s} f(sx)$ with the same shape. This scale can be fixed by requiring that the asymptotic value $\lim_{x\to\infty} f(x) = 1$, so that $\lim_{L\to\infty} S(L) = \alpha\, k_F L \log(\Lambda\xi)$. However, as the cost to compute $S(L)$ grows quite rapidly in L, namely as $\mathcal{O}(L^6)$, the calculations are restricted to moderate values of L. Hence, in practice, the scale is chosen schematically as demonstrated in Fig. 3.5, i.e. by setting $f(x) = 1$ for $x = L/\xi$ for the largest L and for the smallest D in our set, where the asymptotic regime is approximately reached. Once the correlation length for *one* bond

dimension is fixed, the correlation lengths for the GfTNS at other values of D can be fixed by the collapse.

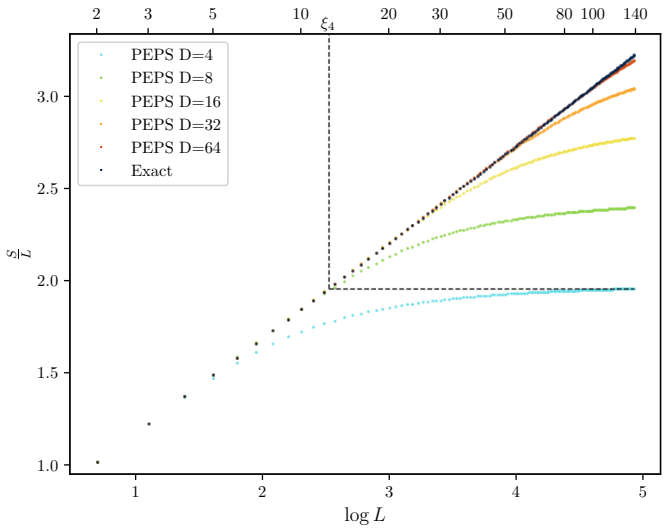

Figure 3.5: Illustration of the procedure to extract the correlation length from the EE data (here for the same data as in Fig. 3.3). For the GfTNS with bond dimension D, the crossover from the $\log L$-Fermi surface regime to the area law regime is long. When the crossover is completed, S/L enters into a plateau with value $y_{\text{plateau},D} = S_D/L$. We identify the correlation length ξ_D to be the length scale at which the exact Fermi surface S_{exact}/L reaches the value $y_{\text{plateau},D}$.

3.B GfTNS in 1D cannot reproduce the power law relation between correlation length and bond dimension

In Ref. [117], the authors showed that GfMPS approximate critical states significantly less efficiently than generic MPS. Here we back this claim from another perspective, namely by showing that GfMPS cannot reproduce the power-law relation $\Delta e \sim D^{-\omega}$ (recall that Δe is the error in the energy density), which is known to hold for generic MPS approximations to one-dimensional critical ground states [53, 54, 122]. Here we study a one-dimensional fermion system, with antiperiodic boundary condition, described by the following hopping Hamiltonian,

$$H = -\sum_{\langle ij \rangle} \left(f_i^\dagger f_j + f_j^\dagger f_i \right) . \tag{3.25}$$

We work with system size $N_s = 100\,000$, and $\mu = 0$ to ensure half-filling. Using the GVW formalism, we optimised GfMPS of $D = 4, \ldots, 4096$. For the optimised GfMPS, the energy density errors are plotted in Fig. 3.7. A closer examination of the data shows a

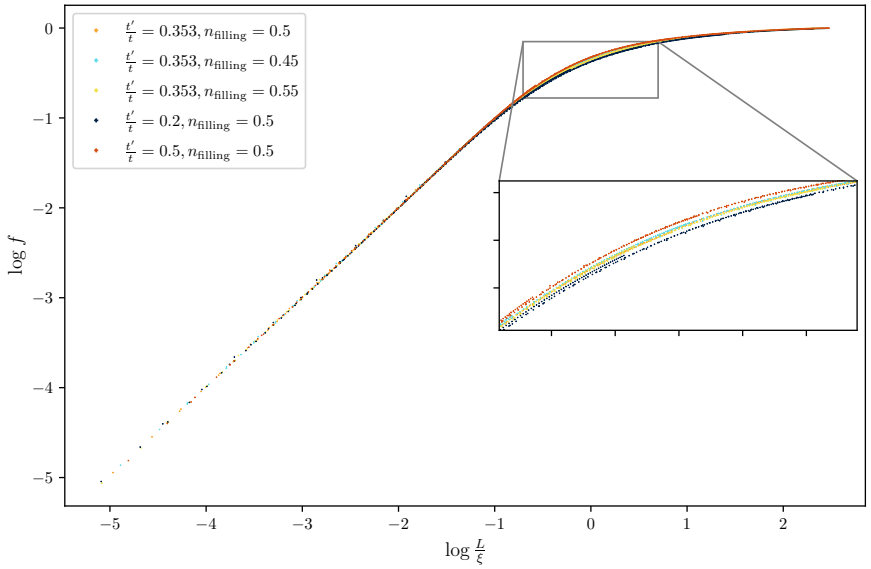

Figure 3.6: The scaling collapse of EE data for different Fermi surfaces. the fuzziness near the transition region indicates that the scaling function for the spinless case could be Fermi surface dependent after all.

clear deviation from the power-law behavior. Since our bond dimensions satisfy $D \equiv 2^M$, $\frac{\Delta e(M+1)}{\Delta e(M)}$ would be a constant if the power law relation is satisfied. However, as we can see in Table. 3.2, this is clearly not the case. Moreover, in the generic MPS case, $\frac{\Delta e(M+1)}{\Delta e(M)} = 5.28$ for the model we wrote down. Thus the data presented in Table. 3.2 shows that GfMPS are not able to approximate critical states as nearly as well as generic MPS with comparable bond dimension.

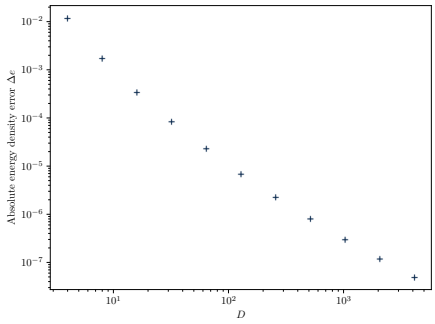

Figure 3.7: The energy density error of optimised GfMPS.

This behaviour is quite well understood for GfMPS. For a bipartition of the ground state (with open boundary conditions) into a left and right half, the reduced density matrix is also Gaussian, and can be diagonalised to take the form $\exp\left(-\sum_m \nu_m b_m^\dagger b_m\right)$. For the

M	2	3	4	5	6	7	8	9	10	11
$\frac{\Delta e(M+1)}{\Delta e(M)}$	6.6962	4.9788	4.1240	3.6087	3.2619	3.0111	2.8206	2.6707	2.5500	2.4519

Table 3.2: The energy density error ratios between adjacent GfMPS.

Hamiltonian in Eq. 3.25 in particular, the values ν_m are proportional to the nonnegative integers in the thermodynamic limit, i.e. $\nu_m \sim m$. The entanglement spectrum (logarithm of the spectrum of Schmidt coefficients) can then be scaled to also correspond to the integers (now including zero), where each value n has a degeneracy given by the number of strict partitions $q(n)$ of that integer. A GfMPS approximation of the true ground state with M virtual fermions (or Grassmann numbers) corresponds to an MPS with bond dimension 2^M, but can only capture the values $\nu_m \sim m$ for $m = 1, \ldots, M$. As a consequence, the distribution of the entanglement spectrum of the GfMPS captures the right degeneracy only up to the value $n = M$, even though it contains values all the way up to $n = M(M+1)/2$. Hence, only the first $\sum_{n=1}^{M} q(n) \ll 2^M$ Schmidt coefficients are correct, with in particular $\lim_{M\to 0} 2^{-M} \sum_{n=1}^{M} q(n) = 0$, i.e. the relative fraction of correct Schmidt coefficients decreases for increasing M. A generic MPS of bond dimension 2^M is not bound by this free-fermion structure of the entanglement spectrum and can capture all Schmidt coefficients up to its full bond dimension correctly.

Whether this behaviour extends to the GfPEPS case is unclear. As there is no clear entanglement interpretation to a single PEPS bond, it is impossible to make an informed prediction about the role of the free-fermion structure in the PEPS truncation.

Chapter 4

Quantum spin liquids on the trillium lattice

4.1 Introduction

In this work, we consider the classification of symmetric spin liquid states on the trillium lattice [123]. Trillium is a network of corner-sharing triangles—like the more well-known kagome and hyperkagome lattices— in three dimensions. The lattice is displayed in Fig. 4.1. Trillium is the magnetic lattice of MnSi, or that of the Ce moments in CeIrSi— which has been considered before in the context of frustrated magnetism [124, 123]. Recent characterisations of the quantum spin liquid material $K_2Ni_2SO_4$ [125, 126, 127] show that the magnetic Ni^{2+} ions lie on two interconnected trillium lattices, having the same set of symmetries as a single trillium lattice— implying, that these structures share the classification of symmetric spin liquid states in terms of projective symmetry groups. Our interest in trillium is also seeded by its remarkable similarity to the hyperhyperkagome (HHK) lattice which describes the network of coupled Cu^{2+} ions in $PbCuTe_2O_6$, which was shown to host a QSL ground state in a series of recent experiments [128, 129, 130], leading to theoretical work on spin liquid states on the underlying HHK structure [131, 132]. Both trillium and HHK are three-dimensional networks of corner-sharing triangles with a cubic Bravais lattice where each site is a part of three corner-sharing triangles. Classical frustrated magnets on these lattices share similar phenomenology [124]: a large regime with classical-spin-liquid behaviour until eventual ordering into co-planar configurations at very low temperatures. For both lattices, large-N approaches yield "partial ordering" [133, 124, 134, 135] ; this implies a macroscopic but sub-extensive number of ordering wave vectors: the manifold of

Chapter heading: dragon motif, detail of the *pan*, Shang dynasty, Yinxu period (circa 14th- 12th/11th centuries B.C.), Meiyintang Collection # 180.

ordering wave-vectors is a line (HHK) or surface (trillium) in three dimensional momentum space. It is instructive to contrast this to order and spin-liquid behaviour in the large-N approach: "Order" corresponds to a single ordering wave-vector, or a few, subextensive number of symmetry-related ordering wave vectors; Disorder or classical spin liquid behaviour — such as ones obtained in the pyrochlore, kagome and hyperkagome lattices — correspond to an extensive manifold of ordering wave-vectors [136, 137, 138]. In the context of QSLs, it is also pertinent to mention the three-dimensional hyperkagome lattice, in which each site is shared by two corner-sharing triangles. The hyperkagome structure describes the magnetic lattice of the well-known candidate spin liquid material $Na_4Ir_3O_8$ [139, 140, 141, 142]; and have invited numerous theoretical investigations of its ordered and spin-liquid states [138, 143, 144, 145, 146, 132]. The hyperkagome lattice has the same space group and therefore has the same classification of PSGs as the HHK lattice [131]. The space group

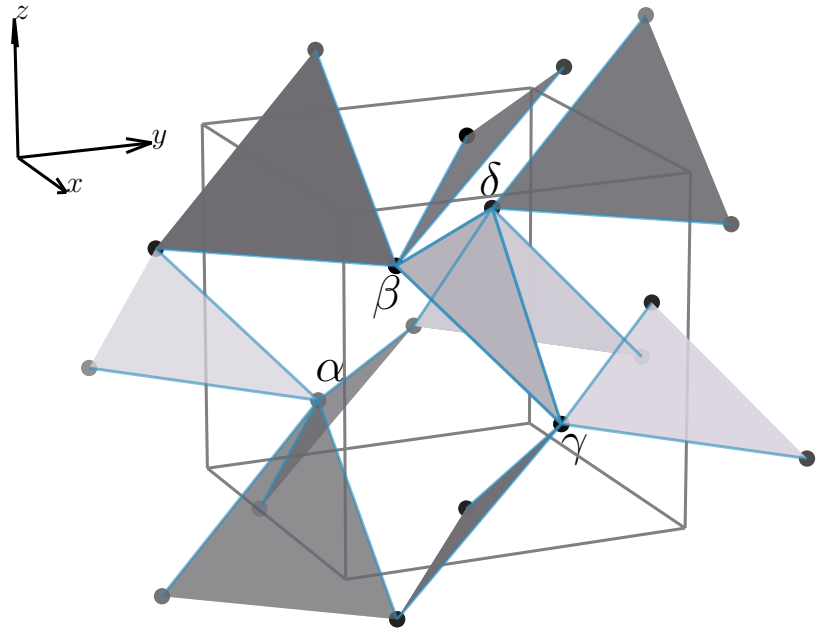

Figure 4.1: The three-dimensional trillium lattice of corner-sharing triangles. Each site is shared by three triangular plaquettes. The Bravais lattice is cubic, with basis of 4 sublattice sites labelled α, β, δ and γ.

of HHK ($\mathsf{P4_132}$) has a 3-fold rotation and a 4-fold non-symmorphic screw operation, where the non-symmorphic screw is known to cause a drastic reduction of total number of QSL states [146, 131]. The space group of trillium, $\mathsf{P2_13}$, has a three-fold rotation, along with two twofold non-symmorphic screw operations [124]. In light of the preceding discussion, it is natural to ask what QSL phases are consistent with the symmetries of the trillium lattice. To this end, in this chapter, we undertake a classification of PSGs for the frustrated

ζ	$\vec{u}_j - \vec{u}_i$	(s_i, s_j)
1	$(0,0,0)$	(β,γ)
2	$(0,0,1)$	(β,γ)
3	$(0,1,1)$	(δ,α)
4	$(0,1,0)$	(δ,α)
5	$(0,0,0)$	(γ,δ)
6	$(1,0,0)$	(γ,δ)
7	$(1,0,1)$	(β,α)
8	$(0,0,1)$	(β,α)
9	$(0,0,0)$	(δ,β)
10	$(0,1,0)$	(δ,β)
11	$(1,1,0)$	(γ,α)
12	$(1,0,0)$	(γ,α)

Table 4.1: The labelling of the 12 translationally inequivalent nearest neighboring links for a unit cell, indexed by ζ. Each link is specified by the unit-cell positions and sublattice indices of the two lattice sites making up the link. For a given label ζ, the head of the bond is labeled i and the end is labeled j. $\vec{u}_{i/j}$ is the position of the unit cell, whereas $s_{i/j}$ is the sub-lattice index.

trillium lattice. We hope this will guide the interpretation of results of future experiments, and add to our theoretical understanding of QSL phases in three dimensions.

Without time-reversal symmetry (TRS) we find 4 Z_2 QSLs, out of which only 2 survive the imposition of TRS. One of them hosts a gapless nodal star protected by projective symmetries— two gapless bands along the lines from the center of the Brillouin zone to its corners. We find two $\mathsf{U}(1)$ QSLs without TRS, out of which only one survive the introduction of TRS— the surviving $\mathsf{U}(1)$ TRS is proximate to the Z_2 QSL without the nodal star. The $\mathsf{U}(1)$ has a spinon Fermi surface. Further, TRS ensures that there aren't any non-vanishing ansatzes for the $\mathsf{SU}(2)$ QSLs [147]: mean-field parameters must vanish for all. As we explain in the main text later, the symmetry group (SG) of trillium has no chiral PSGs, which have also been considered

The rest of this chapter is organised as follows. In Sec. 4.2, we introduce the trillium lattice and the symmetries in its space group, followed by two tables that collect the algebraic solutions of the PSG equations. In Sec. 4.3, we present the mean-field ansatzes of QSL states corresponding to the algebraic PSG solutions and discuss their physical properties, including spinon dispersions and spin structure factors.

4.2 PSGs of the trillium lattice

In Sec. 4.2.1 we introduce the crystal structure of the trillium lattice and the symmetry generators of its space group. In Sec. 4.2.2 we present the symmetry group relations of

	G_x	G_y	G_z	G_a	G_b	G_c	$G_{\mathcal{T}}$
$(\vec{u},\alpha)$	τ_0	τ_0	τ_0	τ_0	$\mathcal{A}^\dagger$	$\mathcal{A}$	$\mathcal{E}$
$(\vec{u},\beta)$	τ_0	τ_0	τ_0	$\mathcal{A}$	$\mathcal{A}^\dagger$	τ_0	$\mathcal{E}$
$(\vec{u},\gamma)$	τ_0	τ_0	τ_0	$\mathcal{A}^\dagger$	$\mathcal{A}$	τ_0	$\mathcal{E}$
$(\vec{u},\delta)$	τ_0	τ_0	τ_0	τ_0	$\mathcal{A}$	τ_0	$\mathcal{E}$

Table 4.2: The Z_2 PSG solutions for the trillium lattice with the symmetry group $\mathsf{P2_13}\times\mathsf{Z}_2^{\mathcal{T}}$. Here $\mathcal{A}=\tau_0, e^{i\frac{2\pi}{3}\tau_z}$, and $\mathcal{E}=\tau_0, i\tau_z$. Thus in total we have 4 Z_2 PSG. We will, however, note that the $\mathcal{E}=\tau_0$ cases do not produce physical mean-field ansatzes. If TRS is not included, we have 2 PSG solutions.

	G_x	G_y	G_z	G_a	G_b	G_c	$G_{\mathcal{T}}$ $(n_{\mathcal{T}}=1)$	$G_{\mathcal{T}}$ $(n_{\mathcal{T}}=0)$
$(\vec{u},\alpha)$	τ_0	τ_0	τ_0	τ_0	$e^{-iA\tau_z}$	$e^{iA\tau_z}$	$i\tau_x e^{iA\tau_z}$	$i\tau_z$
$(\vec{u},\beta)$	τ_0	τ_0	τ_0	$e^{iA\tau_z}$	$e^{-iA\tau_z}$	τ_0	$i\tau_x$	$i\tau_z$
$(\vec{u},\gamma)$	τ_0	τ_0	τ_0	$e^{-iA\tau_z}$	$e^{iA\tau_z}$	τ_0	$i\tau_x e^{-iA\tau_z}$	$i\tau_z$
$(\vec{u},\delta)$	τ_0	τ_0	τ_0	τ_0	$e^{iA\tau_z}$	τ_0	$i\tau_x e^{iA\tau_z}$	$i\tau_z$

Table 4.3: The $\mathsf{U}(1)$ PSG solutions for the trillium lattice with the symmetry group $\mathsf{P2_13}\times\mathsf{Z}_2^{\mathcal{T}}$. When TRS is not included, the PSG solutions are characterised by A, where we have $A=0,\frac{2\pi}{3}$. When TRS is included, there are two classes of PSG solutions. 1.) $n_{\mathcal{T}}=1$: in this class, no new constraint is introduced; 2.) $n_{\mathcal{T}}=0$: in this class, we have $G_{\mathcal{T}}=i\tau_z$ uniformly. Later we will see that only the case with $A=0$ and $n_{\mathcal{T}}=1$ leads to physical nearest neighbor mean field ansatz invariant under the PSG actions. Thus in total we have 4 $\mathsf{U}(1)$ PSG. If TRS is not included, we have 2 PSG solutions.

trillium, and outline the classification of its PSGs using them. We also present the gauge transformations accompanying physical symmetries for all of the PSGs. The details are relegated to Appendices. 4.A and 4.B.

4.2.1 The trillium lattice

Here we introduce the trillium lattice and its spatial symmetries. The spatial symmetries, along with time reversal, will constitute the physical symmetries which our QSL ground states (after projection to the correct Hilbert space) must respect, and is therefore naturally of paramount importance in determining the PSGs on this lattice.

The trillium lattice has a cubic Bravais lattice with four sub-lattices: α,β,γ and δ. The positions of the sublattice sites relative to the unit cell position are given by:

$$\begin{aligned}&\vec{r}^0_\alpha=(\kappa,\kappa,\kappa),\vec{r}^0_\beta=(\frac{1}{2}+\kappa,\frac{1}{2}-\kappa,1-\kappa),\\&\vec{r}^0_\gamma=(1-\kappa,\frac{1}{2}+\kappa,\frac{1}{2}-\kappa),\vec{r}^0_\delta=(\frac{1}{2}-\kappa,1-\kappa,\frac{1}{2}+\kappa),\end{aligned}\tag{4.1}$$

where κ is a free parameter. As mentioned before, connecting up the lattice sites with nearest neighbour links forms a network of corner sharing triangles, with each site being

part of three triangles. These triangles are the elementary motifs seeding frustration in this lattice. We have displayed the trillium lattice in Fig. 4.1.

We denote the position of an unit cell i by the vector $\vec{u_i} = (x, y, z)$, where x, y, z are integers. A generic lattice site i is referred to by specifying its unit cell position and sublattice as $i \equiv (x, y, z; s)$; such site lies at position $\vec{u}_i + \vec{r}_s^0$. Since the mean-field parameters $\{U_{ij}\}$ specifying the ansatz are associated with the links, it is convenient to uniquely label all links for the purpose of further discussion. We exploit the translation invariance of the lattice to do this: there are 12 links per unit cell, none of which are translationally equivalent to another. We introduce the labels $\zeta = (1, 2 \ldots 12)$ for these links, and specify each of these links in Table 4.1.

The space group for the trillium lattice is $\mathsf{P2_13}$, which has the symmetry generators $\{T_x, T_y, T_z, g_a, g_b, g_c\}$. The T_is are the three translational generators, g_c is a threefold rotation, and g_a and g_b are are the generators of non-symmorphic screw symmetries. It has been noted in the literature [146] that non-symmorphic symmetries generally lead to strong constraints on possible PSGs, and a consequent reduction of their number.

The action of the generators g_a, g_b and g_c on a lattice site $i \equiv (x, y, z, s)$ is given by

$$
\begin{aligned}
g_a :&(x, y, z; \alpha) \mapsto (-x, -y - 1, z; \delta),\\
&(x, y, z; \beta) \mapsto (-x - 1, -y - 1, z + 1; \gamma),\\
&(x, y, z; \gamma) \mapsto (-x - 1, -y - 1, z; \beta),\\
&(x, y, z; \delta) \mapsto (-x, -y - 1, z + 1; \alpha),\\
g_b :&(x, y, z; \alpha) \mapsto (-x - 1, y, -z; \gamma),\\
&(x, y, z; \beta) \mapsto (-x - 1, y, -z - 1; \delta),\\
&(x, y, z; \gamma) \mapsto (-x - 1, y + 1, -z; \alpha),\\
&(x, y, z; \delta) \mapsto (-x - 1, y + 1, -z - 1; \beta),\\
g_c :&(x, y, z; \alpha) \mapsto (z, x, y; \alpha),\\
&(x, y, z; \beta) \mapsto (z, x, y; \gamma),\\
&(x, y, z; \gamma) \mapsto (z, x, y; \delta),\\
&(x, y, z; \delta) \mapsto (z, x, y; \beta)
\end{aligned}
\tag{4.2}
$$

4.2.2 PSG classification on the trillium lattice

The PSG involves the group of the transformations $(G_g(n), g)$ that leaves the mean-field ansatz invariant. Here g is a physical symmetry transformation, and $G_g(n) \in \mathsf{SU(2)}$ is

the associated site-dependent gauge transformation, with n denoting the physical site. $(G_g(n), g)$ acts on a mean-field parameter U_{ij} as

$$(G_g(n), g) : U_{ij} \mapsto G_g(i) U_{g^{-1}(i)g^{-1}(j)} G_g^\dagger(j). \tag{4.3}$$

Since the elements of the IGG $\mathcal{G}$ are pure gauge transformations which leave the ansatz invariant, it is clear that whenever $(G_g(i), g)$ is an element of the PSG, $(WG_g(i), g)$, for all $W \in \mathcal{G}$, is also an element of the PSG. If one considers a gauge-equivalent ansatz, $W_i U_{ij} W_j^\dagger$, the PSG element $(G_g(i), g)$ changes to $(W_i G_g(i) W_{g(i)}^\dagger)$. PSGs related by such gauge transformations are equivalent; they are associated with gauge-equivalent ansatzes and represent the same QSL phase. Our task is to find all such equivalence classes; in other words, to find out one representative from each class, singled out by fixing the gauge freedom.

It is convenient to carry out this task purely "algebraically", *i.e.*, by making no reference to the ansatz. To do this, we note that given a physical symmetry group and the IGG $\mathcal{G}$, the PSG can be viewed as a group equipped with a projection $\mathcal{P}$ to the physical symmetry group, such that $\mathcal{P} : (G_g(i), g) \mapsto g$. From the discussion in the previous paragraph, $\mathcal{P} : (WG_g(i), g) \mapsto g$ for $W \in \mathcal{G}$. As a specific corollary, $\mathcal{P}$ projects pure gauge transformations in the IGG back to the identity element, $\mathcal{P} : (W, e) \mapsto e$ for $W \in \mathcal{G}$.

The projection map between the PSG and the physical symmetry group implies that the gauge transformation $G_g(i)$ associated with the symmetry transformation g is constrained by the relations between symmetry group elements g. These constraints on G_g can be used to enumerate all gauge-inequivalent choices of G_g for all symmetry transformations g, and hence enumerate all PSGs.

To see this, one starts with the relations between the symmetry generators $\{T_x, T_y, T_z, g_a, g_b, g_c, \mathcal{T}\}$ which completely specify the group. Each such relation will lead to a equation constraining the associated PSG elements. The minimal set of such relations that specify the group is called the "presentation" of the group. We have used GAP[148] to obtain the finite presentation of the space group of trillium:

$$g_c^3 = e, \tag{4.4a}$$
$$T_z^{-1} g_a^2 = e, \tag{4.4b}$$
$$T_y^{-1} g_b^2 = e, \tag{4.4c}$$
$$T_x^{-1} T_y^{-1} T_x T_y = e, \tag{4.4d}$$
$$T_y^{-1} T_z^{-1} T_y T_z = e, \tag{4.4e}$$
$$T_z^{-1} T_x^{-1} T_z T_x = e, \tag{4.4f}$$
$$g_a^{-1} T_x g_a T_x = e, \tag{4.4g}$$

$$g_a^{-1}T_y g_a T_y = e, \tag{4.4h}$$
$$g_a^{-1}T_z^{-1} g_a T_z = e, \tag{4.4i}$$
$$g_b^{-1}T_x g_b T_x = e, \tag{4.4j}$$
$$g_b^{-1}T_y^{-1} g_b T_y = e, \tag{4.4k}$$
$$g_b^{-1}T_z g_b T_z = e, \tag{4.4l}$$
$$g_c^{-1}T_y^{-1} g_c T_x = e, \tag{4.4m}$$
$$g_c^{-1}T_z^{-1} g_c T_y = e, \tag{4.4n}$$
$$g_c^{-1}T_x^{-1} g_c T_z = e, \tag{4.4o}$$
$$g_a^{-1}g_c^{-1}g_b^{-1}T_x^{-1}T_y g_a g_c = e, \tag{4.4p}$$
$$g_b^{-1}g_a^{-1}T_x T_y^{-1}T_z g_b g_a = e, \tag{4.4q}$$
$$g_c^{-1}g_b^{-1}T_x^{-1}T_y g_a g_b g_c g_b = e, \tag{4.4r}$$

where e denotes the identity of the symmetry group.

We also consider spin liquid phases on the trillium lattice which respect time-reversal symmetry (TRS). The TRS operator $\mathcal{T}$ acts on the mean-field ansatz by complex conjugating the mean-field parameters U_{ij} and μ_i. It is convenient to include a global gauge transformation $i\tau_2$ in the definition of $G_\mathcal{T}$, such that we have

$$\begin{aligned}(G_\mathcal{T}, \mathcal{T}) : U_{ij} \mapsto & G_\mathcal{T}(i) i\tau_2 U_{ij}^* (-i\tau_2) G_\mathcal{T}^\dagger(j) \\ = & - G_\mathcal{T}(i) U_{ij} G_\mathcal{T}^\dagger(j).\end{aligned} \tag{4.5}$$

The introduction of the TRS brings the following relators, expressing the fact that $\mathcal{T}$ commutes with generators in the space group:

$$\mathcal{T}^2 = e, \tag{4.6a}$$
$$\mathcal{T}^{-1}T_x^{-1}\mathcal{T}T_x = e, \tag{4.6b}$$
$$\mathcal{T}^{-1}T_y^{-1}\mathcal{T}T_y = e, \tag{4.6c}$$
$$\mathcal{T}^{-1}T_z^{-1}\mathcal{T}T_z = e, \tag{4.6d}$$
$$\mathcal{T}^{-1}g_a^{-1}\mathcal{T}g_a = e, \tag{4.6e}$$
$$\mathcal{T}^{-1}g_b^{-1}\mathcal{T}g_b = e, \tag{4.6f}$$
$$\mathcal{T}^{-1}g_c^{-1}\mathcal{T}g_c = e. \tag{4.6g}$$

Chiral spin liquids, which break TRS and some lattice symmetries separately while preserving their combinations, have also been considered in the literature [147, 149, 150]. For chiral PSGs, one considers the symmetry group generated by $g\mathcal{T}^{\epsilon_g}$ instead of the usual symmetry group generated by $\{g\}$ [149, 147]. $\epsilon_g = \{0, 1\}$ specifies whether the lattice symmetry g is

preserved on its own ($\epsilon_g = 0$), or preserved only up to TRS ($\epsilon_g = 1$). In the context of trillium and, the SG relations given by Eqs. 4.4a-4.4r impose the constraint $\epsilon_g = 0$ for all generators. This can be easily seen from the fact that for each generator g, there exists one SG relation which has only an odd number of appearances of that generator— imposing $\epsilon_g = 0$. Therefore, there are no chiral PSGs for trillium. Ground states for classical spins on the trillium lattice [124] are also known to be non-chiral (or, as it boils down to for classical spin configurations, co-planar). Despite this, we have collected the PSG solutions without the presence of TRS as well.

The projective relation between the symmetry group elements and the corresponding PSG elements allow us to translate the above symmetry relations (Eqs 4.4a- 4.6g) into constraint equations for the PSG elements. Consider a general symmetry group relation among a set of elements , $\prod_\nu g_\nu = e$. The product of the corresponding PSG elements are given by $(\tilde{G}, \prod_\nu g_\nu = e)$, where $\tilde{G}$ can be constructed from the matrices $G_{g_\nu}(i)$ using Eq. **??**. Under the projection $\mathcal{P}$ to the symmetry group elements mentioned above, $(\tilde{G}, e) \mapsto e)$; this immediately implies a constraint equation expressing that $\tilde{G}$ must be a member of the IGG, $\tilde{G} \in \mathcal{G}$.

The unknowns in these equations are of two kinds: first, the site-dependent gauge transformation matrices $\{G_x, G_y, G_z, G_a, G_b, G_c, G_\mathcal{T}\}$ accompanying each symmetry transformation in $\{T_x, T_y, T_z, g_a, g_b, g_z, \mathcal{T}\}$; and second, an element of the IGG $W \in \mathcal{G}$ corresponding to each symmetry group relation in Eqs 4.4a-4.6g. Solving these equations, along with choice of gauge described earlier, leads to the different inequivalent PSGs that we are after.

The explicit procedures of solving these equations in a fixed gauge is detailed for specific lattices in the seminal work of Wen (Ref. [66]), as well as several later works classifying PSGs in different spatial lattices [146, 147]. We have undertaken this procedure to enumerate and classify all symmetric spin liquids with the IGG set to both Z_2 and $\mathsf{U}(1)$. The calculations are tedious, and we have relegated their detailed presentation to the Appendices. 4.A and 4.B to preserve the clarity of the presentation. Each inequivalent PSG is uniquely specified by the expressions for site-dependent gauge transformations $\{G_x, G_y, G_z, G_a, G_b, G_c, G_\mathcal{T}\}$ which accompany the symmetry transformations, and here we present the results of our calculations by specifying these gauge transformations for all the PSGs we find.

When the IGG is fixed to Z_2, we find 4 inequivalent PSGs. Once the global gauge freedoms are fixed, the gauge transformation matrices associated with lattice translations turn out to be uniform, with no position or sublattice dependence for all PSGs, *i.e.*, $G_x = G_y = G_z = 1$. The PSGs can be uniquely indexed by constraints on the gauge transformation matrices obtained from the PSG equations. First, the transformation corresponding to time-reversal $G_\mathcal{T}$ takes the values τ_0 or $i\tau_z$, though the PSGs corresponding

to $G_{\mathcal{T}} = \tau_0$ do not lead to any non-zero mean-field ansatzes. Gauge transformation matrices associated with other symmetry generators are also unit-cell independent, although they retain a sublattice dependence. Second, the gauge transformation associated with the rotation g_c acting on sites of sublattice α, $G_c(\alpha) = \mathcal{A}$, takes the 2 values $\exp(ik(2\pi/3)\tau_z)$ for $k = \{0, 1\}$. All other gauge transformations can be specified in terms of these three, as detailed in Table 4.2. The 2 possible values of $G_c(\alpha)$ and the 2 possible values of $G_{\mathcal{T}}$ lead to 4 inequivalent PSGs, out of which only 2 (corresponding to $G_{\mathcal{T}} = i\tau_z$) lead to non-zero mean field ansatzes.

Then, we fix the IGG to $\mathsf{U}(1)$. As in the case of Z_2, the gauge transformations corresponding to the three translations are uniform, $G_x = G_y = G_z = 1$. The other gauge transformations, however, acquire both a unit-cell and a sublattice dependence. The PSGs can again be indexed by the parameters specifying certain gauge transformations. The gauge transformation associated with the rotation g_c acting on sites of sublattice α, $G_c(\alpha) = \mathcal{A}$, takes the 2 values $\exp(ik(2\pi/3)\tau_z)$ for $k = \{0, 1\}$. On including time reversal, we find two possibilities for the associated gauge-transformation $G_{\mathcal{T}}$: first, $G_{\mathcal{T}}$ can be $i\tau_z$ uniformly, and this case does not lead to any physical spin-liquid ansatz with non-zero mean-field parameters— and we do not consider these PSGs further; second, $G_{\mathcal{T}}$ can acquire a space-dependent form depending on A which leads to physical spin liquids. Following the second possibility, therefore, we have one $\mathsf{U}(1)$ spin liquid, as we will later show that only the $k = 0$ case leads to nearest neighbor mean field spin liquid states. We specify the PSGs by expressing all gauge transformations in terms of the parameters A in Table 4.3. In the next section, we will construct mean-field ansatzes for spin liquids corresponding to these PSGs and proceed to investigate them.

4.3 Mean field spin liquid phases

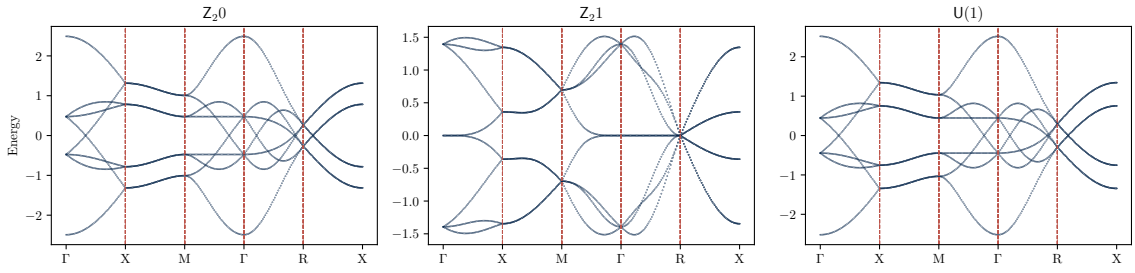

Figure 4.2: In this figure, we collect the band structure of the mean field quantum spin liquids along the high symmetry lines.

QSL label	U_ζ	μ_s
$\mathsf{Z}_2 0$	$U_\zeta = U^x\tau_x + U^y\tau_y, \quad \zeta \in \{1,\ldots,12\}.$	$\mu_s = \mu^x\tau_x + \mu^y\tau_y, \quad s \in \{\alpha,\ldots,\delta\}.$
$\mathsf{Z}_2 1$	$U_\zeta = U^x\tau_x + U^y\tau_y, \quad \zeta \in \{1,2,3,4,5,6,9,10\},$	$\mu_s = 0, \quad s \in \{\alpha,\ldots,\delta\}.$
	$U_\zeta = U^{x'}\tau_x + U^{y'}\tau_y, \quad \zeta \in \{11,12\},$	
	$U_\zeta = U^{x''}\tau_x + U^{y''}\tau_y, \quad \zeta \in \{7,8\}.$	
$\mathsf{U}(1)$	$U_\zeta = U^z\tau_z, \quad \zeta \in \{1,\ldots,12\}.$	$\mu_s = \mu^z\tau_z, \quad s \in \{\alpha,\ldots,\delta\}.$

Table 4.4: In this table, we collect the forms of the nearest neighbor mean field ansatz that correspond to the algebraic PSG solutions obtained. Given a generic label $\mathsf{Z}_2 x$, we can read off the phases in our PSG solutions: $\mathcal{A} = \exp(ix\frac{2\pi}{3}\tau_z)$. Note that in certain entries we have parameters denoted as $U^{x'}$ etc., these are related to U^x and U^y via Eq. 4.8.

QSL label	Numerical values of the mean field parameters	Energy density
$\mathsf{Z}_2 0$	$U^x = -0.161242, U^y = -0.333897, \mu^x = 0.115602, \mu^y = 0.239386.$	-1.647184
$\mathsf{Z}_2 1$	$U^x = -0.110700, \quad U^y = 0.330299.$	-1.458114
$\mathsf{U}(1)$	$U^z = 0.370536, \quad \mu^z = -0.295063.$	-1.646913

Table 4.5: In this table, we collect the numerical values of the mean field parameters and their energetics. We note that $\mathsf{Z}_2 1$ QSL state has energy considerately higher than the rest. Although the rest of the QSL states can be discerned by their energies, the differences between the energies are too small to be attributed to physical reasons.

In this section, we construct the mean field QSL solutions to the Heisenberg Hamiltonian on the trillium lattice. For our purposes, we consider only the nearest neighboring J and set $J = 8/3$ uniformly. The form of the ansatzes are constrained by the PSG: different PSGs enforce different forms for the ansatz. Concretely, a given PSG $(G_g, g), g \in \mathsf{P2_13} \times \mathsf{Z}_2^{\mathcal{T}}$ requires that,

$$\begin{aligned} \forall g : & G_g(g(i))U_{g(i)g(j)}G_g^\dagger(g(j)) = U_{ij}, \\ & G_g(g(i))\mu_{g(i)}G_g^\dagger(g(i)) = \mu_i. \end{aligned} \tag{4.7}$$

The form of the ansatzes for each PSG is derived in detail in Appendix. 4.C by systematically imposing Eq. 4.7 using the gauge transformations detailed in Table 4.2 and Table 4.3. Here we have tabulated the results in Table 4.4. The labeling scheme in the table is such that, given a generic label $\mathsf{Z}_2 x$, we can read off the phases in our PSG solutions: $\mathcal{A} = \exp(ix\frac{2\pi}{3}\tau_z)$. There is only 1 $\mathsf{U}(1)$ QSL, which is labeled as such. The primed parameters, i.e. quantities like $U^{x'}$, are defined as follows:

$$\begin{aligned} \begin{bmatrix} U^{x'} \\ U^{y'} \end{bmatrix} &= \frac{1}{2}\begin{bmatrix} -1 & \sqrt{3} \\ -\sqrt{3} & -1 \end{bmatrix}\begin{bmatrix} U^x \\ U^y \end{bmatrix}, \\ \begin{bmatrix} U^{x''} \\ U^{y''} \end{bmatrix} &= \frac{1}{2}\begin{bmatrix} -1 & -\sqrt{3} \\ \sqrt{3} & -1 \end{bmatrix}\begin{bmatrix} U^x \\ U^y \end{bmatrix}. \end{aligned} \tag{4.8}$$

Concretely, this means we need to find $\{U_{ij}, \mu_i\}$ such that the following self-consistency

equations and on-site constraints are satisfied:

$$\begin{aligned}
\chi_{ij} &= \langle f_{i\uparrow}^{\dagger} f_{j\uparrow} \rangle + \langle f_{i\downarrow}^{\dagger} f_{j\downarrow} \rangle, \\
\eta_{ij} &= \langle f_{i\downarrow} f_{j\uparrow} \rangle - \langle f_{i\uparrow} f_{j\downarrow} \rangle, \\
1 &= \langle f_{i\uparrow}^{\dagger} f_{i\uparrow} \rangle + \langle f_{i\downarrow}^{\dagger} f_{i\downarrow} \rangle, \\
0 &= \langle f_{i\uparrow} f_{i\downarrow} \rangle.
\end{aligned} \tag{4.9}$$

We can impose symmetry conditions on the mean field solutions to reduce the number of unknowns, and the PSG determines these symmetry conditions by requiring that We discuss the consequences of the symmetry conditions on the form of the ansatzs in detail in Appendix 4.A and Appendix 4.B, and the results are tabulated in Table 4.5. Once we obtained the form of the mean field Hamiltonians, we can assemble the Hamiltonian using our variational parameters, and solve the non-linear equation set Eq. 4.9 using the NLSolve package [151] available in JULIA [152]. We set up our system with periodic boundary condition (PBC), with $L = 99$ in the three directions. The numerical values of the solutions are tabulated in Table 4.5, where we also record the energies of the QSL states. We note that the $\mathsf{Z}_2 1$ QSL state has energy considerately higher than the rest.

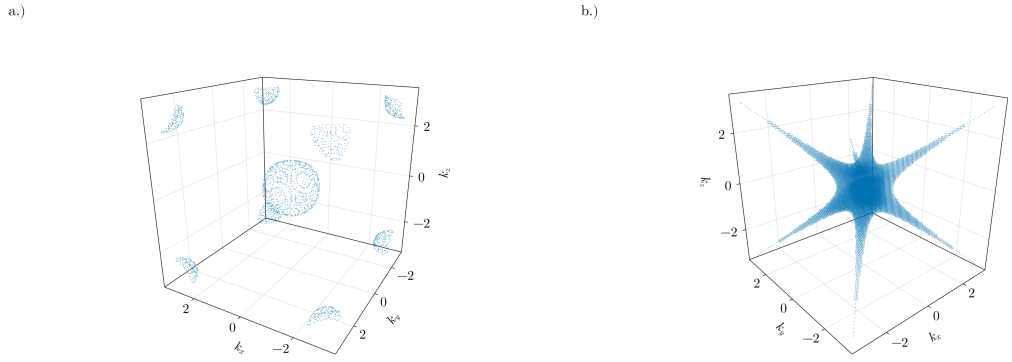

Figure 4.3: In this figure, we plot the collection of gapless points for certain mean field QSL states. a.) $\mathsf{U}(1)$: this state features the two sheeted spinon fermi surfaces, with one located at the center of BZ, and another one at the corners; b.) $\mathsf{Z}_2 1$: this state has a star-shaped gapless manifold, and features a dispersion-less band along the diagonals of the BZ.

4.3.1 Relations between the QSLs

Among the 3 QSL states we obtained, the connection between them is very clear. The parent state of $\mathsf{Z}_2 0$ is $\mathsf{U}(1)$. This can be seen by doing a gauge transformation on $\mathsf{U}(1)$:

$$W(\alpha) = W(\beta) = W(\gamma) = W(\delta) = e^{-i\frac{\pi}{4}\tau_y}, \tag{4.10}$$

which renders, for $\mathsf{U}(1)$:

$$U_\zeta = U^z \tau_x, \quad \zeta \in \{1, \ldots, 12\},$$
$$\mu_s = \mu^z \tau_x, \quad s \in \{\alpha, \ldots, \delta\}, \tag{4.11}$$

It is then clear, that by introducing perturbation $\Delta U_\zeta \sim \tau_y$ and $\Delta \mu_s \sim \tau_y$, we break the $\mathsf{U}(1)$ symmetry and thus $\mathsf{U}(1)$ is reduced to $\mathsf{Z}_2 0$. The $\mathsf{Z}_2 1$ QSL state cannot be obtained by perturbing around the $\mathsf{U}(1)$ QSL state.

4.3.2 The spinon spectra and the nodal star

The spinon band structures for the mean-field QSL states are plotted in Fig. 4.2. Furthermore, in Fig. 4.3, we plot the collections of gapless points in the Brillouin zone (BZ) for $\mathsf{U}(1)$ and $\mathsf{Z}_2 1$.

We note that all the mean field states we obtained are gapless. The $\mathsf{U}(1)$ possesses a spinon fermi surface at the center of the BZ, with another sheet of spinon fermi surface at the corners.

The Z_2 mean-field states are also gapless. The $\mathsf{Z}_2 0$ state has similar spectrum to those of the $\mathsf{U}(1)$, which is due to the fact that the Z_2 mean field state is in the vicinity of the $\mathsf{U}(1)$ states. The $\mathsf{Z}_2 1$ state hosts a spectrum with a "nodal star" of gapless points, with dispersion-less bands running from the center of the BZ to its 8 corners. This can be seen from Fig. 4.3. This nodal star is not a specific property of the short-range ansatz we use to display the bands in Fig. 4.3; rather it is robust to the addition of arbitrary links in the ansatz. In Appendix. 4.C we prove that the gapless nodal star is protected by projective symmetries of the $\mathsf{Z}_2 1$ phase.

Such gapless nodal stars have received significant attention in the pyrochlore lattice [153, 154], where two gapless bands along the nodal star were recently proven to be protected by the projective symmetries [154]. Such lines were also observed in FCC structures in Ref. [155], where the whole mean field Hamiltonian vanishes along the nodal star. Gapless nodal loops were observed in diamond lattice [156] where strong evidence of symmetry-protection was provided by showing that the gapless nodal loops persist despite longer range bond amplitudes being included in the ansatz.

Our proof of the protected nodal star is algebraic and close in spirit to that of Ref. [154]. We look at the symmetries of the mean-field Hamiltonian directly in momentum-space

$$H_{\mathrm{MFT}} = \sum_{\vec{k}} \psi^\dagger(\vec{k}) H_{\mathrm{MFT}}(\vec{k}) \psi(\vec{k}),$$

When the spinors (Eq. 1.80) are arranged as $\psi(\vec{k}) = \big(\psi_1^\alpha(\vec{k}), \psi_1^\beta(\vec{k}), \psi_1^\gamma(\vec{k}), \psi_1^\delta(\vec{k}), \psi_2^\alpha(\vec{k}), \psi_2^\beta(\vec{k}), \psi_2^\gamma(\vec{k}), \psi_2^\delta(\vec{k})\big)$, time-reversal already implies that $H_{\mathrm{MFT}}(\vec{k})$ takes the form

$$H_{\mathrm{MFT}}(\vec{k}) = \begin{pmatrix} 0_{4\times4} & h_{4\times4}(\vec{k}) \\ h^\dagger_{4\times4}(\vec{k}) & 0_{4\times4} \end{pmatrix}. \tag{4.12}$$

This block off-diagonal hermitian structure implies that the eigenvalues come in symmetric pairs of $\pm E(\vec{k})$ everywhere in the BZ. Next, we work out the most general form of $h_{4\times4}(\vec{k})$ allowed by the projective representations of the symmetries $(G_a, g_a), (G_b, g_b)$ and (G_c, g_c). Restricting the general form of $h_{4\times4}(\vec{k})$ to the "nodal star" wavevectors $\vec{k} = (\pm k, \pm k, \pm k)$, we show, using elementary linear algebraic techniques, that it has a maximum rank of 3. This implies that H_{MFT} has a maximum rank of 6 along the nodal star, proving the existence of two gapless bands.

4.3.3 The structure factors

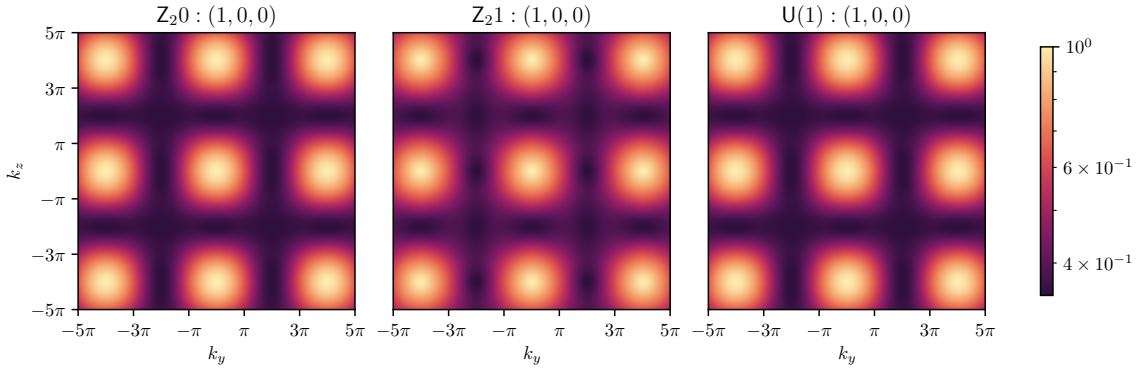

Figure 4.4: In this figure, we collect the static structure factor plots of $\mathsf{Z}_2 0$, $\mathsf{Z}_2 1$ and $\mathsf{U}(1)$ mean field states in the k_y-k_z plane. We note that the $\mathsf{U}(1)$ QSL exhibits remarkably broadened static structure factors, and the $\mathsf{Z}_2 1$ QSL is the most featureful. The seemingly four fold rotation symmetry in the k_y-k_z plane is due to the two screw symmetries on the lattice.

In Fig. 4.4, we plot the static structure factor of $\mathsf{Z}_2 0$, $\mathsf{Z}_2 1$ and $\mathsf{U}(1)$ mean field states in the k_y-k_z plane.

The definition of the static structure factor is:

$$\mathfrak{S}^{s_i,s_j}(\vec{q}) \equiv \frac{1}{N}\sum_{\vec{R}} e^{-i\vec{q}\cdot(\vec{R}+\vec{d}^0_{ij})} \langle \vec{S}_{(0;s_i)} \cdot \vec{S}_{(\vec{R};s_j)} \rangle, \tag{4.13}$$

where s_i and s_j are the sub-lattice indices of site i and j, $\vec{R}$ is the distance between the two unit cells, and $\vec{d}^0_{ij}$ is the distance between the two sub-lattice sites within in the unit cell.

And we compute the sum of all these components:

$$\mathfrak{S}(\vec{q}) \equiv \sum_{s_i,s_j} \mathfrak{S}^{s_i,s_j}(\vec{q}), \tag{4.14}$$

then plot the normalized results.

The structure factor plots indicate that we have obtained remarkable quantum spin liquid states, especially the $\mathsf{U}(1)$ QSLs, which are visibly featureless, implying a sharp departure from the ordered states. We also note that the $\mathsf{Z}_2 1$ state is the most featureful among the three. It is curious to recall that the $\mathsf{Z}_2 1$ state exhibits dispersion-less bands along the diagonals of the BZ, much like the case for the conventional mean field calculations of the Heisenberg model on the trillium lattice, as mentioned in the last section.

4.A IGG = Z_2

One can translate the SG relations to the PSG relations:

$$G_c(g_c^3(i))G_c(g_c^2(i))G_c(g_c(i)) = \eta_c, \tag{4.15a}$$
$$G_z^\dagger(g_a^2(i))G_a(g_a^2(i))G_a(g_a(i)) = \eta_a, \tag{4.15b}$$
$$G_y^\dagger(g_b^2(i))G_b(g_b^2(i))G_b(g_b(i)) = \eta_b, \tag{4.15c}$$
$$G_x^\dagger(T_y^{-1}T_xT_y(i))G_y^\dagger(T_xT_y(i))G_x(T_xT_y(i))G_y(T_y(i)) = \eta_{xy}, \tag{4.15d}$$
$$G_y^\dagger(T_z^{-1}T_yT_z(i))G_z^\dagger(T_yT_z(i))G_y(T_yT_z(i))G_z(T_z(i)) = \eta_{yz}, \tag{4.15e}$$
$$G_z^\dagger(T_x^{-1}T_zT_x(i))G_x^\dagger(T_zT_x(i))G_z(T_zT_x(i))G_x(T_x(i)) = \eta_{zx}, \tag{4.15f}$$
$$G_a^\dagger(T_xg_aT_x(i))G_x(T_xg_aT_x(i))G_a(g_aT_x(i))G_x(T_x(i)) = \eta_{ax}, \tag{4.15g}$$
$$G_a^\dagger(T_yg_aT_y(i))G_y(T_yg_aT_y(i))G_a(g_aT_y(i))G_y(T_y(i)) = \eta_{ay}, \tag{4.15h}$$
$$G_a^\dagger(T_z^{-1}g_aT_z(i))G_z^\dagger(g_aT_z(i))G_a(g_aT_z(i))G_z(T_z(i)) = \eta_{az}, \tag{4.15i}$$
$$G_b^\dagger(T_xg_bT_x(i))G_x(T_xg_bT_x(i))G_b(g_bT_x(i))G_x(T_x(i)) = \eta_{bx}, \tag{4.15j}$$
$$G_b^\dagger(T_y^{-1}g_bT_y(i))G_y^\dagger(g_bT_y(i))G_b(g_bT_y(i))G_y(T_y(i)) = \eta_{by}, \tag{4.15k}$$
$$G_b^\dagger(T_zg_bT_z(i))G_z(T_zg_bT_z(i))G_b(g_bT_z(i))G_z(T_z(i)) = \eta_{bz}, \tag{4.15l}$$
$$G_c^\dagger(T_y^{-1}g_cT_x(i))G_y^\dagger(g_cT_x(i))G_c(g_cT_x(i))G_x(T_x(i)) = \eta_{cyx}, \tag{4.15m}$$
$$G_c^\dagger(T_z^{-1}g_cT_y(i))G_z^\dagger(g_cT_y(i))G_c(g_cT_y(i))G_y(T_y(i)) = \eta_{czy}, \tag{4.15n}$$
$$G_c^\dagger(T_x^{-1}g_cT_z(i))G_x^\dagger(g_cT_z(i))G_c(g_cT_z(i))G_z(T_z(i)) = \eta_{cxz}, \tag{4.15o}$$
$$\begin{aligned} &G_a^\dagger(g_c^{-1}g_b^{-1}T_x^{-1}T_yg_ag_c(i))G_c^\dagger(g_b^{-1}T_x^{-1}T_yg_ag_c(i)) \\ &\times G_b^\dagger(T_x^{-1}T_yg_ag_c(i))G_x^\dagger(T_yg_ag_c(i)) \\ &\times G_y(T_yg_ag_c(i))G_a(g_ag_c(i))G_c(g_c(i)) = \eta_{acb}, \end{aligned} \tag{4.15p}$$
$$G_b^\dagger(g_a^{-1}T_xT_y^{-1}T_zg_bg_a(i))G_a^\dagger(T_xT_y^{-1}T_zg_bg_a(i))$$

$$\times G_x(T_xT_y^{-1}T_zg_bg_a(i))G_y^\dagger(T_zg_bg_a(i))$$
$$\times G_z(T_zg_bg_a(i))G_b(g_bg_a(i))G_a(g_a(i)) = \eta_{ab}, \tag{4.15q}$$
$$G_c^\dagger(g_b^{-1}T_x^{-1}T_yg_ag_bg_cg_b(i))G_b^\dagger(T_x^{-1}T_yg_ag_bg_cg_b(i))$$
$$\times G_x^\dagger(T_yg_ag_bg_cg_b(i))G_y(T_yg_ag_bg_cg_b(i))G_a(g_ag_bg_cg_b(i))$$
$$\times G_b(g_bg_cg_b(i))G_c(g_cg_b(i))G_b(g_b(i)) = \eta_{cba}. \tag{4.15r}$$

The Gs in the above relations are $\mathsf{SU}(2)$ matrices, and are associated with the $\mathsf{SU}(2)$ gauge symmetry, which transforms the G in the following way:

$$G_g(i) \mapsto W(g^{-1}(i))G_g(i)W^\dagger(i), \quad W \in \mathsf{SU}(2); \tag{4.16}$$

This equation can be understood as follows: under gauge transformation, we have:

$$U_{ij} \mapsto \tilde{U}_{ij} \equiv W(i)U_{ij}W^\dagger(j), \tag{4.17}$$

and the requirement for the gauge transformed PSG is:

$$\tilde{G}_g(g(i))\tilde{U}_{g(i)g(j)}\tilde{G}_g^\dagger(g(j)) = \tilde{U}_{ij}. \tag{4.18}$$

From the above relations we derived the gauge transformation of Gs.

Aside from the gauge symmetry, we note that we can replace a generic element G with $\mathfrak{g}G$, where $\mathfrak{g} \in \text{IGG} = \{\tau_0, -\tau_0\}$. Wisely making use of this fact is going to help us reduce the number of phases on the right hand side of the PSG equations.

By performing:

$$\begin{aligned} &G_x \mapsto \eta_{cyx}G_x, \quad G_z \mapsto \eta_{czy}G_z, \\ &G_a \mapsto \eta_{acb}\eta_{cba}G_a, \quad G_b \mapsto \eta_{acb}\eta_{cyx}G_b, \\ &G_c \mapsto \eta_c G_c, \end{aligned} \tag{4.19}$$

we eliminate the phases on the right hand side (RHS) of Eq. 4.15a, Eq. 4.15m, Eq. 4.15n, Eq. 4.15p and Eq. 4.15r.

4.A.1 Solving for the translational Elements

Let us start by considering the following equations Eq.4.15d, Eq.4.15e and Eq.4.15f that arise because of the commutation of translational generators. Canonically, this gives us the following expressions of G_x, G_y, G_z:

$$\begin{aligned} &G_x(x,y,z;s) = \tau_0, G_y(x,y,z;s) = \eta_{xy}^x\tau_0, \\ &G_z(x,y,z;s) = \eta_{zx}^x\eta_{yz}^y\tau_0. \end{aligned} \tag{4.20}$$

4.A.2 Solving for G_c

Using the IGG Z_2 gauge symmetry, we had eliminated the phases on the RHS of Eq.4.15m, Eq.4.15n. To solve for G_c, one then plug the canonical expressions of the translational PSG elements into Eq.4.15m, Eq.4.15n and Eq.4.15o. One arrives at the following expressions:

$$G_c^\dagger(T_y^{-1}(i))\eta_{xy}^{-x}G_c(i) = \tau_0, \tag{4.21a}$$

$$G_c^\dagger(T_z^{-1}(i))\eta_{zx}^{-x}\eta_{yz}^{-y}G_c(i)G_y(g_c^{-1}(i)) = \tau_0, \tag{4.21b}$$

$$G_c^\dagger(T_x^{-1}(i))G_c(i)G_z(g_c^{-1}(i)) = \eta_{cxz}. \tag{4.21c}$$

Further simplifying the expressions, one arrives at:

$$G_c(x,y,z) = \eta_{xy}^{x}G_c(x,y-1,z), \tag{4.22a}$$

$$G_c(x,y,z) = \eta_{zx}^{x}\eta_{yz}^{y}\eta_{xy}^{-y}G_c(x,y,z-1), \tag{4.22b}$$

$$G_c(x,y,z) = \eta_{zx}^{-y}\eta_{yz}^{-z}\eta_{cxz}G_c(x-1,y,z). \tag{4.22c}$$

The above expressions are valid for all sub-lattice indices, and we have suppressed the s indices. One then assumes that the following form is valid for G_c: $G_c \equiv f_c(x,y,z;s)\mathfrak{M}_c(s)$. Because of the mentioned reason, we have $f_c(x,y,z;s) = f_c(x,y,z)$. Then the separation of variable allows one to arrive at:

$$f_c(x,y,z) = \eta_{xy}^{x}f_c(x,y-1,z), \tag{4.23a}$$

$$f_c(x,y,z) = \eta_{zx}^{x}\eta_{yz}^{y}\eta_{xy}^{-y}f_c(x,y,z-1), \tag{4.23b}$$

$$f_c(x,y,z) = \eta_{zx}^{-y}\eta_{yz}^{-z}\eta_{cxz}f_c(x-1,y,z). \tag{4.23c}$$

For f_c to be a path-independent function, there are certain constraints that the phases have to satisfy. For example, one considers two paths to arrive at $f_c(x+1,y+1,z)$: 1.) $f_c(x,y,z) \mapsto f_c(x+1,y,z) \mapsto f_c(x+1,y+1,z)$; 2.) $f_c(x,y,z) \mapsto f_c(x,y+1,z) \mapsto f_c(x+1,y+1,z)$. One then compares the phases resulted from the two paths, and enforce them to be identical. Such a process produces the relevant constraints on the phases. We check the path independence on the xy, yz and zx planes respectively, and arrive at the following constraint:

$$\eta_{xy} = \eta_{zx}^{-1}; \eta_{yz} = \eta_{xy}; \eta_{zx} = \eta_{yz}^{-1}. \tag{4.24}$$

It follows then $\eta_{xy} = \eta_{yz} = \eta_{zx} = \eta_1$. The previous equations on f_c become:

$$f_c(x,y,z) = \eta_1^{x}f_c(x,y-1,z), \tag{4.25a}$$

$$f_c(x,y,z) = \eta_1^{x}f_c(x,y,z-1), \tag{4.25b}$$

$$f_c(x,y,z) = \eta_1^{-(y+z)}\eta_{cxz}f_c(x-1,y,z). \tag{4.25c}$$

Therefore, at this point we claim that $G_c = \eta_1^{xy+xz}\eta_{cxz}^{x}\mathfrak{M}_c(s)$.

Let us take a look at Eq.4.15a. One can eliminate the phase on the RHS by making use of the IGG gauge symmetry. Plugging the above expression into Eq.4.15a, we arrive at:

$$\mathfrak{M}_c^3(\alpha) = \tau_0; \tag{4.26a}$$

$$\mathfrak{M}_c(\delta)\mathfrak{M}_c(\gamma)\mathfrak{M}_c(\beta) = \tau_0; \tag{4.26b}$$

$$\eta_{cxz} = 1. \tag{4.26c}$$

It is useful to make a summary before we close this subsection:
1.) $\eta_c = \eta_{cyx} = \eta_{czy} = \eta_{cxz} = 1$;
2.) $\eta_{xy} = \eta_{yz} = \eta_{zx} = \eta_1$;
3.)$G_c = \eta_1^{xy+xz}\mathfrak{M}_c(s)$, for which the following relations are satisfied:

$$\mathfrak{M}_c^3(\alpha) = \tau_0; \tag{4.27a}$$

$$\mathfrak{M}_c(\delta)\mathfrak{M}_c(\gamma)\mathfrak{M}_c(\beta) = \tau_0; \tag{4.27b}$$

4.A.3 Solving for G_a

To solve for G_a, one plugs the simplified expressions of the translational PSG elements into Eq.4.15g, Eq.4.15h and Eq.4.15i. One arrives at the following expressions:

$$G_a^\dagger(T_x(i))G_a(i) = \eta_{ax}, \tag{4.28a}$$

$$G_a^\dagger(T_y(i))G_y(T_y(i))G_a(i)G_y(g_a^{-1}(i)) = \eta_{ay}, \tag{4.28b}$$

$$G_a^\dagger(T_z^{-1}(i))G_z^\dagger(i)G_a(i)G_z(g_a^{-1}(i)) = \eta_{az}. \tag{4.28c}$$

One makes the usual ansatz $G_a(i) \equiv f_a(x,y,z;s)\mathfrak{M}_a(s)$, only this time one does not have $f_a(x,y,z;s) = f_a(x,y,z)$, for the evaluation of $G_{y/z}(g_a^{-1}(i))$ is not s-independent.
We have, for $s = \alpha/\delta$, the following conditions for f_a:

$$\eta_{ax}^{-1} f_a(x,y,z;\alpha/\delta) = f_a(x+1,y,z;\alpha/\delta), \tag{4.29a}$$

$$\eta_{ay}^{-1} f_a(x,y,z;\alpha/\delta) = f_a(x,y+1,z;\alpha/\delta), \tag{4.29b}$$

$$\eta_{az}\eta_1 f_a(x,y,z;\alpha/\delta) = f_a(x,y,z+1;\alpha/\delta); \tag{4.29c}$$

and for $s = \beta/\gamma$, the following conditions for f_a:

$$\eta_{ax}^{-1} f_a(x,y,z;\beta/\gamma) = f_a(x+1,y,z;\beta/\gamma), \tag{4.30a}$$

$$\eta_{ay}^{-1}\eta_1^{-1} f_a(x,y,z;\beta/\gamma) = f_a(x,y+1,z;\beta/\gamma), \tag{4.30b}$$

$$\eta_{az} f_a(x,y,z;\beta/\gamma) = f_a(x,y,z+1;\beta/\gamma). \tag{4.30c}$$

Note that this time we do not have to check the path independence of f_a, as the phases appearing in the above equations are constants. We then arrive at the following expressions:

$$\begin{aligned} f_a(x,y,z;\alpha/\delta) &= \eta_{ax}^{-x}\eta_{ay}^{-y}\eta_{az}^{z}\eta_1^{z}, \\ f_a(x,y,z;\beta/\gamma) &= \eta_{ax}^{-x}\eta_{ay}^{-y}\eta_1^{-y}\eta_{az}^{z}, \end{aligned} \tag{4.31}$$

from which we write:

$$\begin{aligned} G_a(x,y,z;\alpha/\delta) &= \eta_{ax}^{-x}\eta_{ay}^{-y}\eta_{az}^{z}\eta_1^{z}\mathfrak{M}_a(\alpha/\delta), \\ G_a(x,y,z;\beta/\gamma) &= \eta_{ax}^{-x}\eta_{ay}^{-y}\eta_1^{-y}\eta_{az}^{z}\mathfrak{M}_a(\beta/\gamma). \end{aligned} \tag{4.32}$$

In plugging these expressions into Eq.4.15b, we first consider $i \equiv (x,y,z;\alpha)$. The condition we arrive at is:

$$G_z^{\dagger}(-x,-y-1,z;\delta)G_a(-x,-y-1,z;\delta)G_a(x,y,z;\alpha) = \eta_a, \tag{4.33}$$

which further simplifies to:

$$\eta_1^{x+y+1}\eta_{ay}\mathfrak{M}_a(\delta)\mathfrak{M}_a(\alpha) = \eta_a. \tag{4.34}$$

The above equation dictates that $\eta_1 = 1$. Consequently, one has:

$$\mathfrak{M}_a(\delta)\mathfrak{M}_a(\alpha) = \eta_a\eta_{ay}^{-1}. \tag{4.35}$$

We then consider other sublattice sites, and they give us:

$$G_a(-x-1,-y-1,z+1;\gamma)G_a(x,y,z;\beta) = \eta_a, \tag{4.36a}$$

$$G_a(-x-1,-y-1,z;\beta)G_a(x,y,z;\gamma) = \eta_a, \tag{4.36b}$$

$$G_a(-x,-y-1,z+1;\alpha)G_a(x,y,z;\delta) = \eta_a. \tag{4.36c}$$

Plugging the explicit forms into the above equations, and we arrive at:

$$\mathfrak{M}_a(\gamma)\mathfrak{M}_a(\beta) = \eta_a\eta_{ax}^{-1}\eta_{ay}^{-1}\eta_{az}^{-1}, \tag{4.37a}$$

$$\mathfrak{M}_a(\beta)\mathfrak{M}_a(\gamma) = \eta_a\eta_{ax}^{-1}\eta_{ay}^{-1}, \tag{4.37b}$$

$$\mathfrak{M}_a(\alpha)\mathfrak{M}_a(\delta) = \eta_a\eta_{ay}^{-1}\eta_{az}^{-1}. \tag{4.37c}$$

It is useful to make a summary again before we close this subsection:

1.) $\eta_{xy} = \eta_{yz} = \eta_{zx} = \eta_1 = 1$, and as a result, $G_x = G_y = G_z = \tau_0$;

2.) We have $G_a(x,y,z;s) = \eta_{ax}^{-x}\eta_{ay}^{-y}\eta_{az}^{z}\mathfrak{M}_a(s)$; for which the following relations are satisfied:

$$\mathfrak{M}_a(\delta)\mathfrak{M}_a(\alpha) = \eta_a\eta_{ay}^{-1}, \tag{4.38a}$$

$$\mathfrak{M}_a(\gamma)\mathfrak{M}_a(\beta) = \eta_a\eta_{ax}^{-1}\eta_{ay}^{-1}\eta_{az}^{-1}, \tag{4.38b}$$

$$\mathfrak{M}_a(\beta)\mathfrak{M}_a(\gamma) = \eta_a\eta_{ax}^{-1}\eta_{ay}^{-1}, \tag{4.38c}$$

$$\mathfrak{M}_a(\alpha)\mathfrak{M}_a(\delta) = \eta_a\eta_{ay}^{-1}\eta_{az}^{-1}. \tag{4.38d}$$

4.A.4 Solving for G_b

Now we attack Eq.4.15j, Eq.4.15k and Eq.4.15l. Since G_x, G_y and G_z are trivial now, the equations are reduced to the following form:

$$G_b^\dagger(T_x(i))G_b(i) = \eta_{bx}, \tag{4.39a}$$

$$G_b^\dagger(T_y^{-1}(i))G_b(i) = \eta_{by}, \tag{4.39b}$$

$$G_b^\dagger(T_z(i))G_b(i) = \eta_{bz}. \tag{4.39c}$$

We make the ansatz $G_b \equiv f_b(x,y,z)\mathfrak{M}_b(s)$, where the separation of variables is possible because the above conditions are s-independent. One can quickly arrive at the condition that $G_b = \eta_{bx}^{-x}\eta_{by}^{y}\eta_{bz}^{-z}\mathfrak{M}_b(s)$.

Plugging the expression into Eq.4.15c, one ends up with:

$$G_b(g_b(i))G_b(i) = \eta_b. \tag{4.40}$$

Considering the individual sublattice sites respectively, one arrives at:

$$\mathfrak{M}_b(\gamma)\mathfrak{M}_b(\alpha) = \eta_b\eta_{bx}^{-1}, \tag{4.41a}$$

$$\mathfrak{M}_b(\delta)\mathfrak{M}_b(\beta) = \eta_b\eta_{bx}^{-1}\eta_{bz}^{-1}, \tag{4.41b}$$

$$\mathfrak{M}_b(\alpha)\mathfrak{M}_b(\gamma) = \eta_b\eta_{bx}^{-1}\eta_{by}^{-1}, \tag{4.41c}$$

$$\mathfrak{M}_b(\beta)\mathfrak{M}_b(\delta) = \eta_b\eta_{bx}^{-1}\eta_{by}^{-1}\eta_{bz}^{-1}. \tag{4.41d}$$

A quick summary:
We have $G_b(x,y,z;s) = \eta_{bx}^{-x}\eta_{by}^{y}\eta_{bz}^{-z}\mathfrak{M}_b(s)$; for which the following relations are satisfied:

$$\mathfrak{M}_b(\gamma)\mathfrak{M}_b(\alpha) = \eta_b\eta_{bx}^{-1}, \tag{4.42a}$$

$$\mathfrak{M}_b(\delta)\mathfrak{M}_b(\beta) = \eta_b\eta_{bx}^{-1}\eta_{bz}^{-1}, \tag{4.42b}$$

$$\mathfrak{M}_b(\alpha)\mathfrak{M}_b(\gamma) = \eta_b\eta_{bx}^{-1}\eta_{by}^{-1}, \tag{4.42c}$$

$$\mathfrak{M}_b(\beta)\mathfrak{M}_b(\delta) = \eta_b\eta_{bx}^{-1}\eta_{by}^{-1}\eta_{bz}^{-1}. \tag{4.42d}$$

4.A.5 Solving Eq.4.15p, Eq.4.15q and Eq.4.15r

To attack the remaining three equations, note that we can use the IGG gauge symmetry of G_a and G_b to eliminate η_{acb} and η_{cba}. The equations are reduced to:

$$\begin{aligned} &G_a^\dagger(g_c^{-1}g_b^{-1}(i))G_c^\dagger(g_b^{-1}(i))G_b^\dagger(i) \\ &\times G_a(T_y^{-1}T_x(i))G_c(g_a^{-1}T_y^{-1}T_x(i)) = \tau_0, \\ &G_b^\dagger(g_a^{-1}(i))G_a^\dagger(i)G_b(T_z^{-1}T_yT_x^{-1}(i)) \end{aligned} \tag{4.43}$$

$$\times G_a(g_b^{-1}T_z^{-1}T_yT_x^{-1}(i)) = \eta_{ab}\tau_0, \tag{4.44}$$

$$G_c^\dagger(g_b^{-1}T_x^{-1}T_y(i))G_b^\dagger(T_x^{-1}T_y(i))G_a(i)$$
$$\times G_b(g_a^{-1}(i))G_c(g_b^{-1}g_a^{-1}(i))G_b(g_c^{-1}g_b^{-1}g_a^{-1}(i)) = \tau_0. \tag{4.45}$$

We consider first $i = (x, y, z; \alpha)$. Plugging this into Eq.4.43 gives us the following:

$$G_a^\dagger(y-1, -z, -x-1; \beta)\mathfrak{M}_c(\gamma)G_b^\dagger(x, y, z; \alpha)$$
$$\times G_a(x+1, y-1, z; \alpha)\mathfrak{M}_c(\delta) = \tau_0. \tag{4.46}$$

Recalling $G_a = \eta_{ax}^{-x}\eta_{ay}^{-y}\eta_{az}^{z}\mathfrak{M}_a(s)$ and $G_b = \eta_{bx}^{-x}\eta_{by}^{y}\eta_{bz}^{-z}\mathfrak{M}_b(s)$, the LHS of the above expression is evaluated as:

$$\eta_{ax}^{y-1}\eta_{ay}^{-z}\eta_{az}^{x+1}\mathfrak{M}_a^\dagger(\beta)\mathfrak{M}_c^\dagger(\gamma)$$
$$\times \eta_{bx}^{x}\eta_{by}^{-y}\eta_{bz}^{z}\mathfrak{M}_b^\dagger(\alpha)\eta_{ax}^{-x-1}\eta_{ay}^{-y+1}\eta_{az}^{z}\mathfrak{M}_a(\alpha)\mathfrak{M}_c(\delta)$$
$$=(\eta_{az}\eta_{bx}\eta_{ax}^{-1})^x(\eta_{ax}\eta_{ay}^{-1}\eta_{by}^{-1})^y(\eta_{az}\eta_{bz}\eta_{ay}^{-1})^z\eta_{az}\eta_{ay}$$
$$\times \mathfrak{M}_a^\dagger(\beta)\mathfrak{M}_c^\dagger(\gamma)\mathfrak{M}_b^\dagger(\alpha)\mathfrak{M}_a(\alpha)\mathfrak{M}_c(\delta). \tag{4.47}$$

Since the RHS of the previous expression is unit cell independent, we would have the following equations:

$$\eta_{az}\eta_{bx} = \eta_{ax},$$
$$\eta_{by}\eta_{ay} = \eta_{ax},$$
$$\eta_{az}\eta_{bz} = \eta_{ay}. \tag{4.48}$$

Naming $\eta_2 \equiv \eta_{ax}$, $\eta_3 \equiv \eta_{ay}$ and $\eta_4 \equiv \eta_{az}$, we would have $\eta_{bx} = \eta_2\eta_4^{-1}$, $\eta_{by} = \eta_2\eta_3^{-1}$ and $\eta_{bz} = \eta_3\eta_4^{-1}$. Also, we now have $G_a = \eta_2^{-x}\eta_3^{-y}\eta_4^{z}\mathfrak{M}_a(s)$ and $G_b = \eta_2^{-x+y}\eta_3^{-y-z}\eta_4^{x+z}\mathfrak{M}_b(s)$. The previous constraint becomes:

$$\mathfrak{M}_a^\dagger(\beta)\mathfrak{M}_c^\dagger(\gamma)\mathfrak{M}_b^\dagger(\alpha)\mathfrak{M}_a(\alpha)\mathfrak{M}_c(\delta) = \eta_3^{-1}\eta_4^{-1}. \tag{4.49}$$

What happens now for Eq.4.45? Plugging $i = (x, y, z; \alpha)$ into the equation gives us:

$$\mathfrak{M}_c^\dagger(\gamma)G_b^\dagger(x-1, y+1, z; \alpha)$$
$$\times G_a(x, y, z; \alpha)G_b(-x, -y-1, z-1; \delta)$$
$$\times \mathfrak{M}_c(\beta)G_b(-y-1, -z, x-1; \delta) = \tau_0. \tag{4.50}$$

Evaluating the LHS of the above equation gives us:

$$\eta_2^{x-y}\eta_3^{y+z+1}\eta_4^{-x-z+1}\eta_2^{-x}\eta_3^{-y}\eta_4^{-z}\eta_2^{x-y-1}$$
$$\times \eta_3^{y-z}\eta_4^{-x+z-1}\eta_2^{y+1-z}\eta_3^{z-x+1}\eta_4^{-y+x}$$

$$
\begin{aligned}
&\times \mathfrak{M}_c^\dagger(\gamma)\mathfrak{M}_b^\dagger(\alpha)\mathfrak{M}_a(\alpha)\mathfrak{M}_b(\delta)\mathfrak{M}_c(\beta)\mathfrak{M}_b(\delta)\\
&=(\eta_2^{-1}\eta_3^{-1}\eta_4)^x(\eta_3^{-1}\eta_4^{-1}\eta_2)^y(\eta_4\eta_2^{-1}\eta_3)^z\\
&\quad\times \mathfrak{M}_c^\dagger(\gamma)\mathfrak{M}_b^\dagger(\alpha)\mathfrak{M}_a(\alpha)\mathfrak{M}_b(\delta)\mathfrak{M}_c(\beta)\mathfrak{M}_b(\delta). \qquad (4.51)
\end{aligned}
$$

Again, the unit cell independence gives us an extra condition $\eta_2 = \eta_3\eta_4$. The original equation becomes:

$$
\mathfrak{M}_c^\dagger(\gamma)\mathfrak{M}_b^\dagger(\alpha)\mathfrak{M}_a(\alpha)\mathfrak{M}_b(\delta)\mathfrak{M}_c(\beta)\mathfrak{M}_b(\delta) = \tau_0. \qquad (4.52)
$$

No further conditions on the phases can be derived from the three equations. We are in the position to write $G_a = \eta_3^{-x-y}\eta_4^{-x+z}\mathfrak{M}_a(s)$ and $G_b = \eta_3^{-x-z}\eta_4^{y+z}\mathfrak{M}_b(s)$. Iterating scenarios with different s for $i \equiv (x, y, z; s)$, we arrive at the following constraints:

$$
\begin{aligned}
&\mathfrak{M}_a^\dagger(\beta)\mathfrak{M}_c^\dagger(\gamma)\mathfrak{M}_b^\dagger(\alpha)\mathfrak{M}_a(\alpha)\mathfrak{M}_c(\delta) = \eta_3^{-1}\eta_4^{-1}, && (4.53a)\\
&\mathfrak{M}_a^\dagger(\gamma)\mathfrak{M}_c^\dagger(\delta)\mathfrak{M}_b^\dagger(\beta)\mathfrak{M}_a(\beta)\mathfrak{M}_c(\gamma) = \eta_4, && (4.53b)\\
&\mathfrak{M}_a^\dagger(\alpha)\mathfrak{M}_c^\dagger(\alpha)\mathfrak{M}_b^\dagger(\gamma)\mathfrak{M}_a(\gamma)\mathfrak{M}_c(\beta) = \tau_0, && (4.53c)\\
&\mathfrak{M}_a^\dagger(\delta)\mathfrak{M}_c^\dagger(\beta)\mathfrak{M}_b^\dagger(\delta)\mathfrak{M}_a(\delta)\mathfrak{M}_c(\alpha) = \eta_3, && (4.53d)\\
&\mathfrak{M}_b^\dagger(\delta)\mathfrak{M}_a^\dagger(\alpha)\mathfrak{M}_b(\alpha)\mathfrak{M}_a(\gamma) = \eta_{ab}\eta_3\eta_4, && (4.53e)\\
&\mathfrak{M}_b^\dagger(\gamma)\mathfrak{M}_a^\dagger(\beta)\mathfrak{M}_b(\beta)\mathfrak{M}_a(\delta) = \eta_{ab}\eta_3\eta_4^{-1}, && (4.53f)\\
&\mathfrak{M}_b^\dagger(\beta)\mathfrak{M}_a^\dagger(\gamma)\mathfrak{M}_b(\gamma)\mathfrak{M}_a(\alpha) = \eta_{ab}\eta_3\eta_4^{-1}, && (4.53g)\\
&\mathfrak{M}_b^\dagger(\alpha)\mathfrak{M}_a^\dagger(\delta)\mathfrak{M}_b(\delta)\mathfrak{M}_a(\beta) = \eta_{ab}\eta_3\eta_4^{-1}, && (4.53h)\\
&\mathfrak{M}_c^\dagger(\gamma)\mathfrak{M}_b^\dagger(\alpha)\mathfrak{M}_a(\alpha)\mathfrak{M}_b(\delta)\mathfrak{M}_c(\beta)\mathfrak{M}_b(\delta) = \tau_0, && (4.53i)\\
&\mathfrak{M}_c^\dagger(\delta)\mathfrak{M}_b^\dagger(\beta)\mathfrak{M}_a(\beta)\mathfrak{M}_b(\gamma)\mathfrak{M}_c(\alpha)\mathfrak{M}_b(\alpha) = \eta_3^{-1}, && (4.53j)\\
&\mathfrak{M}_c^\dagger(\alpha)\mathfrak{M}_b^\dagger(\gamma)\mathfrak{M}_a(\gamma)\mathfrak{M}_b(\beta)\mathfrak{M}_c(\delta)\mathfrak{M}_b(\gamma) = \eta_3\eta_4, && (4.53k)\\
&\mathfrak{M}_c^\dagger(\beta)\mathfrak{M}_b^\dagger(\delta)\mathfrak{M}_a(\delta)\mathfrak{M}_b(\alpha)\mathfrak{M}_c(\gamma)\mathfrak{M}_b(\beta) = \eta_4. && (4.53l)
\end{aligned}
$$

4.A.6 Solving for the $\mathfrak{M}$s

We start by performing some $\mathsf{SU}(2)$ gauge transformations. Let us consider a type of gauge transformation $W(i) \equiv W(s)$. Had we started at a generic gauge, we could always make the following gauge transformation:

$$
\begin{aligned}
&W(\alpha) = \mathfrak{M}_a(\alpha), W(\beta) = \mathfrak{M}_c(\beta),\\
&W(\gamma) = \mathfrak{M}_c^\dagger(\delta), W(\delta) = \tau_0. \qquad (4.54)
\end{aligned}
$$

so that:

$$
\begin{aligned}
g.t.: \quad &\mathfrak{M}_c(\delta) \mapsto W(\beta)\mathfrak{M}_c(\beta)W^\dagger(\beta) = \tau_0, && (4.55)\\
&\mathfrak{M}_c(\gamma) \mapsto W(\delta)\mathfrak{M}_c(\delta)W^\dagger(\delta) = \tau_0, && (4.56)
\end{aligned}
$$

$$\mathfrak{M}_a(\delta) \mapsto W(\alpha)\mathfrak{M}_a(\alpha)W^\dagger(\alpha) = \tau_0. \tag{4.57}$$

Now we make use of Eq.4.27b, and arrive at $\mathfrak{M}_c(\beta) = \mathfrak{M}_c(\gamma) = \mathfrak{M}_c(\delta) = \tau_0$. It should be noted that we are silent on $\mathfrak{M}_c(\alpha)$. Indeed, it is not possible to use gauge symmetry alone to trivialise $\mathfrak{M}_c(\alpha)$. However, as we shall see, other equations will bring enough restrictions on the form of $\mathfrak{M}_c(\alpha)$.

Before we take a step further, let us note that taking traces over Eq.4.38a and Eq.4.38d dictates that $\eta_4 = 1$. After the simplification, we have:

$$\mathfrak{M}_c^3(\alpha) = \tau_0, \tag{4.58a}$$
$$\mathfrak{M}_a(\delta)\mathfrak{M}_a(\alpha) = \eta_a\eta_3^{-1}, \tag{4.58b}$$
$$\mathfrak{M}_a(\gamma)\mathfrak{M}_a(\beta) = \eta_a, \tag{4.58c}$$
$$\mathfrak{M}_a(\beta)\mathfrak{M}_a(\gamma) = \eta_a, \tag{4.58d}$$
$$\mathfrak{M}_a(\alpha)\mathfrak{M}_a(\delta) = \eta_a\eta_3^{-1}, \tag{4.58e}$$
$$\mathfrak{M}_b(\gamma)\mathfrak{M}_b(\alpha) = \eta_b\eta_3^{-1}, \tag{4.58f}$$
$$\mathfrak{M}_b(\delta)\mathfrak{M}_b(\beta) = \eta_b, \tag{4.58g}$$
$$\mathfrak{M}_b(\alpha)\mathfrak{M}_b(\gamma) = \eta_b\eta_3^{-1}, \tag{4.58h}$$
$$\mathfrak{M}_b(\beta)\mathfrak{M}_b(\delta) = \eta_b, \tag{4.58i}$$
$$\mathfrak{M}_a^\dagger(\beta)\mathfrak{M}_b^\dagger(\alpha)\mathfrak{M}_a(\alpha) = \eta_3^{-1}, \tag{4.58j}$$
$$\mathfrak{M}_a^\dagger(\gamma)\mathfrak{M}_b^\dagger(\beta)\mathfrak{M}_a(\beta) = \tau_0, \tag{4.58k}$$
$$\mathfrak{M}_a^\dagger(\alpha)\mathfrak{M}_c^\dagger(\alpha)\mathfrak{M}_b^\dagger(\gamma)\mathfrak{M}_a(\gamma) = \tau_0, \tag{4.58l}$$
$$\mathfrak{M}_a^\dagger(\delta)\mathfrak{M}_b^\dagger(\delta)\mathfrak{M}_a(\delta)\mathfrak{M}_c(\alpha) = \eta_3, \tag{4.58m}$$
$$\mathfrak{M}_b^\dagger(\delta)\mathfrak{M}_a^\dagger(\alpha)\mathfrak{M}_b(\alpha)\mathfrak{M}_a(\gamma) = \eta_{ab}\eta_3, \tag{4.58n}$$
$$\mathfrak{M}_b^\dagger(\gamma)\mathfrak{M}_a^\dagger(\beta)\mathfrak{M}_b(\beta)\mathfrak{M}_a(\delta) = \eta_{ab}\eta_3, \tag{4.58o}$$
$$\mathfrak{M}_b^\dagger(\beta)\mathfrak{M}_a^\dagger(\gamma)\mathfrak{M}_b(\gamma)\mathfrak{M}_a(\alpha) = \eta_{ab}\eta_3, \tag{4.58p}$$
$$\mathfrak{M}_b^\dagger(\alpha)\mathfrak{M}_a^\dagger(\delta)\mathfrak{M}_b(\delta)\mathfrak{M}_a(\beta) = \eta_{ab}\eta_3, \tag{4.58q}$$
$$\mathfrak{M}_b^\dagger(\alpha)\mathfrak{M}_a(\alpha)\mathfrak{M}_b(\delta)\mathfrak{M}_b(\delta) = \tau_0, \tag{4.58r}$$
$$\mathfrak{M}_b^\dagger(\beta)\mathfrak{M}_a(\beta)\mathfrak{M}_b(\gamma)\mathfrak{M}_c(\alpha)\mathfrak{M}_b(\alpha) = \eta_3^{-1}, \tag{4.58s}$$
$$\mathfrak{M}_c^\dagger(\alpha)\mathfrak{M}_b^\dagger(\gamma)\mathfrak{M}_a(\gamma)\mathfrak{M}_b(\beta)\mathfrak{M}_b(\gamma) = \eta_3, \tag{4.58t}$$
$$\mathfrak{M}_b^\dagger(\delta)\mathfrak{M}_a(\delta)\mathfrak{M}_b(\alpha)\mathfrak{M}_b(\beta) = \tau_0. \tag{4.58u}$$

Let us first look at Eq.4.58s, which can be rewritten as:

$$\mathfrak{M}_b(\alpha)\mathfrak{M}_b^\dagger(\beta)\mathfrak{M}_a(\beta)\mathfrak{M}_b(\gamma)\mathfrak{M}_c(\alpha) = \eta_3^{-1}.$$

The above expression, when combined with Eq.4.58t and Eq.4.58d, gives us:

$$\mathfrak{M}_b(\alpha)\mathfrak{M}_b(\gamma) = \eta_a^{-1}, \tag{4.59}$$

that, when combined with Eq.4.58h, gives us:

$$\eta_a^{-1} = \eta_b\eta_3^{-1}. \tag{4.60}$$

Now we look at Eq.4.58o, which can be rewritten as:

$$\mathfrak{M}_a(\delta)\mathfrak{M}_b^\dagger(\gamma)\mathfrak{M}_a^\dagger(\beta)\mathfrak{M}_b(\beta) = \eta_{ab}\eta_3.$$

The above expression, when combined with Eq.4.58p and Eq.4.58d, gives us:

$$\mathfrak{M}_a(\delta)\mathfrak{M}_a(\alpha) = \eta_a, \tag{4.61}$$

that, when combined with Eq.4.58b, gives us:

$$\eta_3 = 1. \tag{4.62}$$

Looking at Eq.4.58q and Eq.4.58r, with the help of Eq.4.58b, we reach:

$$\mathfrak{M}_a(\beta) = \eta_{ab}\eta_a\mathfrak{M}_b(\delta). \tag{4.63}$$

Similarly, Eq.4.58n and Eq.4.58u, with the help of Eq.4.58b, give us:

$$\mathfrak{M}_a(\gamma) = \eta_{ab}\eta_a\mathfrak{M}_b(\beta). \tag{4.64}$$

Consider, now, Eq.4.58t and Eq.4.58l. The coupled equations can be manoeuvred to give us:

$$\mathfrak{M}_a(\alpha)\mathfrak{M}_b(\beta)\mathfrak{M}_b(\gamma) = \tau_0. \tag{4.65}$$

The above equation, when paired with Eq.4.58j, gives us (note that $\eta_a = \eta_b$ now):

$$\mathfrak{M}_b(\beta)\mathfrak{M}_a(\beta) = \eta_a^{-1}, \tag{4.66}$$

which can be coupled with Eq.4.58i and Eq.4.63 to give us:

$$\eta_{ab} = \eta_a. \tag{4.67}$$

At this point, there is only one phase left in the problem: $\eta_a = \eta_b = \eta_{ab}$. Let us look at Eq.4.58k, which gives us:

$$\mathfrak{M}_b^3(\beta) = \eta_a^{-1}, \tag{4.68}$$

which then implies that:

$$\mathfrak{M}_b^3(\delta) = \tau_0. \tag{4.69}$$

We note that, at this point, there are four independent $\mathsf{SU}(2)$ matrices, denoted as follows:

$$\mathcal{A} \equiv \mathfrak{M}_c(\alpha), \mathcal{B} \equiv \mathfrak{M}_b(\delta), \mathcal{C} \equiv \mathfrak{M}_a(\alpha), \mathcal{D} \equiv \mathfrak{M}_b(\alpha). \tag{4.70}$$

More completely, the $\mathfrak{M}_a$s and $\mathfrak{M}_b$s are represented as follows:

$$\begin{aligned}
&\mathfrak{M}_a(\alpha) = \mathcal{C}, \\
&\mathfrak{M}_a(\beta) = \mathcal{B}, \\
&\mathfrak{M}_a(\gamma) = \eta_a \mathcal{B}^\dagger, \\
&\mathfrak{M}_a(\delta) = \eta_a \mathcal{C}^\dagger;
\end{aligned} \tag{4.71}$$

and

$$\begin{aligned}
&\mathfrak{M}_b(\alpha) = \mathcal{D}, \\
&\mathfrak{M}_b(\beta) = \eta_a \mathcal{B}^\dagger, \\
&\mathfrak{M}_b(\gamma) = \eta_a \mathcal{D}^\dagger, \\
&\mathfrak{M}_b(\delta) = \mathcal{B}.
\end{aligned} \tag{4.72}$$

There are, in fact, only five independent constraints for these matrices:

$$\mathcal{A}^3 = \tau_0, \tag{4.73}$$

$$\mathcal{B}^3 = \tau_0, \tag{4.74}$$

$$\mathcal{A} = \mathcal{C}\mathcal{B}\mathcal{C}^\dagger, \tag{4.75}$$

$$\mathcal{A} = \mathcal{D}\mathcal{B}\mathcal{D}^\dagger, \tag{4.76}$$

$$\mathcal{A} = \mathcal{D}\mathcal{B}^\dagger\mathcal{C}^\dagger. \tag{4.77}$$

However, note that $\mathcal{C} = \tau_0$ from Eq. 4.57, we immediately have:

$$\mathcal{A} = \mathcal{B}, \quad \mathcal{D} = \mathcal{A}^\dagger. \tag{4.78}$$

In summary:

1.) $G_x = G_y = G_z = \tau_0$;

2.) $G_{a/b/c}(x, y, z; s) = \mathfrak{M}_{a/b/c}(s)$, where the $\mathfrak{M}$s have the following forms:

$$\begin{aligned}
&\mathfrak{M}_a(\alpha) = \tau_0, \mathfrak{M}_a(\beta) = \mathcal{A}, \mathfrak{M}_a(\gamma) = \eta_a \mathcal{A}^\dagger, \mathfrak{M}_a(\delta) = \eta_a \tau_0; \\
&\mathfrak{M}_b(\alpha) = \mathcal{A}^\dagger, \mathfrak{M}_b(\beta) = \eta_a \mathcal{A}^\dagger, \mathfrak{M}_b(\gamma) = \eta_a \mathcal{A}, \mathfrak{M}_b(\delta) = \mathcal{A}; \\
&\mathfrak{M}_c(\alpha) = \mathcal{A}, \mathfrak{M}_c(\beta) = \tau_0, \mathfrak{M}_c(\gamma) = \tau_0, \mathfrak{M}_c(\delta) = \tau_0.
\end{aligned} \tag{4.79}$$

Since we have $\eta_a = \pm 1$, and $\mathcal{A} = \tau_0, e^{i\frac{2\pi}{3}\tau_z}, e^{i\frac{4\pi}{3}\tau_z}$, corresponding to apparently 6 solutions. However, let us note that a further gauge transformation $W(x, y, z; s) \equiv \eta_a^{(x+y+z)}$ leads us

to:

1.) $G_x = G_y = G_z = \eta_a \tau_0$;

2.) $G_{a/b/c}(x, y, z; s) = \mathfrak{M}_{a/b/c}(s)$, where the $\mathfrak{M}$s have the following forms:

$$\begin{aligned}
&\mathfrak{M}_a(\alpha) = \tau_0, \mathfrak{M}_a(\beta) = \mathcal{A}, \mathfrak{M}_a(\gamma) = \mathcal{A}^\dagger, \mathfrak{M}_a(\delta) = \tau_0; \\
&\mathfrak{M}_b(\alpha) = \mathcal{A}^\dagger, \mathfrak{M}_b(\beta) = \mathcal{A}^\dagger, \mathfrak{M}_b(\gamma) = \mathcal{A}, \mathfrak{M}_b(\delta) = \mathcal{A}; \\
&\mathfrak{M}_c(\alpha) = \mathcal{A}, \mathfrak{M}_c(\beta) = \tau_0, \mathfrak{M}_c(\gamma) = \tau_0, \mathfrak{M}_c(\delta) = \tau_0.
\end{aligned} \tag{4.80}$$

Due to the fact that η_a now becomes global signs which are elements of the IGG, we conclude that $\eta_a = \pm 1$ PSGs are equivalent. We also remark that a gauge transformation $W(x, y, z; s) \equiv i\tau_x$ maps the PSG solutions in which $\mathcal{A} = e^{i\frac{2\pi}{3}\tau_z}$ to that in which $\mathcal{A} = e^{i\frac{4\pi}{3}\tau_z}$.

In conclusion, we have:

1.) $G_x = G_y = G_z = \tau_0$;

2.) $G_{a/b/c}(x, y, z; s) = \mathfrak{M}_{a/b/c}(s)$, where the $\mathfrak{M}$s have the following forms:

$$\begin{aligned}
&\mathfrak{M}_a(\alpha) = \tau_0, \mathfrak{M}_a(\beta) = \mathcal{A}, \mathfrak{M}_a(\gamma) = \mathcal{A}^\dagger, \mathfrak{M}_a(\delta) = \tau_0; \\
&\mathfrak{M}_b(\alpha) = \mathcal{A}^\dagger, \mathfrak{M}_b(\beta) = \mathcal{A}^\dagger, \mathfrak{M}_b(\gamma) = \mathcal{A}, \mathfrak{M}_b(\delta) = \mathcal{A}; \\
&\mathfrak{M}_c(\alpha) = \mathcal{A}, \mathfrak{M}_c(\beta) = \tau_0, \mathfrak{M}_c(\gamma) = \tau_0, \mathfrak{M}_c(\delta) = \tau_0,
\end{aligned} \tag{4.81}$$

where $\mathcal{A} = \tau_0, e^{i\frac{2\pi}{3}\tau_z}$, corresponding to 2 solutions.

4.A.7 Adding Time-Reversal Symmetry

Having arrived at the PSG solutions given the space group for the trillium lattice, we are at a position to add time-reversal symmetry (TRS) to the story. The extra relations are translated into the corresponding PSG equations:

$$G_{\mathcal{T}}(i) G_{\mathcal{T}}(i) = \eta_{\mathcal{T}}, \tag{4.82a}$$
$$G^\dagger_{\mathcal{T}}(T_x^{-1}(i)) G^\dagger_x(i) G_{\mathcal{T}}(i) G_x(i) = \eta_{x\mathcal{T}}, \tag{4.82b}$$
$$G^\dagger_{\mathcal{T}}(T_y^{-1}(i)) G^\dagger_y(i) G_{\mathcal{T}}(i) G_y(i) = \eta_{y\mathcal{T}}, \tag{4.82c}$$
$$G^\dagger_{\mathcal{T}}(T_z^{-1}(i)) G^\dagger_z(i) G_{\mathcal{T}}(i) G_z(i) = \eta_{z\mathcal{T}}, \tag{4.82d}$$
$$G^\dagger_{\mathcal{T}}(g_a^{-1}(i)) G^\dagger_a(i) G_{\mathcal{T}}(i) G_a(i) = \eta_{a\mathcal{T}}, \tag{4.82e}$$
$$G^\dagger_{\mathcal{T}}(g_b^{-1}(i)) G^\dagger_b(i) G_{\mathcal{T}}(i) G_b(i) = \eta_{b\mathcal{T}}, \tag{4.82f}$$
$$G^\dagger_{\mathcal{T}}(g_c^{-1}(i)) G^\dagger_c(i) G_{\mathcal{T}}(i) G_c(i) = \eta_{c\mathcal{T}}. \tag{4.82g}$$

We make the ansatz that $G_{\mathcal{T}} \equiv f(x, y, z; s)\mathfrak{M}_{\mathcal{T}}(s)$, and Eq.4.82b, Eq.4.82c and Eq.4.82d immediately tell us that:

$$G_{\mathcal{T}}(i) = \eta^x_{x\mathcal{T}} \eta^y_{y\mathcal{T}} \eta^z_{z\mathcal{T}} \mathfrak{M}_{\mathcal{T}}(s). \tag{4.83}$$

The above form, when plugged into Eq.4.82a, gives us the following constraint:

$$\mathfrak{M}^2_{\mathcal{T}}(s) = \eta_{\mathcal{T}}. \tag{4.84}$$

We now discuss about the consequences of Eq.4.82e, Eq.4.82f and Eq.4.82g.

4.A.7.1 Solving Eq.4.82g

First, we consider $i \equiv (x, y, z; \beta)$, since in this case $G_c(i) = \tau_0$. It is straightforward to reach the following constraint on the phases:

$$\eta_{x\mathcal{T}} = \eta_{y\mathcal{T}} = \eta_{z\mathcal{T}} \equiv \eta_5. \tag{4.85}$$

Also the following constraints for $\mathfrak{M}_{\mathcal{T}}(s)$ arise if we iterate the sub-lattice indices:

$$\mathfrak{M}^\dagger_{\mathcal{T}}(\delta)\mathfrak{M}_{\mathcal{T}}(\beta) = \eta_{c\mathcal{T}}, \tag{4.86a}$$
$$\mathfrak{M}^\dagger_{\mathcal{T}}(\beta)\mathfrak{M}_{\mathcal{T}}(\gamma) = \eta_{c\mathcal{T}}, \tag{4.86b}$$
$$\mathfrak{M}^\dagger_{\mathcal{T}}(\gamma)\mathfrak{M}_{\mathcal{T}}(\delta) = \eta_{c\mathcal{T}}, \tag{4.86c}$$
$$\mathfrak{M}^\dagger_{\mathcal{T}}(\alpha)\mathfrak{M}^\dagger_{c}(\alpha)\mathfrak{M}_{\mathcal{T}}(\alpha)\mathfrak{M}_{c}(\alpha) = \eta_{c\mathcal{T}}. \tag{4.86d}$$

From Eq.4.86a and Eq.4.86b, we can reach $\mathfrak{M}^\dagger_{\mathcal{T}}(\delta)\mathfrak{M}_{\mathcal{T}}(\gamma) = \tau_0$. This statement, when coupled with Eq.4.86c gives us $\eta_{c\mathcal{T}} = 1$.

A quick summary:

1.) $\eta_{x\mathcal{T}} = \eta_{y\mathcal{T}} = \eta_{z\mathcal{T}} \equiv \eta_5$, $\eta_{c\mathcal{T}} = 1$;

2.) We have $G_{\mathcal{T}}(x, y, z; s) = \eta_5^{x+y+z}\mathfrak{M}_{\mathcal{T}}(s)$; for which the following relations are satisfied:

$$\mathfrak{M}^\dagger_{\mathcal{T}}(\alpha)\mathfrak{M}^\dagger_{c}(\alpha)\mathfrak{M}_{\mathcal{T}}(\alpha)\mathfrak{M}_{c}(\alpha) = \tau_0, \tag{4.87}$$
$$\mathfrak{M}_{\mathcal{T}}(\beta) = \mathfrak{M}_{\mathcal{T}}(\gamma) = \mathfrak{M}_{\mathcal{T}}(\delta). \tag{4.88}$$

4.A.7.2 Solving Eq.4.82e and Eq.4.82f

Iterating the sub-lattice indices, we arrive at the following constraints:

$$\mathfrak{M}^\dagger_{\mathcal{T}}(\delta)\mathfrak{M}^\dagger_{a}(\alpha)\mathfrak{M}_{\mathcal{T}}(\alpha)\mathfrak{M}_{a}(\alpha) = \eta_{a\mathcal{T}}, \tag{4.89a}$$
$$\mathfrak{M}^\dagger_{\mathcal{T}}(\gamma)\mathfrak{M}^\dagger_{a}(\beta)\mathfrak{M}_{\mathcal{T}}(\beta)\mathfrak{M}_{a}(\beta) = \eta_{a\mathcal{T}}, \tag{4.89b}$$
$$\mathfrak{M}^\dagger_{\mathcal{T}}(\beta)\mathfrak{M}^\dagger_{a}(\gamma)\mathfrak{M}_{\mathcal{T}}(\gamma)\mathfrak{M}_{a}(\gamma) = \eta_{a\mathcal{T}}\eta_5, \tag{4.89c}$$
$$\mathfrak{M}^\dagger_{\mathcal{T}}(\alpha)\mathfrak{M}^\dagger_{a}(\delta)\mathfrak{M}_{\mathcal{T}}(\delta)\mathfrak{M}_{a}(\delta) = \eta_{a\mathcal{T}}\eta_5, \tag{4.89d}$$
$$\mathfrak{M}^\dagger_{\mathcal{T}}(\gamma)\mathfrak{M}^\dagger_{b}(\alpha)\mathfrak{M}_{\mathcal{T}}(\alpha)\mathfrak{M}_{b}(\alpha) = \eta_{b\mathcal{T}}, \tag{4.89e}$$
$$\mathfrak{M}^\dagger_{\mathcal{T}}(\delta)\mathfrak{M}^\dagger_{b}(\beta)\mathfrak{M}_{\mathcal{T}}(\beta)\mathfrak{M}_{b}(\beta) = \eta_{b\mathcal{T}}\eta_5, \tag{4.89f}$$
$$\mathfrak{M}^\dagger_{\mathcal{T}}(\alpha)\mathfrak{M}^\dagger_{b}(\gamma)\mathfrak{M}_{\mathcal{T}}(\gamma)\mathfrak{M}_{b}(\gamma) = \eta_{b\mathcal{T}}\eta_5, \tag{4.89g}$$
$$\mathfrak{M}^\dagger_{\mathcal{T}}(\beta)\mathfrak{M}^\dagger_{b}(\delta)\mathfrak{M}_{\mathcal{T}}(\delta)\mathfrak{M}_{b}(\delta) = \eta_{b\mathcal{T}}. \tag{4.89h}$$

4.A.7.3 Collection of Constraints

We further specify that $\mathfrak{M}_{\mathcal{T}}(\alpha) \equiv \mathcal{E}$ and $\mathfrak{M}_{\mathcal{T}}(\beta) = \mathfrak{M}_{\mathcal{T}}(\gamma) = \mathfrak{M}_{\mathcal{T}}(\delta) \equiv \mathcal{F}$. We note that Eq.4.89b and Eq.4.89c immediately imply that $\eta_5 = 1$ since $\mathfrak{M}_a(\gamma) = \eta_a \mathfrak{M}_a^\dagger(\beta)$. Furthermore, comparing Eq.4.89b and Eq.4.89h gives us $\eta_{a\mathcal{T}} = \eta_{b\mathcal{T}} \equiv \eta_6$, since $\mathfrak{M}_a(\beta) = \mathfrak{M}_b(\delta)$.

In the end, we reach the following five independent constraints:

$$\mathcal{E}^2 = \eta_{\mathcal{T}}, \tag{4.90a}$$

$$\mathcal{F}^2 = \eta_{\mathcal{T}}, \tag{4.90b}$$

$$\mathcal{E}^\dagger \mathcal{A}^\dagger \mathcal{E} \mathcal{A} = \tau_0, \tag{4.90c}$$

$$\mathcal{F}^\dagger \mathcal{B}^\dagger \mathcal{F} \mathcal{B} = \eta_6, \tag{4.90d}$$

$$\mathcal{C}^\dagger \mathcal{E}^\dagger \mathcal{C} \mathcal{F} = \eta_6. \tag{4.90e}$$

Since $\mathcal{C} = \tau_0$, and $\mathcal{A} = \mathcal{B}$, we can determine that $\eta_6 = 1$ and $\mathcal{E} = \mathcal{F}$. Also, when $\eta_{\mathcal{T}} = 1$, we have $\mathcal{E} = \mathcal{F} = \tau_0$; when $\eta_{\mathcal{T}} = -1$, we have $\mathcal{E} = \mathcal{F} = i\tau_z$. Since without TRS, we had 2 solutions, now we have 4 solutions, as collected in Table 4.2.

4.B IGG = U(1)

In this section, our target is to find the PSG solutions with U(1) IGG. The PSG relations listed in Section 4.A still hold, only with the signs on the RHS being replaced as $\eta_{\mathfrak{g}} \equiv \exp[i\phi_{\mathfrak{g}}]$.

To proceed, we mention a fact which is a blessing for us. In [66], Wen proved that for PSG solutions with U(1) IGG, the Gs always have the following canonical forms:

$$G_g(i) \equiv (i\tau_x)^{n_g} e^{i\theta_g(i)\tau_z}, \quad n_g = 0 \text{ or } 1, \tag{4.91}$$

where $\theta_g \in [0, 2\pi)$. Another thing we would like to mention before moving on is that, in this section θ always stands for *a function* which depends on position i, whereas ϕ always stands for *a constant phase*.

Let us first look at Eq.4.15b, which can be rewritten as:

$$G_a(g_a(i))G_a(i) = G_z(g_a(i))e^{i\phi_a\tau_z}. \tag{4.92}$$

The above equation already dictates that $n_z = 0$. Why? This is straightforward to see if $n_a = 0$. Now supposing $n_a = 1$, we would have:

$$\text{LHS}_{4.92} = e^{i(-\theta_a(g_a(i))+\theta_a(i))\tau_z}, \tag{4.93}$$

which also implies that $n_z = 0$ on the $\text{RHS}_{4.92}$. Similarly, due to Eq.4.15a and Eq.4.15c, we can conclude that $n_y = n_c = 0$.

There is a valuable lesson from the above operation. Given a PSG equation $G_{\mathfrak{g}}G_{\mathfrak{h}}^{\dagger}\cdots = e^{i\phi_{\mathfrak{i}}\tau_z}$, we demand that $(n_{\mathfrak{g}} - n_{\mathfrak{h}}\ldots) = 0 \bmod 2$. Using the above lesson, we see from Eq.4.15q that $n_x = 0$. And Eq.4.15p tells us that $n_b = 0$, whereas Eq.4.15r implies that $n_a = 0$. This is remarkable, for $n_x = n_y = n_z = n_a = n_b = n_c = 0$! What was for us originally a set of coupled $\mathsf{SU}(2)$ matrix equations now reduces to a set of coupled $\mathsf{U}(1)$ matrix equations, which are equations of compact $\mathsf{U}(1)$ phases.

4.B.1 Solving for the Translational Elements and the Simplification

Before we take a step further, let us rewrite the remaining PSG equations in terms of θs:

$$\theta_c(g_c^2(i)) + \theta_c(g_c(i)) + \theta_c(i) = \phi_c, \tag{4.94a}$$
$$-\theta_z(g_a(i)) + \theta_a(g_a(i)) + \theta_a(i) = \phi_a, \tag{4.94b}$$
$$-\theta_y(g_b(i)) + \theta_b(g_b(i)) + \theta_b(i) = \phi_b, \tag{4.94c}$$
$$-\theta_a(T_x(i)) + \theta_x(T_x(i)) + \theta_a(i) + \theta_x(g_a^{-1}(i)) = \phi_{ax}, \tag{4.94d}$$
$$-\theta_a(T_y(i)) + \theta_y(T_y(i)) + \theta_a(i) + \theta_y(g_a^{-1}(i)) = \phi_{ay}, \tag{4.94e}$$
$$-\theta_a(T_z^{-1}(i)) - \theta_z(i) + \theta_a(i) + \theta_z(g_a^{-1}(i)) = \phi_{az}, \tag{4.94f}$$
$$-\theta_b(T_x(i)) + \theta_x(T_x(i)) + \theta_b(i) + \theta_x(g_b^{-1}(i)) = \phi_{bx}, \tag{4.94g}$$
$$-\theta_b(T_y^{-1}(i)) - \theta_y(i) + \theta_b(i) + \theta_y(g_b^{-1}(i)) = \phi_{by}, \tag{4.94h}$$
$$-\theta_b(T_z(i)) + \theta_z(T_z(i)) + \theta_b(i) + \theta_z(g_b^{-1}(i)) = \phi_{bz}, \tag{4.94i}$$
$$-\theta_c(T_y^{-1}(i)) - \theta_y(i) + \theta_c(i) + \theta_x(g_c^{-1}(i)) = \phi_{cyx}, \tag{4.94j}$$
$$-\theta_c(T_z^{-1}(i)) - \theta_z(i) + \theta_c(i) + \theta_y(g_c^{-1}(i)) = \phi_{czy}, \tag{4.94k}$$
$$-\theta_c(T_x^{-1}(i)) - \theta_x(i) + \theta_c(i) + \theta_z(g_c^{-1}(i)) = \phi_{cxz}, \tag{4.94l}$$
$$\begin{aligned}&-\theta_a(g_c^{-1}g_b^{-1}T_x^{-1}T_y g_a g_c(i)) - \theta_c(g_b^{-1}T_x^{-1}T_y g_a g_c(i))\\ &-\theta_b(T_x^{-1}T_y g_a g_c(i)) - \theta_x(T_y g_a g_c(i))\\ &+\theta_y(T_y g_a g_c(i)) + \theta_a(g_a g_c(i)) + \theta_c(g_c(i)) = \phi_{acb},\end{aligned} \tag{4.94m}$$
$$\begin{aligned}&-\theta_b(g_a^{-1}T_x T_y^{-1}T_z g_b g_a(i)) - \theta_a(T_x T_y^{-1}T_z g_b g_a(i))\\ &+\theta_x(T_x T_y^{-1}T_z g_b g_a(i)) - \theta_y(T_z g_b g_a(i))\\ &+\theta_z(T_z g_b g_a(i)) + \theta_b(g_b g_a(i)) + \theta_a(g_a(i)) = \phi_{ab},\end{aligned} \tag{4.94n}$$
$$\begin{aligned}&-\theta_c(g_b^{-1}T_x^{-1}T_y g_a g_b g_c g_b(i)) - \theta_b(T_x^{-1}T_y g_a g_b g_c g_b(i))\\ &-\theta_x(T_y g_a g_b g_c g_b(i)) + \theta_y(T_y g_a g_b g_c g_b(i))\\ &+\theta_a(g_a g_b g_c g_b(i)) + \theta_b(g_b g_c g_b(i))\\ &+\theta_c(g_c g_b(i)) + \theta_b(g_b(i)) = \phi_{cba}.\end{aligned} \tag{4.94o}$$

These θs and ϕs in the above equations are compact $\mathsf{U}(1)$ phase factors, and an equation $\theta = \phi$ means $\theta = \phi \bmod 2\pi$. The θs are associated with the $\mathsf{SU}(2)$ gauge symmetry like before, specifically the $\mathsf{U}(1)$ subgroup of $\mathsf{SU}(2)$ transforms the θ in the following way:

$$\theta_U(i) \mapsto \theta_U(i) - \varphi(i) + \varphi(U^{-1}(i)), \quad \varphi \in [0, 2\pi); \tag{4.95}$$

note that since we do not want to spoil the choice of τ_z, we consider only the $\mathsf{U}(1)$ subgroup of $\mathsf{SU}(2)$.

Similar to the Z_2 case, we eliminate the phases on the right hand side of Eq. 4.94a, Eq. 4.94j, Eq. 4.94k, Eq. 4.94m and Eq. 4.94o.

4.B.2 Solving for the translational Elements

Let us start by considering the equations that arise because of the commutation of translational generators. Canonically, this gives us the following expressions of G_x, G_y, G_z after a gauge fixing:

$$\begin{aligned} &G_x(x, y, z; s) = \tau_0, G_y(x, y, z; s) = e^{ix\phi_{xy}\tau_z}, \\ &G_z(x, y, z; s) = e^{i(x\phi_{zx} + y\phi_{yz})\tau_z}. \end{aligned} \tag{4.96}$$

In other words, we have the following representation:

$$\begin{aligned} &\theta_x(x, y, z; s) = 0, \theta_y(x, y, z; s) = x\phi_{xy}, \\ &\theta_z(x, y, z; s) = x\phi_{zx} + y\phi_{yz}. \end{aligned} \tag{4.97}$$

4.B.3 Solving for θ_c

Using the IGG gauge symmetry, one can eliminate the phases on the RHS of Eq.4.94j, Eq.4.94k and Eq.4.94l, as each of θ_x, θ_y and θ_z appears only once in these equations. To solve for θ_c, one then plug the canonical expressions of the translational PSG elements into Eq.4.94j, Eq.4.94k and Eq.4.94l. We make an ansatz analogous to the one we made in the Z_2 case: $\theta(i) \equiv f(x, y, z; s) + \mathfrak{m}(s)$. We realise that the equations under attention are valid for all sub-lattice indices, therefore we have $f_c(x, y, z; s) \equiv f_c(x, y, z)$, and:

$$f_c(x, y, z) = f_c(x, y - 1, z) + x\phi_{xy}, \tag{4.98}$$

$$\begin{aligned} f_c(x, y, z) = f_c(x, y, z - 1) \\ + x\phi_{zx} + y\phi_{yz} - y\phi_{xy}, \end{aligned} \tag{4.99}$$

$$\begin{aligned} f_c(x, y, z) = f_c(x - 1, y, z) \\ - y\phi_{zx} - z\phi_{yz} + \phi_{cxz}. \end{aligned} \tag{4.100}$$

Checking the path-independency of f_c, we arrive at the following constraint:

$$\phi_{xy} = \phi_{yz} = -\phi_{zx} \equiv \phi_1. \tag{4.101}$$

Eventually we arrive at the conclusion that $f_c(x, y, z) = (xy - xz)\phi_1$.

Let us look at Eq.4.94a. We had eliminated the phase on the RHS by making use of the IGG gauge symmetry. Plugging the above expression into Eq.4.94a, we arrive at:

$$3\mathfrak{m}_c(\alpha) = 0, \tag{4.102}$$

$$\mathfrak{m}_c(\beta) + \mathfrak{m}_c(\gamma) + \mathfrak{m}_c(\delta) = 0, \tag{4.103}$$

$$\phi_{cxz} = 0. \tag{4.104}$$

Before moving on, we make a brief summary:

$$\begin{aligned} &\theta_x(i) = 0, \theta_y(i) = x\phi_1, \theta_z(i) = (y - x)\phi_1, \\ &\theta_c(i) = (xy - xz)\phi_1 + \mathfrak{m}_c(s). \end{aligned} \tag{4.105}$$

4.B.4 Solving for θ_a

To solve for θ_a, one plugs the simplified expressions of the translational PSG elements into Eq.4.94d, Eq.4.94e and Eq.4.94f. One arrives at the following expressions:

$$\theta_a(T_x(i)) = \theta_a(i) - \phi_{ax}, \tag{4.106}$$

$$\begin{aligned} \theta_a(T_y(i)) = \theta_a(i) &+ \theta_y(T_y(i)) \\ &+ \theta_y(g_a^{-1}(i)) - \phi_{ay}, \end{aligned} \tag{4.107}$$

$$\begin{aligned} \theta_a(i) = \theta_a(T_z^{-1}(i)) &+ \phi_{az} \\ &+ \theta_z(i) - \theta_z(g_a^{-1}(i)). \end{aligned} \tag{4.108}$$

One makes the usual ansatz $\theta_a \equiv f_a(x, y, z; s) + \mathfrak{m}_a(s)$, only this time one does not have $f_a(x, y, z; s) = f_a(x, y, z)$, for the evaluation of $\theta_{y/z}(g_a^{-1}(i))$ is not s-independent.
We have, for $s = \alpha/\delta$, the following conditions for f_a:

$$f_a(x + 1, y, z; \alpha/\delta) = f_a(x, y, z; \alpha/\delta) - \phi_{ax}, \tag{4.109}$$

$$f_a(x, y + 1, z; \alpha/\delta) = f_a(x, y, z; \alpha/\delta) - \phi_{ay}, \tag{4.110}$$

$$\begin{aligned} f_a(x, y, z; \alpha/\delta) = f_a(x, y, z - 1; \alpha/\delta) \\ + \phi_{az} + (2y - 2x + 1)\phi_1; \end{aligned} \tag{4.111}$$

and for $s = \beta/\gamma$, the following conditions for f_a:

$$f_a(x + 1, y, z; \beta/\gamma) = f_a(x, y, z; \beta/\gamma) - \phi_{ax}, \tag{4.112}$$

$$f_a(x, y+1, z; \beta/\gamma) = f_a(x, y, z; \beta/\gamma) - \phi_{ay} - \phi_1, \tag{4.113}$$

$$\begin{aligned} f_a(x, y, z; \beta/\gamma) = f_a(x, y, z-1; \beta/\gamma) + \phi_{az} \\ + (2y - 2x)\phi_1. \end{aligned} \tag{4.114}$$

Checking the path-independency of f_a, we arrive at the following constraint:

$$2\phi_1 = 0 \Rightarrow \phi_1 = 0 \text{ or } \pi. \tag{4.115}$$

After the path-independency is guaranteed, we arrive at the following expressions:

$$f_a(x, y, z; \alpha/\delta) = -x\phi_{ax} - y\phi_{ay} + z(\phi_{az} + \phi_1), \tag{4.116}$$

$$f_a(x, y, z; \beta/\gamma) = -x\phi_{ax} - y(\phi_{ay} + \phi_1) + z\phi_{az}. \tag{4.117}$$

Plugging the forms of $\theta_a \equiv f_a(x, y, z; s) + \mathfrak{m}_a(s)$ into Eq.4.94b, further constraints can be derived. Specifically, we iterate the sub-lattice index. Let us consider $i \equiv (x, y, z; \alpha)$, we have:

$$-\theta_z(-x, -y-1, z; \delta) + \theta_a(-x, -y-1, z; \delta) + \theta_a(x, y, z; \alpha) = \phi_a, \tag{4.118}$$

which gives us:

$$\begin{aligned} \phi_a &= -(-y-1+x)\phi_1 + (x\phi_{ax} + (y+1)\phi_{ay} \\ &\quad + z(\phi_{az} + \phi_1)) + (-x\phi_{ax} - y\phi_{ay} \\ &\quad + z(\phi_{az} + \phi_1)) + \mathfrak{m}_a(\alpha) + \mathfrak{m}_a(\delta) \\ &= -(-y-1+x)\phi_1 + \phi_{ay} + 2z\phi_{az} \\ &\quad + \mathfrak{m}_a(\alpha) + \mathfrak{m}_a(\delta). \end{aligned} \tag{4.119}$$

The implication from the above equation is that:

$$\phi_1 = 0, \quad 2\phi_{az} = 0; \quad \mathfrak{m}_a(\alpha) + \mathfrak{m}_a(\delta) = \phi_a - \phi_{ay}. \tag{4.120}$$

For $i \equiv (x, y, z; \beta)$, we have:

$$\theta_a(-x-1, -y-1, z+1; \gamma) + \theta_a(x, y, z; \beta) = \phi_a, \tag{4.121}$$

which gives us:

$$\begin{aligned} \phi_a &= ((x+1)\phi_{ax} + (y+1)\phi_{ay} + (z+1)\phi_{az}) \\ &\quad + (-x\phi_{ax} - y\phi_{ay} + z\phi_{az}) \\ &\quad + \mathfrak{m}_a(\beta) + \mathfrak{m}_a(\gamma) \\ &= \phi_{ax} + \phi_{ay} + \phi_{az} + \mathfrak{m}_a(\beta) + \mathfrak{m}_a(\gamma). \end{aligned} \tag{4.122}$$

For $i \equiv (x, y, z; \gamma)$, we have:

$$\theta_a(-x-1, -y-1, z; \beta) + \theta_a(x, y, z; \gamma) = \phi_a, \tag{4.123}$$

which gives us:

$$\begin{aligned}\phi_a &= ((x+1)\phi_{ax} + (y+1)\phi_{ay} + z\phi_{az}) \\ &\quad + (-x\phi_{ax} - y\phi_{ay} + z\phi_{az}) \\ &\quad + \mathfrak{m}_a(\beta) + \mathfrak{m}_a(\gamma) \\ &= \phi_{ax} + \phi_{ay} + \mathfrak{m}_a(\beta) + \mathfrak{m}_a(\gamma).\end{aligned} \tag{4.124}$$

Combining with the equation for $i \equiv (x, y, z; \beta)$, we have:

$$\phi_{az} = 0; \quad \mathfrak{m}_a(\beta) + \mathfrak{m}_a(\gamma) = \phi_a - \phi_{ay} - \phi_{ax}. \tag{4.125}$$

Lastly, the case for $i \equiv (x, y, z; \delta)$ does not give us new relations.
Before moving on, we make a brief summary:

$$\theta_{x/y/z}(i) = 0, \theta_a(i) = -x\phi_{ax} - y\phi_{ay} + \mathfrak{m}_a(s). \tag{4.126}$$

4.B.5 Solving for θ_b

To solve for θ_b, one plugs the simplified expressions of the translational PSG elements into Eq.4.94g, Eq.4.94h and Eq.4.94i. One arrives at the following expressions:

$$\begin{aligned}\theta_b(T_x(i)) &= \theta_b(i) - \phi_{bx}, \\ \theta_b(i) &= \theta_b(T_y^{-1}(i)) + \phi_{by}, \\ \theta_b(T_z(i)) &= \theta_b(i) - \phi_{bz}.\end{aligned} \tag{4.127}$$

One makes the usual ansatz $\theta_b \equiv f_b(x, y, z; s) + \mathfrak{m}_b(s)$, we arrive at

$$f_b(x, y, z; s) = -x\phi_{bx} + y\phi_{by} - z\phi_{bz}. \tag{4.128}$$

Plugging the forms of $\theta_b \equiv f_b(x, y, z; s) + \mathfrak{m}_b(s)$ into Eq.4.94c, further constraints can be derived. Specifically, we iterate the sub-lattice index. Let us consider $i \equiv (x, y, z; \alpha)$, we have:

$$\theta_b(-x-1, y, -z; \gamma) + \theta_b(x, y, z; \alpha) = \phi_b, \tag{4.129}$$

which gives us:

$$\begin{aligned}\phi_b &= ((x+1)\phi_{bx} + y\phi_{by} + z\phi_{bz}) \\ &\quad + (-x\phi_{bx} + y\phi_{by} - z\phi_{bz})\end{aligned}$$

$$
\begin{aligned}
&+ \mathfrak{m}_b(\alpha) + \mathfrak{m}_b(\gamma) \\
&= \phi_{bx} + 2y\phi_{by} + \mathfrak{m}_b(\alpha) + \mathfrak{m}_b(\gamma).
\end{aligned} \tag{4.130}
$$

The implication from the above equation is that:

$$
2\phi_{by} = 0; \quad \mathfrak{m}_b(\alpha) + \mathfrak{m}_b(\gamma) = \phi_b - \phi_{bx}. \tag{4.131}
$$

For $i \equiv (x, y, z; \beta)$, we have:

$$
\theta_b(-x-1, y, -z-1; \delta) + \theta_b(x, y, z; \beta) = \phi_b, \tag{4.132}
$$

which gives us:

$$
\begin{aligned}
\phi_b &= ((x+1)\phi_{bx} + y\phi_{by} + (z+1)\phi_{bz}) \\
&\quad + (-x\phi_{bx} + y\phi_{by} - z\phi_{bz}) \\
&\quad + \mathfrak{m}_b(\beta) + \mathfrak{m}_b(\delta) \\
&= \phi_{bx} + \phi_{bz} + \mathfrak{m}_b(\beta) + \mathfrak{m}_b(\delta).
\end{aligned} \tag{4.133}
$$

For $i \equiv (x, y, z; \gamma)$, we have:

$$
\theta_b(-x-1, y+1, -z; \alpha) + \theta_b(x, y, z; \gamma) = \phi_b, \tag{4.134}
$$

which gives us:

$$
\begin{aligned}
\phi_b &= ((x+1)\phi_{bx} + (y+1)\phi_{by} + z\phi_{bz}) \\
&\quad + (-x\phi_{bx} + y\phi_{by} - z\phi_{bz}) \\
&\quad + \mathfrak{m}_b(\alpha) + \mathfrak{m}_b(\gamma) \\
&= \phi_{bx} + \phi_{by} + \mathfrak{m}_b(\alpha) + \mathfrak{m}_b(\gamma).
\end{aligned} \tag{4.135}
$$

Combining with the equation for $i \equiv (x, y, z; \alpha)$, we have:

$$
\phi_{by} = 0; \quad \mathfrak{m}_b(\alpha) + \mathfrak{m}_b(\gamma) = \phi_b - \phi_{bx}. \tag{4.136}
$$

Lastly, the case for $i \equiv (x, y, z; \delta)$ gives us the same relation from the case for $i \equiv (x, y, z; \beta)$, which is:

$$
\mathfrak{m}_b(\beta) + \mathfrak{m}_b(\delta) = \phi_b - \phi_{bx} - \phi_{bz}. \tag{4.137}
$$

Before moving on, we make a brief summary:

$$
\theta_b(i) = -x\phi_{bx} - z\phi_{bz} + \mathfrak{m}_b(s). \tag{4.138}
$$

4.B.6 Solving Eq. 4.94m

The equation Eq. 4.94m is then reduced to:

$$\begin{aligned}&-\theta_a(g_c^{-1}g_b^{-1}T_x^{-1}T_y(i)) - \theta_c(g_b^{-1}T_x^{-1}T_y(i))\\&-\theta_b(T_x^{-1}T_y(i)) + \theta_a(i) + \theta_c(g_a^{-1}(i)) = 0.\end{aligned} \tag{4.139}$$

For $i \equiv (x, y, z; \alpha)$, the above equation is:

$$\begin{aligned}0 = &-\theta_a(y, -z, -x; \beta) - \theta_c(-x, y, -z; \gamma)\\&-\theta_b(x-1, y+1, z; \alpha)\\&+\theta_a(x, y, z; \alpha) + \theta_c(-x, -y-1, z-1; \delta)\\&= x(\phi_{bx} - \phi_{ax}) + y(\phi_{ax} - \phi_{ay}) + z(\phi_{bz} - \phi_{ay}) - \phi_{bx}\\&-\mathfrak{m}_a(\beta) - \mathfrak{m}_c(\gamma) - \mathfrak{m}_b(\alpha) + \mathfrak{m}_a(\alpha) + \mathfrak{m}_c(\delta).\end{aligned} \tag{4.140}$$

We can conclude from the above equation that $\phi_2 \equiv \phi_{ax} = \phi_{ay} = \phi_{bx} = \phi_{bz}$. Thus we have $f_a(x, y, z) = -(x + y)\phi_2$ and $f_b(x, y, z) = -(x + z)\phi_2$.
For $i \equiv (x, y, z; \beta)$, the above equation is:

$$\begin{aligned}0 = &-\theta_a(y, -z-1, -x; \gamma) - \theta_c(-x, y, -z-1; \delta)\\&-\theta_b(x-1, y+1, z; \beta) + \theta_a(x, y, z; \beta)\\&+\theta_c(-x-1, -y-1, z; \gamma)\\&= -2\phi_2 - \mathfrak{m}_a(\gamma) - \mathfrak{m}_c(\delta) - \mathfrak{m}_b(\beta)\\&+\mathfrak{m}_a(\beta) + \mathfrak{m}_c(\gamma).\end{aligned} \tag{4.141}$$

For $i \equiv (x, y, z; \gamma)$, the above equation is:

$$\begin{aligned}0 = &-\theta_a(y+1, -z, -x; \alpha) - \theta_c(-x, y+1, -z; \alpha)\\&-\theta_b(x-1, y+1, z; \gamma) + \theta_a(x, y, z; \gamma)\\&+\theta_c(-x-1, -y-1, z-1; \beta)\\&= -\mathfrak{m}_a(\alpha) - \mathfrak{m}_c(\alpha) - \mathfrak{m}_b(\gamma) + \mathfrak{m}_a(\gamma) + \mathfrak{m}_c(\beta).\end{aligned} \tag{4.142}$$

For $i \equiv (x, y, z; \delta)$, the above equation is:

$$\begin{aligned}0 = &-\theta_a(y+1, -z-1, -x; \delta) - \theta_c(-x, y+1, -z-1; \beta)\\&-\theta_b(x-1, y+1, z; \delta) + \theta_a(x, y, z; \delta)\\&+\theta_c(-x, -y-1, z; \alpha)\\&= -\phi_2 - \mathfrak{m}_a(\delta) - \mathfrak{m}_c(\beta) - \mathfrak{m}_b(\delta)\\&+\mathfrak{m}_a(\delta) + \mathfrak{m}_c(\alpha).\end{aligned} \tag{4.143}$$

4.B.7 Solving Eq. 4.94n

The equation is reduced to:

$$\begin{aligned} &- \theta_b(g_a^{-1}T_xT_y^{-1}T_z(i)) - \theta_a(T_xT_y^{-1}T_z(i)) \\ &+ \theta_b(i) + \theta_a(g_b^{-1}(i)) = \phi_{ab}. \end{aligned} \tag{4.144}$$

For $i \equiv (x, y, z; \alpha)$, the above equation is:

$$\begin{aligned} \phi_{ab} &= -\theta_b(-x-1, -y, z; \delta) - \theta_a(x+1, y-1, z+1; \alpha) \\ &\quad + \theta_b(x, y, z; \alpha) + \theta_a(-x-1, y-1, -z; \gamma) \\ &= \phi_2 - \mathfrak{m}_b(\delta) - \mathfrak{m}_a(\alpha) + \mathfrak{m}_b(\alpha) + \mathfrak{m}_a(\gamma). \end{aligned} \tag{4.145}$$

For $i \equiv (x, y, z; \beta)$, the above equation is:

$$\begin{aligned} \phi_{ab} &= -\theta_b(-x-2, -y, z+1; \gamma) - \theta_a(x+1, y-1, z+1; \beta) \\ &\quad + \theta_b(x, y, z; \beta) + \theta_a(-x-1, y-1, -z-1; \delta) \\ &= \phi_2 - \mathfrak{m}_b(\gamma) - \mathfrak{m}_a(\beta) + \mathfrak{m}_b(\beta) + \mathfrak{m}_a(\delta). \end{aligned} \tag{4.146}$$

For $i \equiv (x, y, z; \gamma)$, the above equation is:

$$\begin{aligned} \phi_{ab} &= -\theta_b(-x-2, -y, z; \beta) - \theta_a(x+1, y-1, z+1; \gamma) \\ &\quad + \theta_b(x, y, z; \gamma) + \theta_a(-x-1, y, -z; \alpha) \\ &= -\phi_2 - \mathfrak{m}_b(\beta) - \mathfrak{m}_a(\gamma) + \mathfrak{m}_b(\gamma) + \mathfrak{m}_a(\alpha). \end{aligned} \tag{4.147}$$

For $i \equiv (x, y, z; \delta)$, the above equation is:

$$\begin{aligned} \phi_{ab} &= -\theta_b(-x-1, -y, z+1; \alpha) - \theta_a(x+1, y-1, z+1; \delta) \\ &\quad + \theta_b(x, y, z; \delta) + \theta_a(-x-1, y, -z-1; \beta) \\ &= \phi_2 - \mathfrak{m}_b(\alpha) - \mathfrak{m}_a(\delta) + \mathfrak{m}_b(\delta) + \mathfrak{m}_a(\beta). \end{aligned} \tag{4.148}$$

4.B.8 Solving Eq. 4.94o

The equation Eq.4.94o is then reduced to:

$$\begin{aligned} &- \theta_c(g_b^{-1}T_x^{-1}T_y(i)) - \theta_b(T_x^{-1}T_y(i)) + \theta_a(i) \\ &+ \theta_b(g_a^{-1}(i)) + \theta_c(g_b^{-1}g_a^{-1}(i)) \\ &+ \theta_b(g_c^{-1}g_b^{-1}g_a^{-1}(i)) = 0. \end{aligned} \tag{4.149}$$

For $i \equiv (x, y, z; \alpha)$, the above equation is:

$$0 = -\theta_c(-x, y, -z; \gamma) - \theta_b(x-1, y+1, z; \alpha)$$

$$
\begin{aligned}
&+\theta_a(x,y,z;\alpha)+\theta_b(-x,-y-1,z-1;\delta)\\
&+\theta_c(x-1,-y-1,-z;\beta)+\theta_b(-y-1,-z,x-1;\delta)\\
&=2\phi_2-\mathfrak{m}_c(\gamma)-\mathfrak{m}_b(\alpha)+\mathfrak{m}_a(\alpha)\\
&+\mathfrak{m}_b(\delta)+\mathfrak{m}_c(\beta)+\mathfrak{m}_b(\delta).
\end{aligned}
\tag{4.150}
$$

For $i\equiv(x,y,z;\beta)$, the above equation is:

$$
\begin{aligned}
0=&-\theta_c(-x,y,-z-1;\delta)-\theta_b(x-1,y+1,z;\beta)\\
&+\theta_a(x,y,z;\beta)+\theta_b(-x-1,-y-1,z;\gamma)\\
&+\theta_c(x,-y-1,-z;\alpha)+\theta_b(-y-1,-z,x;\alpha)\\
&=\phi_2-\mathfrak{m}_c(\delta)-\mathfrak{m}_b(\beta)+\mathfrak{m}_a(\beta)\\
&+\mathfrak{m}_b(\gamma)+\mathfrak{m}_c(\alpha)+\mathfrak{m}_b(\alpha).
\end{aligned}
\tag{4.151}
$$

For $i\equiv(x,y,z;\gamma)$, the above equation is:

$$
\begin{aligned}
0=&-\theta_c(-x,y+1,-z;\alpha)-\theta_b(x-1,y+1,z;\gamma)\\
&+\theta_a(x,y,z;\gamma)+\theta_b(-x-1,-y-1,z-1;\beta\\
&)+\theta_c(x,-y-2,-z;\delta)+\theta_b(-y-2,-z,x;\gamma)\\
&=3\phi_2-\mathfrak{m}_c(\alpha)-\mathfrak{m}_b(\gamma)+\mathfrak{m}_a(\gamma)\\
&+\mathfrak{m}_b(\beta)+\mathfrak{m}_c(\delta)+\mathfrak{m}_b(\gamma).
\end{aligned}
\tag{4.152}
$$

For $i\equiv(x,y,z;\delta)$, the above equation is:

$$
\begin{aligned}
0=&-\theta_c(-x,y+1,-z-1;\beta)-\theta_b(x-1,y+1,z;\delta)\\
&\theta_a(x,y,z;\delta)+\theta_b(-x,-y-1,z;\alpha)\\
&+\theta_c(x-1,-y-2,-z;\gamma)+\theta_b(-y-2,-z,x-1;\beta)\\
&=2\phi_2-\mathfrak{m}_c(\beta)-\mathfrak{m}_b(\delta)+\mathfrak{m}_a(\delta)\\
&+\mathfrak{m}_b(\alpha)+\mathfrak{m}_c(\gamma)+\mathfrak{m}_b(\beta).
\end{aligned}
\tag{4.153}
$$

4.B.9 Collected equations for $\mathfrak{m}$s

In this subsection, we collect the coupled equations to solve for $\mathfrak{m}$s. Before doing so, we note that we can use the $\mathsf{SU}(2)$ gauge symmetry to fix certain $\mathfrak{m}$s. Recall that the action of the gauge transformation is:

$$
g.t.:\theta_U(i)\mapsto w(i)-\theta_U(i)+w(U^{-1}(i)).
\tag{4.154}
$$

We start off in a generic gauge where all $\mathfrak{m}$s are non-trivial. We first perform the gauge transformation $w(\beta)=\mathfrak{m}_c(\beta)$ and $w(\gamma)=-\mathfrak{m}_c(\delta)$. The consequence is that $\mathfrak{m}_c(\beta)=$

$\mathfrak{m}_c(\delta) = 0$. And because $\mathfrak{m}_c(\beta) + \mathfrak{m}_c(\gamma) + \mathfrak{m}_c(\delta) = 0$ from one of our constraints, we have $\mathfrak{m}_c(\gamma) = 0$. We then perform the gauge transformation $w(\alpha) = \mathfrak{m}_a(\alpha)$, such that $\mathfrak{m}_a(\alpha) = 0$. And because $\mathfrak{m}_a(\alpha) + \mathfrak{m}_a(\delta) = \phi_a - \phi_2$ from one of our constraints, we have $\mathfrak{m}_a(\delta) = \phi_a - \phi_2$.

The remaining equations after the reductions are:

$$3\mathfrak{m}_c(\alpha) = 0, \tag{4.155a}$$
$$\mathfrak{m}_a(\beta) + \mathfrak{m}_a(\gamma) = \phi_a - 2\phi_2, \tag{4.155b}$$
$$\mathfrak{m}_b(\alpha) + \mathfrak{m}_b(\gamma) = \phi_b - \phi_2, \tag{4.155c}$$
$$\mathfrak{m}_b(\beta) + \mathfrak{m}_b(\delta) = \phi_b - 2\phi_2, \tag{4.155d}$$
$$-\mathfrak{m}_a(\beta) - \mathfrak{m}_b(\alpha) = \phi_2, \tag{4.155e}$$
$$-\mathfrak{m}_a(\gamma) - \mathfrak{m}_b(\beta) + \mathfrak{m}_a(\beta) = 2\phi_2, \tag{4.155f}$$
$$-\mathfrak{m}_c(\alpha) - \mathfrak{m}_b(\gamma) + \mathfrak{m}_a(\gamma) = 0, \tag{4.155g}$$
$$-\mathfrak{m}_b(\delta) + \mathfrak{m}_c(\alpha) = \phi_2, \tag{4.155h}$$
$$-\mathfrak{m}_b(\delta) + \mathfrak{m}_b(\alpha) + \mathfrak{m}_a(\gamma) = \phi_{ab} - \phi_2, \tag{4.155i}$$
$$-\mathfrak{m}_b(\gamma) - \mathfrak{m}_a(\beta) + \mathfrak{m}_b(\beta) = \phi_{ab} - \phi_a, \tag{4.155j}$$
$$-\mathfrak{m}_b(\beta) - \mathfrak{m}_a(\gamma) + \mathfrak{m}_b(\gamma) = \phi_{ab} + \phi_2, \tag{4.155k}$$
$$-\mathfrak{m}_b(\alpha) + \mathfrak{m}_b(\delta) + \mathfrak{m}_a(\beta) = \phi_{ab} + \phi_a - 2\phi_2, \tag{4.155l}$$
$$-\mathfrak{m}_b(\alpha) + \mathfrak{m}_b(\delta) + \mathfrak{m}_b(\delta) = -2\phi_2, \tag{4.155m}$$
$$-\mathfrak{m}_b(\beta) + \mathfrak{m}_a(\beta) + \mathfrak{m}_b(\gamma) + \mathfrak{m}_c(\alpha) + \mathfrak{m}_b(\alpha) = -\phi_2, \tag{4.155n}$$
$$-\mathfrak{m}_c(\alpha) - \mathfrak{m}_b(\gamma) + \mathfrak{m}_a(\gamma) + \mathfrak{m}_b(\beta) + \mathfrak{m}_b(\gamma) = -3\phi_2, \tag{4.155o}$$
$$-\mathfrak{m}_b(\delta) + \mathfrak{m}_b(\alpha) + \mathfrak{m}_b(\beta) = -\phi_a - \phi_2. \tag{4.155p}$$

We now set $A \equiv \mathfrak{m}_c(\alpha)$, $B \equiv \mathfrak{m}_a(\beta)$, $C \equiv \mathfrak{m}_b(\alpha)$ and $D \equiv \mathfrak{m}_b(\beta)$. Eq. 4.155e tells us that $-B - C = \phi_2$. Also, Eq. 4.155f tells us that $D = 2B - \phi_a$. Thus all the $\mathfrak{m}$s can be represented using A and B, as deduced from Eq. 4.155a to Eq. 4.155f:

$$\begin{aligned}
\mathfrak{m}_a(\alpha) &= 0, \\
\mathfrak{m}_a(\beta) &= B, \\
\mathfrak{m}_a(\gamma) &= \phi_a - 2\phi_2 - B, \\
\mathfrak{m}_a(\delta) &= \phi_a - \phi_2, \\
\mathfrak{m}_b(\alpha) &= -\phi_2 - B, \\
\mathfrak{m}_b(\beta) &= 2B - \phi_a, \\
\mathfrak{m}_b(\gamma) &= \phi_b + B, \\
\mathfrak{m}_b(\delta) &= \phi_b - 2\phi_2 + \phi_a - 2B,
\end{aligned}$$

$$\begin{aligned}
\mathfrak{m}_c(\alpha) &= A, \\
\mathfrak{m}_c(\beta) &= 0, \\
\mathfrak{m}_c(\gamma) &= 0, \\
\mathfrak{m}_c(\delta) &= 0.
\end{aligned} \tag{4.156a}$$

Eq. 4.155g tells us that:

$$A + 2B = \phi_a - \phi_b - 2\phi_2, \tag{4.157}$$

whereas Eq. 4.155h tells us that:

$$A + 2B = \phi_a + \phi_b - \phi_2. \tag{4.158}$$

From which we can see that $\phi_2 = -2\phi_b$. Now if we look at Eq. 4.155i, we have $\phi_{ab} = -\phi_b$. In fact, Eq. 4.155j to Eq. 4.155l do not tell us more than this. Eq. 4.155m tells us that $3B = 4\phi_b + 2\phi_a$, Eq. 4.155n tells us that $A - B = -\phi_a - \phi_b$, Eq. 4.155o tells us that $A - B = -2\phi_b$ and finally Eq. 4.155p tells us that $3B = \phi_a + \phi_b - 2\phi_2$. The above relations allow us to assert that:

$$\phi_3 \equiv -\phi_{ab} = \phi_a = \phi_b, \quad \phi_2 = -2\phi_3, \quad B = A + 2\phi_3, \tag{4.159}$$

and:

$$\begin{aligned}
\mathfrak{m}_a(\alpha) &= 0, \\
\mathfrak{m}_a(\beta) &= A + 2\phi_3, \\
\mathfrak{m}_a(\gamma) &= 3\phi_3 - A, \\
\mathfrak{m}_a(\delta) &= 3\phi_3, \\
\mathfrak{m}_b(\alpha) &= -A, \\
\mathfrak{m}_b(\beta) &= -A + 3\phi_3, \\
\mathfrak{m}_b(\gamma) &= 3\phi_3 + A, \\
\mathfrak{m}_b(\delta) &= 2\phi_3 + A, \\
\mathfrak{m}_c(\alpha) &= A, \\
\mathfrak{m}_c(\beta) &= 0, \\
\mathfrak{m}_c(\gamma) &= 0, \\
\mathfrak{m}_c(\delta) &= 0.
\end{aligned} \tag{4.160}$$

We also have:

$$f_a(i) = 2(x + y)\phi_3, \quad f_b(i) = 2(x + z)\phi_3. \tag{4.161}$$

Similar to the Z_2 case, we now consider a further gauge transformation:

$$\begin{aligned} w(x,y,z;\alpha) &= -2\phi_3 + \phi_3(x+y+z), \\ w(x,y,z;\beta/\gamma/\delta) &= \phi_3(x+y+z), \end{aligned} \tag{4.162}$$

we see that:

1.) $G_x = G_y = G_z = e^{-i\phi_3\tau_z}$;

2.) $G_{a/b/c}(x,y,z;s) = e^{i\mathfrak{m}_{a/b/c}(s)\tau_z}$, where the $\mathfrak{m}$s have the following forms:

$$\begin{aligned} &\mathfrak{m}_a(\alpha) = 0, \mathfrak{m}_a(\beta) = A, \mathfrak{m}_a(\gamma) = -A, \mathfrak{m}_a(\delta) = 0; \\ &\mathfrak{m}_b(\alpha) = -A, \mathfrak{m}_b(\beta) = -A, \mathfrak{m}_b(\gamma) = A, \mathfrak{m}_b(\delta) = A; \\ &\mathfrak{m}_c(\alpha) = A, \mathfrak{m}_c(\beta) = 0, \mathfrak{m}_c(\gamma) = 0, \mathfrak{m}_c(\delta) = 0. \end{aligned} \tag{4.163}$$

Due to the fact that ϕ_3 now becomes global signs which are elements of the IGG, we conclude that ϕ_3 is redundant. We also remark that a gauge transformation $W(x,y,z;s) \equiv i\tau_x$ maps the PSG solutions in which $\mathcal{A} = e^{i\frac{2\pi}{3}\tau_z}$ to that in which $\mathcal{A} = e^{i\frac{4\pi}{3}\tau_z}$.

In conclusion, we have:

1.) $G_x = G_y = G_z = \tau_0$;

2.) $G_{a/b/c}(x,y,z;s) = e^{i\mathfrak{m}_{a/b/c}(s)\tau_z}$, where the $\mathfrak{m}$s have the following forms:

$$\begin{aligned} &\mathfrak{m}_a(\alpha) = 0, \mathfrak{m}_a(\beta) = A, \mathfrak{m}_a(\gamma) = -A, \mathfrak{m}_a(\delta) = 0; \\ &\mathfrak{m}_b(\alpha) = -A, \mathfrak{m}_b(\beta) = -A, \mathfrak{m}_b(\gamma) = A, \mathfrak{m}_b(\delta) = A; \\ &\mathfrak{m}_c(\alpha) = A, \mathfrak{m}_c(\beta) = 0, \mathfrak{m}_c(\gamma) = 0, \mathfrak{m}_c(\delta) = 0, \end{aligned} \tag{4.164}$$

where $\mathcal{A} = \tau_0, e^{i\frac{2\pi}{3}\tau_z}$.

4.B.10 Adding Time-Reversal Symmetry

We firstly write the algebraic relations:

$$G_{\mathcal{T}}(i)G_{\mathcal{T}}(i) = e^{i\phi_{\mathcal{T}}\tau_z}, \tag{4.165a}$$

$$G^\dagger_{\mathcal{T}}(T_x^{-1}(i))G^\dagger_x(i)G_{\mathcal{T}}(i)G_x(i) = e^{i\phi_{x\mathcal{T}}\tau_z}, \tag{4.165b}$$

$$G^\dagger_{\mathcal{T}}(T_y^{-1}(i))G^\dagger_y(i)G_{\mathcal{T}}(i)G_y(i) = e^{i\phi_{y\mathcal{T}}\tau_z}, \tag{4.165c}$$

$$G^\dagger_{\mathcal{T}}(T_z^{-1}(i))G^\dagger_z(i)G_{\mathcal{T}}(i)G_z(i) = e^{i\phi_{z\mathcal{T}}\tau_z}, \tag{4.165d}$$

$$G^\dagger_{\mathcal{T}}(g_a^{-1}(i))G^\dagger_a(i)G_{\mathcal{T}}(i)G_a(i) = e^{i\phi_{a\mathcal{T}}\tau_z}, \tag{4.165e}$$

$$G^\dagger_{\mathcal{T}}(g_b^{-1}(i))G^\dagger_b(i)G_{\mathcal{T}}(i)G_b(i) = e^{i\phi_{b\mathcal{T}}\tau_z}, \tag{4.165f}$$

$$G^\dagger_{\mathcal{T}}(g_c^{-1}(i))G^\dagger_c(i)G_{\mathcal{T}}(i)G_c(i) = e^{i\phi_{c\mathcal{T}}\tau_z}. \tag{4.165g}$$

As usual, the canonical form of $G_{\mathcal{T}}(i) = (i\tau_x)^{n_{\mathcal{T}}} e^{i\theta_{\mathcal{T}}(i)\tau_z}$. Later we can show that when $n_{\mathcal{T}} = 0$, the PSG solutions do not produce mean field $\mathsf{U}(1)$ spin liquids. At the moment, let us focus on the case when $n_{\mathcal{T}} = 1$.

Let us first look at Eq. 4.165a, we straightforwardly conclude that $\phi_{\mathcal{T}} = \pi$. We denote $\theta_{\mathcal{T}} \equiv f_{\mathcal{T}}(x, y, z; s) + \mathfrak{m}_{\mathcal{T}}(s)$. Then Eq. 4.165b to Eq. 4.165d tell us that:

$$f_{\mathcal{T}}(x, y, z; s) = x\phi_{x\mathcal{T}} + y\phi_{y\mathcal{T}} + z\phi_{z\mathcal{T}}. \tag{4.166}$$

We would like to plug the above results into Eq. 4.165g. We arrive at the folllowing constraint:

$$-\theta_{\mathcal{T}}(g_c^{-1}(i)) + 2\theta_c(i) + \theta_{\mathcal{T}}(i) = \phi_{c\mathcal{T}}. \tag{4.167}$$

For the case with $i = (x, y, z; \alpha)$, we have:

$$\begin{aligned}\phi_{c\mathcal{T}} &= -\theta_{\mathcal{T}}(y, z, x; \alpha) + 2A + \theta_{\mathcal{T}}(x, y, z; \alpha) \\ &= x(\phi_{x\mathcal{T}} - \phi_{y\mathcal{T}}) + y(\phi_{y\mathcal{T}} - \phi_{z\mathcal{T}}) \\ &+ z(\phi_{z\mathcal{T}} - \phi_{x\mathcal{T}}) + 2A,\end{aligned} \tag{4.168}$$

we arrive at $\phi_4 \equiv \phi_{x\mathcal{T}} = \phi_{y\mathcal{T}} = \phi_{z\mathcal{T}}$, and $\phi_{c\mathcal{T}} = -A$, where we used $3A = 0$.
For the case with $i = (x, y, z; \beta)$, we have:

$$\begin{aligned}\phi_{c\mathcal{T}} &= -\theta_{\mathcal{T}}(y, z, x; \delta) + \theta_{\mathcal{T}}(x, y, z; \beta) \\ &= -\mathfrak{m}_{\mathcal{T}}(\delta) + \mathfrak{m}_{\mathcal{T}}(\beta).\end{aligned} \tag{4.169}$$

For the case with $i = (x, y, z; \gamma)$, we have:

$$\begin{aligned}\phi_{c\mathcal{T}} &= -\theta_{\mathcal{T}}(y, z, x; \beta) + \theta_{\mathcal{T}}(x, y, z; \gamma) \\ &= -\mathfrak{m}_{\mathcal{T}}(\beta) + \mathfrak{m}_{\mathcal{T}}(\gamma).\end{aligned} \tag{4.170}$$

For the case with $i = (x, y, z; \delta)$, we have:

$$\begin{aligned}\phi_{c\mathcal{T}} &= -\theta_{\mathcal{T}}(y, z, x; \gamma) + \theta_{\mathcal{T}}(x, y, z; \delta) \\ &= -\mathfrak{m}_{\mathcal{T}}(\gamma) + \mathfrak{m}_{\mathcal{T}}(\delta).\end{aligned} \tag{4.171}$$

Thus if we denote $\mathfrak{m}_{\mathcal{T}}(\beta) \equiv E$, we have $\mathfrak{m}_{\mathcal{T}}(\gamma) = E - A$ and $\mathfrak{m}_{\mathcal{T}}(\delta) = E + A$.

We now look at Eq. 4.165e. Similar to the case before:

$$-\theta_{\mathcal{T}}(g_a^{-1}(i)) + 2\theta_a(i) + \theta_{\mathcal{T}}(i) = \phi_{a\mathcal{T}}. \tag{4.172}$$

For the case with $i = (x, y, z; \alpha)$, we have:

$$\phi_{a\mathcal{T}} = -\theta_{\mathcal{T}}(-x, -y - 1, z - 1; \delta)$$

$$
\begin{aligned}
&+ 2\mathfrak{m}_a(\alpha) + \theta_{\mathcal{T}}(x, y, z; \alpha) \\
&= -(-x - y - 1 + z - 1)\phi_4 - \mathfrak{m}_{\mathcal{T}}(\delta) \\
&+ (x + y + z)\phi_4 + \mathfrak{m}_{\mathcal{T}}(\alpha) \\
&= x(2\phi_4) + y(2\phi_4) \\
&+ 2\phi_4 + \mathfrak{m}_{\mathcal{T}}(\alpha) - \mathfrak{m}_{\mathcal{T}}(\delta),
\end{aligned} \tag{4.173}
$$

from which we have:

$$
2\phi_4 = 0, \quad \mathfrak{m}_{\mathcal{T}}(\alpha) - \mathfrak{m}_{\mathcal{T}}(\delta) = \phi_{a\mathcal{T}}. \tag{4.174}
$$

For the case with $i = (x, y, z; \beta)$, we have:

$$
\begin{aligned}
\phi_{a\mathcal{T}} &= -\theta_{\mathcal{T}}(-x - 1, -y - 1, z; \gamma) \\
&\quad + 2\mathfrak{m}_a(\beta) + \theta_{\mathcal{T}}(x, y, z; \beta) \\
&= \mathfrak{m}_{\mathcal{T}}(\beta) - \mathfrak{m}_{\mathcal{T}}(\gamma) + 2A \\
&= 0.
\end{aligned} \tag{4.175}
$$

For the case with $i = (x, y, z; \gamma)$, we have:

$$
\begin{aligned}
\phi_{a\mathcal{T}} &= -\theta_{\mathcal{T}}(-x - 1, -y - 1, z - 1; \beta) \\
&\quad + 2\mathfrak{m}_a(\gamma) + \theta_{\mathcal{T}}(x, y, z; \gamma) \\
&= 3\phi_4 + \mathfrak{m}_{\mathcal{T}}(\gamma) - \mathfrak{m}_{\mathcal{T}}(\beta) - 2A \\
&= 3\phi_4.
\end{aligned} \tag{4.176}
$$

Note that this relation combined with the one before, gives us that $\phi_4 = 0$.
For the case with $i = (x, y, z; \delta)$, we have:

$$
\begin{aligned}
\phi_{a\mathcal{T}} &= -\theta_{\mathcal{T}}(-x, -y - 1, z; \alpha) \\
&\quad + 2\mathfrak{m}_a(\delta) + \theta_{\mathcal{T}}(x, y, z; \delta) \\
&= \phi_4 + \mathfrak{m}_{\mathcal{T}}(\delta) - \mathfrak{m}_{\mathcal{T}}(\alpha).
\end{aligned} \tag{4.177}
$$

Combining the above constraints, we arrive at a set of relations summarised here:

$$
\begin{aligned}
&\phi_{a\mathcal{T}} = \phi_4 = 0 \\
&\mathfrak{m}_{\mathcal{T}}(\alpha) = \mathfrak{m}_{\mathcal{T}}(\delta), \quad \mathfrak{m}_{\mathcal{T}}(\beta) = \mathfrak{m}_{\mathcal{T}}(\gamma) + A.
\end{aligned} \tag{4.178}
$$

Let us now look at Eq. 4.165f:

$$
-\theta_{\mathcal{T}}(g_b^{-1}(i)) + 2\theta_b(i) + \theta_{\mathcal{T}}(i) = \phi_{b\mathcal{T}}. \tag{4.179}
$$

For the case with $i = (x, y, z; \alpha)$, we have:

$$\begin{aligned}\phi_{b\mathcal{T}} &= -\theta_{\mathcal{T}}(-x-1, y-1, -z; \gamma) \\ &\quad + 2\mathfrak{m}_b(\alpha) + \theta_{\mathcal{T}}(x, y, z; \alpha) \\ &= -2A + \mathfrak{m}_{\mathcal{T}}(\alpha) - \mathfrak{m}_{\mathcal{T}}(\gamma).\end{aligned} \tag{4.180}$$

For the case with $i = (x, y, z; \beta)$, we have:

$$\begin{aligned}\phi_{b\mathcal{T}} &= -\theta_{\mathcal{T}}(-x-1, y-1, -z-1; \delta) \\ &\quad + 2\mathfrak{m}_b(\beta) + \theta_{\mathcal{T}}(x, y, z; \beta) \\ &= -2A + \mathfrak{m}_{\mathcal{T}}(\beta) - \mathfrak{m}_{\mathcal{T}}(\delta).\end{aligned} \tag{4.181}$$

For the case with $i = (x, y, z; \gamma)$, we have:

$$\begin{aligned}\phi_{b\mathcal{T}} &= -\theta_{\mathcal{T}}(-x-1, y, -z; \alpha) \\ &\quad + 2\mathfrak{m}_b(\gamma) + \theta_{\mathcal{T}}(x, y, z; \gamma) \\ &= 2A + \mathfrak{m}_{\mathcal{T}}(\gamma) - \mathfrak{m}_{\mathcal{T}}(\alpha).\end{aligned} \tag{4.182}$$

For the case with $i = (x, y, z; \delta)$, we have:

$$\begin{aligned}\phi_{b\mathcal{T}} &= -\theta_{\mathcal{T}}(-x-1, y, -z-1; \beta) \\ &\quad + 2\mathfrak{m}_b(\delta) + \theta_{\mathcal{T}}(x, y, z; \delta) \\ &= 2A + \mathfrak{m}_{\mathcal{T}}(\delta) - \mathfrak{m}_{\mathcal{T}}(\beta).\end{aligned} \tag{4.183}$$

Combining the above constraints, we arrive at $\phi_{b\mathcal{T}} = 0$ and no new relations.

We can then summarise:

$$\begin{aligned}\mathfrak{m}_{\mathcal{T}}(\alpha) &= E + A, \\ \mathfrak{m}_{\mathcal{T}}(\beta) &= E, \\ \mathfrak{m}_{\mathcal{T}}(\gamma) &= E - A, \\ \mathfrak{m}_{\mathcal{T}}(\delta) &= E + A.\end{aligned} \tag{4.184}$$

In the above, E is a free $\mathsf{U}(1)$ phase. However, note that we did not make use of the IGG gauge degrees of freedom associated with TRS. Recalling that $G_{\mathcal{T}} \sim G_{\mathcal{T}} W_{\mathcal{T}}$, where $W_{\mathcal{T}} \in \mathsf{U}(1)$. We choose $W_{\mathcal{T}} \equiv \exp(-iE)$, thus eliminating the free phase in our solutions. We collect the $\mathsf{U}(1)$ PSG solutions into Table 4.3. Thus we have:

$$\begin{aligned}G_{\mathcal{T}}(\vec{r}, \alpha) &= i\tau_x e^{iA\tau_z}, \\ G_{\mathcal{T}}(\vec{r}, \beta) &= i\tau_x, \\ G_{\mathcal{T}}(\vec{r}, \gamma) &= i\tau_x e^{-iA\tau_z}, \\ G_{\mathcal{T}}(\vec{r}, \delta) &= i\tau_x e^{iA\tau_z}.\end{aligned} \tag{4.185}$$

4.C Mean-field ansatzes for the PSG solutions

Our PSG classification obtains a set of gauge-inequivalent transformations G_g for all $g \in \mathsf{P2_13}\times\mathsf{Z}_2$. In this appendix, we derive the constraints imposed on the mean-field parameters U_{ij} and μ_i by requiring that an element of the PSG leaves the ansatz invariant. We repeat this condition for convenience:

$$\begin{aligned}\forall g :& G_g(g(i))U_{g(i)g(j)}G_g^\dagger(g(j)) = U_{ij},\\ & G_g(g(i))\mu_{g(i)}G_g^\dagger(g(i)) = \mu_i.\end{aligned} \tag{4.7}$$

4.C.1 Z_2

Here we specify the ansatzes for the PSGs corresponding to the IGG being Z_2. As derived in Appendix 4.A and displayed in Table 4.2 in the main text, the four Z_2 PSGs can be indexed by , $\mathcal{A} = \exp(i2\pi n/3)$ for $i = 0, 1$, and $\mathcal{E} = \tau_0$ or $\mathcal{E} = i\tau_z$, in terms of which all gauge transformations are listed in Table 4.2.

We note that if $G_\mathcal{T} = \tau_0$ then the invariance of the ansatz under time-reversal requires $U_{ij} = -U_{ij}$ and $\mu_i = -\mu_i$, leading to no non-zero mean-field ansatzes.

For $G_\mathcal{T} = i\tau_z$, the invariance under TRS requires the following form for all links and sites:

$$U_{ij} = U_{ij}^x\tau_x + U_{ij}^y\tau_y \tag{4.186}$$

$$\mu_i = \mu_i^x\tau_x + \mu_i^y\tau_y. \tag{4.187}$$

Finally, since $G_x = G_y = G_z = \tau_0$ in our solutions, we must require U_{ij} and μ_{ij} to be translationally invariant. We then encode the dependence of the parameters U_{ij} on the link (ij) by determining U for each of the unique links in Table 4.1, and determining the functions U_i^x, U_i^y, where $i \in \{1, 2\cdots 12\}$ specifies the link in Table 4.1. The on-site parameters are described as $\mu_\alpha, \mu_\beta, \mu_\gamma$ and μ_δ, where the subscripts denote the sublattice dependence.

Imposing the invariance of the ansatz under the action of (G_c, g_c), we get the following relations between 4 groups of links that are closed under the application of g_c

$$\begin{aligned}U_1 &= U_5 = U_9\\ U_2 &= U_6 = U_{10}\\ U_3 &= \mathcal{A}U_7 = \mathcal{A}^2U_{11}\\ U_4 &= \mathcal{A}U_8 = \mathcal{A}^2U_{12}\end{aligned} \tag{4.188}$$

The relations between different groups of links are obtained by the invariance under (G_b, g_b) and (G_a, g_a). The action of (G_a, g_a) gives us

$$\begin{aligned} U_1 &= U_2 \\ U_3 &= U_4 \\ U_5 &= \mathcal{A}^2 U_7 \\ U_6 &= \mathcal{A}^2 U_8 \\ U_9 &= \mathcal{A} U_{12} \\ U_{10} &= \mathcal{A} U_{11} \end{aligned} \tag{4.189}$$

Similarly, the invariance of all links under (G_b, g_b) give us the conditions

$$\begin{aligned} U_1 &= U_3 \\ U_2 &= U_4 \\ U_5 &= \mathcal{A}^2 U_8 \\ U_6 &= \mathcal{A}^2 U_7 \\ U_9 &= U_{10} \\ U_{11} &= U_{12} \end{aligned} \tag{4.190}$$

Combining the conditions in Eqs. 4.188, 4.189 and 4.190 we find that the U_{ij} for all links can be specified in terms of only two parameters U^x and U^y:

$$\begin{aligned} &U_1 = U^x \tau_x + U^y \tau_y; \\ &U_2 = U_1; \qquad U_3 = U_1; \qquad U_4 = U_1; \\ &U_5 = U_1; \qquad U_6 = U_1; \qquad U_7 = \mathcal{A}^2 U_1; \\ &U_8 = \mathcal{A}^2 U_1; \qquad U_9 = U_1; \qquad U_{10} = U_1; \\ &U_{11} = \mathcal{A}^2 U_1; \qquad U_{12} = \mathcal{A}^2 U_1 \end{aligned} \tag{4.191}$$

Similarly, demanding the invariance of μ_i under (G_c, g_c) gives us $\mu_\gamma = \mu_\delta = \mu_\beta$, and $\mu_\alpha = \mathcal{A}^2 \mu_\alpha$. Under (G_a, g_a), we have $\mu_\alpha = \mu_\delta$ and $\mu_\beta = \mathcal{A}^2 \mu_\gamma$. This already implies that when $\mathcal{A} \neq 1$, $\mu = 0$ on all sites. When $\mathcal{A} = 1$, site-independent on-site terms of the form $\mu^x \tau_x + \mu^y \tau_y$ are allowed in the ansatz.

4.C.2 U(1)

The U(1) spin liquid mean field ansatz has the following form:

$$U_{ij} = i U^0_{ij} \tau_0 + U^z_{ij} \tau_z, \tag{4.192}$$

dictated by the fact that the ansatz is invariant under the $\mathsf{U}(1)$ IGG gauge transformation. We would like to investigate how the PSG solutions we obtained constrain the nearest neighbor mean field ansatz by subjecting them to the following test:

$$\forall g \in \mathsf{P2}_1\mathsf{3} \times \mathsf{Z}_2^{\mathcal{T}} : \hat{G}_g \hat{g}(U_{ij}) = U_{ij}. \tag{4.193}$$

Among the PSGs we have, we first study the class in which $A = 0$. After enumerating all the conditions imposed by the PSG, we arrive at the following nearest neighbor mean field ansatz in the class where $A = 0$.:

$$U_i = \lambda \tau_z, \quad \text{where } i \in \{1, \ldots, 12\}. \tag{4.194}$$

Next we would like to argue that, when $A \neq 0$, there would be no nearest neighbor mean field ansatz. We write $U_{1/3} \equiv i\mathfrak{U}_{1/3} \exp[i\varphi_{1/3}\tau_z]$. The TRS conditions on these two bonds give:

$$2\varphi_1 + A = \pi, \quad \varphi_3 = \pi/2. \tag{4.195}$$

However, the condition $\hat{G}_b \hat{g}_b(U_1) = U_1$ gives us:

$$\varphi_3 + 2A + 4\phi_3 = \varphi_1. \tag{4.196}$$

We time the above equation by 2, and combined with the last two relations, we would immediately arrive at $5A = 0$. Note that we had $3A = 0$. Thus the ansatz does not vanish only when $A = 0$.

We conclude that we obtain only one nearest neighbor $\mathsf{U}(1)$ mean field ansatz:

$$\begin{aligned} U_\zeta &= \lambda \tau_z, \quad \zeta \in \{1, \ldots, 12\} \\ a_s &= \omega \tau_z, \quad i \in \{\alpha, \ldots, \delta\}. \end{aligned} \tag{4.197}$$

Chapter 5

Conclusion and outlooks

In Chapter 2, we have established via an explicit construction that all inversion-symmetric higher-order topological insulators and superconductors (except for AZ class C) admit gapped surfaces with anomalous topological order. While we have done so for the case of inversion symmetric electronic phases, we expect it to hold more generally for both Bosonic and electronic three-dimensional higher-order phases with various spatial symmetries. This consequently extends the list of symmetric surface terminations of 3D second and third-order topological phases to include 'anomalous gapped surfaces'. A technical consequence of this work is the study of spatial symmetries and their anomalies in 2D topological orders. In this regard, there is a recent systematic algebraic framework to study the spatial symmetry enrichment of modular tensor categories [157]. In particular, obstructions to such symmetry enrichment must precisely encode anomalies that in turn can be compensated by crystalline topological phases in one higher dimension. It would be interesting to pursue this direction in future work.

In Chapter 3, we have shown that the theory of finite-entanglement scaling can be generalized from 1D gapless systems to 2D states with a Fermi surface. Our main result is that $S_{\mathrm{fTNS}}(L, D)$, the EE of a $L \times L$ spatial region in the optimal bond-dimension-D fTNS approximation of a metallic state, can be written as $S_{\mathrm{fTNS}}(L, D) \sim L \log(\xi_D f(L/\xi_D)$, where ξ_D is a finite infrared length scale which results from the area-law structure (and thus the finite bond dimension D) of the tensor network state, and $f(x)$ is a scaling function which depends on the shape of the Fermi surface, but not on the length scale k_F^{-1}, with k_F the Fermi momentum. It will be interesting to explore quantitatively the Fermi surface dependence of the scaling function.

Fermionic tensor networks are being used in a variety of different ways, e.g., for numerical studies of lattice gauge theories [158, 159, 160], as numerically tractable Gutzwiller-

Chapter heading: bird motifs, *zun*, Middle Western Zhou dynasty (circa 10th – 8th centuries B.C.), Meiyintang Collection # 193.

projected states [161, 162, 163, 164, 165, 166, 167], as a tool for large-scale mean-field calculations [168, 169], as trial states for topological phases [50, 110, 170, 116, 102, 171, 172], and as a general class of variational states for numerical simulations of strongly interacting systems [48, 173, 174, 175, 176, 177]. The results presented in this work show how these applications of fTNS can be extended to metallic states. In particular, being able to perform a scaling collapse for the EE provides solid numerical evidence for the existence of a Fermi surface, and hence can be used to numerically determine whether the ground state of Hubbard-type models (e.g., those obtained from the flat bands of twisted transition-metal dichalcogenides) are metallic or insulating. Similarly, a scaling collapse for the EE can be used to determine whether a frustrated spin model has a spin liquid ground state with a spinon Fermi surface. Furthermore, the scaling collapse significantly enhances the accuracy of the numerically obtained Widom prefactor, and hence provides more reliable information about the fermiology of the metallic ground states.

In Chapter 4, we have computed the PSGs for the trillium lattice, with and without time reversal symmetry. Considering the presence of TRS, the algebraic information of PSGs leads us to write down the nearest neighbor mean field (fermionic) parton Hamiltonian of the corresponding quantum spin liquid states, and we report 2 such Z_2 QSLs, and 1 such $\mathsf{U}(1)$ QSL. We further evaluate the band structure and the static structure factors to provide physical information about the QSLs.

The main result of our chapter is Table. 4.2 and Table. 4.3, since we hope that our results will guide the theoretical studies of the recently reported quantum spin liquid material $K_2Ni_2SO_4$. The natural next step is to apply our PSG classifications to the double trillium lattice of $K_2Ni_2SO_4$, and perform Monte Carlo studies of the Gutzwiller projected mean field QSL wavefunctions to compare with the available experimental data.

Bibliography

[1] Plato. Timaeus and Critias. Oxford University Press, Nov. 2008.

[2] Lev Landau. In: *Zh.Eksp.Teor.Fiz.* (1937). DOI: 10.1016/c2013-0-01806-3.

[3] Vitaly Ginzburg and Lev Landau. In: *Zh.Eksp.Teor.Fiz.* (1950).

[4] C. L. Kane and E. J. Mele. In: *Physical Review Letters* 95.22 (22 Nov. 2005), p. 226801. ISSN: 1079-7114. DOI: 10.1103/PhysRevLett.95.226801. URL: https://link.aps.org/doi/10.1103/PhysRevLett.95.226801.

[5] B. Andrei Bernevig and Shou-Cheng Zhang. In: *Physical Review Letters* 96.10 (10 Mar. 2006), p. 106802. ISSN: 1079-7114. DOI: 10.1103/PhysRevLett.96.106802. URL: https://link.aps.org/doi/10.1103/PhysRevLett.96.106802.

[6] Yuan-Ming Lu and Ashvin Vishwanath. In: *Phys. Rev. B* 86.12 (2012). [Erratum: Phys.Rev.B 89, 199903 (2014)], p. 125119. DOI: 10.1103/PhysRevB.86.125119. arXiv: 1205.3156 [cond-mat.str-el].

[7] Michael Levin and Ady Stern. In: *Physical Review B* 86.11 (Sept. 2012), p. 115131. ISSN: 1550-235X. DOI: 10.1103/physrevb.86.115131.

[8] Xie Chen et al. In: *Physical Review B* 87.15 (15 Apr. 2013), p. 155114. ISSN: 1550-235X. DOI: 10.1103/PhysRevB.87.155114. URL: https://link.aps.org/doi/10.1103/PhysRevB.87.155114.

[9] Zheng-Cheng Gu and Xiao-Gang Wen. In: *Physical Review B* 90.11 (11 Sept. 2014), p. 115141. ISSN: 1550-235X. DOI: 10.1103/PhysRevB.90.115141. URL: https://link.aps.org/doi/10.1103/PhysRevB.90.115141.

[10] Xiao-Gang Wen. In: *Reviews of Modern Physics* 89.4 (Dec. 2017), p. 041004. ISSN: 1539-0756. DOI: 10.1103/revmodphys.89.041004.

[11] Xiao-Gang Wen. In: *Physical Review D* 88.4 (Aug. 2013), p. 045013. ISSN: 1550-2368. DOI: 10.1103/physrevd.88.045013.

[12] Yuji Tachikawa and Kazuya Yonekura. In: *Progress of Theoretical and Experimental Physics* 2017.3 (Mar. 2017). 033B04. ISSN: 2050-3911. DOI: https://doi.org/10.1093/ptep/ptx010. URL: https://doi.org/10.1093/ptep/ptx010.

[13] Chenjie Wang and Michael Levin. In: *Physical Review Letters* 119.13 (13 Sept. 2017), p. 136801. ISSN: 1079-7114. DOI: 10.1103/PhysRevLett.119.136801. URL: https://link.aps.org/doi/10.1103/PhysRevLett.119.136801.

[14] Edward Witten. In: *Physical Review B* 94.19 (19 Nov. 2016), p. 195150. ISSN: 2469-9969. DOI: 10.1103/PhysRevB.94.195150. URL: https://link.aps.org/doi/10.1103/PhysRevB.94.195150.

[15] Edward Witten. In: *Reviews of Modern Physics* 88.3 (3 July 2016), p. 035001. ISSN: 1539-0756. DOI: 10.1103/RevModPhys.88.035001. URL: https://link.aps.org/doi/10.1103/RevModPhys.88.035001.

[16] Eugen Wigner. Vieweg+Teubner Verlag, 1931. ISBN: 9783663025559. DOI: 10.1007/978-3-663-02555-9.

[17] G. 't Hooft. In: *Recent Developments in Gauge Theories*. Springer US, 1980, pp. 135–157. ISBN: 9781468475715. DOI: 10.1007/978-1-4684-7571-5_9.

[18] Ruben Verresen, Roderich Moessner, and Frank Pollmann. In: *Physical Review B* 96.16 (16 Oct. 2017), p. 165124. ISSN: 2469-9969. DOI: 10.1103/PhysRevB.96.165124. URL: https://link.aps.org/doi/10.1103/PhysRevB.96.165124.

[19] Xie Chen, Lukasz Fidkowski, and Ashvin Vishwanath. In: *Physical Review B* 89.16 (16 Apr. 2014), p. 165132. ISSN: 1550-235X. DOI: 10.1103/PhysRevB.89.165132. URL: https://link.aps.org/doi/10.1103/PhysRevB.89.165132.

[20] Parsa Bonderson, Chetan Nayak, and Xiao-Liang Qi. In: *Journal of Statistical Mechanics: Theory and Experiment* 2013.09 (Sept. 2013), P09016. ISSN: 1742-5468. DOI: 10.1088/1742-5468/2013/09/p09016. URL: https://doi.org/10.1088%2F1742-5468%2F2013%2F09%2Fp09016.

[21] Xie Chen et al. In: *Physical Review X* 5.4 (4 Oct. 2015), p. 041013. ISSN: 2160-3308. DOI: 10.1103/PhysRevX.5.041013. URL: https://link.aps.org/doi/10.1103/PhysRevX.5.041013.

[22] Lukasz Fidkowski, Xie Chen, and Ashvin Vishwanath. In: *Physical Review X* 3.4 (4 Nov. 2013), p. 041016. ISSN: 2160-3308. DOI: 10.1103/PhysRevX.3.041016. URL: https://link.aps.org/doi/10.1103/PhysRevX.3.041016.

[23] F. J. Burnell et al. In: *Physical Review B* 90.24 (Dec. 2014), p. 245122. ISSN: 1550-235X. DOI: 10.1103/physrevb.90.245122.

[24] Gregory Moore and Nicholas Read. In: *Nuclear Physics B* 360.2 (Aug. 1991), pp. 362–396. ISSN: 0550-3213. DOI: https://doi.org/10.1016/0550-3213(91)90407-O. URL: http://www.sciencedirect.com/science/article/pii/055032139190407O.

[25] Alexei Kitaev. In: *Annals of Physics* 321.1 (Jan. 2006), pp. 2–111. ISSN: 0003-4916. DOI: 10.1016/j.aop.2005.10.005.

[26] Frank Schindler et al. In: *Science Advances* 4.6 (June 2018). ISSN: 2375-2548. DOI: 10.1126/sciadv.aat0346. URL: https://advances.sciencemag.org/content/4/6/eaat0346.

[27] Eslam Khalaf. In: *Physical Review B* 97.20 (20 May 2018), p. 205136. ISSN: 2469-9969. DOI: 10.1103/PhysRevB.97.205136. URL: https://link.aps.org/doi/10.1103/PhysRevB.97.205136.

[28] Don N. Page. In: *Physical Review Letters* 71.9 (Aug. 1993), pp. 1291–1294. ISSN: 0031-9007. DOI: 10.1103/physrevlett.71.1291.

[29] S. K. Foong and S. Kanno. In: *Physical Review Letters* 72.8 (Feb. 1994), pp. 1148–1151. ISSN: 0031-9007. DOI: 10.1103/physrevlett.72.1148.

[30] Siddhartha Sen. In: *Physical Review Letters* 77.1 (July 1996), pp. 1–3. ISSN: 1079-7114. DOI: 10.1103/physrevlett.77.1.

[31] M B Hastings. In: *Journal of Statistical Mechanics: Theory and Experiment* 2007.08 (Aug. 2007), P08024. DOI: 10.1088/1742-5468/2007/08/P08024. URL: https://dx.doi.org/10.1088/1742-5468/2007/08/P08024.

[32] Itai Arad, Zeph Landau, and Umesh Vazirani. In: *Physical Review B* 85.19 (May 2012), p. 195145. ISSN: 1550-235X. DOI: 10.1103/physrevb.85.195145.

[33] Itai Arad et al. In: (Jan. 7, 2013). DOI: 10.48550/ARXIV.1301.1162. arXiv: 1301.1162 [quant-ph].

[34] Anurag Anshu, Itai Arad, and David Gosset. In: *Proceedings of the 54th Annual ACM SIGACT Symposium on Theory of Computing (STOC 2022)*. STOC '22 (Mar. 3, 2021). DOI: 10.1145/3519935.3519962. arXiv: 2103.02492 [quant-ph].

[35] M. Cramer et al. In: *Physical Review A* 73.1 (Jan. 2006), p. 012309. ISSN: 1094-1622. DOI: 10.1103/physreva.73.012309.

[36] Steven R. White. In: *Physical Review Letters* 69.19 (Nov. 1992), pp. 2863–2866. ISSN: 0031-9007. DOI: 10.1103/physrevlett.69.2863.

[37] Steven R. White. In: *Physical Review B* 48.14 (Oct. 1993), pp. 10345–10356. ISSN: 1095-3795. DOI: 10.1103/physrevb.48.10345.

[38] J Dukelsky et al. In: *Europhysics Letters (EPL)* 43.4 (Aug. 1998), pp. 457–462. ISSN: 1286-4854. DOI: 10.1209/epl/i1998-00381-x.

[39] Stellan Östlund and Stefan Rommer. In: *Physical Review Letters* 75.19 (Nov. 1995), pp. 3537–3540. ISSN: 1079-7114. DOI: 10.1103/physrevlett.75.3537.

[40] F. Verstraete, D. Porras, and J. I. Cirac. In: *Physical Review Letters* 93.22 (Nov. 2004), p. 227205. ISSN: 1079-7114. DOI: 10.1103/physrevlett.93.227205.

[41] F. Verstraete and J. I. Cirac. In: *Physical Review B* 73.9 (Mar. 2006), p. 094423. ISSN: 1550-235X. DOI: 10.1103/physrevb.73.094423.

[42] Laurens Vanderstraeten, Jutho Haegeman, and Frank Verstraete. In: *SciPost Physics Lecture Notes* (Jan. 2019). ISSN: 2590-1990. DOI: 10.21468/scipostphyslectnotes.7.

[43] F. Verstraete et al. In: *Physical Review Letters* 96.22 (June 2006), p. 220601. ISSN: 1079-7114. DOI: 10.1103/physrevlett.96.220601.

[44] Glen Evenbly. In: *Physical Review B* 98.8 (Aug. 2018), p. 085155. ISSN: 2469-9969. DOI: 10.1103/physrevb.98.085155.

[45] Jonas Haferkamp et al. In: *Physical Review Research* 2.1 (Jan. 2020), p. 013010. ISSN: 2643-1564. DOI: 10.1103/physrevresearch.2.013010.

[46] Norbert Schuch et al. In: *Physical Review Letters* 98.14 (Apr. 2007), p. 140506. ISSN: 1079-7114. DOI: 10.1103/physrevlett.98.140506.

[47] J. Jordan et al. In: *Physical Review Letters 101, 250602 (2008)* 101.25 (Mar. 29, 2007), p. 250602. ISSN: 1079-7114. DOI: 10.1103/physrevlett.101.250602. arXiv: cond-mat/0703788 [cond-mat.str-el].

[48] Philippe Corboz et al. In: *Phys. Rev. B* 81 (16 Apr. 2010), p. 165104. DOI: 10.1103/PhysRevB.81.165104. URL: https://link.aps.org/doi/10.1103/PhysRevB.81.165104.

[49] Michael P. Zaletel and Frank Pollmann. In: *Phys. Rev. Lett.* 124 (3 Jan. 2020), p. 037201. DOI: 10.1103/PhysRevLett.124.037201. URL: https://link.aps.org/doi/10.1103/PhysRevLett.124.037201.

[50] Nick Bultinck et al. In: *Phys. Rev. B* 95 (7 Feb. 2017), p. 075108. DOI: 10.1103/PhysRevB.95.075108. URL: https://link.aps.org/doi/10.1103/PhysRevB.95.075108.

[51] Pasquale Calabrese and John Cardy. In: *Journal of Statistical Mechanics: Theory and Experiment* 2004.06 (June 2004), P06002. DOI: 10.1088/1742-5468/2004/06/P06002. URL: https://dx.doi.org/10.1088/1742-5468/2004/06/P06002.

[52] Pasquale Calabrese and John Cardy. In: *Journal of Physics A: Mathematical and Theoretical* 42.50 (Dec. 2009), p. 504005. DOI: 10.1088/1751-8113/42/50/504005. URL: https://dx.doi.org/10.1088/1751-8113/42/50/504005.

[53] L. Tagliacozzo et al. In: *Phys. Rev. B* 78 (2 July 2008), p. 024410. DOI: 10.1103/PhysRevB.78.024410. URL: https://link.aps.org/doi/10.1103/PhysRevB.78.024410.

[54] Frank Pollmann et al. In: *Phys. Rev. Lett.* 102 (25 June 2009), p. 255701. DOI: 10.1103/PhysRevLett.102.255701. URL: https://link.aps.org/doi/10.1103/PhysRevLett.102.255701.

[55] Dimitri Gioev and Israel Klich. In: *Phys. Rev. Lett.* 96 (10 Mar. 2006), p. 100503. DOI: 10.1103/PhysRevLett.96.100503. URL: https://link.aps.org/doi/10.1103/PhysRevLett.96.100503.

[56] Weifei Li et al. In: *Physical Review B* 74.7 (Aug. 2006), p. 073103. ISSN: 1550-235X. DOI: 10.1103/physrevb.74.073103.

[57] R. Helling, H. Leschke, and W. Spitzer. In: *International Mathematics Research Notices* (June 2010). ISSN: 1687-0247. DOI: 10.1093/imrn/rnq085.

[58] Brian Swingle. In: *Phys. Rev. Lett.* 105 (5 July 2010), p. 050502. DOI: 10.1103/PhysRevLett.105.050502. URL: https://link.aps.org/doi/10.1103/PhysRevLett.105.050502.

[59] Luca V. Delacrétaz et al. In: *Physical Review Research* 4.3 (Aug. 2022), p. 033131. ISSN: 2643-1564. DOI: 10.1103/physrevresearch.4.033131.

[60] Junping Shao et al. In: *Physical Review Letters* 114.20 (May 2015), p. 206402. ISSN: 1079-7114. DOI: 10.1103/physrevlett.114.206402.

[61] Ryan V. Mishmash and Olexei I. Motrunich. In: *Physical Review B* 94.8 (Aug. 2016), p. 081110. ISSN: 2469-9969. DOI: 10.1103/physrevb.94.081110.

[62] Kang-Le Cai and Meng Cheng. 2024. DOI: 10.48550/ARXIV.2404.04334.

[63] P.W. Anderson. In: *Materials Research Bulletin* 8.2 (Feb. 1973), pp. 153–160. ISSN: 0025-5408. DOI: 10.1016/0025-5408(73)90167-0.

[64] S. Liang, B. Doucot, and P. W. Anderson. In: *Physical Review Letters* 61.3 (July 1988), pp. 365–368. ISSN: 0031-9007. DOI: 10.1103/physrevlett.61.365.

[65] P. W. Anderson. In: *Science* 235.4793 (Mar. 1987), pp. 1196–1198. ISSN: 1095-9203. DOI: 10.1126/science.235.4793.1196.

[66] Xiao-Gang Wen. In: *Phys. Rev. B* 65 (16 Apr. 2002), p. 165113. DOI: 10.1103/PhysRevB.65.165113. URL: https://link.aps.org/doi/10.1103/PhysRevB.65.165113.

[67] X. G. Wen. In: *Phys. Rev. B* 44 (6 Aug. 1991), pp. 2664–2672. DOI: 10.1103/PhysRevB.44.2664. URL: https://link.aps.org/doi/10.1103/PhysRevB.44.2664.

[68] Ming-Hao Li et al. In: *Physical Review B* 106.12 (Sept. 2022), p. 125121. ISSN: 2469-9969. DOI: 10.1103/physrevb.106.125121.

[69] Quinten Mortier et al. In: *Physical Review Letters* 131.26 (Dec. 2023), p. 266202. ISSN: 1079-7114. DOI: 10.1103/physrevlett.131.266202.

[70] Apoorv Tiwari et al. In: *Physical Review Letters* 124.4 (4 Jan. 2020), p. 046801. ISSN: 1079-7114. DOI: 10.1103/PhysRevLett.124.046801. URL: https://link.aps.org/doi/10.1103/PhysRevLett.124.046801.

[71] Matthew S. Foster and Emil A. Yuzbashyan. In: *Physical Review Letters* 109.24 (Dec. 2012), p. 246801. ISSN: 1079-7114. DOI: 10.1103/physrevlett.109.246801.

[72] Karl Jansen. In: *Physics Reports* 273.1 (Aug. 1996), pp. 1–54. ISSN: 0370-1573. DOI: 10.1016/0370-1573(95)00081-X.

[73] X. G. Wen. In: *Physical Review B* 41.18 (18 June 1990), pp. 12838–12844. ISSN: 1095-3795. DOI: 10.1103/PhysRevB.41.12838. URL: https://link.aps.org/doi/10.1103/PhysRevB.41.12838.

[74] Xiao-Gang Wen. In: *Advances in Physics* 44.5 (Oct. 1995), pp. 405–473. ISSN: 1460-6976. DOI: 10.1080/00018739500101566. URL: http://dx.doi.org/10.1080/00018739500101566.

[75] D. Sénéchal. In: *Theoretical Methods for Strongly Correlated Electrons*. New York, NY: Springer New York, 2004, pp. 139–186. ISBN: 978-0-387-21717-8. URL: https://doi.org/10.1007/0-387-21717-7_4.

[76] Jan von Delft and Herbert Schoeller. In: *Annalen der Physik* 7.4 (Nov. 1998), pp. 225–305. ISSN: 0003-3804. DOI: http://dx.doi.org/10.1002/(SICI)1521-3889(199811)7:4<225::AID-ANDP225>3.0.CO;2-L. URL: http://dx.doi.org/10.1002/(SICI)1521-3889(199811)7:4<225::AID-ANDP225>3.0.CO;2-L.

[77] Eslam Khalaf et al. In: *Physical Review X* 8.3 (3 Sept. 2018), p. 031070. ISSN: 2160-3308. DOI: 10.1103/PhysRevX.8.031070. URL: https://link.aps.org/doi/10.1103/PhysRevX.8.031070.

[78] R. Jackiw and C. Rebbi. In: *Physical Review D* 13.12 (12 June 1976), pp. 3398–3409. ISSN: 0556-2821. DOI: 10.1103/PhysRevD.13.3398. URL: https://link.aps.org/doi/10.1103/PhysRevD.13.3398.

[79] Meng Cheng. In: *Physical Review Letters* 120.3 (3 Jan. 2018), p. 036801. ISSN: 1079-7114. DOI: 10.1103/PhysRevLett.120.036801. URL: https://link.aps.org/doi/10.1103/PhysRevLett.120.036801.

[80] Sharmistha Sahoo, Zhao Zhang, and Jeffrey C. Y. Teo. In: *Physical Review B* 94.16 (16 Oct. 2016), p. 165142. ISSN: 2469-9969. DOI: 10.1103/PhysRevB.94.165142. URL: https://link.aps.org/doi/10.1103/PhysRevB.94.165142.

[81] P. Di Francesco, P. Mathieu, and D. Senechal. Graduate Texts in Contemporary Physics. New York: Springer-Verlag, 1997. ISBN: 978-0-387-94785-3, 978-1-4612-7475-9.

[82] C. N. Yang. In: *Reviews of Modern Physics* 34.4 (4 Oct. 1962), pp. 694–704. ISSN: 0034-6861. DOI: 10.1103/RevModPhys.34.694. URL: https://link.aps.org/doi/10.1103/RevModPhys.34.694.

[83] Max Geier et al. In: *Physical Review B* 97.20 (20 May 2018), p. 205135. ISSN: 2469-9969. DOI: 10.1103/PhysRevB.97.205135. URL: https://link.aps.org/doi/10.1103/PhysRevB.97.205135.

[84] Sheng-Jie Huang et al. In: *Physical Review B* 96.20 (20 Nov. 2017), p. 205106. ISSN: 2469-9969. DOI: 10.1103/PhysRevB.96.205106. URL: https://link.aps.org/doi/10.1103/PhysRevB.96.205106.

[85] Hao Song et al. In: *Physical Review X* 7.1 (1 Feb. 2017), p. 011020. ISSN: 2160-3308. DOI: 10.1103/PhysRevX.7.011020. URL: https://link.aps.org/doi/10.1103/PhysRevX.7.011020.

[86] Ching-Kai Chiu et al. In: *Reviews of Modern Physics* 88.3 (3 Aug. 2016), p. 035005. ISSN: 1539-0756. DOI: 10.1103/RevModPhys.88.035005. URL: https://link.aps.org/doi/10.1103/RevModPhys.88.035005.

[87] Y. X. Zhao and Z. D. Wang. In: *Physical Review B* 90.11 (11 Sept. 2014), p. 115158. ISSN: 1550-235X. DOI: 10.1103/PhysRevB.90.115158. URL: https://link.aps.org/doi/10.1103/PhysRevB.90.115158.

[88] Xiao-Gang Wen. In: *Oxford University Press on Demand* (Sept. 2007). DOI: https://doi.org/10.1093/acprof:oso/9780199227259.001.0001. URL: https://oxford.universitypressscholarship.com/view/10.1093/acprof:oso/9780199227259.001.0001/acprof-9780199227259.

[89] X. G. Wen and A. Zee. In: *Physical Review B* 46.4 (4 July 1992), pp. 2290–2301. ISSN: 1095-3795. DOI: 10.1103/PhysRevB.46.2290. URL: https://link.aps.org/doi/10.1103/PhysRevB.46.2290.

[90] Juven C. Wang and Xiao-Gang Wen. In: *Physical Review B* 91.12 (12 Mar. 2015), p. 125124. ISSN: 1550-235X. DOI: 10.1103/PhysRevB.91.125124. URL: https://link.aps.org/doi/10.1103/PhysRevB.91.125124.

[91] Philippe Corboz et al. In: *Phys. Rev. X* 8 (3 July 2018), p. 031031. DOI: 10.1103/PhysRevX.8.031031. URL: https://link.aps.org/doi/10.1103/PhysRevX.8.031031.

[92] Michael Rader and Andreas M. Läuchli. In: *Phys. Rev. X* 8 (3 July 2018), p. 031030. DOI: 10.1103/PhysRevX.8.031030. URL: https://link.aps.org/doi/10.1103/PhysRevX.8.031030.

[93] Piotr Czarnik and Philippe Corboz. In: *Phys. Rev. B* 99 (24 June 2019), p. 245107. DOI: 10.1103/PhysRevB.99.245107. URL: https://link.aps.org/doi/10.1103/PhysRevB.99.245107.

[94] Bram Vanhecke et al. In: *Phys. Rev. Lett.* 129 (20 Nov. 2022), p. 200601. DOI: 10.1103/PhysRevLett.129.200601. URL: https://link.aps.org/doi/10.1103/PhysRevLett.129.200601.

[95] Christina V. Kraus et al. In: *Phys. Rev. A* 81 (5 May 2010), p. 052338. DOI: 10.1103/PhysRevA.81.052338. URL: https://link.aps.org/doi/10.1103/PhysRevA.81.052338.

[96] Thomas Barthel, Carlos Pineda, and Jens Eisert. In: *Phys. Rev. A* 80 (4 Oct. 2009), p. 042333. DOI: 10.1103/PhysRevA.80.042333. URL: https://link.aps.org/doi/10.1103/PhysRevA.80.042333.

[97] Zheng-Cheng Gu, Frank Verstraete, and Xiao-Gang Wen. In: *arXiv e-prints*, arXiv:1004.2563 (Apr. 2010), arXiv:1004.2563. DOI: 10.48550/arXiv.1004.2563. arXiv: 1004.2563.

[98] Zheng-Cheng Gu. In: *Phys. Rev. B* 88 (11 Sept. 2013), p. 115139. DOI: 10.1103/PhysRevB.88.115139. URL: https://link.aps.org/doi/10.1103/PhysRevB.88.115139.

[99] Nick Bultinck et al. In: *Journal of Physics A: Mathematical and Theoretical* 51.2 (Dec. 2017), p. 025202. DOI: 10.1088/1751-8121/aa99cc. URL: https://dx.doi.org/10.1088/1751-8121/aa99cc.

[100] F.A. Berezin. Pure and Applied Physics : A Series of Monographs and Textbooks. Vol. 24. Academic Press, 1966. ISBN: 9780120894505. URL: https://books.google.co.uk/books?id=fAlRAAAAMAAJ.

[101] B. Béri and N. R. Cooper. In: *Phys. Rev. Lett.* 106 (15 Apr. 2011), p. 156401. DOI: 10.1103/PhysRevLett.106.156401. URL: https://link.aps.org/doi/10.1103/PhysRevLett.106.156401.

[102] J. Dubail and N. Read. In: *Phys. Rev. B* 92 (20 Nov. 2015), p. 205307. DOI: 10.1103/PhysRevB.92.205307. URL: https://link.aps.org/doi/10.1103/PhysRevB.92.205307.

[103] Shaoyu Yin, Nigel R. Cooper, and Benjamin Béri. In: *Phys. Rev. B* 99 (19 May 2019), p. 195125. DOI: 10.1103/PhysRevB.99.195125. URL: https://link.aps.org/doi/10.1103/PhysRevB.99.195125.

[104] Elliott Lieb, Theodore Schultz, and Daniel Mattis. In: *Annals of Physics* 16.3 (1961), pp. 407–466. ISSN: 0003-4916. DOI: https://doi.org/10.1016/0003-4916(61)90115-4. URL: https://www.sciencedirect.com/science/article/pii/0003491661901154.

[105] Ian Affleck. In: *Phys. Rev. B* 37 (10 Apr. 1988), pp. 5186–5192. DOI: 10.1103/PhysRevB.37.5186. URL: https://link.aps.org/doi/10.1103/PhysRevB.37.5186.

[106] Masaki Oshikawa. In: *Phys. Rev. Lett.* 84 (7 Feb. 2000), pp. 1535–1538. DOI: 10.1103/PhysRevLett.84.1535. URL: https://link.aps.org/doi/10.1103/PhysRevLett.84.1535.

[107] M. B. Hastings. In: *Phys. Rev. B* 69 (10 Mar. 2004), p. 104431. DOI: 10.1103/PhysRevB.69.104431. URL: https://link.aps.org/doi/10.1103/PhysRevB.69.104431.

[108] Nick Bultinck and Meng Cheng. In: *Phys. Rev. B* 98 (16 Oct. 2018), p. 161119. DOI: 10.1103/PhysRevB.98.161119. URL: https://link.aps.org/doi/10.1103/PhysRevB.98.161119.

[109] Norbert Schuch, Ignacio Cirac, and David Pérez-García. In: *Annals of Physics* 325.10 (2010), pp. 2153–2192. ISSN: 0003-4916. DOI: https://doi.org/10.1016/j.aop.2010.05.008. URL: https://www.sciencedirect.com/science/article/pii/S0003491610000990.

[110] N. Bultinck et al. In: *Annals of Physics* 378 (2017), pp. 183–233. ISSN: 0003-4916. DOI: https://doi.org/10.1016/j.aop.2017.01.004. URL: https://www.sciencedirect.com/science/article/pii/S0003491617300040.

[111] Andras Molnar et al. In: *arXiv e-prints*, arXiv:2204.05940 (Apr. 2022), arXiv:2204.05940. DOI: 10.48550/arXiv.2204.05940. arXiv: 2204.05940.

[112] Alberto Ruiz-de-Alarcon et al. In: *arXiv e-prints*, arXiv:2204.06295 (Apr. 2022), arXiv:2204.06295. DOI: 10.48550/arXiv.2204.06295. arXiv: 2204.06295.

[113] Thorsten B. Wahl et al. In: *Phys. Rev. B* 90 (11 Sept. 2014), p. 115133. DOI: 10.1103/PhysRevB.90.115133. URL: https://link.aps.org/doi/10.1103/PhysRevB.90.115133.

[114] N. Read and Dmitry Green. In: *Physical Review B* 61.15 (15 Apr. 2000), pp. 10267–10297. ISSN: 1095-3795. DOI: 10.1103/PhysRevB.61.10267. URL: https://link.aps.org/doi/10.1103/PhysRevB.61.10267.

[115] Quinten Mortier et al. In: *Phys. Rev. Lett.* 129 (20 Nov. 2022), p. 206401. DOI: 10.1103/PhysRevLett.129.206401. URL: https://link.aps.org/doi/10.1103/PhysRevLett.129.206401.

[116] T. B. Wahl et al. In: *Phys. Rev. Lett.* 111 (23 Dec. 2013), p. 236805. DOI: 10.1103/PhysRevLett.111.236805. URL: https://link.aps.org/doi/10.1103/PhysRevLett.111.236805.

[117] Adrián Franco-Rubio and J. Ignacio Cirac. In: *Physical Review B* 106.23, 235136 (Dec. 2022), p. 235136. ISSN: 2469-9969. DOI: 10.1103/PhysRevB.106.235136. arXiv: 2204.02478.

[118] Brian Swingle and T. Senthil. In: *Phys. Rev. B* 87 (4 Jan. 2013), p. 045123. DOI: 10.1103/PhysRevB.87.045123. URL: https://link.aps.org/doi/10.1103/PhysRevB.87.045123.

[119] HG Becker. In: *Lettere al Nuovo Cimento (1971-1985)* 8 (1973), pp. 185–188.

[120] Patrick Kofod Mogensen et al. Version v1.7.4. Nov. 2022. DOI: 10.5281/zenodo.7350608. URL: https://doi.org/10.5281/zenodo.7350608.

[121] Bram Vanhecke et al. In: *Phys. Rev. Lett.* 123 (25 Dec. 2019), p. 250604. DOI: 10.1103/PhysRevLett.123.250604. URL: https://link.aps.org/doi/10.1103/PhysRevLett.123.250604.

[122] B. Pirvu et al. In: *Phys. Rev. B* 86 (7 Aug. 2012), p. 075117. DOI: 10.1103/PhysRevB.86.075117. URL: https://link.aps.org/doi/10.1103/PhysRevB.86.075117.

[123] John M. Hopkinson and Hae-Young Kee. In: *Phys. Rev. B* 74 (22 Dec. 2006), p. 224441. DOI: 10.1103/PhysRevB.74.224441. URL: https://link.aps.org/doi/10.1103/PhysRevB.74.224441.

[124] Sergei V. Isakov, John M. Hopkinson, and Hae-Young Kee. In: *Phys. Rev. B* 78 (1 July 2008), p. 014404. DOI: 10.1103/PhysRevB.78.014404. URL: https://link.aps.org/doi/10.1103/PhysRevB.78.014404.

[125] Ivica Živković et al. In: *Phys. Rev. Lett.* 127.15 (15 Oct. 2021), p. 157204. ISSN: 1079-7114. DOI: 10.1103/PhysRevLett.127.157204. URL: https://link.aps.org/doi/10.1103/PhysRevLett.127.157204.

[126] M. G. Gonzalez et al. 2023. arXiv: 2308.11746 [cond-mat.str-el].

[127] Weiliang Yao et al. 2023. arXiv: 2303.16384 [cond-mat.str-el].

[128] B. Koteswararao et al. In: *Phys. Rev. B* 90 (3 July 2014), p. 035141. DOI: 10.1103/PhysRevB.90.035141. URL: https://link.aps.org/doi/10.1103/PhysRevB.90.035141.

[129] Shravani Chillal et al. In: *Nature Communications* 11.1 (May 11, 2020), p. 2348. ISSN: 2041-1723. DOI: 10.1038/s41467-020-15594-1. URL: https://doi.org/10.1038/s41467-020-15594-1.

[130] P. Khuntia et al. In: *Phys. Rev. Lett.* 116 (10 Mar. 2016), p. 107203. DOI: 10.1103/PhysRevLett.116.107203. URL: https://link.aps.org/doi/10.1103/PhysRevLett.116.107203.

[131] Li Ern Chern and Yong Baek Kim. In: *Phys. Rev. B* 104 (9 Sept. 2021), p. 094413. DOI: 10.1103/PhysRevB.104.094413. URL: https://link.aps.org/doi/10.1103/PhysRevB.104.094413.

[132] Hui-Ke Jin and Yi Zhou. In: *Phys. Rev. B* 101 (5 Feb. 2020), p. 054408. DOI: 10.1103/PhysRevB.101.054408. URL: https://link.aps.org/doi/10.1103/PhysRevB.101.054408.

[133] Benjamin Canals and Claudine Lacroix. In: *Phys. Rev. B* 61 (17 May 2000), pp. 11251–11254. DOI: 10.1103/PhysRevB.61.11251. URL: https://link.aps.org/doi/10.1103/PhysRevB.61.11251.

[134] Fa Wang, Ashvin Vishwanath, and Yong Baek Kim. In: *Phys. Rev. B* 76 (9 Sept. 2007), p. 094421. DOI: 10.1103/PhysRevB.76.094421. URL: https://link.aps.org/doi/10.1103/PhysRevB.76.094421.

[135] Sounak Biswas and Kedar Damle. In: *Phys. Rev. B* 97 (11 Mar. 2018), p. 115102. DOI: 10.1103/PhysRevB.97.115102. URL: https://link.aps.org/doi/10.1103/PhysRevB.97.115102.

[136] D. A. Garanin and Benjamin Canals. In: *Phys. Rev. B* 59 (1 Jan. 1999), pp. 443–456. DOI: 10.1103/PhysRevB.59.443. URL: https://link.aps.org/doi/10.1103/PhysRevB.59.443.

[137] S. V. Isakov et al. In: *Phys. Rev. Lett.* 93 (16 Oct. 2004), p. 167204. DOI: 10.1103/PhysRevLett.93.167204. URL: https://link.aps.org/doi/10.1103/PhysRevLett.93.167204.

[138] John M. Hopkinson et al. In: *Phys. Rev. Lett.* 99 (3 July 2007), p. 037201. DOI: 10.1103/PhysRevLett.99.037201. URL: https://link.aps.org/doi/10.1103/PhysRevLett.99.037201.

[139] Yoshihiko Okamoto et al. In: *Phys. Rev. Lett.* 99 (13 Sept. 2007), p. 137207. DOI: 10.1103/PhysRevLett.99.137207. URL: https://link.aps.org/doi/10.1103/PhysRevLett.99.137207.

[140] Yogesh Singh et al. In: *Phys. Rev. B* 88 (22 Dec. 2013), p. 220413. DOI: 10.1103/PhysRevB.88.220413. URL: https://link.aps.org/doi/10.1103/PhysRevB.88.220413.

[141] Rebecca Dally et al. In: *Phys. Rev. Lett.* 113 (24 Dec. 2014), p. 247601. DOI: 10.1103/PhysRevLett.113.247601. URL: https://link.aps.org/doi/10.1103/PhysRevLett.113.247601.

[142] A. C. Shockley et al. In: *Phys. Rev. Lett.* 115 (4 July 2015), p. 047201. DOI: 10.1103/PhysRevLett.115.047201. URL: https://link.aps.org/doi/10.1103/PhysRevLett.115.047201.

[143] Michael J. Lawler et al. In: *Phys. Rev. Lett.* 101 (19 Nov. 2008), p. 197202. DOI: 10.1103/PhysRevLett.101.197202. URL: https://link.aps.org/doi/10.1103/PhysRevLett.101.197202.

[144] Michael J. Lawler et al. In: *Phys. Rev. Lett.* 100 (22 June 2008), p. 227201. DOI: 10.1103/PhysRevLett.100.227201. URL: https://link.aps.org/doi/10.1103/PhysRevLett.100.227201.

[145] Yi Zhou et al. In: *Phys. Rev. Lett.* 101 (19 Nov. 2008), p. 197201. DOI: 10.1103/PhysRevLett.101.197201. URL: https://link.aps.org/doi/10.1103/PhysRevLett.101.197201.

[146] Biao Huang, Yong Baek Kim, and Yuan-Ming Lu. In: *Phys. Rev. B* 95 (5 Feb. 2017), p. 054404. DOI: 10.1103/PhysRevB.95.054404. URL: https://link.aps.org/doi/10.1103/PhysRevB.95.054404.

[147] Samuel Bieri, Claire Lhuillier, and Laura Messio. In: *Phys. Rev. B* 93 (9 Mar. 2016), p. 094437. DOI: 10.1103/PhysRevB.93.094437. URL: https://link.aps.org/doi/10.1103/PhysRevB.93.094437.

[148] The GAP Group. 2022. URL: \url{https://www.gap-system.org}.

[149] Laura Messio, Claire Lhuillier, and Grégoire Misguich. In: *Phys. Rev. B* 87 (12 Mar. 2013), p. 125127. DOI: 10.1103/PhysRevB.87.125127. URL: https://link.aps.org/doi/10.1103/PhysRevB.87.125127.

[150] Benedikt Schneider, Jad C. Halimeh, and Matthias Punk. In: *Phys. Rev. B* 105 (12 Mar. 2022), p. 125122. DOI: 10.1103/PhysRevB.105.125122. URL: https://link.aps.org/doi/10.1103/PhysRevB.105.125122.

[151] Patrick Kofod Mogensen et al. Version v4.5.1. Dec. 2020. DOI: 10.5281/zenodo.4404703. URL: https://doi.org/10.5281/zenodo.4404703.

[152] Jeff Bezanson et al. In: *SIAM Review* 59.1 (2017), pp. 65–98. DOI: 10.1137/141000671. URL: https://epubs.siam.org/doi/10.1137/141000671.

[153] F. J. Burnell, Shoibal Chakravarty, and S. L. Sondhi. In: *Phys. Rev. B* 79 (14 Apr. 2009), p. 144432. DOI: 10.1103/PhysRevB.79.144432. URL: https://link.aps.org/doi/10.1103/PhysRevB.79.144432.

[154] Chunxiao Liu, Gábor B. Halász, and Leon Balents. In: *Phys. Rev. B* 104 (5 Aug. 2021), p. 054401. DOI: 10.1103/PhysRevB.104.054401. URL: https://link.aps.org/doi/10.1103/PhysRevB.104.054401.

[155] Jonas Sonnenschein et al. In: *Phys. Rev. B* 102 (12 Sept. 2020), p. 125140. DOI: 10.1103/PhysRevB.102.125140. URL: https://link.aps.org/doi/10.1103/PhysRevB.102.125140.

[156] Aishwarya Chauhan et al. 2023. arXiv: 2306.12032 [cond-mat.str-el].

[157] Naren Manjunath and Maissam Barkeshli. In: (Dec. 2020). DOI: https://doi.org/10.48550/arXiv.2012.11603. arXiv: 2012.11603.

[158] Erez Zohar et al. In: *Annals of Physics* 363 (2015), pp. 385–439. ISSN: 0003-4916. DOI: https://doi.org/10.1016/j.aop.2015.10.009. URL: https://www.sciencedirect.com/science/article/pii/S0003491615003802.

[159] Patrick Emonts and Erez Zohar. In: *SciPost Phys. Lect. Notes* (2020), p. 12. DOI: 10.21468/SciPostPhysLectNotes.12. URL: https://scipost.org/10.21468/SciPostPhysLectNotes.12.

[160] Patrick Emonts and Erez Zohar. In: *arXiv e-prints*, arXiv:2304.06744 (Apr. 2023), arXiv:2304.06744. DOI: 10.48550/arXiv.2304.06744.

[161] Ying-Hai Wu, Lei Wang, and Hong-Hao Tu. In: *Phys. Rev. Lett.* 124 (24 June 2020), p. 246401. DOI: 10.1103/PhysRevLett.124.246401. URL: https://link.aps.org/doi/10.1103/PhysRevLett.124.246401.

[162] Hui-Ke Jin, Hong-Hao Tu, and Yi Zhou. In: *Phys. Rev. B* 101 (16 Apr. 2020), p. 165135. DOI: 10.1103/PhysRevB.101.165135. URL: https://link.aps.org/doi/10.1103/PhysRevB.101.165135.

[163] Gabriel Petrica et al. In: *Phys. Rev. B* 103 (12 Mar. 2021), p. 125161. DOI: 10.1103/PhysRevB.103.125161. URL: https://link.aps.org/doi/10.1103/PhysRevB.103.125161.

[164] Hui-Ke Jin, Hong-Hao Tu, and Yi Zhou. In: *Phys. Rev. B* 104 (2 July 2021), p. L020409. DOI: 10.1103/PhysRevB.104.L020409. URL: https://link.aps.org/doi/10.1103/PhysRevB.104.L020409.

[165] Jheng-Wei Li, Jan von Delft, and Hong-Hao Tu. In: *arXiv e-prints*, arXiv:2208.04623 (Aug. 2022), arXiv:2208.04623. DOI: 10.48550/arXiv.2208.04623. arXiv: 2208.04623.

[166] Qi Yang et al. In: *arXiv e-prints*, arXiv:2208.04566 (Aug. 2022), arXiv:2208.04566. DOI: 10.48550/arXiv.2208.04566. arXiv: 2208.04566.

[167] Hui-Ke Jin et al. In: *Phys. Rev. B* 105 (8 Feb. 2022), p. L081101. DOI: 10.1103/PhysRevB.105.L081101. URL: https://link.aps.org/doi/10.1103/PhysRevB.105.L081101.

[168] Matthew T. Fishman and Steven R. White. In: *Phys. Rev. B* 92 (7 Aug. 2015), p. 075132. DOI: 10.1103/PhysRevB.92.075132. URL: https://link.aps.org/doi/10.1103/PhysRevB.92.075132.

[169] Norbert Schuch and Bela Bauer. In: *Phys. Rev. B* 100 (24 Dec. 2019), p. 245121. DOI: 10.1103/PhysRevB.100.245121. URL: https://link.aps.org/doi/10.1103/PhysRevB.100.245121.

[170] C. Wille, O. Buerschaper, and J. Eisert. In: *Phys. Rev. B* 95 (24 June 2017), p. 245127. DOI: 10.1103/PhysRevB.95.245127. URL: https://link.aps.org/doi/10.1103/PhysRevB.95.245127.

[171] Anna Hackenbroich et al. In: *Phys. Rev. B* 101 (11 Mar. 2020), p. 115134. DOI: 10.1103/PhysRevB.101.115134. URL: https://link.aps.org/doi/10.1103/PhysRevB.101.115134.

[172] Sujeet K. Shukla, Tyler D. Ellison, and Lukasz Fidkowski. In: *Phys. Rev. B* 101 (15 Apr. 2020), p. 155105. DOI: 10.1103/PhysRevB.101.155105. URL: https://link.aps.org/doi/10.1103/PhysRevB.101.155105.

[173] Lei Wang, Philippe Corboz, and Matthias Troyer. In: *New Journal of Physics* 16.10 (Oct. 2014), p. 103008. DOI: 10.1088/1367-2630/16/10/103008. URL: https://dx.doi.org/10.1088/1367-2630/16/10/103008.

[174] Bo-Xiao Zheng et al. In: *Science* 358.6367 (2017), pp. 1155–1160. DOI: 10.1126/science.aam7127. URL: https://www.science.org/doi/abs/10.1126/science.aam7127.

[175] Zhehao Dai et al. In: *arXiv e-prints*, arXiv:2211.00043 (Oct. 2022), arXiv:2211.00043. DOI: 10.48550/arXiv.2211.00043. arXiv: 2211.00043.

[176] Yixin Ma, Shenghan Jiang, and Chao Xu. 2023. arXiv: 2302.03879 [cond-mat.str-el].

[177] Chao Xu, Yixin Ma, and Shenghan Jiang. 2023. arXiv: 2308.06543 [cond-mat.str-el].